SYNTHESIS AND STRUCTURAL STUDIES OF DONOR-BRIDGE-ACCEPTOR COMPLEXES BASED ON CO(III)(CYCLAM) ACETYLIDES
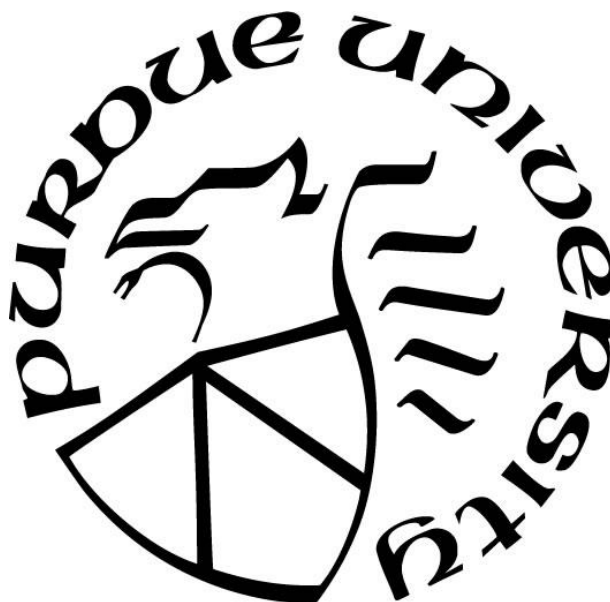
by

Susannah D. Banziger

A Dissertation

Submitted to the Faculty of Purdue University

In Partial Fulfillment of the Requirements for the degree of

Doctor of Philosophy

Department of Chemistry

West Lafayette, Indiana

August 2019

THE PURDUE UNIVERSITY GRADUATE SCHOOL
STATEMENT OF COMMITTEE APPROVAL

Dr. Tong Ren, Chair
  School of Science

Dr. Suzanne Bart
  School of Science

Dr. Libai Huang
  School of Science

Dr. Corey Thompson
  School of Science

Approved by:
  Dr. Christine Hrycyna
    Head of the Graduate Program

This thesis is dedicated to my mother who held me to the highest standards of excellence and first introduced me to the scientific method, my father who instilled in me a great love of literature and knowledge, to my sister who has forever been the greatest of lab partners and best of friends, and to my husband whose love and support has been instrumental to my success.

ACKNOWLEDGMENTS

Firstly, I would like to express my sincere gratitude to my advisor Prof. Tong Ren for the continuous support of my PhD study and related research, for his patience, motivation, and ability to guide me to the answer. His expertise was invaluable during my PhD and the writing of this thesis.

Besides my advisor, I would like to thank the rest of my thesis committee: Prof. Suzanne Bart, Prof. Corey Thompson, and Prof. Libai Huang, for their insightful comments and encouragement. My sincere thanks to Prof. David McMillin, who provided me many spectroscopic answers and taught me to how to ask bigger questions.

I thank my fellow lab mates, past and present, for the stimulating discussions and for the and for all the fun we have had. In particular, I am grateful to Dr. Sarah Robey and Dr. Eileen Judkins for sharing their love of research with me so I could forever dwell in my "excited state". I would also like to thank my friends, who were of great support in deliberating over our problems and findings, as well as providing happy distraction to rest my mind outside of my research.

Last but not the least, I would like to thank my family: especially, my husband, my parents, my sister and her wonderful family for supporting me throughout writing this thesis and my life in general with words of encouragements, happy memories, and the very best artwork to adorn my desk with.

TABLE OF CONTENTS

LIST OF TABLES

LIST OF FIGURES

LIST OF SCHEMES

LIST OF CHARTS

LIST OF ABBREVIATIONS

A-B-A = Acceptor-Bridge-Acceptor

B-A = Bridge-Acceptor

CSS = Charge separated state

Cyclam = 1,4,8,11-tetraazacyclotetradecane

Cyclam′ = *C*-substituted derivatives of 1,4,8,11-tetraazacyclotetradecane

CV = cyclic voltammogram

D-B-A = Donor-Bridge-Acceptor

DFT = Density functional theory

DMBA = tetrakis-*N*-*N*′-dimethylbenzamidinate

DMC = 5,12-dimethyl-1,4,8,11-tetraazacyclotetradecane

DMD = 5,12-dimethyl-1,4,8,11-tetraazacyclotetradiene

HMC = 5,7,7,12,14,14-hexamethyl-1,4,8,11-tetraazacyclotetradecane

HMD = 5,7,7,12,14,14-hexamethyl-1,4,8,11-tetraazacyclotetradeca-4,11-diene

HOMO = Highest occupied molecular orbital

LMCT = Ligand to metal charge transfer

LUMO = Lowest unoccupied molecular orbital

MEC = 5,12-diethyl-7,14-dimethyl-1,4,8,11-tetraazacyclotetradecane

MED = 5,12-diethyl-7,14-dimethyl-1,4,8,11-tetraazacyclotetradeca-4,11-diene

MLCT = Metal to ligand charge transfer

MPC = 5,12-dimethyl-7,14-diphenyl-1,4,8,11-tetraazacyclotetradecane

MPD = 5,12-dimethyl-7,14-diphenyl-1,4,8,11-tetraazacyclotetradeca-4,11-diene

NAP^R = *N*-R-1,8-naphthalimide; R = isopropyl (iPr), mesityl (Mes), methyl (Me),
1-ethylpropyl (Pen), 2-ethylhexyl (2-ethhex), or octyl (Oct)

SOMO = Singularly occupied molecular orbital

TMC = 1,4,8,11-tetramethyl-1,4,8,11-tetraazacyclotetradecane

TD-DFT = Time differentiated density functional theory

ABSTRACT

Author: Banziger, Susannah, D. PhD
Institution: Purdue University
Degree Received: August 2019
Title: Synthesis and Structural Studies of Donor-Bridge-Acceptor Complexes based on Co(III)(cyclam) acetylides

Committee Chair: Dr. Tong Ren

Obtaining a greater understanding of photo-induced electron-transfer (PET) processes is key to synthesizing photovoltaic materials with enhanced efficiency. Gaining knowledge about the structure property relationship in photo-active donor-bridge-acceptor (*D-B-A*) dyads will help to optimize electronic and photoelectronic materials. Metal acetylide complexes have attracted increasing interest for their potential applications as building blocks for electronic and photoelectronic materials. Their unique $\upsilon(C\equiv C)$ (2000-2100 cm^{-1}) allows for selective excitation, making them an appealing target for attenuating PET processes across a metal acetylide backbone. The following topics will be discussed: i.) an overview of M(cyclam′) alkynyl chemistry, where M = Cr, Fe, Co, or Ni, with a focus on reactivity and spectroscopy, ii.) selective synthesis of dissymmetric species, utilizing a Co^{III}(cyclam) (1,4,8,11-tetraazacyclotetradecane) alkynyl bridge, iii) synthesis and characterization of metal alkynyl *D-B-A* dyads *trans*-[R′$_2$N-4-C$_6$H$_4$C$_2$-Co^{III}(cyclam)-C$_n$-NAP^R]$^+$ (n = 2 or 4), where the chromophore acceptor is NAP^{iPr} (*N*-isopropyl-1,8-napthalimide) and the putative donor is -C$_6$H$_4$-4-NR′$_2$ (R′ = Me or Ph-4-OMe), iv.) design and synthesis of *D-B-A* derivatives, alter NAP^R (R = mesityl, methyl, 1-ethylpropyl, 2-ethylhexyl, or octyl) to tune reactivity and crystallinity, v.) electronic and spectroscopic influence the bridging center on *A*, and vi.) effect of η^2

coordination of MX_2 (MX_2 = $CuCl_2$ or $Ag(NO_3)_2$) to the alkyne bridge on electron transfer.

Both the *B-A* and *D-B-A* type compounds have been structurally characterized through single crystal X-ray diffraction, and spectroscopically characterized through UV-vis, FTIR, and fluorescence spectroscopy. It is concluded based on both the voltammetric and spectroscopic analysis of *D-B-A* that (i) the HOMO and LUMO are localized on donor and acceptor respectively; (ii) the π-π* transition localized on NAP^R (*ca.* 390 nm) is the primary Franck-Condon excitation; and (iii) the emissions of both the *B-A* and *D-B-A* moieties are fluorescent in nature and dominated by NAP^R when R' = Me. Through collaborations, we are currently probing the evolution of initial excited state(s) in *D-B-A* and its vibronic attenuation using ultra-fast timescale pump(UV)-probe(IR) and pump(UV)-pump(IR)-probe(IR) techniques, respectively.

CHAPTER 1.   SYNTHESES, STRUCTURES AND BONDING OF 3D METAL ALKYNYL COMPLEXES OF CYCLAM AND ITS DERIVATIVES

Abstract: Described in this review is the chemistry of 3*d* metal alkynyls based on tetraaza macrocyclic ligands. Both the abundance of 3*d* metals and easy access to the tetraazacyclotetradecane type ligands make these compounds more affordable and sustainable alternatives to metal alkynyls based on precious metals. Taking advantage of a rich variety of starting materials available in literature, the *trans*-[M(cyclam)(C$_2$R)$_2$]X type (cyclam = 1,4,8,11-tetraazacyclotetradecane) compounds have been prepared from the reactions between [M(cyclam)X$_2$]X (M = Cr, Fe and Co; X = Cl or OTf) and LiC$_2$R. With [Co(cyclam)Cl$_2$]$^+$, both the {*trans*-[Co(cyclam)Cl]$_2$(μ-(C≡C)$_n$)}$^{2+}$ and *trans*-[Co(cyclam)(C$_2$R)Cl]$^+$ type compounds can be prepared through a dehydrohalogenation reaction. The latter type compounds can undergo a second alkynylation reaction with LiC$_2$R´ to afford the dissymmetric *trans*-[Co(cyclam)(C$_2$R)(C$_2$R´)]$^+$ type compounds, including the *trans*-[Co(cyclam)(C$_2$A)(C$_2$D)]$^+$ dyads with *A* and *D* as acceptor and donor chromophores respectively. These compounds are being studied to probe photo-induced electron transfer and related photophysical/photochemical processes. The *trans*-[Co(cyclam)(C$_2$R)(NCMe)]$^{2+}$ type complexes react with unactivated HC$_2$R´ in the presence of a weak base to provide *trans*-[Co(cyclam)(C$_2$R)(C$_2$R´)]$^+$ in high yields. Similar alkynylation chemistry with complexes of cyclam derivatives, like TMC (1,4,8,11-tetramethyl-1,4,8,11-tetraazacyclotetradecane),   HMC   (5,7,7,12,14,14-

hexamethyl-1,4,8,11-tetraazacyclotetradecane) and DMC (5,12-dimethyl-1,4,8,11-tetraazacyclotetradecane), has been demonstrated with the studies of $[Ni(TMC)(C_2R)]^+$, *trans-/cis*-$[Cr(HMC/DMC)(C_2R)_2]^+$ and *trans*-$[Co(DMC)(C_2R)_2]^+$.

1.1 Introduction

Early examples of metal alkynyl chemistry can be traced back to homoleptic $[M(C{\equiv}CR)_6]^{n-}$ (M = Cr, Mn, Fe and Co), $[M(C{\equiv}CR)_4]^{n-}$ (M = Mn, Ni, Pd, Pt, Zn, Cd and Hg), and $[M(C{\equiv}CR)_2]^{n-}$ (M = Cu, Ag and Au) complexes developed by Nast and co-workers.[1] Similar species based on complexes of d^0 metal ions, such as Ta, Hf, Zr,[2] as well as M^{III} complexes (M= Cr, Co, and Fe)[3] were studied to further understand the structure-property relationship using modern structural and computational techniques. Formation of rigid-rod polymers $[M\text{-}C{\equiv}C\text{-}Ar\text{-}C{\equiv}C]_n$ (M = Ni, Pd and Pt) can be traced back to work by Hagihara *et al.* in the late 70s and early 80s.[4] Lewis and co-workers developed similar motifs with metals of groups 8-10 in the 90s by utilizing a trimethyl tin reagent and CuI to induce polymerization.[5,6] While these polymers display wire-like rigid rod structures, they are poor conductors. Square planar d^8 configuration Pd and Pt poly-ynes exhibited band gaps greater than 3 eV, based on their absorption edges, thereby acting as insulators ($R \sim 10^7 \Omega cm$).[7] The synthetic chemistry of metal alkynyls, their electronic structures as well as their applications in opto-electronics have been investigated by many groups and these efforts have been reviewed elsewhere.[8-12]

Since the pioneering studies of the C_4-bridged dirhenium compounds by Gladysz[13] and C_4-bridged diiron compounds by Lapinte,[14] the focus of wire like M-$(C{\equiv}C)_n$-M type compounds has been based on *middle* transition metals. There have been many examples of bimetallic compounds with an oligoyn-diyl bridge, including M as

Mn,[15] Ru,[16] W,[17] and Pt.[18] Examples of oligoen-diyl bridged species are scarce and limited largely to those capped with Ru(II) by the laboratories of Jia[19-21] and Liu.[22-24] Electron movement across the oligoyn-diyl bridge has been studied via voltammetric techniques and analysed using the framework of the classic Taube-Creutz mixed valency.[25] Drawing motivation from the work of Cotton[26] and Bear-Kadish[27,28] we reported the first diruthenium compounds with oligoyn-diyl bridges.[29] The Lehn laboratory published on similar compounds shortly thereafter[30] Since the late 90s, our laboratory has continued to probe diruthenium alkynyls as prototypical molecular wires.[31-33] Electrochemical and spectroelectrochemical analysis of the electronic couplings (H_{ad}) between two Ru_2 termini in Ru_2-$(C\equiv C)_n$-Ru_2 type compounds (n = 2-10), where $Ru_2(ap)_4$ is the capping unit (ap = 2-anilinopyridinate), showed good electronic coupling with a Robin-Day class II behaviour.[34-36] Similar studies were conducted for -$(C\equiv C)_n$-$Ru_2(DMBA)_4$-$(C\equiv C)_n$- bridge (n = 1 − 4; DMBA = N,N'-dimethylbenzamidinate) end-capped with ferrocenyls, and Robin-Day class II-III behaviours were observed for the [Fc-bridge-Fc]$^+$ moieties.[37-39] STM and break-junction techniques have been utilized to study how conductivity in Ru_2 alkynyl species compare to similar organic systems, and revealed that the Ru_2 systems perform better overall.[40,41] Since then, Ru_2-alkynyls have been incorporated and studied in flash-memory devices.[42-44] Facile electronic delocalization facilitated by metal-alkynyl linkage has also been demonstrated with high nuclearity clusters, such as linear Ru_3 array[45] and Os-carbonyl clusters.[46-49]

In an effort to advance metal alkynyl chemistry towards more sustainable materials, we have transitioned towards earth abundant $3d$ metal complexes supported by tetraaza macrocycles. The previously discussed alkynyl chemistry is primarily based on

4d and 5d metals, with only a few examples of 3d metals, more specifically based on Fe[14,50] and Mn.[15] First row transition metals originally gained popularity for their rich coordination chemistry developed to study bioinorganic modelling.[51,52] Use of a *hard* base as the supporting ligand in place of the soft polarizable ligands, previously mentioned, could result in different reactivity and applications for metal alkynyl species. When our laboratory began looking into Fe[III](cyclam) alkynyls in 2010,[53] examples of M(cyclam) alkynyl chemistry were restricted to a few Cr(III) bis-alkynyl compounds in two publications from the laboratories of Wagenknecht[54] and Nishi[55] and a dissertation chapter by Berben.[3] In less than 10 years, this family of compounds has been expanded to include metals such as Cr, Fe, Co, and Ni coordinated to simple alkynyls, cross-conjugated alkynyls, like *gem*-DEE (*geminal*-diethynyleneethene), and simple alkynyl chromophores. The majority of this review will discuss both the synthesis and structural characterizations of these compounds. It is worth noting that the scope of cyclam-based organometallic chemistry remains very limited. Besides the metal alkynyl chemistry described herein, Martins and co-workers have investigated extensively the Zr[IV](R$_2$cyclam)X$_2$ type compounds, where R is *N* benzyl / allyl susbstitutent at 1- and 8-positions, 4- and 11-nitrogen are amido (deprotonated), and X can be halide or alkyl.[56-59] Among many Zr[IV] species isolated are mono- and bis-phenylacetylide complexes based on Zr[IV](Bn$_2$cyclam),[59] though the X-ray structures of these compounds were not established.

There are many derivatives of cyclam, both *N*- and *C*-substituted, available in literature. It is well established that the coordination chemistry of TMC (TMC = 1,4,8,11-tetramethyl-1,4,8,11-tetraazacyclotetradecane, Chart 1.1) is significantly different from

that of cyclam,[60] and alkynyl compounds based on M(TMC) should be unique as well. The *C*-substituted cyclams have been subject to intense scrutiny in recent years because of the CO_2 reduction activity for their Ni^{II} and $Co^{II/III}$ complexes.[61,62] Particularly attractive are the M(HMC) complexes (5,7,7,12,14,14-hexamethyl-1,4,8,11-tetraazacyclotetradecane, Chart 1.1) due to the facile and inexpensive ligand synthesis. A number of Co(III) and Cr(III) alkynyl complexes of DMC (5,12-dimethyl-1,4,8,11-tetraazacyclotetradecane), HMC and MPC (4,14-Dimethyl-7,12-di-p-tolyl-1,4,8,11-tetraazacyclo-tetradecane) are described herein. The capacity of the 1,4,8,11-tetraazacyclotetradeca-4,11-diene macrocycle to support metal alkynyl complexes has also been recently demonstrated.[63]

Cyclam
(1,4,8,11-tetraazacyclotetradecane)

TMC
(1,4,8,11-tetramethyl-1,4,8,11-tetraazacyclotetradecane)

HMC
(5,7,7,12,14,14-hexamethyl-1,4,8,11-tetraazacyclotetradecane)

DMC
(5,12-dimethyl-1,4,8,11-tetraazacyclotetradecane)

MEC
(5,12-diethyl-7,14-dimethyl-1,4,8,11-tetraazacyclotetradecane)

MPC
(5,12-dimethyl-7,14-diphenyl-1,4,8,11-tetraazacyclotetradecane)

MED
(5,12-diethyl-7,14-dimethyl-1,4,8,11-tetraazacyclotetradeca-4,11-diene)

MPD
(5,12-dimethyl-7,14-diphenyl-1,4,8,11-tetraazacyclotetradeca-4,11-diene)

Chart 1.1. Tetraazamacrocycle Ligands

1.2 Alkynyl Complexes of M(cyclam)

1.2.1 Symmetric bis-alkynyl compounds
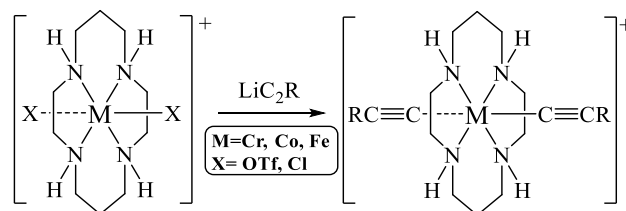
Scheme 1.1. Synthesis of bis-alkynyl M(III) cyclam complexes

Traditionally, *trans*-M(cyclam)(C$_2$R)$_2$ type complexes are prepared through the reaction between [M(cyclam)(OTf)$_2$]$^+$ and LiC$_2$R (Scheme 1.1). Berben first applied this technique to prepare several [Cr(cyclam)(C$_2$R)$_2$]$^+$ species (R= -SiMe$_3$ and -C$_6$H$_4$-3-C$_2$H).[3] Wagenknecht *et al.* further expanded on this class of symmetric alkynyl compounds with R as -Ph, -C$_6$H$_4$-4-CH$_3$ and -C$_6$H$_4$-4-CF$_3$,[54] R as -C$_6$H$_4$-4-F, cyclohexyl, 1-naphthalenyl and 9-phenanthrenyl[64] and -C$_6$F$_5$.[65] Further experiments carried out by Wagenknecht *et al.* revealed ways to i) suppress hydroamination byproducts formed from deprotonation of the –NH groups on the cyclam ring by replacing *n*-BuLi with lithium diisopropylamide,[66] and ii) enhance the yields of *cis*-isomer with the use of diethyl ether in place of THF.[64] Analogous Cr^{III}(cyclam) complexes bearing cross-conjugated *geminal*-diethynylethene (*gem*-DEE) type ligands were prepared from the reactions between [Cr(cyclam)(OTf)$_2$]$^+$ and Li(*gem*-DEE) through a collaboration between our lab and Wagenknecht.[67] Contemporary to the work of Wagenknecht, Nishijo and coworkers prepared a series of [Cr(cyclam)(C$_2$Ar)$_2$]$^+$ (Ar = thiophene, 6-methoxynaphthalene and tetrathiafulvalene (TTF)) and investigated the weak ferromagnetism therein.[55,68-72] Similar reactivity is observed for [Fe(cyclam)(OTf)$_2$]$^+$ and [Co(cyclam)(OTf)$_2$]$^+$, which upon treatment with LiC$_2$R afforded [Fe(cyclam)(C$_2$R)$_2$]$^+$ with R as -Ph, -Si^{i}Pr$_3$ (structure

shown in Figure 1.1), -C$_2$SiMe$_3$, -C$_4$SiMe$_3$ and -Fc,[53,73] and, [Co(cyclam)(C$_2$R)$_2$]$^+$ with R as -CF$_3$, -Fc, -Ph, -C$_6$H$_4$-4-CH$_3$, -C$_6$H$_4$-4-CN and -C$_6$H$_4$-4-CF$_3$, respectively.[74] The products of the above mentioned reactions are predominantly observed in the *trans*-isomer form, despite the fact that the [M(cyclam)(OTf)$_2$]$^+$ starting materials are generally a mixture of *trans*-(minor) and *cis*-(major) isomers. These reactions utilize alkynyl lithium reagents and are an effective route to form symmetric [M(cyclam)(C$_2$R)$_2$]$^+$.
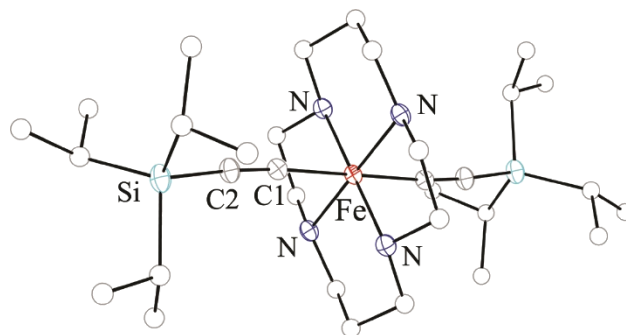
Figure 1.1. Molecular structure of [Fe(cyclam)(C$_2$Si^{i}Pr$_3$)$_2$]$^+$ (generated from CCDC 844147, originally reported in Ref. [53]).

On the other hand, selective formation of mono-alkynyl species, for example [M(cyclam)(C$_2$R)X]$^+$, has remained elusive for the majority of 3d metals. The exceptions are currently limited to Co^{III}(cyclam). Synthesis of *trans*-[Co(cyclam)(C$_2$Ph)Cl]Cl was achieved through reaction of HC$_2$Ph and [Co(cyclam)Cl$_2$]Cl in a weakly basic solution by Shores and coworkers (Scheme 1.2).[75] Similar conditions were employed to produce *trans*-[Co(cyclam)((C≡C)$_m$H)Cl]$^+$ (m = 1 − 3) through the reaction of MeSiC$_{2m}$SiMe$_3$ with [Co(cyclam)Cl$_2$]Cl,[76] several *trans*-[Co(cyclam)(C$_2$R)Cl]$^+$ type compounds (R = -C$_6$H$_4$-4-NO$_2$ (structure shown in Figure 1.2), -Fc and -C$_6$H$_4$-4-SC$_2$H$_4$SiMe$_3$),[77] as well as *trans*-[Co(cyclam)(C$_2$C$_6$F$_5$)Cl]$^+$ and *trans*-[Co(cyclam)(C$_2$C$_6$H$_4$-4-NMe$_2$)Cl]$^+$.[78,79] The mild conditions required to alkynylate Co^{III}(cyclam) has allowed for simple chromophores to

be coupled to the metal center. These species include *trans*-[Co(cyclam)(C$_2$Np)Cl]$^+$ (Np = naphthalene),[80] *trans*-[Co(cyclam)(C$_2$ANT)Cl]$^+$ (ANT = anthracene),[80] and *trans*-[Co(cyclam)(C$_2$NAP^{iPr})Cl]$^+$ (NAP^{iPr} = *N*-isopropyl-1,8-naphthalimide).[81]
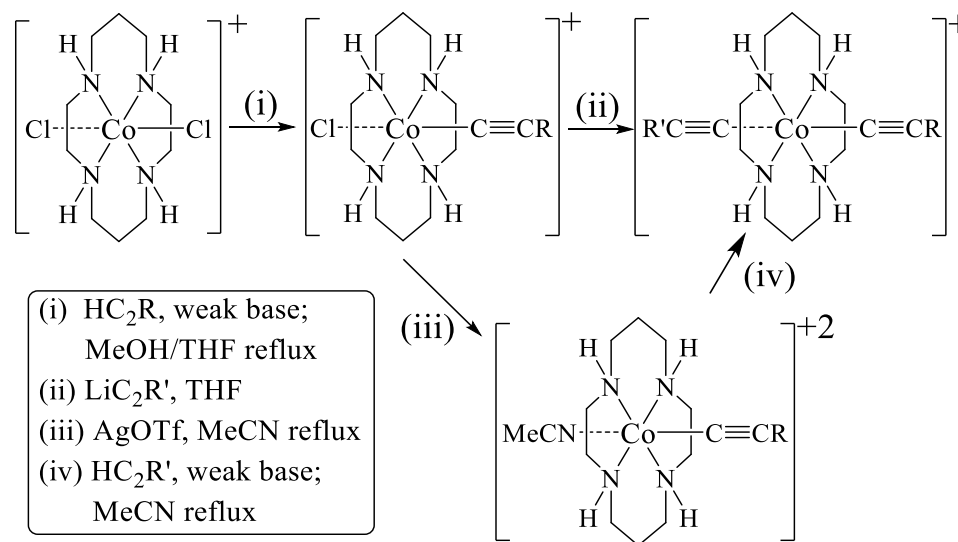
Scheme 1.2. Stepwise synthesis of dissymmetric Co^{III}(cyclam)-bis-alkynyl.
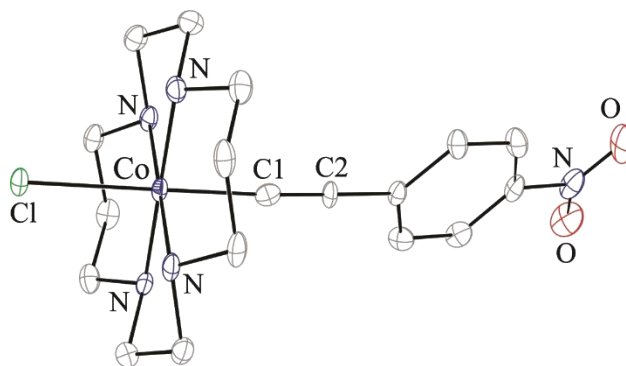
Figure 1.2. Molecular structure of *trans*-[Co(cyclam)(C$_2$-C$_6$H$_4$-4-NO$_2$)Cl]$^+$ (generated from CCDC 1411094, originally reported in Ref. [77]).

More recently, it was demonstrated that, with a Co^{III} species, stepwise formation of a bis-alkynyl species could be achieved under ambient conditions through a [Co(cyclam)(C$_2$R)(NCMe)]$^{2+}$ intermediate (Scheme 1.2). This reaction can also be

employed to selectively form both symmetric and dissymmetric *trans*-alkynyl complexes; the dissymmetric species will be discussed later on.[78,79] Refluxing a MeCN solution containing [Co(cylam)(C$_2$C$_6$F$_5$)Cl]Cl with AgOTf led to the formation of [Co(cyclam)(C$_2$C$_6$F$_5$)(NCMe)](OTf)$_2$ and AgCl. Formation of [Co(cyclam)(C$_2$C$_6$F$_5$)$_2$]OTf was accomplished through the reaction of [Co(cyclam)(C$_2$C$_6$F$_5$)(NCMe)](OTf)$_2$ with excess HC$_2$C$_6$F$_5$ in the presence of Et$_3$N under reflux.[79] Similar conditions afforded [Co(cyclam)(C$_2$C$_6$H$_4$-4-NMe$_2$)$_2$]OTf,[79] and [Co(cyclam)(C$_2$Np)$_2$]OTf (structure shown in Figure 1.3).[80] Unless specified otherwise, the compounds mentioned above adopt a *trans*-[M(cyclam)(C$_2$R)X]$^+$ and *trans*-[M(cyclam)(C$_2$R)$_2$]$^+$ pseudo-octahedral coordination geometry. Isomerically pure *cis*-[Cr(cyclam)(C$_2$Ph)$_2$]$^+$ was isolated from a solution containing the *trans*-counterpart through careful precipitation using THF and ether.[64] The M-C bond lengths observed in the symmetric *trans*-[M(cyclam)(C$_2$R)$_2$]$^+$ type compounds, 2.08 Å for Cr^{III}, 1.95 Å for Fe^{III} and 1.90 Å for Co^{III}, are consistent with gradual decrease of covalent radii across the periodic table from left to right.
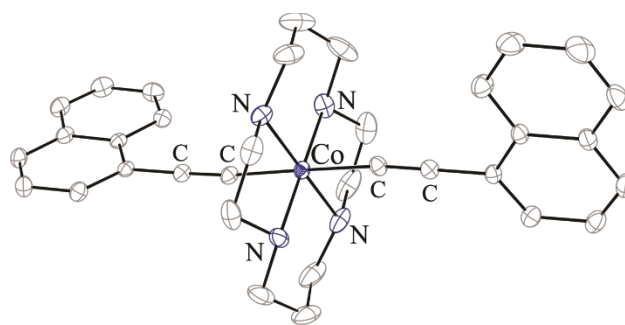
Figure 1.3. Molecular structure of *trans*-[Co(cyclam)(C$_2$Np)$_2$]$^+$ (generated from CCDC 1590057, originally reported in Ref. [80]).

1.2.2 Dissymetric D-B-A alkynyl compounds
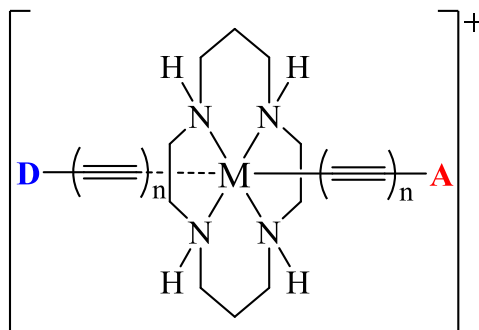
Chart 1.2. D-B-A type compounds based on M(III) cyclam.

Stepwise alkynylation unlocked the potential to form dissymmetric bis-alkynyl metal complexes. Reaction of *trans*-[Co(cyclam)(C$_2$Ph)Cl]$^+$ with LiC$_2$Ph and LiC$_2$SiMe$_3$ resulted in *trans*-[Co(cyclam)(C$_2$Ph)$_2$]$^{+}$[75] and *trans*-[Co(cyclam)(C$_2$Ph)(C$_2$SiMe$_3$)]$^+$,[82] respectively. The dissymmetric species, *trans*-[Co(cyclam)(C$_2$Ph)(C$_2$SiMe$_3$)]$^+$, is intriguing from the electronic point of view and provided a synthetic platform that was further expanded on to form a pseudo Donor-Bridge-Acceptor (D-B-A) species, *trans*-[Co(cyclam)(C$_2$-C$_6$H$_4$-4-NO$_2$)(C$_2$Ph)]$^+$ (structure shown in Figure 1.4). Formation of this complex was achieved through reaction of LiC$_2$Ph with *trans*-[Co(cyclam)(C$_2$C$_6$H$_4$-4-NO$_2$)Cl]$^+$.[77] However, these reactions suffered from low reaction yields and often resulted in scrambling to form both symmetric and dissymmetric products that were impractical to separate. Since then, two routes have been established to promote selective alkynylation i) the previously mentioned method, in which an intermediate species with a more labile leaving group is generated[78,79] and ii) cooling the lithiation to -78°C thereby kinetically promoting the formation of the dissymmetric *trans*-[Co(cyclam)(C$_2$R)(C$_2$R´)]Cl species.[81] Under the former conditions, formation of *trans*-[Co(cyclam)(C$_2$C$_6$H$_4$-4-NMe$_2$)(C$_2$C$_6$F$_5$)]OTf and *trans*-[Co(cyclam)(C$_2$C$_6$F$_5$)(C$_2$Ph)]OTf

have been observed.[78,79] Utilizing the latter conditions, formation of the first true Co^{III} D-B-A species was realized. The addition of 1.1 equivalents of $LiC_2C_6H_4$-4-NMe_2 to 1 equivalent of *trans*-[Co(cyclam)(C_2NAP^{iPr})Cl]$^+$, at -78°C, results in selective formation of the dissymmetric *trans*-[Co(cyclam)(C_2NAP^{iPr})($C_2C_6H_4$-4-NMe_2)]$^+$ species in 50% yield. This method was also utilized to synthesize *trans*-[Co(cyclam)(C_2NAP^{iPr})(C_2TPA)]$^+$, a panchromic D-B-A species (TPA = 4-*N,N*-bis(4-methoxyphenyl)aniline), and *trans*-[Co(cyclam)(C_2NAP^{iPr})(C_2Ph)]$^{+}$.[81] These compounds are actively being probed to understand the dynamics of photo-induced electron-transfer in comparison to their Pt^{II} counterparts, *trans*-(4-ethynyl-*N*-octyl-1,8-naphthalimide)(*N*-(4-ethynyl-benzyl)-phenothiazine)Pt(PBu_3)$_2$ and *trans*-(4-ethynyl-*N*-octyl-1,8-naphthalimide)(C_2Ph)Pt(PBu_3)$_2$.[83-85]
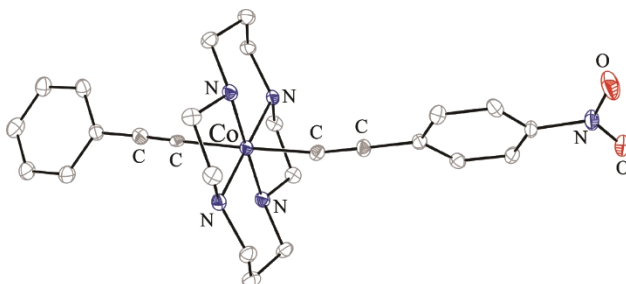
Figure 1.4. Molecular structure of *trans*-[Co(cyclam)(C_2-C_6H_4-4-NO_2)(C_2Ph)Cl]$^+$ (generated from CCDC 1411097, originally reported in Ref. [77]).

1.3   Alkynyl Complexes of M(cyclam′)

1.3.1   M(cyclam′)

While M(cyclam) alkynyl complexes are still being investigated, the more sterically crowded derivatives such as TMC (1,4,8,11-tetramethyl-1,4,8,11-tetraazacyclotetradecane), DMD (5,12-dimethyl-1,4,8,11-tetraazacyclotetradiene), its

reduced form DMC (5,12-dimethyl-1,4,8,11-tetraazacyclotetradecane), MPD (4,14-Dimethyl-7,12-di-p-tolyl-1,4,8,11-tetraazacyclo-tetradiene), its reduced form MPC (4,14-Dimethyl-7,12-di-p-tolyl-1,4,8,11-tetraazacyclo-tetradecane), HMD (5,7,7,12,14,14-hexamethyl-1,4,8,11-tetraazacyclotetradeca-4,11-diene) and its reduced form HMC (5,7,7,12,14,14-hexamethyl-1,4,8,11-tetraazacyclotetradecane) have also drawn interest for their differing structural and electrochemical properties when compared to M(cyclam) species. Alkynyl chemistry based on TMC was championed by our group: reaction between $[Ni(TMC)X]^+$ (X = Cl or OTf) and LiC_2R yielded a variety of $[Ni(TMC)(C_2R)]^+$ type complexes with R = -SiMe$_3$, -Si^{i}Pr$_3$, -Ph (structure shown in Figure 1.5) and -C$_2$H.[86] The facile synthesis coupled with the low cost of starting materials to synthesize the aforementioned alkyl substituted macrocycles give them a significant advantage over cyclam and TMC. Both MPD and HMD can readily be synthesized via a Schiff base condensation reaction between singly protonated ethylene diamine and the corresponding vinyl ketone,[87] both of which are inexpensive reagents. Reduction of MPD or HMD by NaBH$_4$ in an alcoholic solvent resulted in MPC and HMC respectively, both in high yields. DMC is prepared similarly, albeit in lower yields.[88].
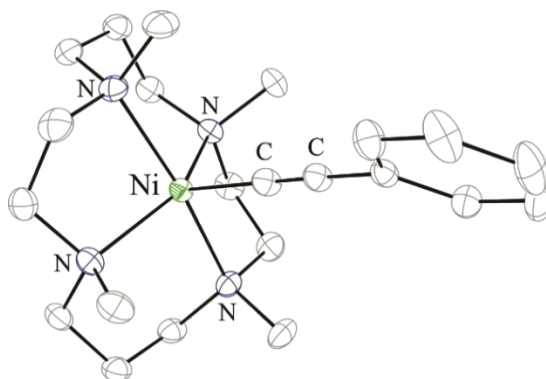
Figure 1.5. Molecular structure of $[Ni(TMC)(C_2Ph)]^+$ (generated from CCDC 1889854, originally reported in Ref. [86])

1.3.2   Mono/Bis-alkynyl Cr(cyclam′)

As mentioned previously, Cr(cyclam) alkynyl chemistry has been a fertile ground with a variety of interesting outcomes. Recent work has focused on elucidating how the configuration, *cis* vs *trans,* affects its spectral properties such as absorption and emission.[80,89,90] In contrast to cyclam, the steric crowding caused by the *C*-substitution in HMC ligand and DMC ligand results in intriguing coordination geometry. For example, the reaction of Cr[III] with HMC results in the formation of two easily separated isomers: the more soluble *trans*-[Cr[III](HMC)Cl$_2$]Cl and the less soluble *cis*-[Cr[III](HMC)Cl$_2$]Cl.[91] The *trans* and *cis* configurations are primarily dictated by the stereochemistry of the ligand with *meso*-HMC forming *trans* product and *rac*-HMC *cis* product.[89] Furthermore, it has been demonstrated that the respective *cis/trans* configuration of the starting material is retained upon alkynylation.[80,89,92] The two stereoisomers can readily be differentiated, where the *rac*-HMC is commonly folded across the nitrogen plane and the *meso*-HMC is planar (Scheme 1.3). While under certain reaction conditions the *rac*-HMC ligand can rearrange from folded to planar, it cannot rearrange to form the *meso*-HMC.[93-95] Similarly, *trans*-[Cr[III](DMC)Cl$_2$]Cl and *cis*-[Cr[III](DMC)Cl$_2$]Cl can also be prepared and readily separated,[96] however the stereochemistry observed in the starting materials is not necessarily retained upon alkynylation.[90]

tet-a (meso)   *tet-b (rac)*
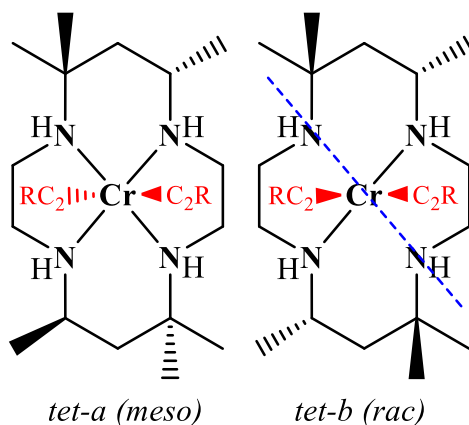
Scheme 1.3. Stereoisomers of HMC; the folding axis for *cis*–[Cr(*rac*–HMC)(C$_2$R)$_2$]Cl complexes is shown as the blue dashed line.

When reacted with LiC$_2$R *trans*-[Cr^{III}(*meso*-HMC)Cl$_2$]Cl and *cis*-[Cr^{III}(*rac*-HMC)Cl$_2$]Cl result in the formation of *trans*-[Cr^{III}(*meso*-HMC)(C$_2$R)$_2$]$^+$ and *cis*-[Cr^{III}(*rac*-HMC)(C$_2$R')$_2$]$^+$ (R = -Ph and -C$_2$H; R' = -Ph and -C$_2$TMS), respectively.[89] The crystal structure of *cis*-[Cr(HMC)(C$_4$TMS)$_2$]Cl is shown in Figure 1.6. Analogous to the alkynyl chemistry of Cr(HMC), the product stereochemistry of the reaction between Cr^{III}(DMC)Cl$_3$ and LiC$_4$TMS/H is dependent on the starting material, with *cis*-[Cr^{III}(DMC)Cl$_2$]Cl forming *cis*-[Cr^{III}(DMC)(C$_4$TMS)$_2$]Cl and *trans*-[Cr^{III}(DMC)Cl$_2$]Cl forming *trans*-[Cr^{III}(DMC)(C$_4$H)$_2$]Cl. However, unlike with Cr^{III}(HMC), isomerization of *cis*-[Cr^{III}(DMC)(C$_4$TMS)$_2$]Cl to the thermodynamically favored *trans*-[Cr^{III}(DMC)(C$_4$H)$_2$]Cl could be observed in polar solvents via UV-Vis and ESI-MS.[90] In the presence of bulkier alkynes, the reaction of LiC$_2$R with *cis*-[Cr^{III}(DMC)Cl$_2$]Cl and *trans*-[Cr^{III}(DMC)Cl$_2$]Cl both resulted in the formation of *trans*-[Cr^{III}(DMC)(C$_2$R)$_2$]Cl (R = -Ph and -Fc (structure shown in Figure 1.7)), producing lower yields when starting from the *cis* species.[90]
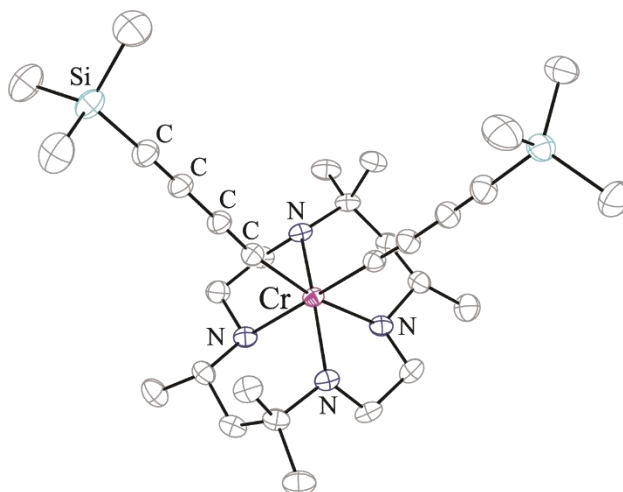
Figure 1.6. Molecular structure of *cis*-[Cr^{III}(HMC)(C$_4$TMS)$_2$]$^+$ (generated from CCDC 1507917, originally reported in Ref. [89])
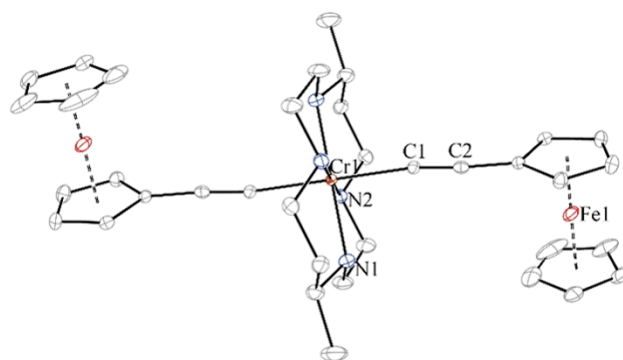
Figure 1.7. Molecular structure of *trans*-[Cr^{III}(DMC)(C$_2$Fc)$_2$]$^+$ (generated from CCDC 1531350, originally reported in Ref. [90])

Recent efforts have shifted focus towards the isolation of mono-alkynyl species [Cr(HMC)(C$_2$R)Cl]Cl, which would be the obvious precursor for the dissymmetric [Cr(HMC)(C$_2$R)(C$_2$R')]$^+$ type complexes. Early experimental work has shown that formation of both *cis*-[Cr(HMC)(C$_2$Ph)Cl]$^+$ and *trans*-[Cr(HMC)(C$_2$Ph)Cl]$^+$ can be achieved through controlled acid degradation of *cis*-[Cr(HMC)(C$_2$Ph)$_2$]$^+$ and *trans*-[Cr(HMC)(C$_2$Ph)$_2$]$^+$, respectively.[92] While formation of dissymmetric *cis*-

[M(cyclam′)(C$_2$R)(C$_2$R′)]$^+$ has yet to be achieved, this early work represents a considerable stepping stone towards making these types of compounds.

1.3.3   Mono/Bis-alkynyl Co(cyclam′)

The success in isolating *cis*-Cr(cyclam′) alkynyl species[80,89,90] raised the possibility of preparing *cis*-Co(cyclam′) alkynyl species in a stepwise fashion. Use of an electrochemically active metal center, like Co, in place of electrochemically silent Cr would allow for the study of how altering the stereochemistry could affect the cyclic voltammetry, which will be discussed later. Recently, it was demonstrated that Co alkynyl species supported by MPD, its reduced form MPC, and the less sterically bulky DMC could be used to form both mono and bis-alkynyl species. Synthesis of mono-alkynyl complexes *trans*-[Co(MPD)(C$_2$Ph)Cl]Cl, *trans*-[Co(MPC)(C$_2$Ph)Cl]Cl, and *trans*-[Co(DMC)(C$_2$Ph)Cl]Cl were achieved under weak base conditions.[63,97] Formation of *trans*-[Co(MPD)(C$_2$Ph)$_2$]Cl and *trans*-[Co(MPC)(C$_2$Ph)$_2$]Cl was achieved in the presence of excess LiC$_2$Ph.[63] The stepwise weak-base reaction pathway, discussed previously,[79] was utilized to form *trans*-[Co(DMC)(C$_2$Ph)$_2$]OTf via the *in situ* reaction of *trans*-[Co(DMC)(C$_2$Ph)Cl]Cl with AgOTf, followed by the addition of HC$_2$Ph and Et$_3$N.[97] While *cis*-Co(cyclam′) alkynyl species remain elusive, the ability for *C*-substituted macrocycles to support Co proves promising. Additionally, formation of *trans*-[Co(MPD)(C$_2$Ph)Cl]Cl (structure shown in Figure 1.8) and *trans*-[Co(MPD)(C$_2$Ph)$_2$]Cl is noteworthy as they are the first examples of metal acetylide complexes based on a 1,4,7,11-tetra-azacyclotetradeca-4,11-diene type ligand.[63] When comparing *trans*-[Co(MPC)(C$_2$Ph)$_2$]Cl, *trans*-[Co(DMC)(C$_2$Ph)$_2$]OTf, and *trans*-[Co(cyclam)(C$_2$Ph)$_2$]Cl, there is a noticeable trend tied to increased *C*-substitution of the

macrocycle and relative length of the both the Co-N bond lengths and the Co-C bonds lengths. The most substituted macrocycle, *trans*-[Co(MPC)(C₂Ph)₂]Cl has the longest Co-N bond, 2.004(2) Å, and the shortest Co-C bond, 1.924(3) Å.[63] By comparison, *trans*-[Co(cyclam)(C₂Ph)₂]Cl has the shortest Co-N bond length of 1.983(2) and the longest Co-C bond length of 2.001(3).[75] *trans*-[Co(DMC)(C₂Ph)₂]OTf falls in the middle with an average Co-N bond length of 1.992(2) Å and a Co-C bond length of 1.927(2) Å.[97] While these metric parameters differ slightly from the unsubstituted cyclam variant, they are within the range of previously reported Co-N and Co-C bond lengths.[77-80,98]
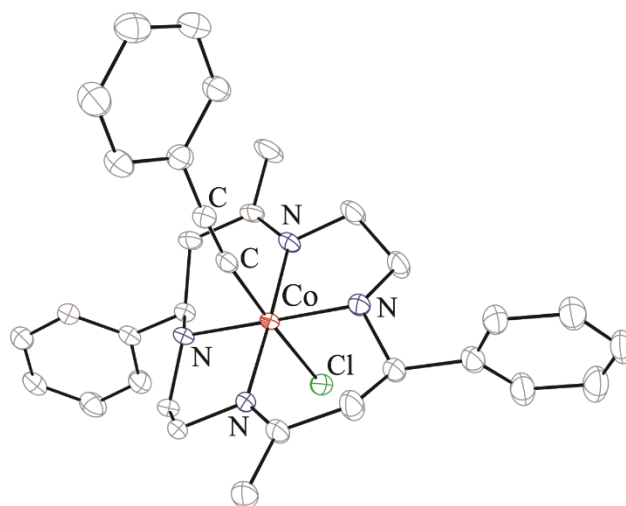
Figure 1.8. Molecular structure of *trans*-[Co(MPD)(C₂Ph)Cl]⁺ (generated from CCDC 1872102, originally reported in Ref. [63])

1.4   Physical and Material Properties

1.4.1   Spectroscopic-Emission

The characteristic absorption spectra of the compounds discussed herein feature LMCT bands in the UV region and *d-d* transition bands of weak to modest intensity in the visible region, with the weakest *d-d* transitions occurring in M(cyclam′) complexes

with aryl substituted macrocycles.[63,99] The LMCT bands are attributed to both the N centers and C≡C bonds.[100] Highly structured *d-d* bands were observed for *cis/trans*-[Cr(HMC)(C_2Ph)_2]^+ and for *cis/trans*-[Cr(HMC)(C_4R)_2]^+ (R= H or TMS), which were attributed to vibronic coupling. The vibronic progressions for the former ranged from 800-900 cm^{-1} and likely arose from aromatic C-H bending, N-H bending, and CH_2 rocking; the vibronic progressions of the latter ranged from 2023-1971 cm^{-1} and correlated well with the experimentally observed C≡C stretches.[89] Until recently, the only cyclam species that displayed emission were Cr^{III} based, which possess phosphorescence originating from the ligand-field excitations.[66,67,80,89,90] The *trans*-[Cr(cyclam)(C_2R)_2]^+ type compounds were found to emit from both the ^2E_g and $^2T_{1g}$ states with a lifetime of about 1 μs.[66] A similar trend was also observed for several [Cr(HMC)(C_2R)_2]^+ and [Cr(DMC)(C_2R)_2]^+ type compounds.[80,89,90] The *trans*-[Cr(cyclam)(*gem*-DEE)_2]^+ type compounds were found to phosphoresce as well but only from the ^2E_g state.[67] As shown in Table 1.1, the *cis*-Cr^{III} species tend to have a shorter lifetime that is difficult to measure at room temperature. This is attributed to additional geometric strain caused by the *cis* configuration, which favours nonradiative decay in comparison to its *trans* counterpart.[101] Comparison of the λ_{em} of the *cis* and *trans* pairings, for example *cis*-[Cr(HMC)(C_2Ph)_2]^+ vs. *trans*-[Cr(HMC)(C_2Ph)_2]^+ or *cis*-[Cr(HMC)(C_2Np)_2]^+ vs. *trans*-[Cr(HMC)(C_2Np)_2]^+, reveals that the λ_{em} of the *cis* species is shifted to lower energy, which is likely a consequence of differing stereochemistry between the *cis* and *trans* species (Table 1.1).

Table 1.1. Photophysical Data for Cr(cyclam′) Complexes

	Room Temperature[a]			Frozen Glass[b/b*]		
	λ_{ex} (nm)	λ_{em} (nm)	τ (µs)	λ_{ex} (nm)	λ_{em} (nm)	τ (µs)
cis-[Cr(HMC)(C$_2$Ph)$_2$]$^+$ [c]	424	764	-	425	763	212
trans-[Cr(HMC)(C$_2$Ph)$_2$]$^+$ [c]	425	746	-	425	744	469
cis-[Cr(HMC)(C$_4$TMS)$_2$]$^+$ [c]	402	771	-	443	777	129
trans-[Cr(HMC)(C$_4$H)$_2$]$^+$ [c]	402	746	-	405	771	455
cis-[Cr(HMC)(C$_2$Np)$_2$]$^+$ [d]	430	777	-	430	777	97
trans-[Cr(HMC)(C$_2$Np)$_2$]$^+$ [d]	445	747	218	445	747	447
				445	727	362
cis-[Cr(DMC)(C$_4$TMS)$_2$]$^+$ [e]	427	777	68	427	780	160
trans-[Cr(DMC)(C$_4$H)$_2$]$^+$ [e]	403	755	113	403	777	358
trans-[Cr(DMC)(C$_2$Ph)$_2$]$^+$ [e]	420	750	95	424	745	380
				424	728	222
trans-[Cr(cyclam)(C$_2$Ph)$_2$]$^+$ [f]	380	748	225	430*	745*	343*
trans-[Cr(cyclam)(C$_2$Np)$_2$]$^+$ [f]	440	749	250	360*	748*	343*

[a]In degassed acetonitrile. [b]Dissolved in 4:1 EtOH:MeOH glass, taken at 77K. [b*] Indicates dissolved in H$_2$O/DMSO glass, taken at 77K.. [c] From ref [89]. [d] From ref [80]. [e] From ref [90]. [f] From ref [66]. Cyclam′ refers to *C*-substituted derivatives of cyclam.

Use of a fluorophore ligand in conjunction with Cr^{III} was theorized to alter the emission properties. However, it was found for cis-[Cr(HMC)(C$_2$Np)$_2$]Cl,[80] trans-[Cr(HMC)(C$_2$Np)$_2$]Cl,[80] and trans-[Cr(cyclam)(C$_2$Np)$_2$]Cl[66] that the emission was dominated by the excited states at the Cr^{III} metal center. Figure 1.9 provides a direct visual comparison between the emission of free Me$_3$SiC$_2$Np, trans-[Cr(HMC)(C$_2$Np)$_2$]Cl, and trans-[Co(cyclam)(C$_2$Np)$_2$]Cl, where the organic chromophore emission dominates when coordinated to Co(cyclam).[80]
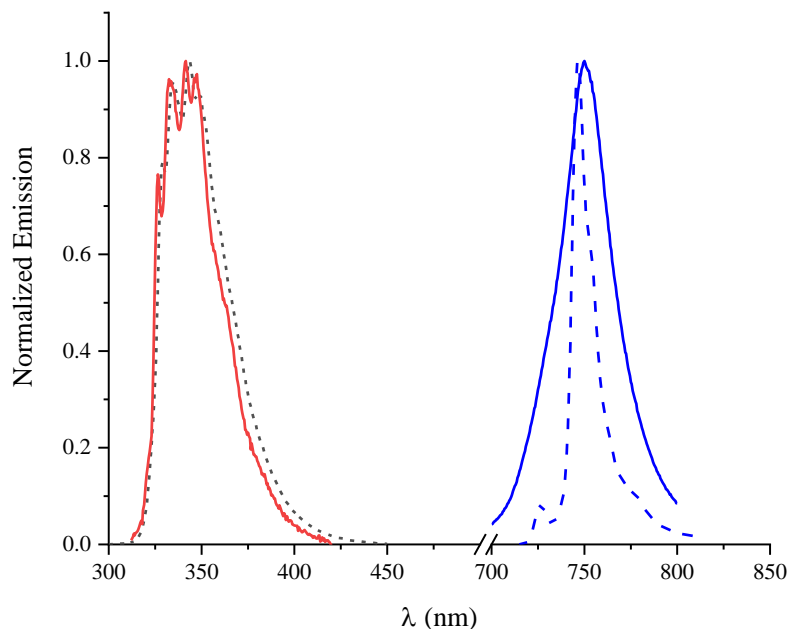
Figure 1.9. Normalized emission spectra for [Co(cyclam)(C$_2$Np)$_2$]OTf (red) in DCM at RT, free ligand Me$_3$SiC$_2$Np (black) in DCM at RT and *trans*-[Cr(HMC)(C$_2$Np)$_2$]Cl emission (blue) in 4:1 EtOH:MeOH at RT (solid) and 77K (dash), plotted using data from Ref. [80].

In parallel to Cr^{III} overshadowing the chromophore emission, quenching effects were observed for Ru$_2$(DMBA)$_4$(C$_2$Ar)$_2$ (Ar = 1-naphthalene (Np), 9-anthracene (ANT), *N*-isopropyl-1, 8-naphthalimide (NAP^{iPr}), *N*-methyl-1, 8-naphthalimide (NAP^{Me})) where the fluorescence of the free ligands (listed in Table 1.2) were completely quenched.[102] This led our laboratory to perturb the emission properties of alkynyl chromophores when coordinated to a non-emissive metal center like Co^{III}(cyclam). While florescence quenching by the metal center is still apparent (Table 1.2) for Co-bound Me$_3$SiC$_2$ANT,[80] Me$_3$SiC$_2$Np,[80] and HC$_2$NAP^{iPr},[81] it is notable that emission is observed for this previously non-emissive Co species. Furthermore, the distinct shift in emission, hypsochromic for [Co(cyclam)(C$_2$ANT)Cl]Cl[80] and bathochromic for [Co(cyclam)(C$_2$NAP^{iPr})(C$_2$R)]Cl,[81] suggests that coordination to Co^{III} alters the electronic ground state of the chromophore

ligand (Table 1.2). Emission, based on Φ, tended to be significantly stronger for the panchromic Co^{III}(cyclam) complexes such as [Co(cyclam)(C_2NAP^{iPr})_2]Cl and [Co(cyclam)(C_2NAP^{iPr})(C_2TPA)]Cl than the singly chromophore containing species like [Co(cyclam)(C_2NAP^{iPr})Cl]Cl and [Co(cyclam)(C_2NAP^{iPr})(C_2Ph)]Cl.[81] The Φ for [Co(cyclam)(C_2Np)Cl]Cl and [Co(cyclam)(C_2Np)_2]OTf could not be determined due to instrument limitations.[80]

Table 1.2. Photophysical Data for Co(cyclam) Complexes & Respective Chromophore Ligands

	λ_{ex} (nm)	λ_{em} (nm)	Φ
trans-[Co(cyclam)(C_2ANT)Cl]^{+ a}	263	408	0.022
Me_3SiC_2ANT ^a	263	414	0.633
trans-[Co(cyclam)(C_2Np)Cl]^{+ a}	298	342	-
trans-[Co(cyclam)(C_2Np)_2]^{+ a}	234	341.5	-
Me_3SiC_2Np ^a	290	343.5	-
trans-[Co(cyclam)(C_2NAP^{iPr})Cl]^{+ b}	400	438	0.0066
trans-Co(cyclam)(C_2NAP^{iPr})(C_2Ph)]^{+ b}	400	437	0.0043
trans-[Co(cyclam)(C_2NAP^{iPr})_2]^{+ b}	400	439	0.0143
trans-[Co(cyclam)(C_2NAP^{iPr})(C_2C_6H_4-4-NMe_2)]^{+ b}	400	439	0.0068
trans-[Co(cyclam)(C_2NAP^{iPr})(C_2TPA)]^{+ b}	400	461	0.0104
HC_2NAP^{iPr b}	340	401	0.423

All photophysical data collected in CH_2Cl_2 at room temperature. [a]From ref [80]. [b]From ref [81].

1.4.2 Voltammetry

An important criterion for metal alkynyl species functioning as molecular wires is the ability to undergo multiple reversible redox processes.[31,103,104] Some of the most notable examples include [Cp(PPh_3)_2Ru]_2(μ-C_4), which exhibits four stepwise one-electron oxidations,[16] [Ru_2(ap)_4]_2(μ-C_4), which has a pair of one-electron oxidations and

a pair of one-electron reductions,[29] and Ru$_2$(ap)$_4$(C$_2$C$_6$H$_4$P(O)(OH)$_2$) which functions as

the active species in a highly robust flash memory device.[44] Furthermore, compounds

containing multiple reversible one-electron couples are of interest because they allow for

the study of intervalence charge transfer processes between two metal centers across a

polyyn-diyl bridge resulting in mixed valence compounds such as (M^{+n}-(C≡C)$_m$-

M$^{+(n+1)}$).[105,106] Specifically, using voltammetric and spectroelectrochemical studies, our

group demonstrated significant electronic coupling between capping Ru$_2$ units in

[Ru$_2$(Xap)$_4$]$_2$(μ-C$_{2m}$) with m ranging from 2-10.[36] However, the electrochemical

behaviors of 3d M-cyclam compounds are vastly different from 4d and 5d metal

compounds. Generally, Co^{III} species display multiple irreversible couples[74,75,77,82] and

Cr^{III} species are redox inactive.[54,67]
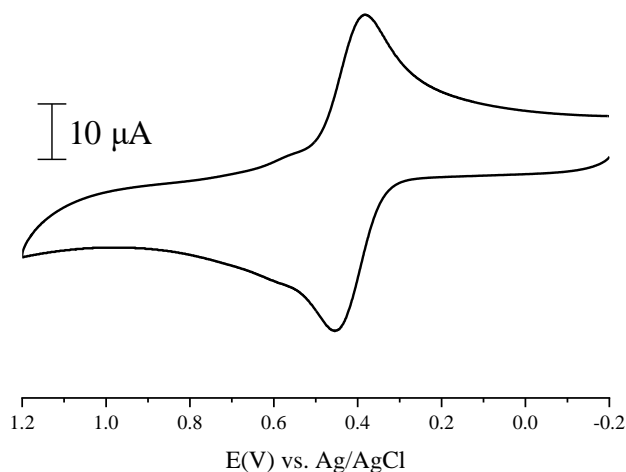
Figure 1.10. Cyclic voltammogram of a 1.0 mM solution of *trans*-
[Cr^{III}(DMC)(C$_2$Fc)$_2$]ClO$_4$ in a 0.2 M solution of Bu$_4$NPF$_6$ in acetonitrile at scan rate of
100 mV/s), plotted using data from Ref. [90].

To study the Fc-Fc coupling across a 3d metal center, *trans*-[M^{III}(cyclam)(C$_2$Fc)$_2$]$^+$ (M =

Fe, Cr, and Co) type compounds have been prepared and their voltammetric responses

analyzed using the Richardson and Taube method;[107] the two ferrocenyl capping groups are only weakly coupled across the C_2-M^{III}-C_2 bridge.[67,73,74] To determine the effect of the supporting macrocycle on coupling, *trans*-[Cr^{III}(DMC)(C_2Fc)$_2$]ClO$_4$ was synthesized and studied electrochemically. Figure 1.10 shows the observed quasi-reversible 2e$^-$ oxidation for *trans*-[Cr^{III}(DMC)(C_2Fc)$_2$]ClO$_4$ with an estimated ΔE value of 50 mV based on Richardson-Taube method, suggesting a weak coupling between the two ferrocenyl groups.[90]
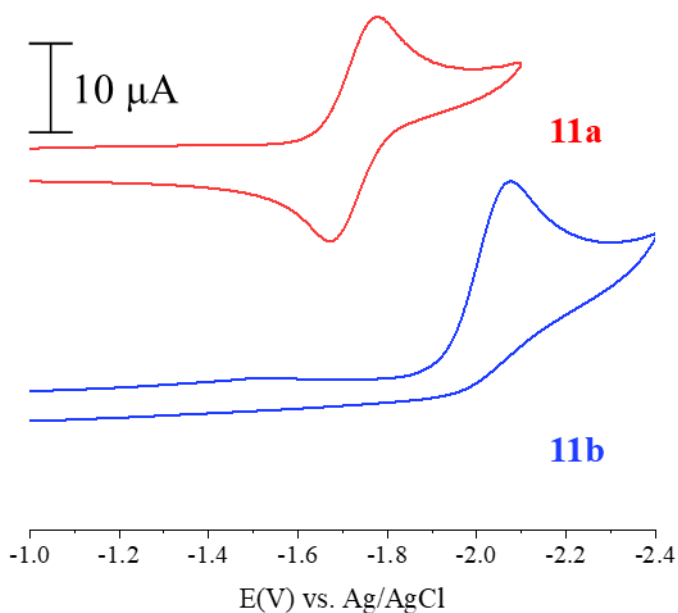
Figure 1.11. Cyclic voltammograms of a 1.0 mM solution of [Co^{III}(cyclam)($C_2C_6F_5$)$_2$]OTf (**11a**) and [Co^{III}(cyclam)($C_2C_6H_4$-4-NMe$_2$)$_2$]OTf (**11b**) in a 0.2 M solution of Bu$_4$NPF$_6$ in DCM at scan rate of 100 mV/s, plotted using data from Ref. [79].

The only cyclam complexes that consistently display reversible metal-center redox couples are Fe^{III} species,[53,73,108] all of which undergo a one electron reduction. It was noted recently that Co^{III}(cyclam) species bearing electron withdrawing ligands, such as pentafluorophenylacetylide,[65,79] and trifluoropropynyl,[65,109] underwent reversible one

electron reductions and was attributed to the π-accepting nature of the acetylide ligand. Figure 1.11 shows a direct comparison of the Co(+3/+2) couple for $[Co^{III}(cyclam)(C_2C_6F_5)_2]OTf$ (**11a**) versus $[Co^{III}(cyclam)(C_2C_6H_4-4-NMe_2)_2]OTf$ (**11b**). Coordination of the electron withdrawing pentafluorophenylacetylide ligand to Co(cyclam) resulted in a reversible Co(+3/+2) couple that occurs at a more positive potential than that of the irreversible Co(+3/+2) couple observed for the Co(cyclam) complex bearing the electron donating 4-ethynyl-*N,N*-dimethylaniline ligand. A quasi-reversible reduction attributed to Co was also observed for $[Co(MPC)(C_2Ph)_2]Cl$, but in this case was thought to be a result of increased electron density on the metal center from MPC.[63] These observations suggest that reversible electrochemical couples can be achieved in 3*d*-M cyclam species with careful attenuation of both the axial alkynyl and supporting macrocyle ligands.

1.4.3 Magnetism

Bis-alkynyl complexes of Co(III) are always diamagnetic, while those of Fe(III) are of an $S = 1/2$ ground state. Bis-alkynyl complexes of Cr(cyclam) and Cr(cyclam') are consistently paramagnetic with an $S = 3/2$ ground state. Temperature dependence of magnetic susceptibility between 5 – 300 K were examined for several $[Cr^{III}(HMC)(C_2R)_2]^+$ complexes, which is consistent with a zero-field splitting (ZFS) of an $S = 3/2$ species, and a *D* of *ca.* -0.5 cm^{-1}.[89] Using 3-Th (3-thiophene) and TTF (tetrathiafulvalene) containing acetylides, Nishijo and coworkers demonstrated the formation of 1-D and 2-D coordination polymers based on $[Cr^{III}(cyclam)(C_2R)_2]^+$, which exhibit interesting ferri- and ferro-magnetic ordering through the π-π stacking of TTF rings.[55,68-72] Room temperature magnetic susceptibility measurements of

[Ni(TMC)(C$_2$R)]$^+$ type compounds yielded effective magnetic moments that were consistent with an S = 1 ground state and were further corroborated by both CASSCF and density functional theory calculations.[86]

1.5   Conclusions and Outlook

The strategies applied here to synthesize metal alkynyl species supported by tetraaza macrocyclic ligands mainly employ lithiation or weak base dehydrohalogenation techniques. Therefore, the main obstacle for 3*d* metal alkynyl complexes is the development of alternative synthetic routes with both improved yields and selectivity. Recently, our lab was able to selectively synthesize dissymmetric [Co(cyclam)(C$_2$R)(C$_2$R')]$^+$ type compounds utilizing a triflate intermediate.[79] However, this method only works for a limited scope of alkynyl compounds and has not been proven as a successful method with more complex ligands. This led us to revaluate lithiation techniques as a means to form [Co(cyclam)(C$_2$R)(C$_2$R')]$^+$ compounds. Early attempts were plagued by low reaction yields as a result of poor selectivity, as products could include the symmetric [Co(cyclam)(C$_2$R)$_2$]$^+$ and [Co(cyclam)(C$_2$R')$_2$]$^+$ in addition to the target compound.[77] This issue has since been circumvented by cooling the lithiation reaction down to -78°C.[81] These approaches are restricted to complexes based on Co^{III}(cyclam) and Co^{III} (DMC) and are unsuccessful thus far for other 3*d* metals.

Other synthetic strategies that are being investigated include i) organo-tin activated arylalkynyls, ii) Hagihara coupling (CuI / organic amine) as a variation of the dehydrohalogenation reactions, and iii) controlled acid degradation of symmetric M acetylides. Lewis and coworkers employed organo-tin activated arylalkynyls to numerous *trans*-bisalkynyl   Ru(II)   compounds,[8]   including   dissymmetric   *trans*-

[(dppe)$_2$Ru(C$_2$Ar)(C$_2$Ar′)] (dppe = 1,2-bis(diphenylphosphino)ethane).[6] The Hagihara dehydrohalogenation reaction, has been effectively utilized to form Pt^{II}, Pd^{II} and Ni^{II} alkynyl compounds.[85,110,111] We speculate that the Hagihara reaction could be a good fit for M(cyclam′) alkynyl compounds due to their robust nature towards organic amines.[112] This is further substantiated by the work done on arylalkynyls of cobalamin that were prepared using Hagihara coupling conditions.[113] Finally, the prospect of using controlled acid degradation to isolate new mono-alkynyl Cr(HMC) species shows promise. While only simple alkynyl species were studied, namely [Cr(HMC)(C$_2$Ph)Cl]$^+$, this method is relatively new and work is actively being done to isolate more complex species.[92]

In looking towards the future, the synthetic strategies mentioned above will be instrumental in developing new 3d metal alkynyl species for studying electron transfer processes. Synthesis of the first true D-B-A species, with a Co^{III}(cyclam) bridge, has been achieved and is actively being probed to understand the role of the bridging metal center.[81] It is important to acknowledge that all the M(cyclam) and M(cyclam′) discussed herein (M = Cr, Fe, and Co) are stable under an ambient atmosphere, an essential quality for optoelectronic devices. Additionally, use of earth abundant 3d metals paired with the inexpensive and facile synthesis of cyclam′ derivatives continue to make these complexes a valuable target for further development.

1.6   References

(1)   Nast, R. Coordination Chemistry of Metal Alkynyl Compounds. *Coord. Chem. Rev.* **1982**, *47*, 89-124.

(2)   Vaid, T. P.; Veige, A. S.; Lobkovsky, E. B.; Glassey, W. V.; Wolczanski, P. T.; Rheingold, A. L.; Cundari, T. R. Structural Dichotomy in Six-Coordinate d0 Complexes: Trigonal Prismatic (tBu3SiC[Image]C)6Ta- and Octahedral (tBu3SiC [Image]C)6M2- (M = Zr, Hf). *J. Am. Chem. Soc.* **1998**, *120*, 10067-10079.

(3)   Berben, L. A. Toward acetylide- and N-hetercycle-bridged materials with strong electronic and magnetic coupling.Ph.D. Dissertation, University of California, 2005.

(4)   Hagihara, N.; Sonogashira, K.; Takahashi, S. Linear Polymers Containing Transition Metals in the Main Chain. *Adv. Polym. Sci.* **1981**, *40*, 149-179.

(5)   Khan, M. S.; Pasha, N. A.; Kakkar, A. K.; Raithby, P. R.; Lewis, J.; Fuhrmann, K.; Friend, R. H. Synthesis and Optical Spectroscopy of Monomeric and Polymeric Cobalt Sigma-Acetylide Complexes. *J. Mater. Chem.* **1992**, *2*, 759-760.

(6)   Younus, M.; Long, N. J.; Raithby, P. R.; Lewis, J.; Page, N. A.; White, A. J. P.; Williams, D. J.; Colbert, M. C. B.; Hodge, A. J.; Khan, M. S.; Parker, D. G. Synthesis and characterisation of mono-acetylide and unsymmetrical bis-acetylide complexes of ruthenium and osmium: X-ray structure determinations on [(dppe)(2)Ru(Cl)(C C-C6H4-p- NO2)], [(dppe)(2)Ru(Cl)(C C-C6H3-o-CH3-p-NO2)] and [(dppm)(2)Os(C C-C6H4-p-CH3)(C C-C6H4-p-NO2)]. *J. Organomet. Chem.* **1999**, *578*, 198-209.

(7)   Dray, A. E.; Wittmann, F.; Friend, R. H.; Donald, A. M.; Khan, M. S.; Lewis, J.; Johnson, B. F. G. Structure and Electronic-Structure of Transition Metal-Containing Poly-Ynes. *Synth. Met.* **1991**, *41*, 871-874.

(8)   Long, N. J.; Williams, C. K. Metal Alkynyl Complexes: Synthesis and Materials. *Angew. Chem. Int. Ed. Engl.* **2003**, *42*, 2586-2617.

(9)   Manna, J.; John, K. D.; Hopkins, M. D. The Bonding of Metal-Alkynyl Complexes. *Adv. Organomet. Chem.* **1995**, *38*, 79-154.

(10)   Low, P. J.; Bruce, M. I. Transition Metal Chemistry of 1,3-Diynes, Poly-ynes, and Related compounds. *Adv. Organomet. Chem.* **2001**, *48*, 71-288.

(11)   Haque, A.; Al-Balushi, R. A.; Al-Busaidi, I. J.; Muhammad S. Khan; Raithby, P. R. Rise of Conjugated Poly-ynes and Poly(Metalla-ynes): From Design Through Synthesis to Structure–Property Relationships and Applications. *Chem. Rev.* **2018**, *118*, 8474-8597.

(12)   Ho, C. L.; Wong, W. Y. Metal-containing polymers: Facile tuning of photophysical traits and emerging applications in organic electronics and photonics. *Coord. Chem. Rev.* **2011**, *255*, 2469-2502.

(13)   Zhou, Y. L.; Seyler, J. W.; Weng, W.; Arif, A. M.; Gladysz, J. A. New Families of Coordinated Carbon: Oxidative Coupling of an Ethynyl Complex to Isolable and Crystallographically Characterized MC=CC=CM amd +MC=CC=CM+ Assemblies. *J. Am. Chem. Soc.* **1993**, *115*, 8509-8510.

(14) Le Narvor, N.; Lapinte, C. First C_4 Bridged Mixed-valence Iron(II)-Iron(III) Complex Delocalized on the Infrared Timescale. *J. Chem. Soc., Chem. Commun.* **1993**, 357-359.

(15) Kheradmandan, S.; Heinze, K.; Schmalle, H. W.; Berke, H. Electronic Communication in C4-Bridged Binuclear Complexes with Paramagnetic Bisphosphane Manganese End Groups. *Angew. Chem. Int. Ed.* **1999**, *38*, 2270-2273.

(16) Bruce, M. I.; Low, P. J.; Costuas, K.; Halet, J.-F.; Best, S. P.; Heath, G. A. Oxidation Chemistry of Metal-Bonded C4 Chains: A Combined Chemical, Spectroelectrochemical, and Computational Study. *J. Am. Chem. Soc.* **2000**, *122*, 1949-1962.

(17) Semenov, S. N.; Blacque, O.; Fox, T.; Venkatesan, K.; Berke, H. Electronic Communication in Dinuclear C4-Bridged Tungsten Complexes. *J. Am. Chem. Soc.* **2010**, *132*, 3115–3127.

(18) Zheng, Q.; Gladysz, J. A. A Synthetic Breakthrough into an Unanticipated Stability Regime: Readily Isolable Complexes in which C16-C28 Polyynediyl Chains Span Two Platinum Atoms. *J. Am. Chem. Soc.* **2005**, *127*, 10508-10509.

(19) Jia, G.; Xia, H. P.; Wu, W. F.; Ng, W. S. Dimeric ruthenium complexes w/ C_5H_2 and C5H Bridges. *Organometallics* **1996**, *15*, 3634-3636.

(20) Xia, H. P.; Jia, G. C5H5-Bridged Dimeric Ruthenium Complexes. *Organometallics* **1997**, *16*, 1.

(21) Liu, S. H.; Chen, Y.; Wan, K. L.; Wen, T. B.; Zhou, Z.; Lo, M. F.; Williams, I. D.; Jia, G. Synthesis and Characterization of Linear (CH)8-Bridged Bimetallic Ruthenium Complexes. *Organometallics* **2002**, *21*, 4984-4992.

(22) Yuan, P.; Wu, X. H.; Yu, G. A.; Du, D.; Liu, S. H. Synthesis and characterization of bimetallic ruthenium complexes connected through linear (CH)(14) chain. *J. Organomet. Chem.* **2007**, *692*, 3588-3592.

(23) Lin, Y.; Yuan, J.; Hu, M.; Cheng, J.; Yin, J.; Jin, S.; Liu, S. H. Syntheses and Properties of Binuclear Ruthenium Vinyl Complexes with Dithienylethene Units as Multifunction Switches. *Organometallics* **2009**, *28*, 6402–6409.

(24) Xia, J. L.; Ou, Y. P.; Meng, X. G.; Yin, J.; Yu, G. A.; Liu, S. H. Synthesis and Characterization of Dithia 3.3 metaparacyclophane-Bridged Dimetallic Ruthenium Acetylide Complexes. *Eur. J. Inorg. Chem.* **2014**, *2014*, 247-255.

(25) Creutz, C. Mixed Valence Complexes of d^5-d^6 Metal Centers. *Prog. Inorg. Chem.* **1983**, *30*, 1-73.

(26) Chakravarty, A. R.; Cotton, F. A. A New Diruthenium(II,III) Compound, Ru$_2$(CCPh)(PhNPy)$_4$·2CH$_2$Cl$_2$, with an Axial η^1−Acetylide Ligand. *Inorg. Chim. Acta* **1986**, *113*, 19.

(27) Li, Y.; Han, B.; Kadish, K. M.; Bear, J. L. A Novel Diamagnetic Diruthenium(III) Complex Bridged by Four Unsymmetrical Carboxylate Type Ligands. Synthesis, Molecular Structure, Electrochemistry, and Spectroelectrochemistry of Ru$_2$(pfap)$_4$(CCC$_6$H$_5$)$_2$, Where pfap Is 2,3,4,5,6-Pentafluoro-2-anilinopyridinate. *Inorg. Chem.* **1993**, *32*, 4175.

(28) Bear, J. L.; Han, B. C.; Huang, S. R.; Kadish, K. M. Effect of axial ligands on the oxidation state, structure, and electronic configuration of diruthenium complexes. Synthesis and characterization of Ru-2(dpf)(4)Cl, Ru-2(dpf)(4)(C CC6H5), Ru-2(dpf)4(C CC6H5)(2), and Ru-2(dpf)4(CN)(2) (dpf equals N,N'-diphenylformamidinate). *Inorg. Chem.* **1996**, *35*, 3012-3021.

(29) Ren, T.; Zou, G.; Alvarez, J. C. Facile Electronic Communication between Bimetallic Termini Bridged by Elemental Carbon Chains. *Chem. Commun.* **2000**, 1197-1198.

(30) Wong, K.-T.; Lehn, J.-M.; Peng, S.-M.; Lee, G.-H. Nanoscale molecular organometallo-wires containing diruthenium cores. *Chem. Commun.* **2000**, 2259-2260.

(31) Ren, T. Diruthenium σ-Alkynyl Compounds: A New Class of Conjugated Organometallics. *Organometallics* **2005**, *24*, 4854-4870.

(32) Ren, T.; Xu, G.-L. Diruthenium Metallaynes: Versatile Chromophores and Electrophores. *Comm. Inorg. Chem.* **2002**, *23*, 355-380.

(33) Xi, B.; Ren, T. Wire-like Diruthenium -Alkynyl Compounds and Charge Mobility Therein. *C. R. Chimie* **2009**, *12*, 321-331.

(34) Xu, G.-L.; Zou, G.; Ni, Y.-H.; DeRosa, M. C.; Crutchley, R. J.; Ren, T. Polyyn-diyls Capped by Diruthenium Termini: A New Family of Carbon-Rich Organometallic Compounds and Distance Dependent Electronic Coupling Therein. *J. Am. Chem. Soc.* **2003**, *125*, 10057-10065.

(35) Xi, B.; Liu, I. P. C.; Xu, G.-L.; Choudhuri, M. M. R.; DeRosa, M. C.; Crutchley, R. J.; Ren, T. Modulation of Electronic Couplings within Metal-Polyyne Frameworks. *J. Am. Chem. Soc.* **2011**, *133*, 15094-15104.

(36) Cao, Z.; Xi, B.; Jodoin, D. S.; Zhang, L.; Cummings, S. P.; Gao, Y.; Tyler, S. F.; Fanwick, P. E.; Crutchley, R. J.; Ren, T. Diruthenium-Polyyn-diyl-Diruthenium Wires: Electronic Couplings in the Long Distance Regime. *J. Am. Chem. Soc.* **2014**, *136*, 12174-12183.

(37) Xu, G.-L.; DeRosa, M. C.; Crutchley, R. J.; Ren, T. *Trans*-Bis(alkynyl)-Diruthenium(III) Tetra(amidinate): An Effective Facilitator of Electronic Delocalization. *J. Am. Chem. Soc.* **2004**, *126*, 3728-3729.

(38) Xu, G.-L.; Crutchley, R. J.; DeRosa, M. C.; Pan, Q.-J.; Zhang, H.-X.; Wang, X.; Ren, T. Strong Electronic Couplings between Ferrocenyl Centers Mediated by Bis-Ethynyl/Butadiynyl Diruthenium Bridges. *J. Am. Chem. Soc.* **2005**, *127*, 13354-13363.

(39) Xi, B.; Xu, G.-L.; Fanwick, P. E.; Ren, T. Diruthenium Complexes of Axial Ferrocenylpolyynyl Ligands: the Cases of C6Fc and C8Fc. *Organometallics* **2009**, *28*, 2338-2341.

(40) Blum, A. S.; Ren, T.; Parish, D. A.; Trammell, S. A.; Moore, M. H.; Kushmerick, J. G.; Xu, G.-L.; Deschamps, J. R.; Pollack, S. K.; Shashidhar, R. Ru$_2$(ap)$_4$(σ-oligo(phenyleneethynyl)) Molecular Wires: Synthesis and Electronic Characterization. *J. Am. Chem. Soc.* **2005**, *127*, 10010-10011.

(41) Mahapatro, A. K.; Ying, J.; Ren, T.; Janes, D. B. Electronic Transport through Ruthenium Based Redox-Active Molecules in Metal-Molecule-Metal Nanogap Junctions. *Nano Lett* **2008**, *8*, 2131-2136.

(42) Pookpanratana, S.; Savchenko, I.; Natoli, S. N.; Cummings, S. P.; Richter, L. J.; Robertson, J. W. F.; Richter, C. A.; Ren, T.; Hacker, C. A. Attachment of a Diruthenium Compound to Au and SiO2/Si Surfaces by "Click" Chemistry. *Langmuir* **2014**, *30*, 10280-10289.

(43) Pookpanratana, S.; Zhu, H.; Bittle, E. G.; Natoli, S. N.; Ren, T.; Gundlach, D. J.; Richter, C. A.; Li, Q.; Hacker, C. A. Non-volatile Memory Devices with Redox-active Diruthenium Molecular Compound. *J. Phys.: Condens. Mat.* **2016**, *28*, 094009.

(44) Zhu, H.; Pookpanratana, S. J.; Bonevich, J. E.; Natoli, S. N.; Hacker, C. A.; Ren, T.; Suehle, J. S.; Richter, C. A.; Li, Q. Redox-Active Molecular Nanowire Flash Memory for High-Endurance and High-Density Non-Volatile Memory Applications. *ACS Appl. Mater. Interfaces* **2015**, *7*, 27306-27313.

(45) Kuo, C.; Chang, J.; Yeh, C.; Lee, G.; Wang, C.; Peng, S. Synthesis, structures, magnetism and electrochemical properties of triruthenium-acetylide complexes. *Dalton Trans.* **2005**, 3696-3701.

(46) Adams, R. D.; Qu, B. Effect of Metals on the Electronic Communication through a Molecular Wire Model. *Organometallics* **2000**, *19*, 2411-2413.

(47) Adams, R. D.; Kwon, O.-S.; Qu, B.; Smith, M. D. Structures and Electrocommunication between Ferrocenyl Groups in Osmium Cluster Complexes of 1,8-Bis(ferrocenyl)octatetrayne. *Organometallics* **2001**, *20*, 5225-5232.

(48)   Adams, R. D.; Qu, B.; Smith, M. D. Synthesis and characterization of 1,12-bis(ferrocenyl)-1,3,5,7,9,11-dodecahexayne and its coordination to triosmium and dicobalt carbonyls. *Organometallics* **2002**, *21*, 3867-3872.

(49)   Adams, R. D.; Qu, B.; Smith, M. D.; Albright, T. A. Syntheses, Structures, Bonding, and Redox Behavior of 1,4-Bis(ferrocenyl)butadiyne Coordinated Osmium Clusters. *Organometallics* **2002**, *21*, 2970-2978.

(50)   Lissel, F.; Fox, T.; Blacque, O.; Polit, W.; Winter, R. F.; Venkatesan, K.; Berke, H. Stepwise Construction of an Iron-Substituted Rigid-Rod Molecular Wire: Targeting a Tetraferra–Tetracosa–Decayne. *J. Am. Chem. Soc.* **2013**, *135*, 3826-3833.

(51)   Lindoy, L. F. *The chemistry of macrocyclic ligand complexes*; Cambridge University Press: Cambridge, 1989.

(52)   *Macrocyclic Chemistry: Current Trends and Future Perspectives*; Gloe, K., Ed.; Springer: Berlin, 2005.

(53)   Cao, Z.; Forrest, W. P.; Gao, Y.; Fanwick, P. E.; Zhang, Y.; Ren, T. New Fe(III) Bis-Acetylide Compounds Based on the Fe-Cyclam Motif. *Inorg. Chem.* **2011**, *50*, 7364-7366.

(54)   Grisenti, D. L.; Thomas, W. W.; Turlington, C. R.; Newsom, M. D.; Priedemann, C. J.; VanDerveer, D. G.; Wagenknecht, P. S. Emissive Chromium(III) Complexes with Substituted Arylethynyl Ligands. *Inorg. Chem.* **2008**, *47*, 11452-11454.

(55)   Nishijo, J.; Judai, K.; Numao, S.; Nishi, N. Chromium Acetylide Complex Based Ferrimagnet and Weak Ferromagnet. *Inorg. Chem.* **2009**, *48*, 9402-9408.

(56)   Alves, L. G.; Madeira, F.; Munha, R. F.; Maulide, N.; Veiros, L. F.; Martins, A. M. Cooperative Metal-Ligand Hydroamination Catalysis Supported by C-H Activation in Cyclam Zr(IV) Complexes. *Inorg. Chem.* **2018**, *57*, 13034-13045.

(57)   Munha, R. F.; Ballmann, J.; Veiros, L. F.; Patrick, B. O.; Fryzuk, M. D.; Martins, A. M. Dinuclear Cationic Zirconium Hydrides Stabilized by the N,N-Dibenzylcyclam Ancillary Ligand. *Organometallics* **2012**, *31*, 4937-4940.

(58)   Antunes, M. A.; Munha, R. F.; Alves, L. G.; Schafer, L. L.; Martins, A. M. Intramolecular hydroamination catalysis using trans-N,N '-dibenzylcyclam zirconium complexes. *J. Organomet. Chem.* **2011**, *696*, 2-6.

(59)   Munha, R. F.; Antunes, M. A.; Alves, L. G.; Veiros, L. F.; Fryzuk, M. D.; Martins, A. M. Structure and Reactivity of Neutral and Cationic trans-N,N '-Dibenzylcyclam Zirconium Alkyl Complexes. *Organometallics* **2010**, *29*, 3753-3764.

(60) Barefield, E. K. Coordination chemistry of N-tetraalkylated cyclam ligands-A status report. *Coord. Chem. Rev.* **2010**, *254*, 1607-1627.

(61) Schneider, J.; Jia, H.; Muckerman, J. T.; Fujita, E. Thermodynamics and kinetics of CO2, CO, and H+ binding to the metal centre of CO2 reduction catalysts. *Chem. Soc. Rev.* **2012**, *41*, 2036-2051.

(62) Schneider, J.; Jia, H. F.; Kobiro, K.; Cabelli, D. E.; Muckerman, J. T.; Fujita, E. Nickel(II) macrocycles: highly efficient electrocatalysts for the selective reduction of CO2 to CO. *Energy Environ. Sci.* **2012**, *5*, 9502-9510.

(63) Mash, B. L.; Ren, T. Co(III) Phenylacetylide Complexes Supported By Tetraazamacrocyclic Ligands: Syntheses and Characterizations. *J. Organomet. Chem.* **2019**, *880*, 143-149.

(64) Thakker, P. U.; Sun, C.; Khulordava, L.; McMillen, C. D.; Wagenknecht, P. S. Synthetic control of the cis/trans geometry of M(cyclam)(CCR)(2) OTf complexes and photophysics of cis- Cr(cyclam)(CCCF3)(2) OTf and cis- Rh(cyclam)(CCCF3)(2) OTf. *J. Organomet. Chem.* **2014**, *772*, 107-112.

(65) Eddy, L. E.; Thakker, P. U.; McMillen, C. D.; Pienkos, J. A.; Cordoba, J. J.; Edmunds, C. E.; Wagenknecht, P. S. A comparison of the metal-ligand interactions of the pentafluorophenylethynyl and trifluoropropynyl ligands in transition metal cyclam complexes. *Inorg. Chim. Acta* **2019**, *486*, 141-149.

(66) Sun, C.; Turlington, C. R.; Thomas, W. W.; Wade, J. H.; Stout, W. M.; Grisenti, D. L.; Forrest, W. P.; VanDerveer, D. G.; Wagenknecht, P. S. Synthesis of cis and trans Bis-alkynyl Complexes of Cr(III) and Rh(III) Supported by a Tetradentate Macrocyclic Amine: A Spectroscopic Investigation of the M(III)–Alkynyl Interaction. *Inorg. Chem.* **2011**, *50*, 9354-9364.

(67) Forrest, W. P.; Cao, Z.; Hambrick, R.; Prentice, B. M.; Fanwick, P. E.; Wagenknecht, P. S.; Ren, T. Photoactive Cr(III)(cyclam) Complexes with Axially Bound geminal-Diethynylethenes. *Eur. J. Inorg. Chem.* **2012**, 5616-5620.

(68) Nishijo, J.; Judai, K.; Nishi, N. Weak Ferromagnetism and Strong Spin-Spin Interaction Mediated by the Mixed-Valence Ethynyltetrathiafulvalene-Type Ligand. *Inorg. Chem.* **2011**, *50*, 3464-3470.

(69) Nishijo, J.; Enomoto, M. A Series of Weak Ferromagnets Based on a Chromium-Acetylide-TTF Type Complex: Correlation of the Structures and Magnetic Properties and Origin of the Weak Ferromagnetism. *Inorg. Chem.* **2013**, *52*, 13263-13268.

(70) Nishijo, J. Chromium-ethynyltetrathiafulvalene complex based magnetic materials. *Polyhedron* **2013**, *66*, 43-47.

(71)   Nishijo, J.; Enomoto, M. Synthesis, structure and magnetic properties of [CrCyclam(Ctriple bond; length of mdashC-6-methoxynaphthalene)2](TCNQ)n(1,2-dichloroethane) (n = 1, 2). *Inorg. Chim. Acta* **2015**, *437*, 59-63.

(72)   Nishijo, J.; Shima, Y.; Enomoto, M. Synthesis, crystal structures and magnetic properties of new chromium(III)–acetylide–TTF type complexes. *Polyhedron* **2017**, *136*, 35-41.

(73)   Cao, Z.; Forrest, W. P.; Gao, Y.; Fanwick, P. E.; Ren, T. trans-[Fe(cyclam)(C2R)2]+: A New Family of Fe(III) Bis-Alkynyl Compounds. *Organometallics* **2012**, *31*, 6199-6206.

(74)   Thakker, P. U.; Aru, R. G.; Sun, C.; Pennington, W. T.; Siegfried, A. M.; Marder, E. C.; Wagenknecht, P. S. Synthesis of trans bis-alkynyl complexes of Co(III) supported by a tetradentate macrocyclic amine: A spectroscopic, structural, and electrochemical analysis of Ï€-interactions and electronic communication in the CCMCC structural unit. *Inorg. Chim. Acta* **2014**, *411*, 158-164.

(75)   Hoffert, W. A.; Kabir, M. K.; Hill, E. A.; Mueller, S. M.; Shores, M. P. Stepwise acetylide ligand substitution for the assembly of ethynylbenzene-linked Co(III) complexes. *Inorg. Chim. Acta* **2012**, *380*, 174-180.

(76)   Cook, T. D.; Natoli, S. N.; Fanwick, P. E.; Ren, T. Dimeric Complexes of CoIII(cyclam) with Polyyndiyl Bridge. *Organometallics* **2015**, *34*, 686-689.

(77)   Banziger, S. D.; Cook, T. D.; Natoli, S. N.; Fanwick, P. E.; Ren, T. Synthetic and Structural Studies of Mono-acetylide and Unsymmetric Bis-acetylide Complexes based on CoIII-cyclam. *J. Organomet. Chem.* **2015**, *799-800*, 1-6.

(78)   Natoli, S. N.; Zeller, M.; Ren, T. Stepwise Synthesis of Bis-Alkynyl CoIII(cyclam) Complexes under Ambient Conditions. *Inorg. Chem.* **2016**, *55*, 5756-5758.

(79)   Natoli, S. N.; Zeller, M.; Ren, T. An Aerobic Synthetic Approach toward Bis-Alkynyl Cobalt(III) Compounds. *Inorg. Chem.* **2017**, *56*, 10021-10031.

(80)   Judkins, E. C.; Zeller, M.; Ren, T. Synthesis and Characterizations of Macrocyclic Cr(III) and Co(III) 1-Ethynyl Naphthalene and 9-Ethynyl Anthracene Complexes: An Investigation of Structural and Spectroscopic Properties. *Inorg. Chem.* **2018**, *57*, 2249-2259.

(81)   Banziger, S. D.; Li, X.; Qasim, L. N.; Zeller, M.; Rubtsov, I.; Ren, T. Unsymmetrical Bis-Alkynyl Complexes Based on Co(III)(cyclam): Preparation, Molecular and Electronic Structures and Excited State Dynamics. *Inorg. Chem.* **2019**, manuscript in preparation.

(82)   Cook, T. D.; Fanwick, P. E.; Ren, T. Unsymmetric Mononuclear and Bridged Dinuclear Co(III)-cyclam Acetylides. *Organometallics* **2014**, *33*, 4621-4624.

(83)   Delor, M.; Keane, T.; Scattergood, P. A.; Sazanovich, I. V.; Greetham, G. M.; Towrie, M.; Meijer, A. J. H. M.; Weinstein, J. A. On the mechanism of vibrational control of light-induced charge transfer in donor–bridge–acceptor assemblies. *Nature Chem.* **2015**, *7*, 689-695.

(84)   Delor, M.; Scattergood, P. A.; Sazanovich, I. V.; Parker, A. W.; Greetham, G. M.; Meijer, A. J. H. M.; Towrie, M.; Weinstein, J. A. Toward control of electron transfer in donor-acceptor molecules by bond-specific infrared excitation. *Science* **2014**, *346*, 1492-1495.

(85)   Scattergood, P. A.; Delor, M.; Sazanovich, I. V.; Bouganov, O. V.; Tikhomirov, S. A.; Stasheuski, A. S.; Parker, A. W.; Greetham, G. M.; Towrie, M.; Davies, E. S.; Meijer, A. J. H. M.; Weinstein, J. A. Electron transfer dynamics and excited state branching in a charge-transfer platinum(II) donor-bridge-acceptor assembly. *Dalton Trans.* **2014**, *43*, 17677-17693.

(86)   Tyler, S. F.; Natoli, S. N.; Vlaisavljevich, B.; Fanwick, P. E.; Ren, T. Turning a New Leaf on Metal-TMC Chemistry: NiII(TMC) Acetylides. *Inorg. Chem.* **2015**, *54*, 10058-10064.

(87)   Curtis, N. F. The advent of macrocyclic chemistry. *Supramol. Chem.* **2012**, *24*, 439-447.

(88)   Hay, R. W.; Piplani, D. P. Transition-metal complexes of the macrocyclic ligand C-meso-5,12-dimethyl-1,4,8,11-tetra-azacyclotetradecane. *J. Chem. Soc., Dalton Trans.* **1977**, 1956-1962.

(89)   Tyler, S. F.; Judkins, E. C.; Song, Y.; Cao, F.; McMillin, D. R.; Fanwick, P. E.; Ren, T. Cr(III)-HMC (HMC = 5,5,7,12,12,14-Hexamethyl-1,4,8,11-tetraazacyclotetradecane) Alkynyl Complexes: Preparation and Emission Properties. *Inorg. Chem.* **2016**, *55*, 8736-8743.

(90)   Judkins, E. C.; Tyler, S. F.; Zeller, M.; Fanwick, P. E.; Ren, T. Synthesis and Investigation of Macrocyclic CrIII Bis(alkynyl) Complexes: Structural and Spectroscopic Properties. *Eur. J. Inorg. Chem.* **2017**, *2017*, 4068-4076.

(91)   House, D. A.; Hay, R. W.; Ali, M. A. The Preparation and Characterization of Chromium(Iii) Complexes of C-Meso and C-Racemic-5,7,7,12,14,14-Hexamethyl-1,4,8,11-Tetraazacyclotetradecane (Tet-a and Tet-B). *Inorg. Chim. Acta* **1983**, *72*, 239-245.

(92)   Robey, S. Investigation Of Transition Metal Compounds Of Cyclam Derivatives For Applications In Catalysis, Electronics, and Magnetism.Ph.D. Dissertation, Purdue University, 2017.

(93)   Curtis, N. F. In *Coordination Chemistry of Macrocyclic Compounds*; Melson, G. A., Ed.; Springer, 1979.

(94) Curtis, N. F.; Swann, D. A.; Waters, T. N. Structural studies on co-ordinated macrocyclic ligands. Part III. Preparations and crystal structure analyses of salts of the nickel(II) complex C-rac-5,5,7,12,12,14-hexamethyl-1,4,8,11-tetra-azacyclotetradecane, [Ni(tetb)]2+, in the α-, β-, and γ-configurations. *J. Chem. Soc., Dalton Trans.* **1973**, 1963-1974.

(95) Warner, L. G.; Busch, D. H. Stereoisomers of a macrocyclic nickel(II) complex containing six asymmetric centers. Factors determining the stabilities of configurations and conformations. *J. Am. Chem. Soc.* **1969**, *91*, 4092-4101.

(96) Hay, R. W.; Pujari, M. P.; Bembi, R.; Jeragh, B.; Norman, P. R. The preparation and characterisation of chromium(III) complexes of C-meso-5, 12-dimethyl-1, 4, 8, 11-tetraazacyclotetradecane (LM). Aquation and base hydrolysis kinetics of cis-andtrans-[CrLMCl2]+. *Trans. Metal Chem.* **1989**, *14*, 393-400.

(97) Oxley, B. M.; Mash, B.; Zeller, M.; Banziger, S.; Ren, T. Crystal structures of 5,12-dimethyl-1,4,8,11-tetraazacyclotetradecane cobalt(III) mono-phenylacetylide and bis-phenylacetylide. *Acta Cryst. E* **2018**, *74*, 522-529.

(98) Cook, T. D.; Natoli, S. N.; Fanwick, P. E.; Ren, T. CoIII(cyclam) Oligoynyls: Monomeric Oligoynyl Complexes and Dimeric Complexes with an Oligoyn-diyl Bridge. *Organometallics* **2016**, *35*, 1329-1338.

(99) Cook, T. D.; Tyler, S. F.; McGuire, C. M.; Zeller, M.; Fanwick, P. E.; Evans, D. H.; Peters, D. G.; Ren, T. Nickel Complexes of C-Substituted Cyclams and Their Activity for CO2 and H+ Reduction. *ACS Omega* **2017**, *2*, 3966-3976.

(100) Schenker, R.; Mock, M. T.; Kleber-Emmons, M. T.; Riordan, C. G.; Brunold, T. C. Spectroscopic and computational studies on Ni(tmc)CH3 OTf: Implications for Ni-methyl bonding in the A cluster of acetyl-CoA synthase. *Inorg. Chem.* **2005**, *44*, 3605-3617.

(101) Forster, L. S.; Moensted, O. Low temperature luminescence of chromium(III) complexes coordinated with macrocyclic tetraamine ligands. *J. Phys. Chem.* **1986**, *90*, 5131-5134.

(102) Banziger, S. D.; Judkins, E. C.; Zeller, M.; Ren, T. Diruthenium-DMBA Bis-Alkynyl Compounds with Hetero- and Extended- Aryl Appendant. *Chin. J. Inorg. Chem.* **2017**, *33*, 2103-2109.

(103) Paul, F.; Lapinte, C. Organometallic Molecular Wires and Other Nanoscale-sized Devices. An Approach using the Organoiron (dppe)Cp*Fe Building Block. *Coord. Chem. Rev.* **1998**, *178-180*, 431-509.

(104) Pombeiro, A. J. L. Electron-donor/acceptor properties of carbynes, carbenes, vinylidenes, allenylidenes and alkynyls as measured by electrochemical ligand parameters. *J. Organomet. Chem.* **2005**, *690*, 6021-6040.

(105) Crutchley, R. J. Intervalence Charge Transfer and Electron Exchange Studies of Dinuclear Ruthenium Complexes. *Adv. Inorg. Chem.* **1994**, *41*, 273-325.

(106) Launay, J.-P. Long-distance intervalence electron transfer. *Chem. Soc. Rev.* **2001**, *30*, 386-397.

(107) Richardson, D. E.; Taube, H. Determination of E20-E10 in multistep charge transfer by stationary-electrode pulse and cyclic voltammetry: application to binuclear ruthenium ammines. *Inorg. Chem.* **1981**, *20*, 1278-1285.

(108) Cao, Z.; Fanwick, P. E.; Forrest, W. P.; Gao, Y.; Ren, T. New Fe(III)(cyclam) Complexes Bearing Axially Bound geminal-Diethynylethenes. *Organometallics* **2013**, *32*, 4684-4689.

(109) Sun, C.; Thakker, P. U.; Khulordava, L.; Tobben, D. J.; Greenstein, S. M.; Grisenti, D. L.; Kantor, A. G.; Wagenknecht, P. S. Trifluoropropynyl as a Surrogate for the Cyano Ligand and Intense, Room-Temperature, Metal-Centered Emission from Its Rh(III) Complex. *Inorg. Chem.* **2012**, *51*, 10477-10479.

(110) Sonogashira, K.; Fujikura, Y.; Yatake, T.; Toyoshima, N.; Takahashi, S.; Hagihara, N. Syntheses and Properties of Cis-Dialkynyl and Trans-Dialkynyl Complexes of Platinum(Ii). *J. Organomet. Chem.* **1978**, *145*, 101-108.

(111) Sonogashira, K.; Yatake, T.; Tohda, Y.; Takahashi, S.; Hagihara, N. Novel Preparation of Omicron-Alkynyl Complexes of Transition-Metals by Copper(I) Iodide-Catalyzed Dehydrohalogenation. *J. Chem. Soc., Chem. Commun.* **1977**, 291-292.

(112) Ren, T. Sustainable metal alkynyl chemistry: 3d metals and polyaza macrocyclic ligands. *Chem. Commun.* **2016**, *52*, 3271-3279.

(113) Chrominski, M.; Lewalska, A.; Gryko, D. Reduction-free synthesis of stable acetylide cobalamins. *Chem. Commun.* **2013**, *49*, 11406-11408.

CHAPTER 2.   SYNTHESIS AND STRUCTURAL STUDIES OF MONO-ACETYLIDES AND UNSYMMETRIC BIS-ACETYLIDE COMPLEXES BASED ON CO(III)(CYCLAM)

Abstract: Reported in this contribution are the synthesis and characterization of both mono-acetylide and unsymmetric bis-acetylide compounds based on Co^{III}(cyclam) (cyclam = 1,4,8,11,tetraazacycloctetradecane). Refluxing [Co(cyclam)Cl$_2$]Cl with HC$_2$R in the presence of organic amine resulted in the formation of *trans*-[Co(cyclam)(C$_2$R)Cl]Cl (R = -4-C$_6$H$_4$NO$_2$ (**1a**), -ferrocenyl (**1b**) and -4-C$_6$H$_4$SC$_2$H$_4$SiMe$_3$ (**1c**)) in satisfactory yields. Subsequent reactions between LiC$_2$Ph and *trans*-[Co(cyclam)(C$_2$-4-C$_6$H$_4$NO$_2$)Cl]Cl resulted in a mixture of *trans*-[Co(cyclam)(C$_2$-4-C$_6$H$_4$NO$_2$)(C$_2$Ph)]Cl (**2a**) and *trans*-[Co(cyclam)(C$_2$Ph)$_2$]Cl (trace). Molecular structures of the new compounds were established using single crystal X-ray diffraction. Cyclic voltammetric study revealed that these compounds typically display three Co-based couples: an irreversible 1e$^-$ oxidation, and two 1e$^-$ reductions.

2.1   Introduction

There has been a long standing interest in the synthesis and physical properties of metal acetylide complexes,[1,2] and the recent decades have witnessed much of activity in using metal acetylides as the building blocks for molecular wires,[3-9] non-linear optical chromophores,[10,11] and photovoltaic materials.[12,13] Examples of metal acetylides exhibiting extensive conjugation, a prerequisite for molecular wires, include those based on Fe,[14,15] Ru,[16-18] Re[19,20] and Ru_2.[21-26] Though less frequent, reports of metal acetylides functioning as molecular wires or active materials in devices have also appeared in literature in recent years.[27-33] In addition to the aforementioned study of Ru_2-based acetylides, our laboratory has investigated a number of M^{III}-cyclam (M = Cr, Fe and Co; cyclam = 1,4,8,11-tetraazacyclotetradecane) based acetylide complexes, and elucidated their structural and voltammetric properties.[34-37] It should be noted that other laboratories have also explored the acetylide chemistry of M^{III}-cyclam complexes.[38-43] While the majority of the M^{III}-cyclam acteylides are the symmetric $trans$-$[M(cyclam)(C_2R)_2]^+$ type obtained using lithium acetylide, a unique Co^{III} species, $trans$-$[Co(cyclam)(C_2Ph)Cl]^+$, was prepared using the weak-base assisted alkynylation method by the laboratory of Shores.[44] Subsequently, our laboratory reported that treating $[Co(cyclam)Cl_2]Cl$ with $ca.$ 0.5 equiv of $Me_3SiC_{2n}SiMe_3$ in the presence of weak base resulted in novel oligoyn-diyl bridged compounds $trans$-$\{[Co(cyclam)Cl]_2(\mu\text{-}C_{2n})\}^{2+}$ with $n = 2$ and 3.[45]

In addition to functioning as electronic wires, metal acetylides can also serve as photonic wires. Recently, Weinstein et $al.$ reported that the photo-induced electron transfer within a donor-bridge-acceptor diad (D-B-A) is modulated by selective excitation of C≡C vibration of the $trans$-C≡C-Pt-C≡C bridge.[46,47] This elegant example inspired us

to consider similar D-B-A constructs based on *trans*-[M(cyclam)(C≡C-)$_2$] bridges, which have the advantage of using earth abundant 3d metals. The aforementioned work on Co system is an ideal starting point because of the highly selective formation of *trans*-[Co(cyclam)(C$_2$R)Cl]$^+$.[44] As the first step towards M(cyclam)-based D-B-A dyad, we report herein the synthesis and characterization of new *trans*-[Co(cyclam)(C$_2$R)Cl]$^+$ type compounds (**1a/b/c** in Scheme 2.1) and an unsymmetric compound *trans*-[Co(cyclam)(C$_2$Ph)(C$_2$C$_6$H$_4$-4-NO$_2$)]$^+$ (**2a**).
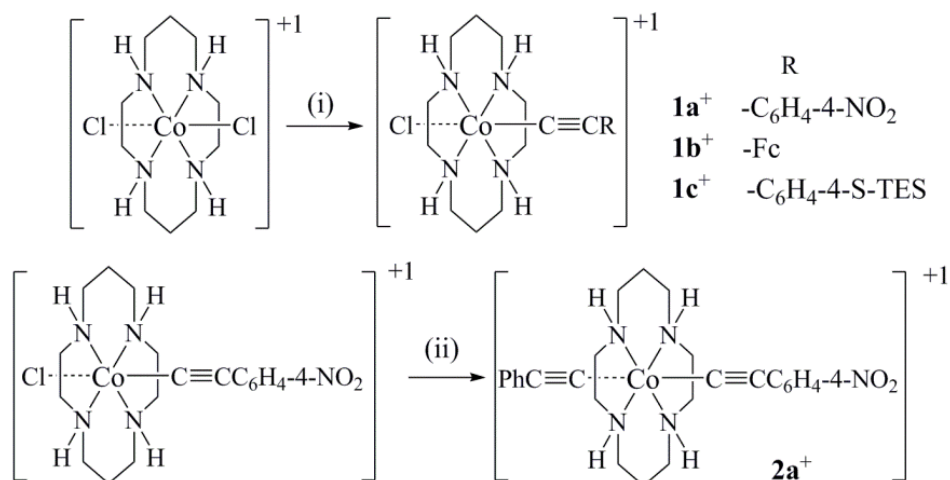
Conditions: (i) 1 equiv HC$_2$R, base (excess), MeOH reflux 12 h;
(ii) 1.0 equiv LiC$_2$Ph, THF; 8 h; Counter ion is chloride in all cases

Scheme 2.1. Synthesis of mono- and bis-acetylide Co(cyclam) Compounds

2.2   Results and Discussion

2.2.1   Synthesis

Compounds **1a/b/c** were prepared by refluxing a methanolic solution of [Co(cyclam)Cl$_2$]Cl and HC$_2$R in the presence of an organic amine overnight. Though the alkynylation did not proceed to 100% completion, the desired product can be readily

separated from the residue [Co(cyclam)Cl$_2$]Cl on a silica column. The nature of organic base also has a subtle role: triethylamine worked very well for the preparation of both **1a** and **1c** while diethylamine led to a much higher yield for **1b**. Compounds **1a/b/c** were isolated in satisfactory yields of 50 – 70%, which are comparable to those reported for [Co(cyclam)(C$_2$Ph)Cl](BPh$_4$), {[Co(cyclam)Cl]$_2$(μ-*p*-DEB)}(BPh$_4$)$_2$ and {[Co(cyclam)Cl]$_3$(μ-1,3,5-TEB)}(BPh$_4$)$_3$ by Shores *et al.* (DEB and TEB are diethnylbenzene and triethynylbenzene, respectively).[44]

The introduction of the second acetylide ligand was achieved through the reaction between **1a** and lithiated phenylacetylene as shown in Scheme 2.1. Reactions between **1a** and one equiv of LiC$_2$Ph yielded compound **2a** (22%). A major limitation of such approach is that while the substitution of the chloro ligand is the primary reaction, acetylide metathesis also occurs as evidenced by the detection of [Co(cyclam)(C$_2$Ph)$_2$]$^+$ in the reaction.

Consistent with the Co^{III} center being a low spin d^6 ion, all compounds reported here are diamagnetic and hence can be characterized by ^{1}H NMR spectroscopy. In addition, all compounds have been characterized by ESI-MS and combustion analysis with satisfactory results.

2.2.2 X-ray and molecular structures of **1a**, **1b, 1c** and **2a**.

Both the mono- and bis-acetylide compounds were readily crystallized from slow diffusion of a less polar solvent (ether or hexanes) into their methanol or methylene chloride solutions. Molecular structures of compounds **1a**, **1b**, **1c** and **2a** were determined using single crystal X-ray diffraction, and the structural plots of the cations are shown in Figures 2.1, 2.2, 2.3 and 2.4, respectively. Selected bond lengths and angles are collected

in Table 2.1, while the relevant crystal data are provided in Table 2.3 at the end of the Experimental section.
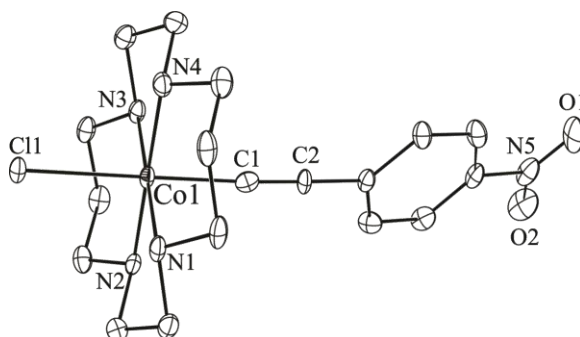
Figure 2.1. ORTEP plot of compound **1a**$^+$ at 30% probability level. Hydrogen atoms were omitted for clarity.

The Co^{III} coordination spheres in **1a**$^+$, **1b**$^+$ and **1c**$^+$ are all pseudo-octahedral, and similar to those reported for [Co(cyclam)(C$_2$Ph)Cl]$^+$ [44] and {[Co(cyclam)Cl]$_2$(μ-C$_{2n}$)}$^{2+}$.[45] The cyclam ligands exhibit very comparable ring conformations, and the Co-N bond lengths in Table 2.1 are within a narrow range of 1.962 – 1.987 Å. Adhering to the pseudo-octahedral geometry, both the C-Co-Cl angles in **1**$^+$ and the C-Co-C angle in **2a**$^+$ are all nearly linear. Among the mono-acetylide species, the Co-C bond lengths are in the order of **1a**$^+$ ~ **1c**$^+$ < **1b**$^+$. Given the fact that *p*-nitrophenylacetylide is the least electron donating of the three, the order of bond lengths is unlikely related solely to the σ-donor strength. It is likely that the Co-C≡C π interactions also play a significant role here. It is established that the π interactions between a transition metal center and σ-acetylide ligand are dominated by the filled-filled antibonding type.[48,49] The *p*-nitro group acts as a strong π-acceptor, which pulls the π(C≡C) electron density away from metal center, and hence significantly reduces the antibonding π interaction between the Co center and C≡C bond. Although ferrocenyl is more electron donating than aryls, the

$\pi(C{\equiv}C)$ of FcC_2 ligand probably has the strongest antibonding interaction with $d\pi(Co)$ and hence the longest Co-C bond for $\mathbf{1b^+}$. The Co-C bond length in $\{[Co(cyclam)Cl]_2(\mu\text{-}C_8)\}^{2+}$ (1.874(3) Å) is slightly shorter than that in $\mathbf{1c^+}$ due to a high degree of electron deficiency in an oligoyn-diyl chain.[45]
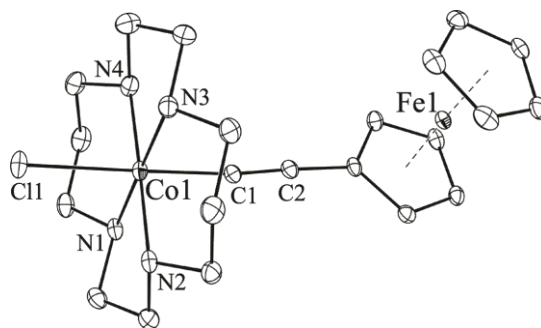
Figure 2.2. ORTEP plot of compound $\mathbf{1b^+}$ at 30% probability level. Hydrogen atoms were omitted for clarity.
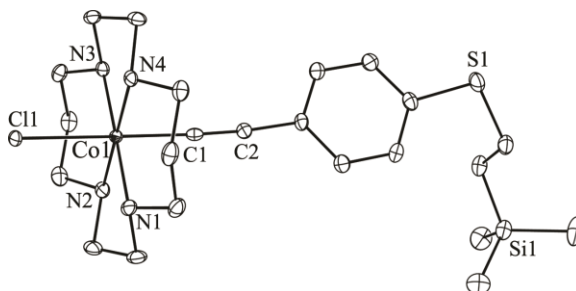
Figure 2.3. ORTEP plot of compound $\mathbf{1c^+}$ at 30% probability level. Hydrogen atoms were omitted for clarity.

Molecular structures of symmetric bis-acetylide compounds, namely $[Co(cyclam)(C_2R)_2]^+$, have been reported for R = Ph by Shores[44] and R = CF_3 by Wagenknecht.[41] Though the coordination sphere of $\mathbf{2a^+}$ is very similar to those of $[Co(cyclam)(C_2Ph)_2]^+$ and $[Co(cyclam)(C_2CF_3)_2]^+$, the molecular structure is unique owing to its asymmetry. Interestingly, the trend of the Co-C distances is $[Co(cyclam)(C_2CF_3)_2]^+$ (1.917) < $\mathbf{2a^+}$ (1.924 and 1.991) < $[Co(cyclam)(C_2Ph)_2]^+$ (2.001,

which parallels the influence of the acetylide ligands on the electron richness of the Co^{III} center. Furthermore, the Co-C(nitrophenylacetylene) bond length of **2a⁺** is slightly longer than that of $[Co(cyclam)(C_2CF_3)_2]^+$, while the Co-C(phenylacetylene) bond length of **2a⁺** is slightly shorter than that of $[Co(cyclam)(C_2Ph)_2]^+$. The shortness of Co-C in $[Co(cyclam)(C_2CF_3)_2]^+$ was previously attributed to a weak π-acidity of $-C_2CF_3$ ligand.[41] However, our DFT calculations on related Co^{III} acetylides generally place $\pi^*(C{\equiv}C)$ significantly above Co $d\pi$ orbitals,[37,45] which makes the former an unlikely acceptor. It is more likely that the electron withdrawing ability of $-CF_3$ and $-C_6H_4-4-NO_2$ significantly reduces the antibonding contribution from $\pi(C{\equiv}C)$ to Co $d\pi$, and hence strengthens the Co-C bond. Also noteworthy is that both Co-C bonds in **2a⁺** are significantly longer than those in compounds **1⁺**. This is because the acetylide is a much stronger donor than the chloro, and both acetylides in **2a⁺** experience the *trans*-influence of each other.
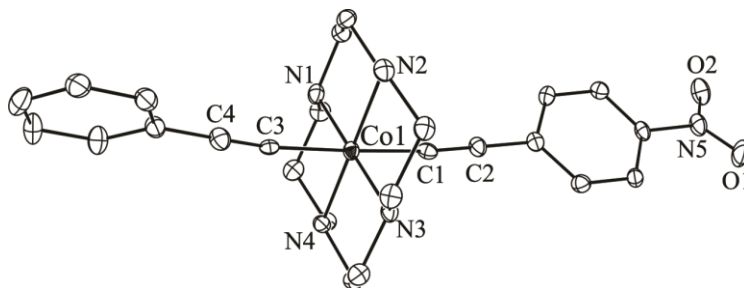
Figure 2.4. ORTEP plot of compound **2a⁺** at 30% probability level. Hydrogen atoms were omitted for clarity.

Table 2.1. Selected bond lengths (Å) and bond angles (°) for **1a⁺**, **1b⁺**, **1c⁺** and **2a⁺**

	1a⁺	**1b⁺**	**1c⁺**	**2a⁺**
Co1-C1	1.877(4)	1.883(2)	1.879(2)	1.924(4)
Co1-C3	--	--	--	1.991(4)
Co1-N1	1.982(4)	1.985(2)	1.970(2)	1.977(4)
Co1-N2	1.976(4)	1.962(2)	1.974(2)	1.991(3)
Co1-N3	1.966(4)	1.970(2)	1.976(2)	1.977(4)
Co1-N4	1.987(4)	1.985(2)	1.972(2)	1.978(3)
Co1-Cl1	2.312(1)	2.3226(6)	2.3185(6)	--
C1-C2	1.215(6)	1.209(3)	1.210(3)	1.214(5)
C3-C4	--	--	--	1.157(5)
Cl1-Co1-C1	177.7(1)	178.42(7)	178.18(7)	--
C3-Co1-C1	--	--	--	177.6(1)
Co1-C1-C2	168.2(4)	173.8(2)	176.9(2)	170.1(3)
C1-C2-C3	176.0(5)	177.1(2)	175.3(3)	--
C1-C2-C11	--	--	--	179.3(5)
Co1-C3-C4	--	--	--	173.9(4)
C3-C4-C5	--	--	--	177.7(5)

2.2.3   Spectroscopic studies

The electronic absorption spectra of both compounds **1** and **2** feature a weak band ($\varepsilon \sim 10^2$) in the visible window and an intense band ($\varepsilon \sim 10^4$) in the UV window, as exemplified by the spectra of **1a** and **2a** in Figure 2.5. The spectral features of **1b** and **1c** are very similar to that of **1a**. The lower energy transitions, peaks at 478 nm for **1a** and 442 nm for **2a**, are likely attributed to the ligand field (*d-d*) transition $^1A_{1g} \rightarrow {}^1T_{1g}$, according to the discussion by Wagenknecht for the symmetric [Co(cyclam)(C₂R)₂]⁺ type

compounds.[41] Wagenknecht also noted that the intensities of *d-d* bands for [Co(cyclam)(C$_2$R)$_2$]$^+$ are about three times of that for [Co(cyclam)(CN)$_2$]$^+$ because of more efficient intensity stealing from the high energy CT band. Interestingly, the *d-d* band of **2a** is further intensified by at least three fold in comparison with those of [Co(cyclam)(C$_2$R)$_2$]$^+$ ($\varepsilon \sim 150$ or less), likely the result of the electronic asymmetry (thus a permanent dipole) along the PhC$_2$-Co-C$_2$C$_6$H$_4$-4-NO$_2$ axis. The higher energy transitions, peaks at 337 nm for **1a** and 270 nm for **2a**, are likely the LMCT transitions from axial chloro / acetylide ligands.[39] The intensity of the LMCT band of **2a** is significantly lower than that of **1a**, implying a prominent contribution from the chloro ligand in the latter.
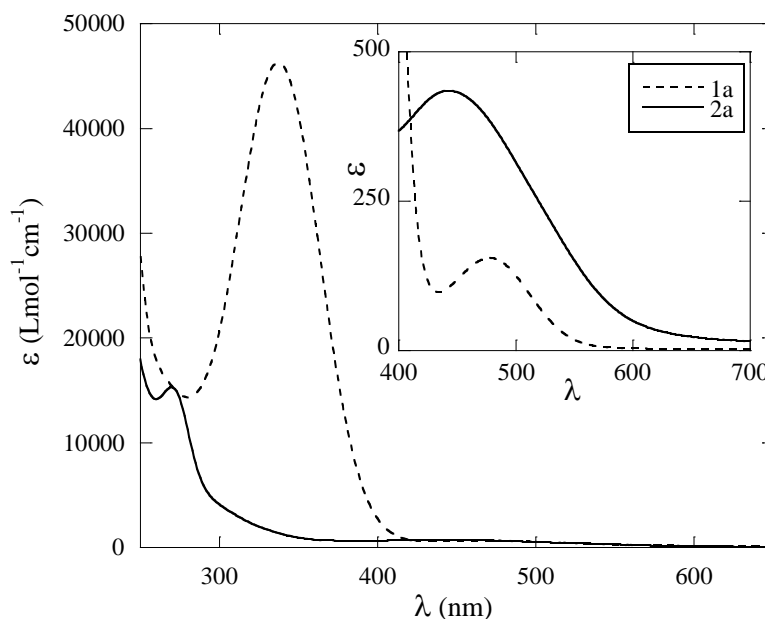
Figure 2.5. UV-Vis spectra of compounds **1a** and **2a** recorded in methanol solution. The inset is the enlargement of the visible region.

2.2.4   Electrochemistry
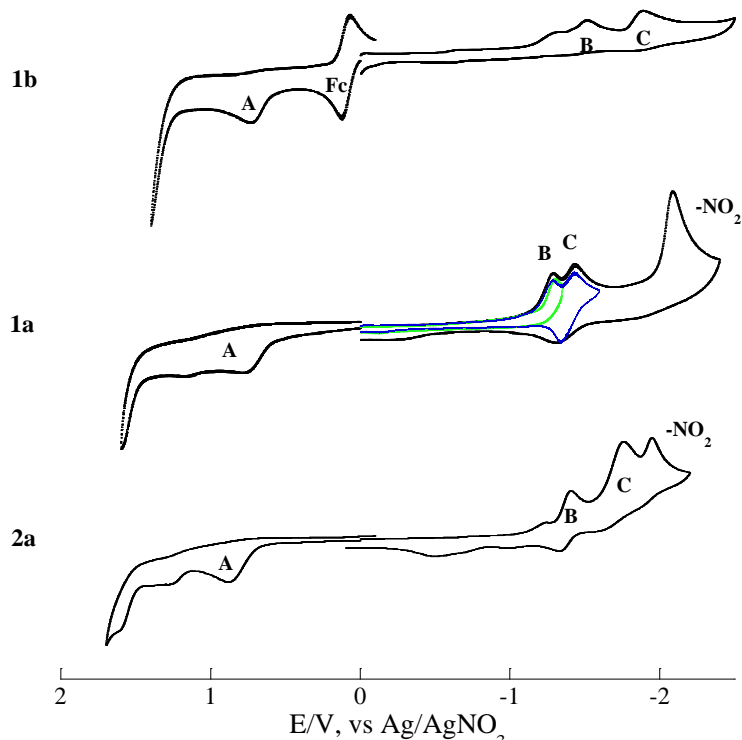
Figure 2.6. Cyclic voltammograms of compounds **1a**, **1b** and **2a** recorded in 0.10 M
Bu$_4$NBF$_4$ acetonitrile solution with a scan rate of 100 mV/s. Description for the green and
blue insets in the CV of **1a** is given in the discussion below.

Compounds **1** and **2** exhibit several 1e$^-$ redox couples in their cyclic

voltammograms (CV), as exemplified by the CVs of **1a**, **1b** and **2a** (Figure 2.6).

Electrode potentials determined for all of the new compounds are listed in Table 2.2. The

CV of the mono-acetylide species **1b** consists of a reversible ferrocenyl oxidation at 0.10

V and an irreversible Co-based oxidation at 0.81 V, and irreversible Co-based reductions

at -1.52 and -1.89 V. The anodic portion of the CV of **1a** has the irreversible oxidation **A**

at a potential slightly more positive than that of **1b**, reflecting the increased electron

deficiency due to the nitrophenyl group. Because of the absence of current on the back

sweep, the Co^{III} species is likely completely degraded passing E$_{pa}$(**A**) and the resultant

species is labeled as "Co^{IV}" in Scheme 2.2. The impact of the nitrophenyl group is more pronounced in the cathodic region: the first (**B**) and second (**C**) reductions are significantly shifted to the positive direction compared with those of **1b**. Furthermore, a substantial anodic wave was observed on the backward sweep immediately beneath the closely spaced cathodic peaks **B** and **C**. To ascertain the origin of this wave, the cathodic scans with the end point shortly past $E_{pc}(\mathbf{B})$ (green) and $E_{pc}(\mathbf{C})$ (blue) were performed and included in Figure 2.6. It is clear from these CVs that the anodic peak is associated with reduction **C** and makes the couple quasi-reversible. This observation is consistent with the prior report of the CVs for $[Co(cyclam)(C_2R)_2]^+$, for which the reversibility of the Co(III/II) couple improves as R becoming more electron withdrawing.[41] Reduction of the nitro-group occurs at very negative potential and results in degradation of the Co compound, as evidenced by the broadening of the anodic peak below **C** and the appearance of a new anodic wave near 0 V when compared to the CVs in green and blue. Based on the voltammetric results of **1b** and **1c**, a simple assignment to explain the observed couples is given in Scheme 2.2 below.
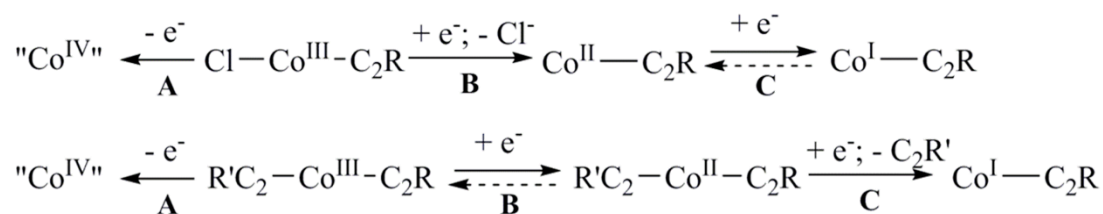
Scheme 2.2. Assignment of Co-based redox couples observed for 1 (top) and 2 (bottom); C₂R′ indicates the less electron deficient acetylide

Compound **2a** exhibits an irreversible 1e⁻ oxidation and three 1e⁻ reductions. In contrast to **1a**, it is the first 1e⁻ reduction **B** that is quasi-reversible, which is consistent

with the prior report of [Co(cyclam)(C$_2$R)$_2$]$^+$.[41] As outlined in Scheme 2.2, the second 1e$^-$

reduction is irreversible because of the dissociation of the less electron deficient acetylide

(-C$_2$Ph). The retention of the nitrophenylacetylide is also supported by the observation of

the reduction of nitro group.

Table 2.2. Electrode potentials of all observed redox couples (V) in compounds **1** and **2**

	E$_{pa}$(**A**)	E$_{pc}$(**B**)	E$_{pc}$(**C**)	E$_{1/2}$(**Fc**)	E$_{pc}$ (**-NO$_2$**)
[Co(cyclam)Cl(C$_2$C$_6$H$_4$-4-NO$_2$)]Cl (**1a**)	0.81	-1.29	-1.42	--	-2.09
[Co(cyclam)Cl(C$_2$Fc)]Cl (**1b**)	0.74	-1.52	-1.89	0.10	--
[Co(cyclam)Cl(C$_2$C$_6$H$_4$-4-SC$_2$H$_4$SiMe$_3$)]Cl (**1c**)	0.81	-.147	-1.79	--	--
[Co(cyclam)(C$_2$Ph)(C$_2$C$_6$H$_4$-4-NO$_2$)]Cl (**2a**)	0.88	-1.41	-1.76	--	-1.95

2.3   Conclusion

Presented in this contribution is the general synthesis of the *trans-*

[Co(cyclam)(C$_2$R)Cl]Cl type compounds **1a/b/c**, and facile conversion of **1a** to the

unsymmetric bis-acetylide derivative *trans-*[Co(cyclam)(C$_2$Ph)(C$_2$C$_6$H$_4$-4-NO$_2$)]Cl (**2a**).

As discussed above, the presence of *para-*nitro substituent and the unsymmetric nature of

2a have significant influence on both the electronic absorption spectra and voltammetric

behaviors of Co(cyclam) acetylides. While the synthetic method for *trans-*

[Co(cyclam)(C$_2$R)Cl]Cl in satisfactory yield and purity has been established, the current

synthesis of the unsymmetric bis-acetylide derivative is of low yield. Preparations of

unsymmetric bis-acetylides that do not involve lithium acetylides have been documented

in literature: the reaction between *trans-*[(dppe)$_2$RuCl(C$_2$Ar)] and Me$_3$SnC$_2$Ar′ resulted in

trans-[(dppe)$_2$Ru(C$_2$Ar)(C$_2$Ar′)] (dppe = 1,2-bis(diphenylphosphino)ethane),[50] and *trans-*

Pt(PBu$_3$)$_2$Cl(C$_2$R) was converted to *trans-*Pt(PBu$_3$)$_2$(C$_2$R)(C$_2$R′) under the Hagihara

conditions (CuI / organic amine).[47]   More selective and higher yield methods for the *trans*-[Co(cyclam)(C$_2$R)(C$_2$R′)]Cl type compounds are being sought in our laboratory.

2.4   Experimental

2.4.1   Materials and Measurements

[Co(cyclam)Cl$_2$]Cl was prepared according to literature procedures.[37] Also prepared according literature procedures were ethynylferrocene,[51] 4-NO$_2$-C$_6$H$_4$C$_2$SiMe$_3$[52] and 4-(Me$_3$SiC$_2$H$_4$S)-C$_6$H$_4$C$_2$H.[53] THF was distilled over Na/benzophenone under a N$_2$ atmosphere. UV-Vis-NIR spectra were obtained with a JASCO V-670 UV-Vis-NIR spectrophotometer. Infrared spectra were obtained on a JASCO FT-IR 6300 spectrometer via ATR on a ZnSe crystal. Mass Spectrometry data were collected on a Waters 600 LC/MS. ^{1}H NMR spectra were recorded on a Varian MERCURY300 NMR spectrometer. Cyclic voltammograms were recorded in 0.1 M n-Bu$_4$NPF$_6$ and 1.0 mM cobalt species solution (CH$_3$CN, Ar degassed) by a CHI620A voltammetric analyzer with a glassy carbon working electrode (diameter = 2 mm), Pt-wire counter electrode, and a Ag/AgNO$_3$ reference electrode with ferrocene used as an external reference (E$_{1/2}$ = 0.12 V).

2.4.2   Synthesis Compounds **1** and **2**

Preparation of **1a**.   [Co(cyclam)Cl$_2$]Cl (220 mg, 0.54 mmol), 4-NO$_2$-C$_6$H$_4$C$_2$SiMe$_3$ (120 mg, 0.54 mmol), and Et$_3$N (4.0 mL) were mixed in 20 mL of methanol, and the mixture was refluxed overnight to yield a muddy red solution. After solvent removal, the crude mixture was loaded onto a short silica gel plug and eluted first with CH$_2$Cl$_2$, then CH$_3$OH/CH$_2$Cl$_2$ (v/v, 1:6). An orange and a green fraction were collected with the second eluent, and identified by ESI-MS as the desired product and the

starting material, respectively. After solvent removal, the orange fraction was recrystallized from ether-methanol to afford 168 mg of **1a** (70% based on Co). When Et_2NH was used in place of Et_3N, the reaction only yielded a mixture of intractable products. Data for **1a**: ESI-MS: $[M]^+$, 440.0. ^1H NMR (CD_3OD, δ): 8.175 (dd, 2H, Ph), 7.645 (dd, 2H, Ph), 5.2 (br s, 4H, NH). UV-vis spectra, λ_{max} (nm, ε (M^{-1} cm^{-1})): 337 (46,300), 478 (155); IR (cm^{-1}): C≡C: 2114(m). Anal. Found (calcd) for $C_{18}H_{30}Cl_2CoN_5O_3$ (**1a**·H_2O): C,43.31 (43.74); H, 5.86 (6.12); N, 13.84 (14.17).

Preparation of **1b**. [Co(cyclam)Cl_2]Cl (200 mg, 0.61 mmol), ethynylferrocene (107 mg, 0.51 mmol) and Et_2NH (2.0 mL) were mixed in 10 mL of methanol, and the mixture was refluxed for overnight to yield a dark red solution. After solvent removal, the crude mixture was loaded onto a short silica gel plug and eluted with first CH_2Cl_2, then CH_3OH/CH_2Cl_2 (v/v, 1:6). Both a red and a green fraction were collected using the latter eluent, and were identified by ESI-MS as the desired product and starting materials, respectively. After solvent removal, the red fraction was recrystallized from ether-methanol to afford 162 mg of **1b** (63% based on ethynylferrocene). When Et_3N was used in place of Et_2NH, the reaction between [Co(cyclam)Cl_2]Cl and ethynylferrocene only resulted in **1b** in *ca*. 10% yield. Data for **1b**: ESI-MS: $[M]^+$, 503.0. ^1H NMR (CD_3OD, δ): 4.990 (br s, 4H, NH), 4.894 (s, 2H, Fc), 4.470 (s, 2H, Fc), 4.206 (s, 5H, Fc). UV-vis spectra, λ_{max} (nm, ε (M^{-1} cm^{-1})): 270 (15,300), 442 (548); IR (cm^{-1}): C≡C, 2132(m). Anal. Found (calcd) for $C_{23}H_{35}Cl_4CoFeN_4$ (**1b**·CH_2Cl_2): C, 44.01 (44.26); H, 5.65 (5.92); N, 8.81 (8.98).

Preparation of **1c**. [Co(cyclam)Cl_2]Cl (110 mg, 0.41 mmol), 4-($Me_3SiC_2H_4S$)-$C_6H_4C_2H$ (110 mg, 0.47 mmol) and Et_3N (1.6 mL) were mixed in 10 mL of methanol,

and the mixture was refluxed for overnight to yield a dark red solution. Solvent was removed under reduced pressure, and the crude residue was loaded onto a short silica gel plug and eluted with first CH_2Cl_2, then CH_3OH/CH_2Cl_2 (v/v, 1:6). Both a red and a green fraction were collected using the latter eluent, and were identified by ESI-MS as the desired product and starting materials, respectively. After solvent removal, the red fraction was recrystallized from ether-methanol to afford 120 mg of **1c** (52% based on Co). Data for **1c**: ESI-MS: $[M]^+$, 527.0. ^1H NMR (CD_3OD, δ): 7.37 (dd, 2H, Ph), 7.23 (dd, 2H, Ph), 5.08 (br s, 4H, NH), 1.94 (m, 2H, CH_2), 1.60 (m, 2H, CH_2), 0.030 (s, 9H, TMS). UV-Vis spectra, λ_{max} (nm, ε (M^{-1} cm^{-1})): 285 (28,500), 491 (112); IR (cm^{-1}): $C{\equiv}C$: 2122(m). Anal. Found (calcd) for $C_{23}H_{37}Cl_2CoN_4O_3SSi$ (**1c**·$3H_2O$): C, 44.70 (44.73); H, 7.66 (7.67); N, 8.97 (9.07)

Preparation of **2a**. Under an N_2 atmosphere, LiC_2Ph in THF (0.29 mmol) was added to a Schlenck flask containing **1a** (119 mg, 0.27 mmol) in 5 mL THF, and the reaction mixture was allowed to stir overnight to yield a brown solution. After solvent removal, the crude residue was loaded onto a short silica gel plug and eluted first with EtOAc, then $CH_3OH/EtOAc$ (v/v 1:6). Both a yellow and an orange fraction were collected using the latter eluent, and were identified by ESI-MS as the desired product and the starting material, respectively. The material from the yellow fraction was recrystallized from ether-methanol to afford 30 mg of **2a** (22% based on **1a**). Data for **2a**: ESI-MS: $[M]^+$, 506.0. ^1H NMR (CD_3OD, δ): 8.17 (dd, 2H, $PhNO_2$), 7.65 (dd, 2H, $PhNO_2$), 7.47 (dd, 2H, Ph), 7.26 (dt, 2H, Ph), 7.17 (dd, 1H, Ph), 4.72 (br s, 4H, NH), UV-Vis spectra, λ_{max} (nm, ε (M^{-1} cm^{-1})): 270 (15,300), 442 (435); IR (cm^{-1}): $C{\equiv}C$, 2054 (w),

2097(s). Anal. Found (calcd) for $C_{26}H_{41}ClCoN_5O_5$ (**2a**·$2H_2O$·CH_3OH): C, 53.49 (53.16); H, 6.59 (6.77); N, 11.50 (11.48).

2.4.3   Structure Determination

Single crystals of compound **1a**, **1b** and **2a** were grown by slow diffusion of ether into methanol at room temperature. Single crystals of **1c** were grown by slow diffusion of hexanes into dichloromethane solution at room temperature. X-ray diffraction data were collected on either a Rigaku Rapid II image plate diffractometer using Cu Kα (**1a** and **2a**) or a Nonius Kappa CCD using Mo Kα (**1b** and **1c**), and the structures were solved using the structure solution program PATTY in DIRDIF99,[54] and refined using SHELX-07.[55] Crystallographic data are listed in Table 2.3.

Table 2.3. Crystal data for compounds **1a, 1b, 1c** and **2a**

	1a·$2CH_3OH$	**1b**·$3CH_3OH$	**1c**·$2CH_2Cl_2$·H_2O	**2a**·$2CH_3OH$
Chemical Formula	$C_{20}H_{36}Cl_2CoN_5O_4$	$C_{25}H_{45}Cl_2CoFeN_4O_3$	$C_{25}H_{47}Cl_6CoN_4OSSi$	$C_{28}H_{41}ClCoN_5O_4$
Formula Weight	540.38	635.35	751.48	606.06
Space Group	$P\bar{1}$	$P2_1$/c	$P\bar{1}$	$P\bar{1}$
a, Å	8.0601(6)	18.9682(5)	9.5458(7)	10.3849(8)
b, Å	10.1925(7)	11.1569(2)	13.291(1)	12.532(1)
c, Å	16.7491(9)	14.1810(3)	14.490(1)	12.705(1)
α °	92.12(5)		94.77(5)	92.40(8)
β °	93.70(6)	105.40(1)	90.69(5)	109.43(7)
γ °	104.24(5)		102.55(4)	108.92(7)
V, Å^3	1328.9(2)	2893.4(1)	1787.4(2)	1454.0(2)
Z	2	4	2	2
T, K	150	150	150	150
λ, Å	1.54184	0.71073	0.71073	1.54184
ρ_{calcd}, g cm^{-3}	1.350	1.458	1.396	1.384
R	0.061	0.037	0.040	0.058
$wR2$	0.152	0.084	0.100	0.148

Supporting Information Available. Crystallographic data for the structural analysis have been deposited with the Cambridge Crystallographic Data Center, CCDC 1411094 - 1411097 for compounds **1a**, **1b**, **1c** and **2a**, respectively.

2.5   References

(1)   Nast, R. Coordination Chemistry of Metal Alkynyl Compounds. *Coord. Chem. Rev.* **1982**, *47*, 89-124.

(2)   Hagihara, N.; Sonogashira, K.; Takahashi, S. Linear Polymers Containing Transition Metals in the Main Chain. *Adv. Polym. Sci.* **1980**, *40*, 149-179.

(3)   Low, P. J.; Brown, N. J. Electronic Interactions Between and Through Covalently-Bonded Polymetallic Complexes. *J. Cluster Sci.* **2010**, *21*, 235-278.

(4)   Ren, T. Diruthenium s-Alkynyl Compounds**:** A New Class of Conjugated Organometallics. *Organometallics* **2005**, *24*, 4854-4870.

(5)   Costuas, K.; Rigaut, S. Polynuclear carbon-rich organometallic complexes: clarification of the role of the bridging ligand in the redox properties. *Dalton Trans.* **2011**, *40*, 5643-5658.

(6)   Zhang, X.-Y.; Zheng, Q. Q.; Chen-Xi, Q.; Zuo, J.-L. Some New Progress on Molecular Wires. *Chinese J. Inorg. Chem.* **2011**, *27*, 1451-1464.

(7)   Hurst, S. K.; Ren, T. Homo-dinuclear sigma-alkynyl complexes: past, present and opportunities. *J. Organomet. Chem.* **2003**, *670*, 188-197.

(8)   Szafert, S.; Gladysz, J. A. Carbon in One Dimension: Structural Analysis of the Higher Conjugated Polyynes. *Chem. Rev.* **2003**, *103*, 4175-4206.

(9)   Szafert, S.; Gladysz, J. A. Update 1 of: Carbon in One Dimension: Structural Analysis of the Higher Conjugated Polyynes. *Chem. Rev.* **2006**, *106*, 1-33.

(10)   Whittall, I. R.; McDonagh, A. M.; Humphrey, M. G.; Samoc, M. Organometallic complexes in nonlinear optics I: Second-order nonlinearities. *Adv. Organomet. Chem.,* **1998**, *42*, 291-362.

(11)   Zhou, G.-J.; Wong, W.-Y. Organometallic acetylides of Pt(II), Au(I) and Hg(II) as new generation optical power limiting materials. *Chem. Soc. Rev.* **2011**, *40*, 2541-2566.

(12)   Wong, W. Y.; Ho, C. L. Heavy metal organometallic electrophosphors derived from multi-component chromophores. *Coord. Chem. Rev.* **2009**, *253*, 1709-1758.

(13)   Wong, W.-Y.; Ho, C.-L. Organometallic Photovoltaics: A New and Versatile Approach for Harvesting Solar Energy Using Conjugated Polymetallaynes. *Acc. Chem. Res.* **2010**, *43*, 1246-1256.

(14)   Tanaka, Y.; Shaw-Taberlet, J. A.; Justaud, F.; Cador, O.; Roisnel, T.; Akita, M.; Hamon, J.-R.; Lapinte, C. Electronic and Magnetic Couplings in Free and ?-Coordinated 1,4-Diethynylnaphthalene-Bridged [Cp*(dppe)Fe]n+ (n = 0, 1) Units. *Organometallics* **2009**, *28*, 4656.

(15)   Le Narvor, N.; Lapinte, C. First C_4 Bridged Mixed-valence Iron(II)-Iron(III) Complex Delocalized on the Infrared Timescale. *J. Chem. Soc., Chem. Commun.* **1993**, 357-359.

(16)   Hamon, P.; Justaud, F.; Cador, O.; Hapiot, P.; Rigaut, S.; Toupet, L.; Ouahab, L.; Stueger, H.; Hamon, J.-R.; Lapinte, C. Redox-Active Organometallics: Magnetic and Electronic Couplings through Carbon-Silicon Hybrid Molecular Connectors. *J. Am. Chem. Soc.* **2008**, *130*, 17372.

(17)   Fox, M. A.; Roberts, R. L.; Baines, T. E.; Guennic, B. L.; Halet, J.-F.; Hartl, F.; Yufit, D. S.; Albesa-Jové, D.; Howard, J. A. K.; Low, P. J. Ruthenium Complexes of C,C'-Bis(ethynyl)carboranes: An Investigation of Electronic Interactions Mediated by Spherical Pseudo-aromatic Spacers. *J. Am. Chem. Soc.* **2008**, *130*, 3566-3578.

(18)   Olivier, C.; Costuas, K.; Choua, S.; Maurel, V.; Turek, P.; Saillard, J.-Y.; Touchard, D.; Rigaut, S. "Chain-Like" Trimetallic Ruthenium Complexes with C7 Carbon-Rich Bridges: Experimental and Theoretical Investigations of Electronic Communication Tuning in Five Distinct Oxidation States. *J. Am. Chem. Soc.* **2010**, *132*, 5638–5651.

(19)   Dembinski, R.; Bartik, T.; Bartik, B.; Jaeger, M.; Gladysz, J. A. Toward Metal-Capped One-Dimensional Carbon Allotropes: Wirelike C6-C20 Polyynediyl Chains That Span Two Redox-Active ([Image]5-C5Me5)Re(NO)(PPh3) Endgroups. *J. Am. Chem. Soc.* **2000**, *122*, 810-822.

(20)   Zhou, Y. L.; Seyler, J. W.; Weng, W.; Arif, A. M.; Gladysz, J. A. New Families of Coordinated Carbon: Oxidative Coupling of an Ethynyl Complex to Isolable and Crystallographically Characterized MC=CC=CM amd +MC=CC=CM+ Assemblies. *J. Am. Chem. Soc.* **1993**, *115*, 8509-8510.

(21)   Ren, T.; Zou, G.; Alvarez, J. C. Facile Electronic Communication between Bimetallic Termini Bridged by Elemental Carbon Chains. *Chem. Comm.* **2000**, 1197-1198.

(22)   Wong, K.-T.; Lehn, J.-M.; Peng, S.-M.; Lee, G.-H. Nanoscale molecular organometallo-wires containing diruthenium cores. *Chem. Commun.* **2000**, 2259-2260.

(23) Xu, G.-L.; Zou, G.; Ni, Y.-H.; DeRosa, M. C.; Crutchley, R. J.; Ren, T. Polyyn-diyls Capped by Diruthenium Termini: A New Family of Carbon-Rich Organometallic Compounds and Distance Dependent Electronic Coupling Therein. *J. Am. Chem. Soc.* **2003**, *125*, 10057-10065.

(24) Ying, J.-W.; Liu, I. P.-C.; Xi, B.; Song, Y.; Campana, C.; Zuo, J.-L.; Ren, T. Linear Diruthenium Trimer of Butadiyn-diyl Bridge - A Unique Electronic Wire. *Angew. Chem. Int. Ed.* **2010**, *49*, 954-957.

(25) Xi, B.; Liu, I. P. C.; Xu, G.-L.; Choudhuri, M. M. R.; DeRosa, M. C.; Crutchley, R. J.; Ren, T. Modulation of Electronic Couplings within Metal-Polyyne Frameworks. *J. Am. Chem. Soc.* **2011**, *133*, 15094-15104.

(26) Cao, Z.; Xi, B.; Jodoin, D. S.; Zhang, L.; Cummings, S. P.; Gao, Y.; Tyler, S. F.; Fanwick, P. E.; Crutchley, R. J.; Ren, T. Diruthenium-Polyyn-diyl-Diruthenium Wires: Electronic Couplings in the Long Distance Regime. *J. Am. Chem. Soc.* **2014**, *136*, 12174-12183.

(27) Inkpen, M. S.; Long, N. J. In *Molecular Design and Applications of Photofunctional Polymers and Materials*, 2012; pp 85-129.

(28) Blum, A. S.; Ren, T.; Parish, D. A.; Trammell, S. A.; Moore, M. H.; Kushmerick, J. G.; Xu, G. L.; Deschamps, J. R.; Pollack, S. K.; Shashidhar, R. Ru-2(ap)(4)(sigma-oligo(phenyleneethynyl)) molecular wires: Synthesis and electronic characterization. *J. Am. Chem. Soc.* **2005**, *127*, 10010-10011.

(29) Mahapatro, A. K.; Ying, J.; Ren, T.; Janes, D. B. Electronic Transport through Ruthenium Based Redox-Active Molecules in Metal-Molecule-Metal Nanogap Junctions. *Nano Lett.* **2008**, *8*, 2131-2136.

(30) Gauthier, N.; Argouarch, G.; Paul, F.; Humphrey, M. G.; Toupet, L.; Ababou-Girard, S.; Sabbah, H.; Hapiot, P.; Fabre, B. Silicon Surface-Bound Redox-Active Conjugated Wires Derived From Mono- and Dinuclear Iron(II) and Ruthenium(II) Oligo(phenyleneethynylene) Complexes. *Adv. Mater.* **2008**, *20*, 1952-1956.

(31) Luo, L.; Benameur, A.; Brignou, P.; Choi, S. H.; Rigaut, S.; Frisbie, C. D. Length and Temperature Dependent Conduction of Ruthenium-Containing Redox-Active Molecular Wires. *J. Phys. Chem. C* **2011**, *115*, 19955-19961.

(32) Meng, F. B.; Hervault, Y. M.; Norel, L.; Costuas, K.; Van Dyck, C.; Geskin, V.; Cornil, J.; Hng, H. H.; Rigaut, S.; Chen, X. D. Photo-modulable molecular transport junctions based on organometallic molecular wires. *Chem. Sci.* **2012**, *3*, 3113-3118.

(33) Meng, F. B.; Hervault, Y. M.; Shao, Q.; Hu, B. H.; Norel, L.; Rigaut, S.; Chen, X. D. Orthogonally modulated molecular transport junctions for resettable electronic logic gates. *Nature Commun.* **2014**, *5*, Art. 3023.

(34) Cao, Z.; Forrest, W. P.; Gao, Y.; Fanwick, P. E.; Ren, T. trans-[Fe(cyclam)(C2R)2]+: A New Family of Fe(III) Bis-Alkynyl Compounds. *Organometallics* **2012**, *31*, 6199-6206.

(35) Forrest, W. P.; Cao, Z.; Hambrick, R.; Prentice, B. M.; Fanwick, P. E.; Wagenknecht, P. S.; Ren, T. Photoactive Cr(III)(cyclam) Complexes with Axially Bound geminal-Diethynylethenes. *Eur. J. Inorg. Chem.* **2012**, 5616-5620.

(36) Cao, Z.; Fanwick, P. E.; Forrest, W. P.; Gao, Y.; Ren, T. New Fe(III)(cyclam) Complexes Bearing Axially Bound geminal-Diethynylethenes. *Organometallics* **2013**, *32*, 4684-4689.

(37) Cook, T. D.; Fanwick, P. E.; Ren, T. Unsymmetric Mononuclear and Bridged Dinuclear Co(III)-cyclam Acetylides. *Organometallics* **2014**, *33*, 4621-4624.

(38) Grisenti, D. L.; Thomas, W. W.; Turlington, C. R.; Newsom, M. D.; Priedemann, C. J.; VanDerveer, D. G.; Wagenknecht, P. S. Emissive Chromium(III) Complexes with Substituted Arylethynyl Ligands. *Inorg. Chem.* **2008**, *47*, 11452-11454.

(39) Sun, C.; Turlington, C. R.; Thomas, W. W.; Wade, J. H.; Stout, W. M.; Grisenti, D. L.; Forrest, W. P.; VanDerveer, D. G.; Wagenknecht, P. S. Synthesis of cis and trans Bis-alkynyl Complexes of Cr(III) and Rh(III) Supported by a Tetradentate Macrocyclic Amine: A Spectroscopic Investigation of the M(III)–Alkynyl Interaction. *Inorg. Chem.* **2011**, *50*, 9354-9364.

(40) Sun, C.; Thakker, P. U.; Khulordava, L.; Tobben, D. J.; Greenstein, S. M.; Grisenti, D. L.; Kantor, A. G.; Wagenknecht, P. S. Trifluoropropynyl as a Surrogate for the Cyano Ligand and Intense, Room-Temperature, Metal-Centered Emission from Its Rh(III) Complex. *Inorg. Chem.* **2012**, *51*, 10477-10479.

(41) Thakker, P. U.; Aru, R. G.; Sun, C.; Pennington, W. T.; Siegfried, A. M.; Marder, E. C.; Wagenknecht, P. S. Synthesis of trans bis-alkynyl complexes of Co(III) supported by a tetradentate macrocyclic amine: A spectroscopic, structural, and electrochemical analysis of Ï€-interactions and electronic communication in the CCMCC structural unit. *Inorg. Chim. Acta* **2014**, *411*, 158-164.

(42) Thakker, P. U.; Sun, C.; Khulordava, L.; McMillen, C. D.; Wagenknecht, P. S. Synthetic control of the cis/trans geometry of M(cyclam)(CCR)(2) OTf complexes and photophysics of cis- Cr(cyclam)(CCCF3)(2) OTf and cis-Rh(cyclam)(CCCF3)(2) OTf. *J. Organomet. Chem.* **2014**, *772*, 107-112.

(43) Nishijo, J.; Enomoto, M. A Series of Weak Ferromagnets Based on a Chromium-Acetylide-TTF Type Complex: Correlation of the Structures and Magnetic Properties and Origin of the Weak Ferromagnetism. *Inorg. Chem.* **2013**, *52*, 13263-13268.

(44)   Hoffert, W. A.; Kabir, M. K.; Hill, E. A.; Mueller, S. M.; Shores, M. P. Stepwise acetylide ligand substitution for the assembly of ethynylbenzene-linked Co(III) complexes. *Inorg. Chim. Acta* **2012**, *380*, 174-180.

(45)   Cook, T. D.; Natoli, S. N.; Fanwick, P. E.; Ren, T. Dimeric Complexes of CoIII(cyclam) with Polyyndiyl Bridge. *Organometallics* **2015**, *34*, 686-689.

(46)   Delor, M.; Scattergood, P. A.; Sazanovich, I. V.; Parker, A. W.; Greetham, G. M.; Meijer, A. J. H. M.; Towrie, M.; Weinstein, J. A. Toward control of electron transfer in donor-acceptor molecules by bond-specific infrared excitation. *Science* **2014**, *346*, 1492-1495.

(47)   Scattergood, P. A.; Delor, M.; Sazanovich, I. V.; Bouganov, O. V.; Tikhomirov, S. A.; Stasheuski, A. S.; Parker, A. W.; Greetham, G. M.; Towrie, M.; Davies, E. S.; Meijer, A. J. H. M.; Weinstein, J. A. Electron transfer dynamics and excited state branching in a charge-transfer platinum(II) donor-bridge-acceptor assembly. *Dalton Trans.* **2014**, *43*, 17677-17693.

(48)   Lichtenberger, D. L.; Renshaw, S. K.; Bullock, R. M. Metal-Acetylide Bonding in $(h^5-C_5H_5)Fe(CO)_2(C=CR)$ Compounds.   Measures of Metal-dp-acetylide-p Interactions from Photoelectron Spectroscopy. *J. Am. Chem. Soc.* **1993**, *115*, 3276-3285.

(49)   Lichtenberger, D. L.; Renshaw, S. K.; Wong, A.; Tagge, C. D. Investigation of Metal-dp-Butadiynyl-p Interactions in $CpFe(CO)_2(C=C-C=CH)$ Using Photoelectron Spectroscopy. *Organometallics* **1993**, *12*, 3522-3526.

(50)   Younus, M.; Long, N. J.; Raithby, P. R.; Lewis, J.; Page, N. A.; White, A. J. P.; Williams, D. J.; Colbert, M. C. B.; Hodge, A. J.; Khan, M. S.; Parker, D. G. Synthesis and characterisation of mono-acetylide and unsymmetrical bis-acetylide complexes of ruthenium and osmium: X-ray structure determinations on [(dppe)(2)Ru(Cl)(C C-C6H4-p- NO2)], [(dppe)(2)Ru(Cl)(C C-C6H3-o-CH3-p-NO2)] and [(dppm)(2)Os(C C-C6H4-p-CH3)(C C-C6H4-p-NO2)]. *J. Organomet. Chem.* **1999**, *578*, 198-209.

(51)   Doisneau, G.; Balavoine, G.; Fillebeen-Khan, T. Synthesis and Some Reactions of Ferrocenylacetylenes. *J. Organomet. Chem.* **1992**, *425*, 113-117.

(52)   Takahashi, S.; Kuriyama, Y.; Sonogashira, K.; Hagihara, N. A Convenient Synthesis of Ethylarenes and Diethynylarenes. *Synthesis* **1980**, 627-630.

(53)   Yu, C. J.; Chong, Y. C.; Kayyem, J. F.; Gozin, M. Soluble ferrocene conjugates for incorporation into self- assembled monolayers. *J. Org. Chem.* **1999**, *64*, 2070-2079.

(54)   *The DIRDIF2008 Program System*; Beurskens, P. T.; Beurskens, G.; deGelder, R.; Garcia-Granda, S.; Gould, R. O.; Smits, J. M. M.; Crystallography Laboratory, University of Nijmegen, The Netherlands, 2008.

(55)   Sheldrick, G. M. A short history of SHELX. *Acta Cryst. A* **2008**, *64*, 112-122.

CHAPTER 3. SYNTHESIS, STRUCTURAL AND SPECTROSCOPIC ANALYSIS OF UNSYMMETRIC DONOR-BRIDGE-ACCEPTOR BIS-ALKYNYL COMPLEXES BASED ON CO(III)(CYCLAM)

Abstract: The reaction between [Co(cyclam)Cl$_2$]Cl and HC$_2$NAP^{iPr} (4-ethynyl-*N*-isopropyl-1,8-naphthalimide) in the presence of Et$_3$N yields [Co(cyclam)(C$_2$NAP^{iPr})Cl]Cl (**1a**, 87%), which reacts with LiC$_2$Y at -78 ^{o}C to afford the donor-bridge-acceptor dyads [Co(cyclam)(C$_2$NAP^{iPr})(C$_2$Y)]Cl with Y as C$_6$H$_4$-4-NMe$_2$ (**2a**, 50%), NAP^{iPr} (**2b**, 37%), Ph (**2c**, 26%) and C$_6$H$_4$-4-N(Ph-4-OMe)$_2$ (**2d**, 19%). [Co(cyclam)(C$_4$NAP^{iPr})Cl]Cl (**1b**, 50%) and [Co(cyclam)(C$_4$NAP^{iPr})(C$_2$C$_6$H$_4$-4-NMe$_2$)]Cl (**2ba**, 28%) were prepared similarly starting from the reaction of [Co(cyclam)Cl$_2$]Cl and TMSC$_4$NAP^{iPr} (4-triethylsilyl-butadiyne-*N*-isopropyl-1,8-naphthalimide) in the presence of Et$_3$N. Molecular structures of **1a** and **2a** were established with single crystal X-ray diffraction, revealing the pseudo-octahedral geometry around the Co(III) center and metric parameters about the first coordination sphere. The redox activities of compounds **1** and **2** were examined using voltammetric techniques, which affirmed that the HOMO and LUMO in **2a, 2d**, and **2ba** were localized on the anilino (donor) and NAP^{iPr} (acceptor), respectively. Steady state emission studies of compounds **1a** and **2a-d** revealed fluorescent profiles similar to that of the free ligand HC$_2$NAP^{iPr}, but with significantly reduced quantum yields. Electronic structures of these compounds were further probed using DFT calculations. Comprehensive examination of the collected data suggests the charge separated state (CSS) undergoes fast charge recombination followed by intersystem crossing and formation of a long-lived ^{T}NAP state.

3.1   Introduction

Donor-bridge-acceptor (*D-B-A*) dyad molecules have received intense interest as the model systems for studying electron transfer processes[1,2] and building blocks for opto-electronic materials.[3,4] Aiming at better understanding and control of the photo-induced electron transfer process in *D-B-A* dyads, several recent studies have probed possible attenuation of the evolution of initial photo-excited states through selective vibrational excitation. Weinstein and coworkers studied a series of *D-B-A* compounds with a *trans*-Pt(II)-bis-alkynyl bridge and found that the photo-induced electron transfer (PET) between phenothiazine (*D*) and naphthalimide (*A*) can be attenuated by the IR excitation of the Pt-bound $C\equiv C$ bonds.[5-8] Rubtsov, Sessler, Beratan and coworkers demonstrated the ET rate retardation by mid-IR excitation in a *D-B-A* ensemble formed by nucleobase pairing (GC),[9] and related the observed modulation to the changes in the density of states in the Marcus curve crossing region.[10]   Rubtsov, Schmehl and coworkers reported a *ca.* 30% enhancement of intramolecular ligand-to-ligand charge transfer rate in a Re(I) compound via selective excitation of the acceptor ligand 4,4'-(dicarboxyethyl)-2,2-bipyridine at 1540 cm^{-1} (ν(bpy)).[11]

Recently, metal alkynyl compounds based on a 3*d* metal supported by cyclam have been investigated by our laboratory.[12] The Co(III)(cyclam) motif is especially attractive because of the feasibility of stepwise alkynylation under mild reaction conditions. This was first demonstrated by Shores and coworkers through the preparation of [Co(cyclam)(C$_2$Ph)Cl]$^+$,[13] and explored by us in attaining the dicobalt complexes bridged by oligoyn-diyls (μ-C$_{2m}$).[14,15] The general preparations of the unsymmetric *trans*-[Co(cyclam)(C$_2$Ar)(C$_2$Ar')]$^+$ type compounds were developed either through an

intermediate *trans*-[Co(cyclam)(C$_2$Ar)(NCMe)][+],[16,17] or via lithiation to install the second

alkynyl.[18] Such Co(III) bis-alkynyls are attractive alternatives to the Pt species studied by

Weinstein since they too provide rigid framework for *D-B-A* dyad, possess vibrationally

excitable Co-C≡C bonds, and due to the inexpensive nature of cobalt. Described in this

chapter are the syntheses of the *trans*-[Co(cyclam)(C$_2$D)(C$_2$A)][+] type complexes, where

D and *A* are C$_6$H$_4$-4-Z (Z = H, NMe$_2$ or N(Ph-4-OMe)$_2$) and *N*-isopropyl-1,8-

napthalimide (NAP^{iPr}), respectively (Scheme 3.1), their structural, spectroscopic and

voltammetric properties.
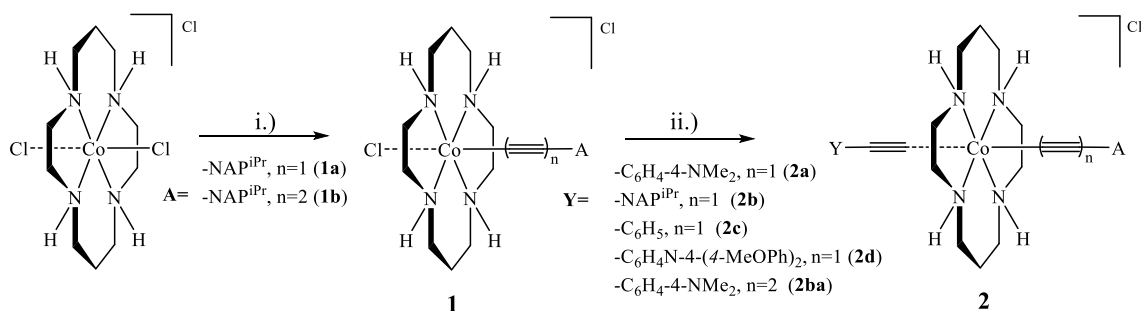
Scheme 3.1. i.) 1.5 equiv HC$_2$NAP^{iPr}/TESC$_4$NAP^{iPr}, CH$_3$OH:THF, reflux, 16h; ii.) 1.2 equiv LiC$_2$Y, THF, -78°C, 4h

3.2   Results and Discussion

3.2.1   Synthesis

As shown in Scheme 3.1, the dissymmetric species were prepared step-wise.

Synthesis of 4-triethylsilyl-butadiyne-*N*-isopropyl-1,8-naphthalimide (TESC$_4$NAP^{iPr}) was

achieved via a modified Cadiot-Chodkiewicz coupling reaction.[19] 4-Ethynyl-*N*-isopropyl-

1,8-naphthalimide[20] (HC$_2$NAP^{iPr}) and 4-ethynyl-*N,N*-bis(4-methoxyphenyl)aniline[21]

(HC$_2$TPA) were prepared according to literature methods. [Co(cyclam)(C$_2$NAP^{iPr})Cl]Cl

(**1a**) was prepared under N$_2$ through the reaction of HC$_2$NAP^{iPr} in weak base conditions

to form an orange microcrystalline solid in 87% yield after purification over silica. [Co(cyclam)(C$_4$NAP^{iPr})Cl]Cl (**1b**) was prepared similarly, resulting in 50% yield of an orange solid.

Synthesis of [Co(cyclam)(C$_2$NAP^{iPr})(C$_2$C$_6$H$_4$-4-NMe$_2$)]Cl (**2a**) was accomplished via addition of 1.2 equiv LiC$_2$C$_6$H$_4$-4-NMe$_2$ in THF to **1a** at -78°C. Reaction at low temperatures prevented scrambling of alkynyl ligands to form a mix of symmetric and dissymmetric products, thereby increasing the synthetic yield of the dissymmetric *D-B-A* species (50%) more than two-fold from the previously published method (20%).[18] [Co(cyclam)(C$_2$NAP^{iPr})$_2$]Cl (**2b**) was prepared similarly in 37% yield, however, its solubility was greatly reduced in comparison to the dissymmetric species. This was attributed to π-π stacking between the planar NAP^{iPr} ligands. Additionally, synthesis of **2b** had to be performed stepwise, as LiC$_2$NAP^{iPr} readily degraded at temperatures above -78°C. [Co(cyclam)(C$_2$NAP^{iPr})(C$_2$Ph)]Cl (**2c**) and [Co(cyclam)(C$_2$NAP^{iPr})(C$_2$TPA)]Cl (**2d**) were prepared like **2a** in 26% and 19% yield respectively after purification. Compounds containing an electron donating substituent (**2a**, **2ba**, and **2d**) yielded a light orange solid. In contrast, synthesis of **2b** and **2c** resulted in bright yellow solids. All compounds presented herein are low spin Co(III) species, and are readily characterized using ^{1}H NMR, UVvis, and FT-IR spectroscopies, ESI mass spectrometry and combustion analysis.

3.2.2 Structure analysis

Molecular structures of complexes **1a** and **2a** were determined using single crystal X-ray diffraction and are shown in Figs 3.1 and 3.2, respectively. Both compounds are in pseudo-octahedral configurations with the cyclam ring encircling the square plane (XY)

and acetylide/chloro ligands occupying the axial positions (Z). The length of the C≡C

bonds were within the expected range, as were the Co-C distances for both **1a** and **2a**

(Table 3.1). In compound **2a** the alkyne bond length varied between C1-C2 and C4-C5,

1.223(4) Å and 1.208(4) Å respectively, due to the *trans* influence. The difference

between the triple bond stretches for **2a** is slightly greater when compared to related

symmetric complexes such as $[Co(cyclam)(C_2Np)_2]OTf$,[23] where the C≡C bonds were

found to be 1.212(5) Å and 1.207(3) Å, owing to the presence of an electron donating

group *trans* to an electron withdrawing group. A similar trend was observed for

$[Co(cyclam)(C_2Ph)(C_2C_6H_4-4-NO_2)]Cl$[18] in which the *acceptor* alkyne bond, 1.214(5) Å,

was longer than the C≡C of the phenyl group, 1.157(5) Å. Similarly, in

$[Co(cyclam)(C_2C_6H_4-4-NMe_2)(C_2Ph)]OTf$,[16] the phenyl C≡C bond, 1.211(6) Å, was

longer than the triple bond of the *donor* group, 1.187(6) Å. Consistent with previously

published structures, the Co-C bond distances in bis-alkynyl **2a** (1.932(3) Å and 1.925(3)

Å) are longer than in mono-alkynyl **1a** (1.888(4)Å) and can be attributed to the greater π

backbonding in **1a** versus **2a**, thereby resulting in a shorter Co-C bond length.[15-18,22]

Investigations into the extended crystal packing revealed that the -NAP^{iPr} substituent of

1a stacked uniformly with the carbonyls at 120° angles with respect to each other to

reduce electron-electron repulsions. Similar stacking was not observed in **2a**, suggesting

the addition of $-C_2C_6H_4-4-NMe_2$ impeded aggregation and helped prevent π-π stacking.

Attempts to grow crystal of the symmetric species, **2b**, have been unsuccessful due to low

solubility.
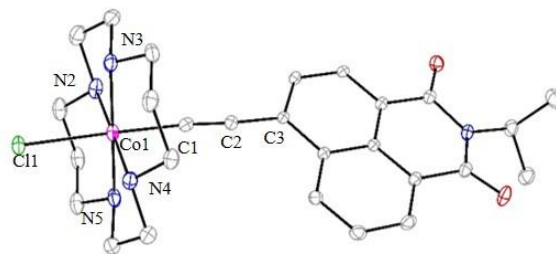
Figure 3.1. ORTEP plot of compound [**1a**]⁺ at 30% probability level; counterion, hydrogen atoms, and solvent molecules were omitted for clarity.
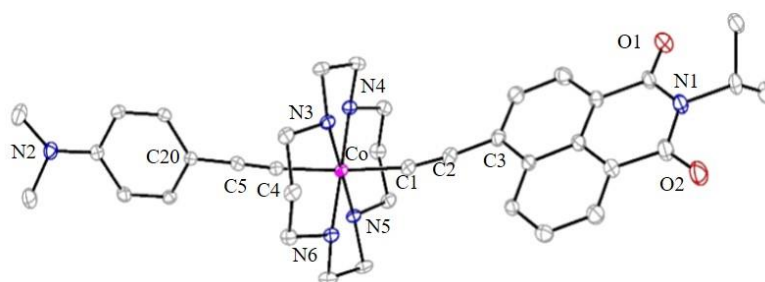
Figure 3.2. ORTEP plot of compound [**2a**]⁺ at 30% probability level; counterion, hydrogen atoms, and solvent molecules were omitted for clarity.

Table 3.1. Selected bond lengths (Å) and angles (°) for compounds [**1a**]⁺and [**2a**]⁺

	[**1a**]⁺	[**2a**]⁺
Co1-C1	1.888 (4)	1.932 (3)
Co1-C4	--	1.925 (3)
Co1-N2/N3*	1.974 (4)	1.989 (2)
Co1-N3/N4*	1.972 (3)	1.996 (2)
Co1-N4/N5*	1.974 (3)	1.981 (2)
Co1-N5/N6*	1.982 (4)	1.9781 (2)
Co1-Cl1	2.3314 (2)	--
C1-C2	1.206 (5)	1.223 (4)
C4-C5	--	1.208 (4)
Cl1-Co-C1	178.51(2)	--
C4-Co-C1	--	176.02 (2)
Co-C1-C2	178.51 (2)	168.6 (2)
C1-C2-C3	176.4 (4)	174.8 (3)
Co1-C4-C5	--	173.6 (2)
C4-C5-C20	--	175.9 (3)

*Indicates nitrogens on the cyclam ring of **2a**

3.2.3   Electrochemistry

The redox profiles of the Co(III)(cyclam) complexes were examined using cyclic voltammetry. The resultant CVs for **1a**, **2a**, **2b, 2c** and **2d** are shown in Fig 3.3 and **1a**, **1b**, **2a**, and **2ba** in Fig 3.4. The electrode potentials (*versus* a ferrocene external standard) for all complexes are collected in Table 3.2. Consistent with previous studies Co^{III} undergoes two irreversible 1e⁻ reductions, (Co^{III}/Co^{II}) and (Co^{II}/Co^{I}), and one irreversible 1e⁻ oxidation (Co^{III}/Co^{IV}), the respective cathodic and anodic waves are indicated in Table 3.2.[18]

Table 3.2. Electrode potentials of all observed redox couples (V) in **1a**, **1b**, **2a-d**, and **2ba**.

	$E_{1/2}$ (**D**)	$E_{1/2}$ (**A**)	E_{pc}(**Co**)	E_{pc}(**Co**)	E_{pa} (**Co**)
1a	−	-1.74 (0.09)	-1.49	-2.25	0.76
2a	0.21 (0.09)	-1.69 (0.06)	-2.11	-2.32	0.98
2b	−	-1.72 (0.08)	-2.14	-2.26	0.70
2c	−	-1.72 (0.06)	-2.09	-2.25	0.64
2d	0.23 (0.07), 0.84 (0.08)	-1.71 (0.07)	-2.11	-2.33	0.81
1b	−	-1.57 (0.06)	-1.39	-1.88	0.71
2ba	0.22 (0.07)	-1.57 (0.07)	-2.10	-2.32	0.98

Data collected vs. Fc⁺/Fc collected in MeCN solutions with 0.1 M n-Bu₄NPF₆ as the supporting electrolyte. Peak separation (ΔE_p) for reversible processes shown in brackets.

For the *D-B-A* dyads **2a** and **2d**, the cyclic voltammograms feature the quasi-reversible 1e⁻ reduction and 1e⁻ oxidation that are ascribed to NAP^{iPr} and the *N*-donor, respectively, from which the electrochemical HOMO-LUMO gap ($E_g = E_{1/2}(D) - E_{1/2}(A)$) are calculated as 1.90 V (**2a**) and 1.94 V (**2d**). For **2d**, the donor species (TPA) undergoes two separate 1e⁻ oxidations at 0.23 V and 0.84 V, where the second oxidation is obscured by the irreversible 1e⁻ oxidation Co^{III}/Co^{IV}. Upon addition of the second alkynyl, the reduction of Co^{III} to Co^{II} shifted approximately 0.62 V to a more negative potential, as shown in Table 3.2. This trend is attributed to increased electron density on the Co center for the bis-alkynyl species. Since the currents of the NAP^{iPr} reduction in **1a** and **2b** are

about the same (Fig 3.3) while the concentration of the latter is one half of the former, **2b** undergoes a quasi-reversible 2e$^-$ reduction, i.e. simultaneous reduction of both NAP^{iPr} groups. It is noteworthy that the reduction potentials of NAP^{iPr} are within a very narrow range for both mono- and bis-acetylide species. Similarly, the reduction of the NAP^{iPr} group was consistently measured at -1.83 V *versus* ferrocene in CH$_2$Cl$_2$ for the Pt(II) based *trans*-acetylide donor-bridge-acceptor species,[7] and the difference in $E_{1/2}$ between the Co(III) and Pt(II) complexes is attributed to the difference in solvents.
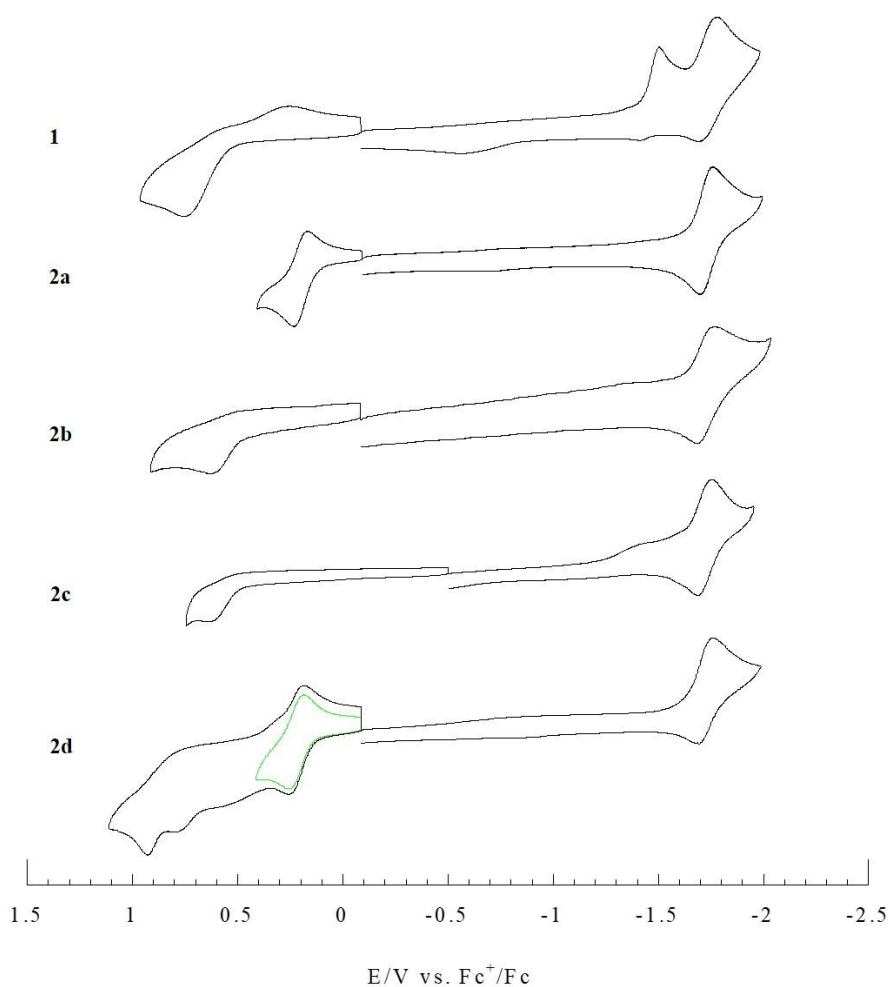
Figure 3.3. Cyclic voltammograms of compounds **1a** and **2a-d** (vs. Fc$^+$/Fc) recorded in 1.0 mM solutions MeCN solutions with 0.1 M n-Bu$_4$NPF$_6$ as the supporting electrolyte. Due to low solubility of **2b**, its CV was recorded in a 0.22 mM solution and scaled to 0.50 mM in the plot.

When the alkynyl bridge is lengthened between Co and -NAP^{iPr}, as is the case for **2ba**, the E$_g$ is reduced to 1.69 V. Comparison of the electrochemical potentials between **2a**, and **2ba** (Table 3.2) show that while the anilino donor is oxidized at similar potentials, 0.21V for **2a** and 0.22V for **2ba**, the acceptor based reduction is shifted to a more positive potential for the -C$_4$NAP^{iPr} species, 0.12 V for **2a** versus **2ba** (Fig 3.4). Compounds **1a** and **1b** follow the same trend with the NAP^{iPr} reduction moving 0.17 V more positive for **1b**. However, DFT experiments suggested this shift is likely an experimental artifact.
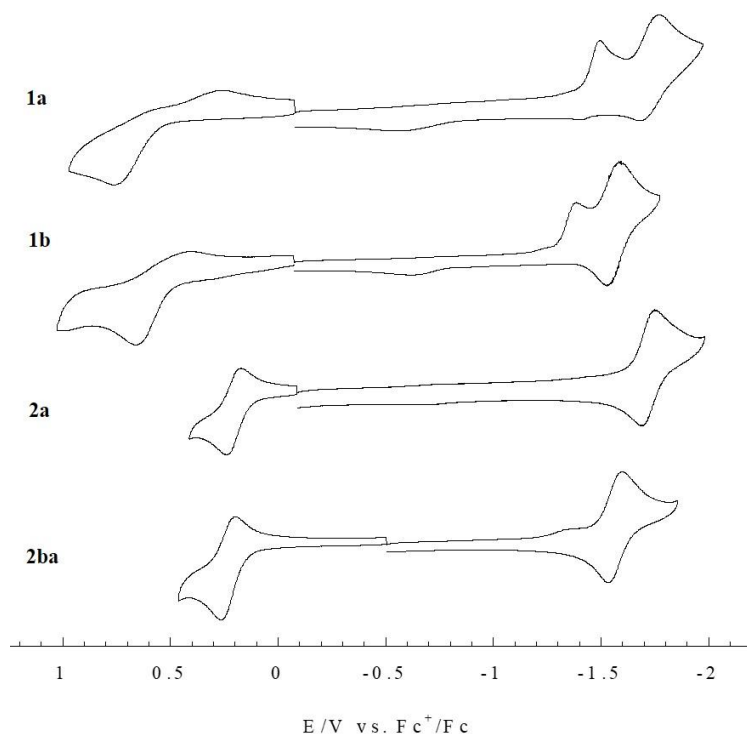
Figure 3.4. Cyclic voltammograms of compounds **1a**, **2a**, **1b**, and **2ba** (vs. Fc$^+$/Fc) collected in 1.0 mM solutions MeCN solutions with 0.1 M n-Bu$_4$NPF$_6$ as the supporting electrolyte.

3.2.4 UV-vis Spectroscopic Analysis

For all of the complexes, the visible window is dominated by a broad and intense peak at 400 nm. The free ligand HC_2NAP^{iPr} displays an intense peak at *ca.* 358 nm (Table 3.2), which is assigned as the $\pi-\pi*$ transition localized on NAP^{iPr}.[7,20] The strong resemblance in the spectral shape and extinction coeffcient between complexes **1a**, **2a-d** and HC_2NAP^{iPr} suggests that the transition at 400 nm has some $\pi-\pi*$ character localized on NAP^{iPr}, an assignment that has been supported by DFT calculations (see discussion below). $[Ru(bpy)_x(PNI\text{-}phen)_y]^{2+}$ (x+y = 3; PNI-phen = 5-(4-piperidinyl1,8-naphthalimide)-1,10-phenanthroline) complexes displayed ground state absorption representing the sum of the chromophores present, which allowed for characterization of the primary absorption transition at 430 nm to be primarily ligand based.[23] Similarly, **2b** has an extinction coefficient at 401 nm, approximately double that of **1a** at 395 nm, further corroborating that the transition occuring *ca.* 400 nm is strongly influenced by $\pi-\pi*$ transition on the NAP^{iPr} ligand (Fig 3.5). The 70 nm red shift from free ligand to complexes **1a** and **2a-d** is clearly due to Co coordination. The broad nature of the 400 nm peak obscures the expected *d-d* ($^1A_{1g} \rightarrow {}^1T_{1g}$, O_h) transition, except in the case of **1a** and **1b** where a weak shoulder peak can be observed around 480 nm. The *D-B-A* species, **2a** and **2d**, display UV bands attributed to the donor ligands. Compound **2a** displays a sharp peak at 290 nm which can be assigned to the π-$\pi*$ transition localized on C_6H_4-4-NMe_2, and compound **2d** has a broad band centered at 330 nm attributed to π-$\pi*$ transitions localized on TPA (Fig 3.5). It should be noted that no such peak is present for **2b** or **2c** due to the absense of a *N*-donor substituent.
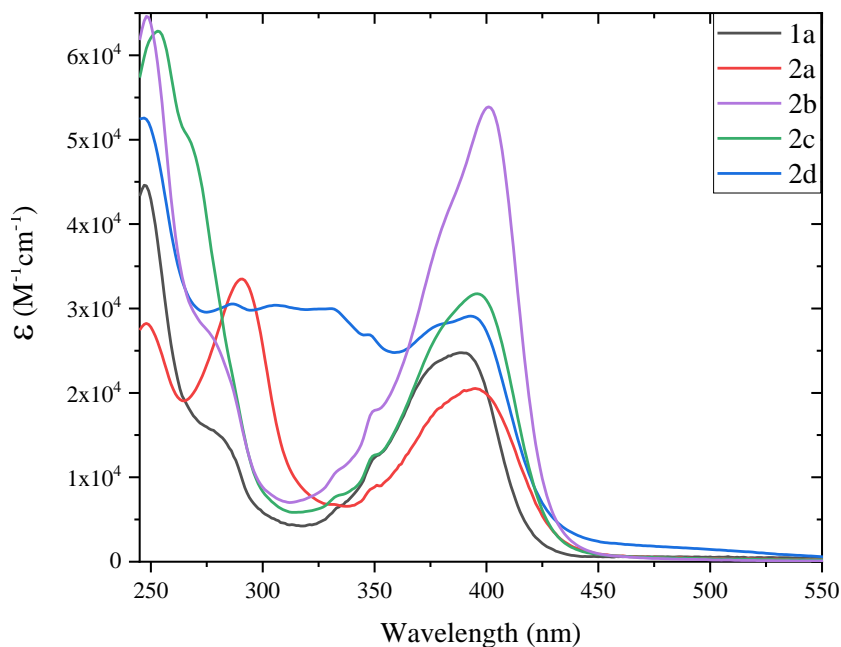
Figure 3.5. Absorption spectra of **1a**, **2a**, **2b**, **2c**, and **2d** in CH_2Cl_2

DFT calculations suggest the transition at 400 nm also possesses both LMCT and MLCT character, molecular orbitals shown in Fig 3.10, involving ligand→$d_{x^2-y^2}/d_z^2$ and partial Co^{III}(cyclam) →NAP charge transfer, respectively (Table 3.4). The mixed metal-ligand character of this transition is consistent with similar *D-B-A* motifs in literature. Weinstein et al. reported a Pt(II) trans-acetylide *D-B-A* species, where *A* = 4-ethynyl-*N*-octyl-1,8-naphthalimide (NAP^Oct), in which the lowest energy transition at 430 nm was assigned to mixed metal-ligand-to-ligand charge transfer (ML/L'CT).[7]
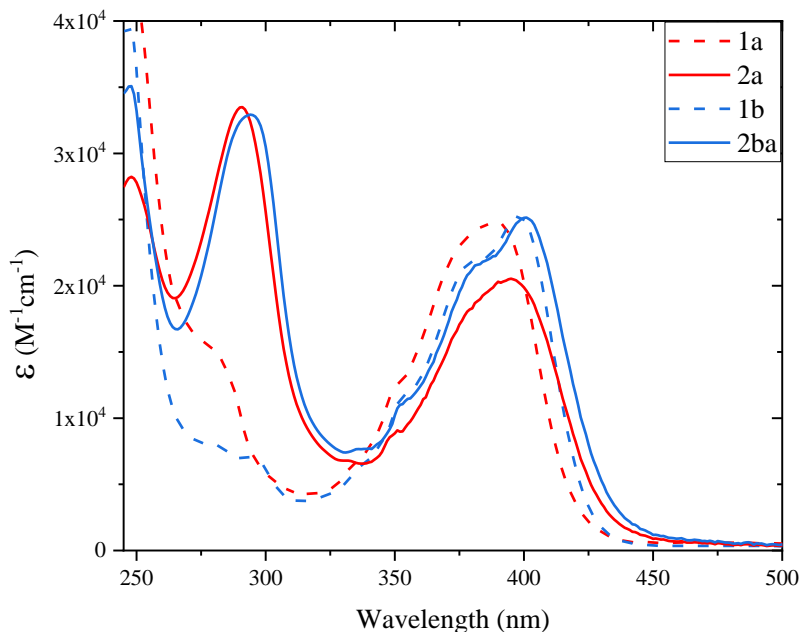
Figure 3.6. Absorption spectrum of **1a** and **2a** (red) versus **1b** and **2b** (blue) in CH_2Cl_2 showing increased fine structuring for the complexes with extended alkyl chains

Comparison of the -C_2NAP^{iPr} (**1a** and **2a**) versus the -C_4NAP^{iPr} species (**1b** and **2b**) in Fig 3.6, shows that the increase in alkynyl chain length results in *ca.* 10 nm shift to longer wavelengths, from 388 nm (**1a**) to 398 nm (**1b**) and 395 nm (**2a**) to 401 nm (**2ba**). The UV-vis profile of the **2a** and **2ba** dyads both display a peak assigned to C_6H_4-4-NMe_2 π-π* transitions at 290 nm and 295 nm respectively. The increased structuring observed in the -C_4NAP^{iPr} series can be attributed to the vibronic progressions on the butadyine bridge; a similar and more discernible trend was observed for Cr^{III}(cyclam′)($C_4TMS/H)_2$ type species (cyclam′ = 5,5,7,12,12,14-hexamethyl-1,4,8,11-tetraazacyclotetradecane or 5,12-dimethyl-1,4,8,11-tetraazacyclotetradecane).[24,25]

3.2.5   Emission Studies

Use of a chromophore as the acceptor group allows for study of emission properties of each complex and the effect of the donor substituent, thereby enabling

elaboration on the structure-property relationship. Initial emission studies revealed that **1a**, **1b**, **2a**, **2b**, **2c**, and **2ba** exhibit similar emission profiles, with a λ_{em} *ca.* 438 nm, that are red-shifted from λ_{em} of the free ligand (401 nm) as shown in Fig 3.7.[26] Literature reports from Castellano and co-workers observed *triplet* emission based on NI/NAP^{Butyl} for Pt(dbbpy)(C$_2$NI)$_2$, where NI = N-butyl-4-ethynylnaphthalimide and dbbpy = 4,4′-di-tert-butyl-2,2′-bipyridine, which was characterized by a large Stokes shift (λ_{em} = 621 nm; λ_{ex} = 420 nm), long lifetime (τ = 124 μs), and high quantum yield (Φ = 21.5%).[27] By comparison, the emission observed for compounds **1** and **2** have low fluorescence quantum yields (Φ_{fl}), small Stokes shifts, and short lifetimes (τ < 1 ns; not observable on the instrument timescale), suggesting it can be attributed to NAP^{iPr} centered *singlet* emission (Table 3.3). Furthermore, the Co(III) center is remote enough to not induce ultrafast intersystem crossing.[26] The mirror image similarity of the absorption and emission spectra and reasonably small Stokes shifts suggest that the observed emission occurs from the same excited state prepared by 400 nm excitation. The emission spectrum in **2d** features a larger peak width and larger Stokes shift, which suggests that different electronic states than the one initially excited are involved in the emission.

Table 3.3. Absorption (λ_{abs}) and emission maxima (λ_{em}) in nm, excitation wavelength (λ_{ex}) in nm, and emission quantum yields (Φ_{fl}) in CH$_2$Cl$_2$

	Φ_{fl}	λ_{abs}	λ_{em}	λ_{ex}
NAP^{iPr}C$_2$H	0.423	350/366	401	340
1a	0.0066	388	438	400
1b	-	398	436	400
2a	0.0068	401	439	400
2ba	-	401	435	400
2b	0.0143	395	439	400
2c	0.0043	397	437	400
2d	0.026	393	461	320
	0.00063	393	461	400

Emission quantum yields were measured for **1a**, **2a-d** and the HC_2NAP^{iPr} ligand (Table 3.3). As expected, the bridging metal center significantly reduces the Φ_{fl} of metal-bound NAP^{iPr} in comparison with that of HC_2NAP^{iPr} (42.3%). For instance, the NAP^{iPr} centered emission was completely quenched when $-C_2NAP^{iPr}$ is axially bonded to Ru_2 in *trans*-$Ru_2(DMBA)_4(C_2NAP^{iPr})_2$.[20]   Compounds **2b** and **2d** had quantum yields of 1.43% and 1.03% respectively, double that of **1**, **2a** and **2c**, which were 0.66%, 0.68%, and 0.43% respectively. This doubling is attributed to the presence of two emissive ligands in the axial positions. While low, these values are comparable to the quantum yields found for Pt bridged *D-B-A* species reported by the Weinstein group, which were *ca.* 5.5%.[7] These quantum yields are also analogous to ferrocenyl naphthalimide donor-acceptor complexes with an alkyl bridge ($\Phi_{fl} = 0.2\%$), where the fluorophore quenching was attributed to the ferrocene redox center.[28]
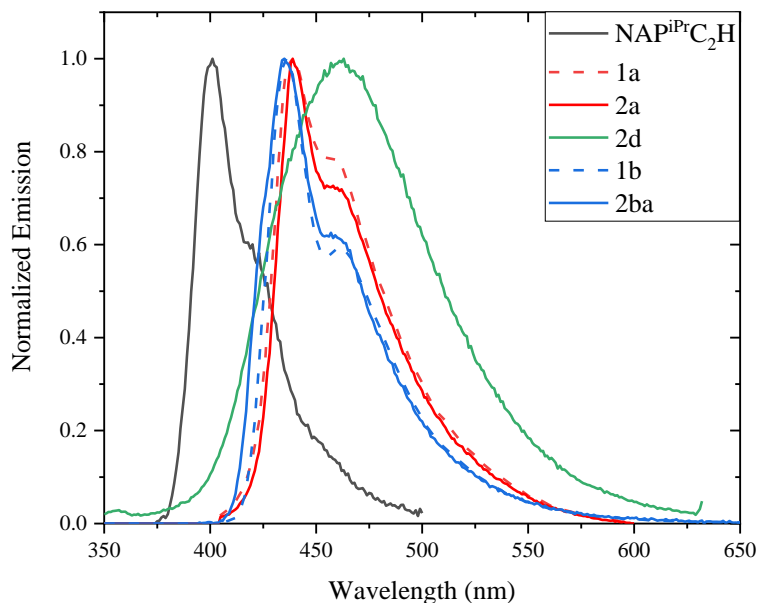
Figure 3.7. Normalized emission spectra in CH_2Cl_2 taken at room temperature, for **1a**, **1b**, **2a**, **2d**, and **2ba** graphed versus $NAP^{iPr}C_2H$

3.2.6 Fourier Transform IR (FT-IR) Spectroscopy

The IR absorption spectra of **1**, **2a** and **2d** are dominated by the asymmetric and symmetric C=O stretching modes of NAP^{iPr} found at 1635 and 1690 cm^{-1} in **1a** and 1653 and 1690 cm^{-1} in **2a** 1648 and 1692 cm^{-1} in **2d** (Fig 3.8). The C≡C stretch in **1a** (2109 cm^{-1}) is significantly stronger and shifted to higher frequency compared to that in **2a** and **2d** (2087 cm^{-1}), suggesting the molecular dipole is altered upon addition of a second alkynyl. This trend is consistent with arguments made by Wageknecht and co-workers[29] in which the presence of the second alkynyl (a strong π acceptor) results in greater antibonding interactions with the filled dπ of the dπ-π(C≡C) than the chloro ligand (a relatively weaker π donor), thereby resulting in a lower υ(C≡C) for **2a** and **2d** than **1a**.
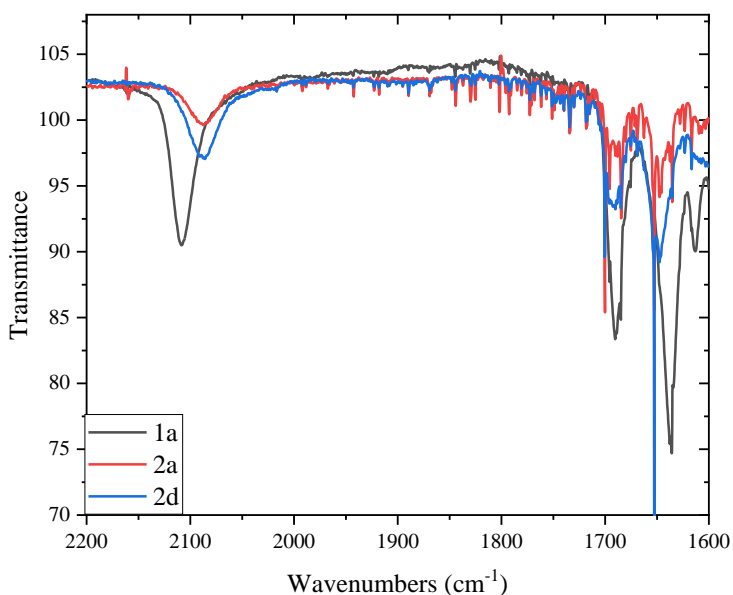
Figure 3.8. ATR-FTIR of **1a** (black), **2a** (red), and **2d** (blue) highlighting C≡C stretch and the C=O stretches.

Lengthening the alkynyl chain between Co and NAP^{iPr} from C$_2$ to a C$_4$ has an effect on both the intensity and separation of the peaks attributed to the C≡C stretches. As

expected, compound **1b** has two C≡C stretches at 2065 cm^{-1} (w) and 2178 cm^{-1} (m), a result of the butadyine bridge. Interestingly, **2ba** has three unique C≡C stretches of varying intensities, 2045 cm^{-1} (w), 2105 cm^{-1} (w), and 2173 cm^{-1} (s), unlike its analogous C$_2$ bridged *D-B-A* compound (**2a**) the C≡C stretches attributed to the *D* and *A* ligands are discernable from each other. Direct comparison of **1a** and **2a** to **1b** and **2ba** (Fig 3.9) suggest the following peak assignments for **2ba**: 2045 cm^{-1} (Co-C≡C-C$_2$*A*), 2105 cm^{-1} (*D*-C≡C-Co), and 2173 cm^{-1} (Co-C$_2$-C≡C-*A*).
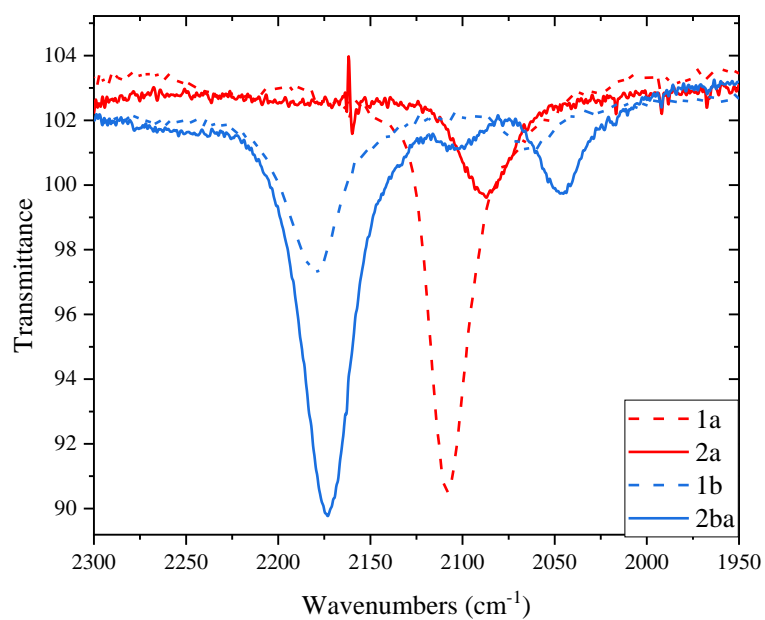
Figure 3.9. FT-IR of **1a** and **2a** (red) versus **1b** and **2ba** (blue) showing the effect extending the alkynyl chain has on υ(C≡C)

3.2.7 Density Functional Theory (DFT) calculations

DFT calculations were performed on geometry optimized structures of [**1a**]$^+$, [**1b**]$^+$, [**2a**]$^+$, [**2b**]$^+$, [**2c**]$^+$, [**2d**]$^+$, and [**2ba**]$^+$ at B3LYP/LanL2DZ level using Gaussian 16 suite,[30] utilizing the crystal structures of [**1a**]$^+$ and [**2a**]$^+$ as the optimization starting point. The energy level results and assumed major transitions are listed in Table 3.4. The calculations and nature of the molecular orbitals (shown in Fig 3.10) suggest that the

absorption band centered at 400 nm is comprised of several transitions likely including (NAP)$\pi \rightarrow \pi^*$ and HOMO$\rightarrow 3d_z^2$ (LMCT). The HOMO orbitals for all compounds have very minor $3d_{xy}$ character, which could be providing a small amount of MLCT character in the ground state absorption spectrum. The HOMO for **2a**, **2ba**, and **2d** is significantly higher in energy than the rest of series due to the electron rich anilino donor, this change in energy is represented in the UV-vis by the presence of the peak *ca.* 300 nm.
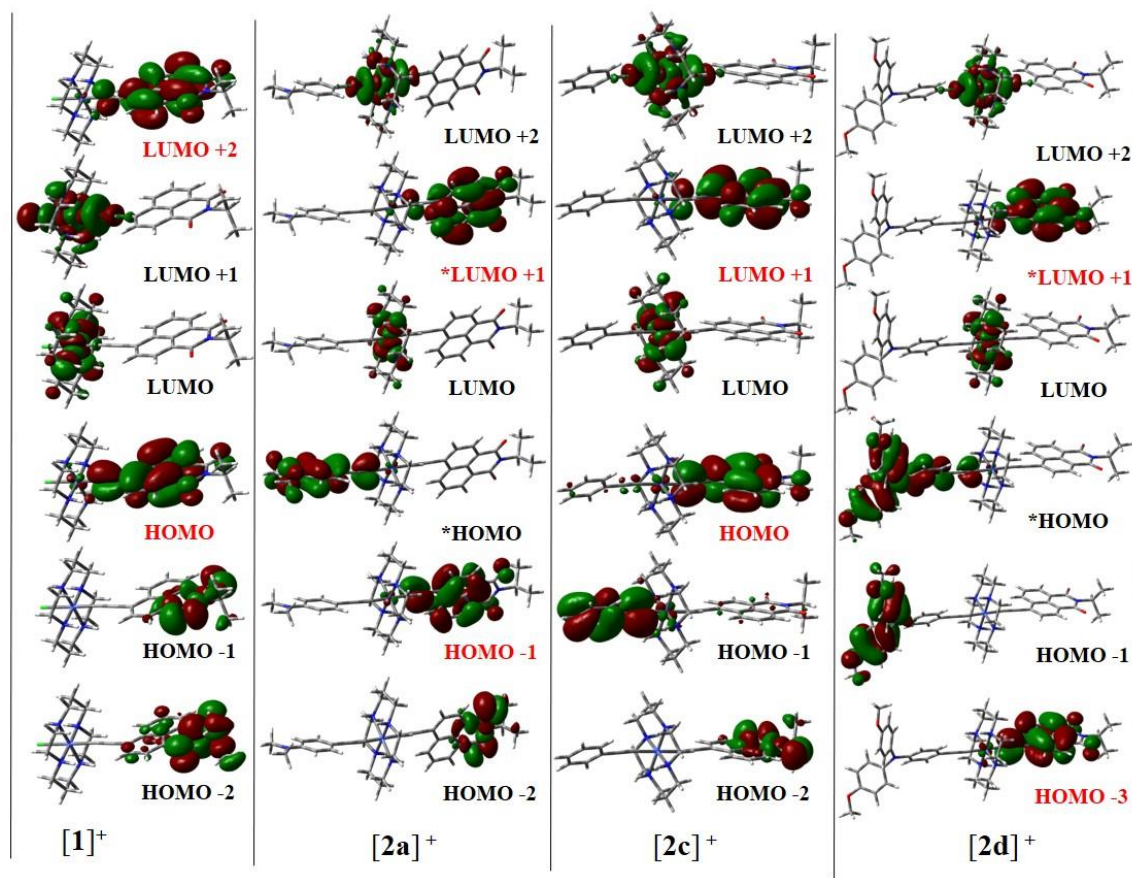
Figure 3.10. Molecular orbital diagrams for [**1a**]⁺, [**2a**]⁺, [**2c**]⁺and, [**2d**]⁺from DFT calculations; the orbitals involved in the (NAP)$\pi \rightarrow \pi^*$ transition are noted in red; *D→A transition for [**2a**]⁺ and [**2d**]⁺

Compounds **1a** and **1b** possess degenerate LUMO and LUMO+1 assigned to the $3d_z^2$ and $3d_{x^2-y^2}$ orbitals. Addition of an alkynyl *trans* to -C₂NAP^{iPr} moves the $3d_z^2$ orbital

to the LUMO+2 for compounds **2a**, **2c**, **2d**, and **2ba** and to the LUMO+3 for **2b**, with the LUMO of all bis-alkynyl species having predominantly Co $3d_{x^2-y^2}$ character with contribution from nitrogens of the cyclam ring. This is in good agreement with electrochemical data in which the first Co reduction (Co^{III}/Co^{II}) moves to more negative potentials in the bis- versus mono- species and the second Co reduction (Co^{II}/Co^{I}) remains relatively constant. The experimentally observed E_g between the donor and acceptor (~2 eV) is also mirrored in the DFT results. *D-B-A* compounds **2a**, **2ba**, and **2d** exhibited a HOMO and LUMO+1 located on the donor and acceptor, respectively (Fig 3.10), with a $\Delta E_{(D \rightarrow A)}$ of 2.45 eV (**2a**), 2.40 eV (2**ba**), and 2.01 eV (**2d**).

Table 3.4. Relative energies (eV) of Molecular Orbitals and major transitions (eV) calculated at B3LYP/LanL2DZ level

	$[1a]^+$	$[1b]^+$	$[2a]^+$	$[2ba]^+$	$[2b]^+$	$[2c]^+$	$[2d]^+$
LUMO+4	-3.05	-3.15	-2.75	-2.72	-3.16	-2.99	-2.78
LUMO+3	-3.21	-3.29	-2.91	-3.02	-4.35	-3.13	-2.94
LUMO+2	-4.82	-4.68	-3.92	-3.92	-4.71	-4.14	-3.92
LUMO+1	-5.12	-5.12	-4.52	-4.41	-4.73	-4.63	-4.52
LUMO	-5.12	-5.12	-4.54	-4.57	-4.98	-4.76	-4.57
HOMO	-8.49	-8.16	-6.97	-6.97	-8.35	-8.25	-6.53
HOMO-1	-9.01	-8.76	-8.14	-7.86	-8.35	-8.44	-7.73
HOMO-2	-9.06	-8.82	-8.76	-8.57	-8.93	-8.84	-7.89
HOMO-3	-9.20	-8.95	-8.82	-8.63	-8.93	-8.90	-8.14
HOMO-4	-9.50	-9.20	-8.84	-8.73	-8.98	-9.03	-8.49
[a]$(NAP)\pi \rightarrow \pi^*$	3.67 (338 nm)	3.48 (356 nm)	3.62 (343 nm)	3.45 (359 nm)	3.62 (343 nm)	3.62 (343 nm)	3.62 (343 nm)
[b]$D \rightarrow A$	--	--	2.45 (506 nm)	2.56 (484 nm)	--	--	2.01 (617 nm)
[c]$HOMO \rightarrow 3d_{x^2-y^2}$	3.37 (368 nm)	3.04 (408 nm)	2.43 (510 nm)	2.40 (517 nm)	3.37 (368 nm)	3.49 (355 nm)	1.96 (633)
[d]$HOMO \rightarrow 3d_{z^2}$	3.37 (368 nm)	3.04 (408 nm)	3.05 (407 nm)	3.05 (407 nm)	4.00 (310 nm)	4.11 (302 nm)	2.61 (475 nm)

[a]**1a** and **1b** (HOMO→L+2); **2a** and **2ba** (H-1→L+2); **2b** and **2c** (HOMO→L+1); **2d** (H-3→L+1) [b]HOMO→L+1. [c] $3d_{x^2-y^2}$ lies on LUMO for all compounds. [d] $3d_{z^2}$ lies on LUMO (**1a** and **1b**), L+2 (**2a**, **2ab**, **2c**, and **2d**) and L+3 (**2b**).

3.3 Conclusions

Through step-wise addition, syntheses of dissymmetric Co(III) *D-B-A* complexes were accomplished in respectable yields in order to probe the CSS with time-resolved infrared (TRIR) spectroscopy. New variations of the *D-B-A* complexes will focus on systematically altering each component of the system. Specific research targets include: i) increasing the robustness and/or complexity of the *D* and *A* substituents and ii) new electronic properties afforded by changing the bridging metal center. Bridging metal

centers of interest include other earth abundant *3d* metals, like Cr, as well as *4d* metal centers like Ru. Use of Cr would introduce a phosphorescent *3d* metal center into the system and could allow for investigation of cis vs. trans chromophore complexes.[22,25] Ru alkynyl species have received attention for use in studying non-linear optics (NLO)[31,32] and promising power conversion efficiencies.[33] Through collaborations, the excited state dynamics for compounds **1a**, **2a**, and **2d** are currently being probed to look at the evolution of initial excited state(s) in *D-B-A* and its vibronic attenuation using ultra-fast timescale pump(UV)-probe(IR) and pump(UV)-pump(IR)-probe(IR) techniques, respectively. Higher level TD-DFT computation is also underway to better understand the nature of the absorption, emission, and excited state dynamics experimentally observed.

3.4   Experimental

3.4.1   Materials and Measurements

[Co(cyclam)Cl$_2$]Cl was prepared according to literature procedures.[34]   Also prepared according to literature procedures was 4-ethynyl-*N*-isopropyl-1,8-naphthalimide (HC$_2$NAP^{iPr})[20] and 4-ethynyl-*N,N*-bis(4-methoxyphenyl)aniline (HC$_2$TPA) via a Sonogashira coupling reaction.[21,35] Tetrahydrofuran (THF) was distilled over Na/benzophenone under a dry N$_2$ atmosphere. Diisopropylamine and triethylamine were purchased from Acros Organics and Fisher chemical, respectively, and then distilled over potassium hydroxide. 4-ethynyl-*N,N*-dimethylaniline (HC$_2$C$_6$H$_4$-4-NMe$_2$) was purchased from Sigma Aldrich. All alkynylation reactions were carried out using Schlenk techniques under dry N$_2$. Crystallographic data for **1a** and **2a** is provided in Table 3.5.

3.4.2   Spectroscopic Measurements and Computational Details

UV-Vis-NIR spectra were obtained with a JASCO V-670 UV-Vis-NIR spectrophotometer. Infrared spectra were obtained on a JASCO FT-IR 6300 spectrometer via ATR on a ZnSe crystal. ESI-MS was carried out on an Advion Mass Spectrometer. ^{1}H NMR spectra were recorded on a Varian INOVA300 NMR with chemical shifts (δ) referenced to the solvent signal (CD_3OD at 4.88 and 3.31 ppm; $CDCl_3$ at 7.26 ppm). Cyclic voltammograms were recorded in 0.1 M n-Bu_4NPF_6 and 1.0 mM cobalt species solution (CH_3CN, Ar degassed) using a CHI620A voltammetric analyzer with a glassy carbon working electrode (diameter = 2 mm), Pt-wire counter electrode, and a Ag/AgCl reference electrode with ferrocene used as an external reference. Emission studies and quantum yields were measured on a Varian Cary Eclipse fluorescence spectrophotometer. Elemental analysis was performed by Atlantic Microlab, Inc in Norcross, GA. Spin-unrestricted DFT calculations were performed with the B3LYP functional and LANL2DZ basis sets, as implemented in the Gaussian 16 program.[30]

Table 3.5. Experimental Crystal Data for Compounds [**1a**]$^+$ and [**2a**]$^+$

Compound	[**1a**]$^+$	[**2a**]$^+$
Chemical Formula	$C_{27}H_{36}ClCoN_5O_2 \cdot$ 0.101(NO$_3$)$\cdot$1.394(CH$_4$O)$\cdot$ 0.899(Cl)	2($C_{37}H_{46}CoN_6O_2$)$\cdot$ $C_4H_{10}O\cdot$0.576(NO$_3$)$\cdot$ 2.386(CH$_4$O)$\cdot$1.42Cl
Formula Weight	639.78	1568.23
Space group	$P2_1/c$	$P2_1/n$
a, Å	10.1281 (4)	10.4954 (8)
b, Å	27.7813 (11)	30.009 (2)
c, Å	33.9862 (13)	12.6240 (9)
β, °	95.2146 (14)	95.882 (3)
V, Å^3	9523.2 (6)	3955.1 (5)
λ, Å	0.71073Å	0.71073Å
Z	12	2
$\Delta\rho_{max}$, $\Delta\rho_{min}$ (e Å^{-3})	0.84, −0.65	0.57, −0.96
T, K	100	100
$(\sin\theta/\lambda)_{max}$ (Å^{-1})	0.667	0.715
R	0.035	0.057
R$_w$ (F^2)	0.149	0.144

3.4.3   Synthesis of Compounds **1a**, **2a**, **2b**, **2c** and **2d**

Synthesis of [Co(cyclam)(C$_2$NAP^{iPr})Cl]Cl (**1a**).   [Co(cyclam)Cl$_2$]Cl (277 mg, 0.76 mmol) was dissolved in 50 mL CH$_3$OH to which a 20 mL solution of THF containing 4-ethynyl-*N*-isopropyl-1,8-naphthalimide (241 mg, 0.91 mmol) was added and purged with N$_2$. Upon addition of Et$_3$N (2.0 mL, 15 mmol) the solution darkened and was refluxed for 16 h. Silica plug purification with CH$_3$OH/CH$_2$Cl$_2$ (v/v, 1:6) eluted the product as an orange band. Recrystallization from methanol and ether yielded 392 mg of **1a** as an orange solid. (87% based on [Co(cyclam)Cl$_2$]Cl). ESI-MS: [M]$^+$, 556.2; ^{1}H NMR (CD$_3$OD, δ): δ 8.93 (dd, *J* = 8.4, 1.3 Hz, 1H), 8.55 (dd, *J* = 7.4, 1.3 Hz, 1H), 8.45 (dd, *J* = 7.7, 2.3 Hz, 1H), 7.95 (dd, *J* = 7.7, 2.2 Hz, 1H), 7.91 – 7.81 (m, 1H), 5.48 – 5.38 (m, 1H), 5.34 (d, *J* = 9.5 Hz, 4H), 3.07 – 2.49 (m, 16H), 2.03 (t, *J* = 13.7 Hz, 2H), 1.76 –

1.67 (m, 1H), 1.58 (dd, J = 6.9, 2.0 Hz, 6H), 1.38 – 1.26 (m, 1H). Visible spectra, λ_{max} (nm, ε (M^{-1} cm^{-1})): 388 (24,800), 478 (314); IR (cm^{-1}): C=O: 1635 (s), 1690 (s); C≡C: 2109 (s). Anal. Found (calcd) for $C_{27}H_{38}N_5O_4Cl_2Co$ (**1a**·$2H_2O$): C, 51.60 (51.06); H, 6.12 (6.41); N, 11.14 (11.14).

Synthesis of [Co(cyclam)(C_2NAP^{iPr})($C_2C_6H_4$-4-NMe_2)]Cl (**2a**). [Co(cyclam)(C_2NAP^{iPr})Cl]Cl (138 mg, 0.23 mmol) was dried under vacuum. A 4 mL THF solution of $LiC_2C_6H_4$-4-NMe_2 (40 mg, 0.28 mmol) was added via cannula while stirring at -78°C. The solution turned dark red and was allowed to slowly warm to room temperature over a period of 8 h. The resulting dark orange solution was purified over silica. The desired product eluted as a yellow band with CH_3OH/CH_2Cl_2 (v/v, 1:6). Recrystallization from methanol and ether yielded 81 mg of **2a**. (50% based on **1a**). ESI-MS: $[M]^+$, 665.4; ^1H NMR (CD_3OD, δ): δ 9.06 (d, J = 8.3 Hz, 1H), 8.55 (d, J = 7.2 Hz, 1H), 8.45 (d, J = 7.7 Hz, 1H), 7.98 (d, J = 7.8 Hz, 1H), 7.85 (t, J = 8.0 Hz, 1H), 7.37 (d, J = 8.4 Hz, 2H), 6.72 (d, J = 8.8 Hz, 2H), 5.47 – 5.36 (m, 1H), 4.83 (s, 4H), 3.06 (d, J = 12.2 Hz, 4H), 2.95 (d, J = 5.0 Hz, 6H), 2.64 (d, J = 41.3 Hz, 14H), 1.95 (d, J = 15.7 Hz, 2H), 1.59 (d, J = 7.4 Hz, 6H). Visible spectra, λ_{max} (nm, ε (M^{-1} cm^{-1})): 291 (33,500), 395 (20,500); IR (cm^{-1}): C=O: 1653 (s), 1690 (s); C≡C: 2087 (w). Anal. Found (calcd) for $C_{38}H_{48}N_6O_2Cl_3Co$ (**2a**·CH_2Cl_2): C, 58.45 (58.06); H, 6.30 (6.15); N, 11.13 (10.69).

Synthesis of [Co(cyclam)(C_2NAP^{iPr})$_2$]Cl (**2b**). To a 20 mL THF solution containing LiC_2NAP^{iPr} (77 mg, 0.29 mmol) was added vacuum dried **1a** (100 mg, 0.17 mmol). The dark red solution was stirred at -78°C for 4 h and then quenched with air. Upon solvent removal, the residue was purified by column chromatography (SiO_2, CH_3OH/CH_2Cl_2 v/v, 1:6) and eluted as a yellow band. The product was then rinsed with

CH$_3$OH, the filtrate collected and recrystallized from CH$_2$Cl$_2$ and ether to yield 57 mg of **2b** as a yellow solid. (37% based on **1a**). ESI-MS: [M]$^+$, 783.4; ^{1}H NMR (CD$_3$OD, δ): δ 9.10 (d, J = 7.5 Hz, 2H), 8.59 (d, J = 6.2 Hz, 2H), 8.49 (d, J = 7.7 Hz, 2H), 8.03 (d, J = 7.7 Hz, 2H), 7.95 – 7.83 (m, 2H), 5.48 – 5.37 (m, 2H), 4.99 (d, J = 20.6 Hz, 4H), 3.06 (d, J = 12.4 Hz, 4H), 2.85 – 2.59 (m, 12H), 2.02 (d, J = 16.1 Hz, 2H), 1.60 (d, J = 6.9 Hz, 12H), 1.13 – 0.90 (m, 2H). Visible spectra, λ$_{max}$ (nm, ε (M^{-1} cm^{-1})): 401 (53,900); IR (cm^{-1}): C=O: 1646 (m), 1685 (m); C≡C: 2086 (w). Anal. Found (calcd) for C$_{44}$H$_{56}$N$_6$O$_8$Cl$_1$Co (**2b**·4H$_2$O): C, 59.67 (59.29); H, 6.33 (6.17); N, 9.10 (9.43).

Synthesis of [Co(cyclam)(C$_2$NAP^{iPr})(C$_2$Ph)]Cl (**2c**). In a 100mL schlenck flask, **1a** (150 mg, 0.25 mmol) was dried under vacuum. A 6 mL THF solution of LiC$_2$Ph (0.28 mmol) was added while stirring at -78°C, turning the solution bright red. After 2 h, the solution was allowed to warm to room temperature, turning from red to orange. Upon quenching with CH$_3$OH, the solution turned light brown. Solvent was removed and the residue was purified by silica plug purification (hexanes/CH$_3$OH/CH$_2$Cl$_2$ v/v, 1:1:8), eluting as a yellow band. Recrystallization from methanol and ether yielded 43 mg of **2c** as a yellow solid. (26% based on **1a**). ESI-MS: [M]$^+$, 622.4; ^{1}H NMR (CD$_3$OD, δ): 9.08 (d, J = 8.1 Hz, 1H), 8.57 (d, J = 7.3 Hz, 1H), 8.47 (d, J = 7.8 Hz, 1H), 7.99 (d, J = 7.6 Hz, 1H), 7.92 – 7.80 (m, 1H), 7.51 (d, J = 7.6 Hz, 2H), 7.29 (t, J = 7.4 Hz, 2H), 7.20 (d, J = 6.1 Hz, 1H), 5.50 – 5.40 (m, 1H), 4.81 (s, 4H), 3.08 – 2.96 (m, 4H), 2.65 (d, J = 38.5 Hz, 14H), 1.96 (d, J = 15.0 Hz, 2H), 1.59 (d, J = 7.2 Hz, 6H). Visible spectra, λ$_{max}$ (nm, ε (M^{-1} cm^{-1})): 396 (31,700); IR (cm^{-1}): C=O: 1645 (s), 1689 (s); C≡C: 2089 (s). Anal. Found (calcd) for C$_{36}$H$_{43}$N$_5$O$_2$Cl$_3$Co (**2c**·CH$_2$Cl$_2$): C, 58.00 (58.19); H, 6.18 (5.83); N, 9.58 (9.43).

Synthesis of [Co(cyclam)(C$_2$NAP^{iPr})(C$_2$TPA)]Cl (**2d**). A 100 mL Schlenck tube was charged with 46 mg (0.08 mmol) of **1a** and dried under vacuum. An 8 mL THF solution of LiC$_2$TPA (52 mg, 0.16 mmol) was added while stirring at -78°C, turning the solution bright red. The solution was allowed to stir for 3 h and then quenched with CH$_3$OH. Solvent was removed, the crude residue was purified by column chromatography (SiO$_2$, CH$_3$OH/CH$_2$Cl$_2$ v/v, 1:6), eluting as an orange band, and recrystallized from CH$_2$Cl$_2$/hexanes to yield 13 mg of orange solid (19% based on **1a**). ESI-MS: [M]$^+$, 849.7; ^{1}H NMR (CD$_3$OD, δ): δ 9.06 (dd, J = 8.3, 1.2 Hz, 1H), 8.55 (dd, J = 7.3, 1.1 Hz, 1H), 8.45 (d, J = 7.7 Hz, 1H), 7.98 (d, J = 7.7 Hz, 1H), 7.85 (t, J = 7.8 Hz, 1H), 7.32 (d, J = 8.7 Hz, 2H), 7.03 – 6.97 (m, 4H), 6.90 – 6.85 (m, 4H), 6.80 (d, J = 8.6 Hz, 2H), 5.41 (hept, J = 13.6, 6.8 Hz, 1H), 4.83 (s, 4H), 3.76 – 3.69 (m, 2H), 3.07 – 2.95 (m, 4H), 2.73 – 2.58 (m, 10H), 2.01 – 1.84 (m, 5H), 1.59 (d, J = 7.0 Hz, 6H). Visible spectra, λ$_{max}$ (nm, ε (M^{-1} cm^{-1})): 306 (30,400), 398 (29,100), 480 (1205); IR (cm^{-1}): C=O: 1648 (s), 1692 (s); C≡C: 2087 (w). Anal. Found (calcd) for C$_{49.5}$H$_{55}$N$_6$O$_4$Cl$_2$Co (**2d**·0.5CH$_2$Cl$_2$): C, 63.50 (64.07); H, 6.33 (5.97); N, 8.79 (9.06).

3.4.4 Synthesis of Compounds TESC$_4$NAP^{iPr}, 1b and 2b

Synthesis of 4-bromo-ethynyl-*N*-isopropyl-1,8-naphthalimide (BrC$_2$NAP^{iPr}). 4-ethynyl-*N*-isopropyl-1,8-naphthalimide (800 mg, 3.0 mmol) was dissolved in acetone with *N*-bromosuccinimide (1.08 grams, 6.1 mmol) and AgNO$_3$ (52 mg, 0.31 mmol). The solution was stirred at room temperature overnight. The crude reaction mixture was purified via a silica gel plug (SiO$_2$, hexanes/CH$_2$Cl$_2$ v/v, 1:1) to yield 980 mg of the desired product as a light yellow solid (94% based on 4-ethynyl-*N*-isopropyl-1,8-naphthalimide). ^{1}H NMR (CDCl$_3$, δ): δ 8.60 (m, 2H), 8.50 (d, J = 7.6 Hz, 1H), 7.88 (d, J

= 7.4 Hz, 1H), 7.82 (t, 1H), 5.43 (h, 1H), 1.59 (d, 6H). IR (cm^{-1}): C=O: 1653 (s), 1693 (s); C≡C: 2188 (s).

Synthesis of 4-triethylsilyl-butadiyne-*N*-isopropyl-1,8-naphthalimide (TESC$_2$NAP^{iPr}). A 3-kneck round bottom flask was fitted with a side-arm containing CuI (450 mg, 2.4 mmol) and charged with triethylsilylacetylene (0.90 mL, 5.0 mmol) and dry THF (10 mL). Upon cooling to -10°C, nBuLi (1.6 M in hexanes, 3.0 mL, 4.8 mmol) was added while stirring and warming to 0°C. After 20 min, CuI was added and the solution immediately turned orange. It was allowed to stir and warm to room temperature for 1h. Pyridine (29 mL) was added while the solution stirred at -10°C. A solution of dry THF (30 mL) and 4-bromo-ethynyl-*N*-isopropyl-1,8-naphthalimide (820 mg, 2.4 mmol) was added dropwise over 1.5 h. The solution turned darker red. Upon complete addition, the reaction was allowed to stir an additional 10 min and quenched with CH$_3$OH. The solvent was removed under vacuum. The crude material was extracted from brine with CH$_2$Cl$_2$ and dried over MgSO$_4$. Purification was achieved by rinsing the red solution through a CH$_2$Cl$_2$ silica plug followed by column chromatography (SiO$_2$, hexanes/CH$_2$Cl$_2$ v/v, 1:1). Recrystallization from CH$_2$Cl$_2$ with CH$_3$OH yielded 757 mg of desired product as a yellow solid. (79% based on 4-bromo-ethynyl-*N*-isopropyl-1,8-naphthalimide). ^{1}H NMR (CDCl$_3$, δ): δ 8.61 (d, *J* = 8.2 Hz, 2H), 8.49 (d, *J* = 7.7 Hz, 1H), 7.93 (d, *J* = 7.6 Hz, 1H), 7.82 (t, 1H), 5.48 – 5.37 (m, 1H), 1.59 (d, *J* = 7.0 Hz, 6H), 1.07 (t, *J* = 7.8 Hz, 9H), 0.72 (q, *J* = 7.9 Hz, 6H).Visible spectra, λ$_{max}$ (nm, ε (M^{-1} cm^{-1})): 367 (31,500), 386 (37,100); IR (cm^{-1}): C=O: 1655 (s), 1695 (s); C≡C: 2097 (s), 2099 (s), 2197 (m).

Synthesis of [Co(cyclam)(C$_4$NAP^{iPr})Cl]Cl (**1b**). 4-triethylsilyl-butadiyne-*N*-isopropyl-1,8-naphthalimide (645 mg, 1.6 mmol) was dissolved in minimal THF, added

to a solution of 50 mL CH_3OH containing [Co(cyclam)Cl_2]Cl (880 mg, 2.42 mmol) and purged with N_2. Upon addition of Et_3N (4.2 mL, 31 mmol), the solution was refluxed for 16 h. The desired product was purified over a silica plug, eluting as an orange band with (CH_3OH/CH_2Cl_2 v/v, 1:7). Recrystallization from methanol and ether yielded 499 mg of **1b** as an orange solid. (50% based on [Co(cyclam)Cl_2]Cl). ESI-MS: [M]$^+$, 579.8; ^{1}H NMR (CD$_3$OD, δ): δ 8.60 (dd, J = 15.4, 7.8 Hz, 2H), 8.45 (d, J = 7.8 Hz, 1H), 7.88 (d, J = 7.8 Hz, 2H), 5.42 (s, 1H), 5.28 (s, 2H), 2.97 – 2.63 (m, 16H), 2.50 (d, J = 10.5 Hz, 2H), 2.08 – 1.92 (m, 2H), 1.57 (d, J = 7.2 Hz, 6H). Visible spectra, λ_{max} (nm, ε (M^{-1} cm^{-1})): 398 (25,300), 480 (196); IR (cm^{-1}): C=O: 1649 (s), 1693 (s); C≡C: 2065 (w), 2178 (m). Anal. Found (calcd) for $C_{31}H_{48}N_5O_6Cl_6Co$ (**1b**·2CH$_2$Cl$_2$·4H$_2$O): C, 42.99 (43.38); H, 6.00 (5.63); N, 8.32 (8.16).

Synthesis of [Co(cyclam)(C$_4$NAP^{iPr})(C$_2$C$_6$H$_4$-4-NMe$_2$)]Cl (**2ba**). To a Schlenck flask containing **1b** (130 mg, 0.21 mmol) was added LiC$_2$C$_6$H$_4$-4-NMe$_2$ (40 mg, 0.28 mmol) in 10 mL THF, while stirring at -78°C. The red solution was allowed to stir, gradually warming to room temperature over a period of 4 h. Solvent was removed, and the crude mixture was purified over a silica gel plug, eluting as a yellow band ($CH_3OH/CHCl_3$ v/v, 1:6). Recrystallization from methanol and ether yielded 43 mg of **2ba** as a yellow solid. (28% based on **1b**). ESI-MS: [M]$^+$, 688.6; Visible spectra, λ_{max} (nm, ε (M^{-1} cm^{-1})): 294 (32,900), 401 (25,200); IR (cm^{-1}): C=O: 1652 (s), 1696 (s); C≡C: 2045 (w), 2105 (w), 2173 (s). Anal. Found (calcd) for $C_{40}H_{47}N_6O_2Cl_4Co$ (**2ba**·CHCl$_3$): C, 56.49 (56.88); H, 6.01 (5.61); N, 9.74 (9.95).

3.4.5 X-ray Crystallographic Analysis

Single crystals of **1a** were obtained from the slow diffusion of hexanes/ether (v/v, 1:2) into CH_3OH containing **1a**. Single crystals of **2a** were grown from slow diffusion of hexanes/ether (v/v, 1:1) into a CH_2Cl_2/CH_3OH (v/v, 1:1) solution containing **2a**. X-ray diffraction data was obtained on a Bruker Quest diffractometer with Mo Kα radiation (λ=0.71073Å) at 100K. Data were collected; reflections were indexed and processed using APEX3.[36] The space groups were assigned and the structures were solved by direct methods using XPREP within the SHELXTL suite of programs[37,38] and refined using Shelxle.[39,40]

3.5 References

(1)   Albinsson, B.; Mårtensson, J. Long-range electron and excitation energy transfer in donor–bridge–acceptor systems. *J. Photochem. Photobiol. C* 2008, *9*, 138-155.

(2)   Gray, H. B.; Halpern, J. Distant charge transport. *Proc Natl Acad Sci U S A* 2005, *102*, 3533 LP - 3533 DO - 10.1073/pnas.0501035102.

(3)   Lin, Y. Z.; Li, Y. F.; Zhan, X. W. Small molecule semiconductors for high-efficiency organic photovoltaics. *Chem. Soc. Rev.* 2012, *41*, 4245-4272.

(4)   Lu, L. Y.; Zheng, T. Y.; Wu, Q. H.; Schneider, A. M.; Zhao, D. L.; Yu, L. P. Recent Advances in Bulk Heterojunction Polymer Solar Cells. *Chem. Rev.* 2015, *115*, 12666-12731.

(5)   Delor, M.; Keane, T.; Scattergood, P. A.; Sazanovich, I. V.; Greetham, G. M.; Towrie, M.; Meijer, A. J. H. M.; Weinstein, J. A. On the mechanism of vibrational control of light-induced charge transfer in donor–bridge–acceptor assemblies. *Nature Chem.* 2015, *7*, 689-695.

(6)   Delor, M.; Scattergood, P. A.; Sazanovich, I. V.; Parker, A. W.; Greetham, G. M.; Meijer, A. J. H. M.; Towrie, M.; Weinstein, J. A. Toward control of electron transfer in donor-acceptor molecules by bond-specific infrared excitation. *Science* 2014, *346*, 1492-1495.

(7)   Scattergood, P. A.; Delor, M.; Sazanovich, I. V.; Bouganov, O. V.; Tikhomirov, S. A.; Stasheuski, A. S.; Parker, A. W.; Greetham, G. M.; Towrie, M.; Davies, E. S.; Meijer, A. J. H. M.; Weinstein, J. A. Electron transfer dynamics and excited state

branching in a charge-transfer platinum(II) donor-bridge-acceptor assembly. *Dalton Trans.* 2014, *43*, 17677-17693.

(8)   Rubtsov, I. V. STATE-SPECIFIC ELECTRON TRANSFER Shake it off. *Nature Chem.* 2015, *7*, 683-684.

(9)   Lin, Z. W.; Lawrence, C. M.; Xiao, D. Q.; Kireev, V. V.; Skourtis, S. S.; Sessler, J. L.; Beratan, D. N.; Rubtsov, I. V. Modulating Unimolecular Charge Transfer by Exciting Bridge Vibrations. *J. Am. Chem. Soc.* 2009, *131*, 18060-18062.

(10)   Ma, Z.; Lin, Z. W.; Lawrence, C.; Rubtsov, I. V.; Antoniou, P.; Skourtis, S. S.; Zhang, P.; Beratan, D. N. How can infra-red excitation both accelerate and slow charge transfer in the same molecule? *Chem. Sci.* 2018, *9*, 6395-6405.

(11)   Yue, Y. K.; Grusenmeyer, T.; Ma, Z.; Zhang, P.; Schmehl, R. H.; Beratan, D. N.; Rubtsov, I. V. Electron transfer rate modulation in a compact Re(I) donor-acceptor complex. *Dalton Trans.* 2015, *44*, 8609-8616.

(12)   Ren, T. A Sustainable Metal Alkynyl Chemistry: 3d Metals and Polyaza Macrocyclic Ligands. *Chem. Commun.* 2016, *52*, 3271-3279.

(13)   Hoffert, W. A.; Kabir, M. K.; Hill, E. A.; Mueller, S. M.; Shores, M. P. Stepwise acetylide ligand substitution for the assembly of ethynylbenzene-linked Co(III) complexes. *Inorg. Chim. Acta* 2012, *380*, 174-180.

(14)   Cook, T. D.; Natoli, S. N.; Fanwick, P. E.; Ren, T. Dimeric Complexes of CoIII(cyclam) with a Polyynediyl Bridge. *Organometallics* 2015, *34*, 686-689.

(15)   Cook, T. D.; Natoli, S. N.; Fanwick, P. E.; Ren, T. CoIII(cyclam) Oligoynyls: Monomeric Oligoynyl Complexes and Dimeric Complexes with an Oligoyn-diyl Bridge. *Organometallics* 2016, *35*, 1329-1338.

(16)   Natoli, S. N.; Zeller, M.; Ren, T. Stepwise Synthesis of Bis-Alkynyl CoIII(cyclam) Complexes under Ambient Conditions. *Inorg. Chem.* 2016, *55*, 5756-5758.

(17)   Natoli, S. N.; Zeller, M.; Ren, T. An Aerobic Synthetic Approach Toward Bis-Alkynyl Cobalt(III) Compounds. *Inorg. Chem.* 2017, *56*, 10021-10031.

(18)   Banziger, S. D.; Cook, T. D.; Natoli, S. N.; Fanwick, P. E.; Ren, T. Synthetic and Structural Studies of Mono-acetylide and Unsymmetric Bis-acetylide Complexes based on CoIII-cyclam. *J. Organomet. Chem.* 2015, *799-800*, 1-6.

(19)   Gibtner, T.; Hampel, F.; Gisselbrecht, J.-P.; Hirsch, A. End-Cap Stabilized Oligoynes: Model Compounds for the Linear sp Carbon Allotrope Carbyne. *Chem. Eur. J.* 2002, *8*, 408-432.

(20) Banziger, S. D.; Judkins, E. C.; Zeller, M.; Ren, T. Diruthenium-DMBA Bis-Alkynyl Compounds with Hetero- and Extended- Aryl Appendant. *Chin. J. Inorg. Chem.* 2017, *33*, 2103-2109.

(21) Heyer, E.; Ziessel, R. Panchromatic Push-Pull Dyes of Elongated Form from Triphenylamine, Diketopyrrolopyrrole, and Tetracyanobutadiene Modules. *Synlett* 2015, *26*, 2109-2116.

(22) Judkins, E. C.; Zeller, M.; Ren, T. Synthesis and Characterizations of Macrocyclic Cr(III) and Co(III) 1-Ethynyl Naphthalene and 9-Ethynyl Anthracene Complexes: An Investigation of Structural and Spectroscopic Properties. *Inorg. Chem.* 2018, *57*, 2249-2259.

(23) Tyson, D. S.; Luman, C. R.; Zhou, X.; Castellano, F. N. New Ru(II) Chromophores with Extended Excited-State Lifetimes. *Inorg. Chem.* 2001, *40*, 4063-4071.

(24) Judkins, E. C.; Tyler, S. F.; Zeller, M.; Fanwick, P. E.; Ren, T. Synthesis and Investigation of Macrocyclic CrIII Bis(alkynyl) Complexes: Structural and Spectroscopic Properties. *Eur. J. Inorg. Chem.* 2017, *2017*, 4068-4076.

(25) Tyler, S. F.; Judkins, E. C.; Song, Y.; Cao, F.; McMillin, D. R.; Fanwick, P. E.; Ren, T. Cr(III)-HMC (HMC = 5,5,7,12,12,14-Hexamethyl-1,4,8,11-tetraazacyclotetradecane) Alkynyl Complexes: Preparation and Emission Properties. *Inorg. Chem.* 2016, *55*, 8736-8743.

(26) Gütlich, P.; Goodwin, H. A. In *Spin Crossover in Transition Metal Compounds I.*; Gütlich, P., Goodwin, H. A., Eds.; Springer: Berlin, Heidelberg, 2004; Vol. 233; pp 1-47.

(27) Guo, H.; Muro-Small, M. L.; Ji, S.; Zhao, J.; Castellano, F. N. Naphthalimide Phosphorescence Finally Exposed in a Platinum(II) Diimine Complex. *Inorg. Chem.* 2010, *49*, 6802-6804.

(28) McAdam, C. J.; Morgan, J. L.; Robinson, B. H.; Simpson, J.; Rieger, P. H.; Rieger, A. L. Tunable Donor-Acceptor Interactions in 4-Ene/Yne-Ferrocenyl and 4-Enamine Naphthalimides with Ferrocenyl Headgroups. *Organometallics* 2003, *22*, 5126-5136.

(29) Thakker, P. U.; Aru, R. G.; Sun, C.; Pennington, W. T.; Siegfried, A. M.; Marder, E. C.; Wagenknecht, P. S. Synthesis of trans bis-alkynyl complexes of Co(III) supported by a tetradentate macrocyclic amine: A spectroscopic, structural, and electrochemical analysis of π-interactions and electronic communication in the C equivalent to C-M-C equivalent to C structural unit. *Inorg. Chim. Acta* 2014, *411*, 158-164.

(30) *Gaussian 16 Rev. B.01*; Frisch, M. J.; Trucks, G. W.; Schlegel, H. B.; Scuseria, G. E.; Robb, M. A.; Cheeseman, J. R.; Scalmani, G.; Barone, V.; Petersson, G. A.;

Nakatsuji, H.; Li, X.; Caricato, M.; Marenich, A. V.; Bloino, J.; Janesko, B. G.; Gomperts, R.; Mennucci, B.; Hratchian, H. P.; Ortiz, J. V.; Izmaylov, A. F.; Sonnenberg, J. L.; Williams; Ding, F.; Lipparini, F.; Egidi, F.; Goings, J.; Peng, B.; Petrone, A.; Henderson, T.; Ranasinghe, D.; Zakrzewski, V. G.; Gao, J.; Rega, N.; Zheng, G.; Liang, W.; Hada, M.; Ehara, M.; Toyota, K.; Fukuda, R.; Hasegawa, J.; Ishida, M.; Nakajima, T.; Honda, Y.; Kitao, O.; Nakai, H.; Vreven, T.; Throssell, K.; Montgomery Jr., J. A.; Peralta, J. E.; Ogliaro, F.; Bearpark, M. J.; Heyd, J. J.; Brothers, E. N.; Kudin, K. N.; Staroverov, V. N.; Keith, T. A.; Kobayashi, R.; Normand, J.; Raghavachari, K.; Rendell, A. P.; Burant, J. C.; Iyengar, S. S.; Tomasi, J.; Cossi, M.; Millam, J. M.; Klene, M.; Adamo, C.; Cammi, R.; Ochterski, J. W.; Martin, R. L.; Morokuma, K.; Farkas, O.; Foresman, J. B.; Fox, D. J.: Wallingford, CT, 2016.

(31)   Durand, R. J.; Gauthier, S. b.; Achelle, S.; Groizard, T.; Kahlal, S.; Saillard, J.-Y.; Barsella, A.; Le Poul, N.; Le Guen, F. R. Push-pull D-p-Ru-p-A chromophores: synthesis and electrochemical, photophysical and second-order nonlinear optical properties. *Dalton Trans.* 2018, *47*, 3965-3975.

(32)   Nisic, F.; Colombo, A.; Dragonetti, C.; Garoni, E.; Marinotto, D.; Righetto, S.; De Angelis, F.; Lobello, M. G.; Salvatori, P.; Biagini, P.; Melchiorre, F. Functionalized Ruthenium Dialkynyl Complexes with High Second-Order Nonlinear Optical Properties and Good Potential as Dye Sensitizers for Solar Cells. *Organometallics* 2015, *34*, 94-104.

(33)   De Sousa, S.; Ducasse, L.; Kauffmann, B.; Toupance, T.; Olivier, C. Functionalization of a Ruthenium-Diacetylide Organometallic Complex as a Next-Generation Push-Pull Chromophore. *Chem. Eur. J.* 2014, *20*, 7017-7024.

(34)   Bosnich, B.; Tobe, M. L.; Webb, G. A. Complexes of Nickel(2) with a Cyclic Tetradentate Secondary Amine. *Inorg. Chem.* 1965, *4*, 1109-1112.

(35)   Planells, M.; Abate, A.; Hollman, D. J.; Stranks, S. D.; Bharti, V.; Gaur, J.; Mohanty, D.; Chand, S.; Snaith, H. J.; Robertson, N. Diacetylene bridged triphenylamines as hole transport materials for solid state dye sensitized solar cells. *J. Mater. Chem. A* 2013, *1*, 6949-6960.

(36)   *APEX3 v2016.9-0, Saint V8.34A, Saint V8.37A*Bruker AXS, Inc.: Madison, WI, 2016.

(37)   *SHELXTL suite of programs, version 6.14*Bruker AXS Inc.: Madison, WI, 2000-2003.

(38)   Sheldrick, G. M. A short history of SHELX. *Acta Crystallogr A* 2008, *64*, 112-122.

(39)   Sheldrick, G. M. Crystal structure refinement with SHELXL. *Acta Crystallogr C* 2015, *71*, 3-8.

(40)   Hübschle, C. B.; Sheldrick, G. M.; Dittrich, B. ShelXle: a Qt graphical user interface for SHELXL. *J. Appl. Cryst.* 2011, *44*, 1281-1284.

CHAPTER 4. UNLOCKING NEW SYNTHETIC ROUTES FOR UNSYMMETRIC DONOR-BRIDGE-ACCEPTOR (D-B-A) SPECIES BASED ON A CO(III)(CYCLAM)(C$_2$NAP^R) MOTIF

4.1 Introduction

The understanding of electron transfer processes is paramount to building enhanced photovoltaic materials.[1,2] Weinstein et al. have utilized Pt motifs to look at photo-induced electron transfer across a linear donor-bridge-acceptor (*D-B-A*) system with a *trans*-Pt(II)-bis-alkynyl bridge,[3-5] as well as a bent or 'fork' donor–bridge–acceptor–bridge–donor system utilizing a *cis*-Pt(II)-bis-alkynyl bridge.[6] Bis-acetylide Pt complexes with diphenylpyranylidene end caps have been studied in TiO$_2$ for dye-sensitized solar cells (DSCs) and exhibited efficiencies as high as 4.7%.[7] It has been well established that the dissymmetric D-C≡C-Pt-C≡C-A type complexes can be readily synthesized under weak base conditions in the presence of a Cu catalyst.[3-7] Other examples of *D-B-A* complexes utilize a Ru(dppe)$_2$ bridge, where dppe = bis(diphenylphosphino)ethane, to study photo-active materials for dye-sensitized solar cells.[8] These types of species have been investigated for their non-linear optical (NLO) properties[9] and can be readily synthesized at room temperature under weak base conditions.[8-10]
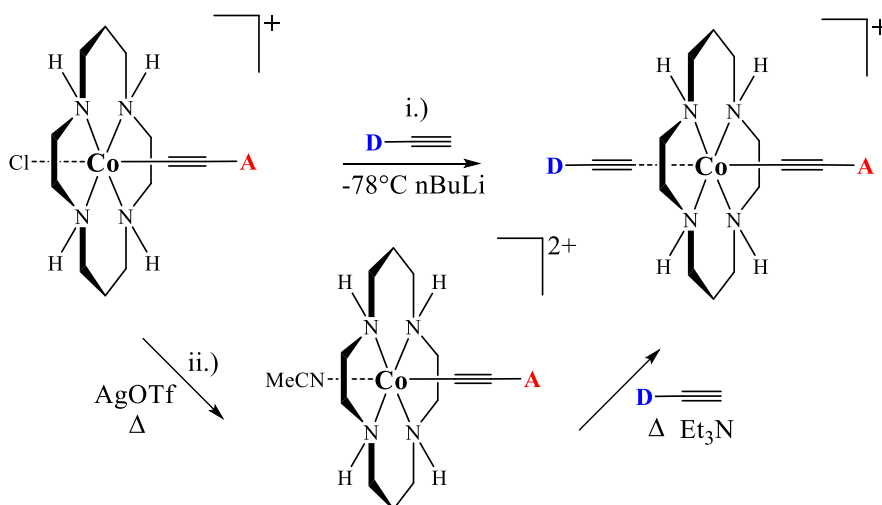
Scheme 4.1. Syntheses of dissymmetric *D-B-A* compounds based on Co^{III}(cyclam). Route i.) proceeds at low temp with a strong base; Route ii.) proceeds through a triflate intermediate in the presence of weak base and heat.

More recently, our group has demonstrated that *D-B-A* compounds based on an earth abundant *3d* metal motif, Co^{III}(cyclam), can be synthesized selectively in high yields[11,12] through two different routes shown in Scheme 4.1. i.) Stepwise alkynylation, with the first step proceeding under weak base conditions and the second utilizing nBuLi,[13,14] and ii.) stepwise alkynylation under weak base conditions via a triflate intermediate.[15,16] These synthetic routes suffer from harsh conditions, with the most notable being use of a strong base (i.) and high temperature (ii.). Previous work to synthesize the first dissymmetric *D-B-A* Co^{III}(cyclam) complexes, where $D = C_6H_4$-4-NR'_2 (R'=Me or Ph-4-OMe) and A= *N*-isopropyl-1,8-naphthalimide (NAP^{iPr}), could only be accomplished using the first route.[11] Since that time, our group has investigated altering the alkyl group directly linked to the imide to tune reactivity, crystallinity, and "robustness" of the naphthalimide unit. Reported herein is the synthesis of new Co^{III}(cyclam)(C_2NAP^R) species (R = mesityl (NAP^{Mes}, **1a**), methyl

(NAP^{Me}, **1b**), 1-ethylpropyl (NAP^{Pen}, **1c**), 2-ethylhexyl (NAP$^{2-ethhex}$, **1d**), or octyl (NAP^{Oct}, **1e**)) and a discussion on their properties and reactivity (Chart 4.1).
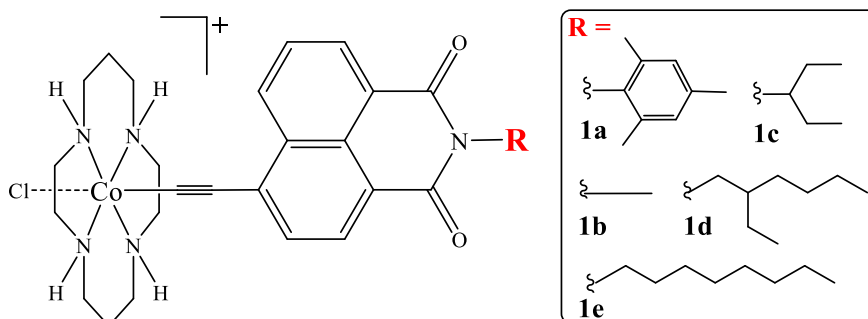
Chart 4.1. [Co(cyclam)(C$_2$NAP^R)Cl]Cl type compounds

4.2   Results and Discussion

4.2.1   Synthesis

As demonstrated in Scheme 4.2, synthesis of the desired 4-ethynyl-*N*-alkyl-1,8-naphthalimide (NAP^R) was readily achieved using a Sonogashira coupling in the presence of excess trimethylsilylacetylene. 4-Ethynyl-*N*-methyl-1,8-naphthalimide (HC$_2$NAP^{Me}),[17]   4-ethynyl-*N*-2-ethylhexyl-1,8-naphthalimide (HC$_2$NAP$^{2-ethhex}$),[18] and 4-ethynyl-*N*-octyl-1,8-naphthalimide (HC$_2$NAP^{Oct})[5] were prepared according to literature methods. Preparation of 4-ethynyl-*N*-mesityl-1,8-naphthalimide (HC$_2$NAP^{Mes}) required increased reaction time compared to the other derivatives, with the insertion of H$_2$NMes into the naphthalic anhydride framework requiring 84 h of reflux, five times longer than any other derivative reported herein. Desilylation of TMSC$_2$NAP^{Mes} formed HC$_2$NAP^{Mes} in high yields and the dimerized NAP^{Mes}C$_4$NAP^{Mes} as a minor byproduct. Formation of 4-ethynyltrimethylsilyl-*N*-1-ethylpropyl-1,8-naphthalimide   (TMSC$_2$NAP^{Pen})   occurred

within 20 min at room temperature. Longer reaction times or extra heating resulted in degradation and formation of $NAP^{Pen}C_4NAP^{Pen}$.
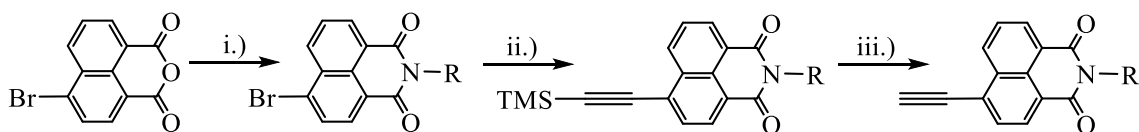
Scheme 4.2. i.) 3 equiv H_2NR (R = mesityl or 1-ethylpropyl), EtOH/^{i}PrOH, reflux, 18-84 h; ii.) 3 equiv TMSA, ^{i}Pr$_2$NH, 2 mol% CuI, 2 mol% Pd(PPh$_3$)$_2$Cl$_2$, 20 min-2 h; iii.) Excess K$_2$CO$_3$, MeOH, 30 min

Synthesis of mono acetylide Co^{III}(cyclam) compounds **1a-1e** was accomplished under N_2 through the reaction of HC$_2$NAP^R (R is defined in Chart 4.1) with [Co(cyclam)Cl$_2$]Cl in the presence of Et$_3$N. Except for **1b**, purification over silica resulted in a bright orange microcrystalline solid in 45-63% yield. Due to low solubility, isolation of **1b** was accomplished by addition of ether to the crude reaction solution to yield a light orange powder in 48% yield. Reaction of AgOTf (5 equiv) with **1a** and **1b** in MeCN resulted in [Co(cyclam)(C$_2$NAP^{Mes})MeCN]OTf$_2$ (**2a**) and [Co(cyclam)(C$_2$NAP^{Me})MeCN]OTf$_2$ (**2b**), respectively as yellow powders. Attempts to synthesize [Co(cyclam)(C$_2$NAP^R)MeCN]OTf$_2$ type triflate intermediates proved unsuccessful for **1c-1e** and attempts to form dissymmetric complexes based on NAP^{Pen}, NAP$^{2-ethhex}$, and NAP^{Oct} was not pursued further. [Co(cyclam)(C$_2$NAP^{Mes})(C$_2$C$_6$H$_4$-4-NMe$_2$)]OTf (**3a**), [Co(cyclam)(C$_2$NAP^{Mes})$_2$]OTf (**3b**), and [Co(cyclam)(C$_2$NAP^{Mes})(C$_2$Ph)]OTf (**3c**) were synthesized from **2a** under N_2 in the presence of excess HC$_2$Ar (Ar = C$_6$H$_4$-4-NMe$_2$, NAP^{Mes}, Ph) and Et$_3$N as shown in Scheme 4.3. Compounds **3b** and **3c** were isolated as bright yellow solids and **3a** as a light orange solid. Low reaction yields for **3a** (39%) and **3b** (11%) was attributed to the hydroamination of -C≡C-NAP^{Mes} to form [Et$_3$NC$_2$H$_2$NAP^{Mes}]OTf. Hydroamination of

alkynes in the presence of perchlorate salts to make formyl vinyl tertiary amines was initially reported by Fischer in 1968.[19] This type of reactivity has been used in the literature to promote carboamination of alkynes in the presence of Pt,[20] Pd,[21] and Au[22] catalysts.
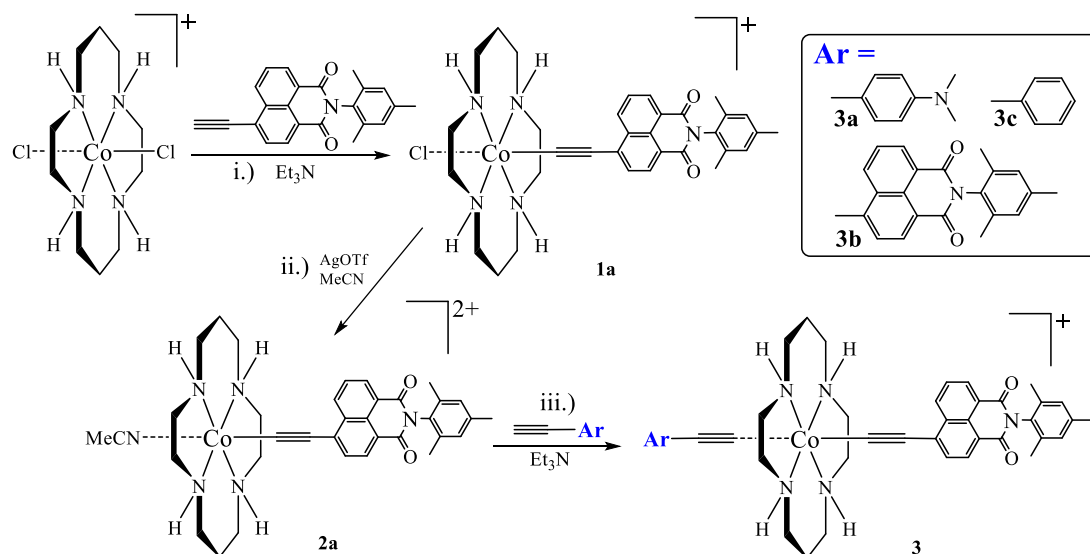
Scheme 4.3. i.) 1.1 equiv HC$_2$NAP^{Mes}, Et$_3$N, CH$_3$OH:THF, reflux, 18h; ii.) 5 equiv AgOTf, MeCN, reflux, 16h; iii.) 4 equiv HC$_2$Ar, Et$_3$N, MeCN, reflux, 24 h

Synthesis of [Co(cyclam)(C$_2$NAP^{Me})(C$_2$C$_6$H$_4$-4-NMe$_2$)]OTf (**3ba**) was accomplished similarly from **2b** in the presence of excess HC$_2$C$_6$H$_4$-4-NMe$_2$ and Et$_3$N to afford a light orange powder in 29% yield after silica plug purification. Poor solubility of **3ba** was attributed to aggregation due to π-π stacking of the NAP^{Me} moiety,[17,23-25] making purification and characterization difficult. Attempts to synthesize new *D-B-A* derivatives based on a NAP^{Me} acceptor was abandoned in favor of the significantly more soluble NAP^{Mes} derivatives. All new Co(cyclam) compounds (**1a**-**1e**, **3a**-**c**, and **3ba**) are diamagnetic, consistent with a low spin Co(III) center.

4.2.2 Structure Analysis

Crystals of HC_2NAP^{Mes} were grown from slow evaporation of a hexanes/CH_2Cl_2 solution, shown in Figure 4.1. Single crystals of $[Et_3NC_2H_2NAP^{Mes}]OTf$, **1a**, **1c** and **3b** were grown from slow diffusion of a less polar solvent into a polar concentrated solution of the respective compound; their cationic structures are shown in Figure 4.2, Figure 4.3, Figure 4.4, and Figure 4.5, respectively. The Co center assumes a pseudo-octahedral geometry with the alkyne and Cl/alkyne *trans*- to each other. Selected bond lengths and angles can be found in Table 4.1 and experimental details are listed in Table 4.4.
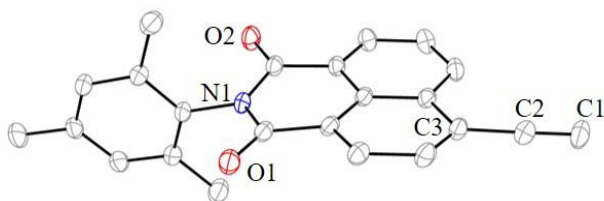
Figure 4.1. ORTEP plot of compound HC_2NAP^{Mes} at 30% probability level; hydrogen atoms and solvent molecules were omitted for clarity.
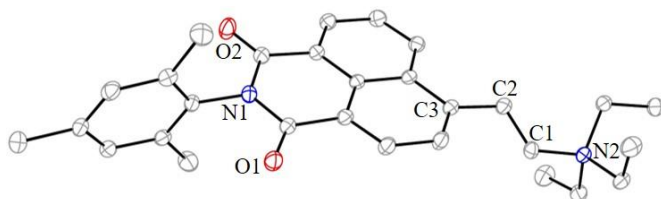
Figure 4.2. ORTEP plot of compound $[Et_3NC_2H_2NAP^{Mes}]^+$ at 30% probability level; counterion, hydrogen atoms and solvent molecules were omitted for clarity.

The C≡C bond length for HC_2NAP^{Mes} (1.185(3) Å) and the C=C (1.325 (3) Å) bond length for $[Et_3NC_2H_2NAP^{Mes}]^+$ are slightly shorter than expected due to the electron withdrawing character of NAP^{Mes}, but are within expected error of the ideal bond lengths for an alkyne and alkene, respectively. The observed bond angles for C1-C2-C3 are also characteristic of a sp (178.8(3)°) hybridized (HC_2NAP^{Mes}) versus a sp^2 (119.5(2)°) hybridized ($[Et_3NC_2H_2NAP^{Mes}]OTf$) carbon.

Table 4.1. Selected bond lengths (Å) and angles (°) for compounds HC_2NAP^{Mes}, $[Et_3NC_2H_2NAP^{Mes}]^+$, $[1a]^+$, $[1c]^+$ and $[3b]^+$

	HC_2NAP^{Mes}	$[Et_3NC_2H_2NAP^{Mes}]^+$	$[1a]^+$	$[1c]^+$	$[3b]^+$
Co1-C1	--	--	1.859(3)	1.866(5)	1.933(4)
Co1-N2	--	--	1.990(2)	1.974(4)	1.982(4)
Co1-N3	--	--	1.973(2)	1.937(4)	1.972(3)
Co1-N4	--	--	1.971(2)	1.981(4)	--
Co1-N5	--	--	1.983(2)	2.019(4)	--
Co1-Cl1	--	--	2.3154(5)	2.317(3)	--
C1-C2	1.185(3)	1.325(3)	1.204(3)	1.213(5)	1.210(5)
Cl1-Co-C1	--	--	176.76(8)	179.4(3)	--
C1´-Co-C1	--	--	--	--	180.0
Co-C1-C2	--	--	174.0(2)	177.4(7)	171.1(4)
C1-C2-C3	178.8(3)	119.5(2)	176.5(2)	178.6(6)	170.4(4)

The shortened C≡C bond length of HC_2NAP^{Mes} compared to that of the organometallic species $[1a]^+$, $[1c]^+$ and $[3b]^+$, can be attributed to the substantial electron withdrawing character of the ligand. As observed in previous work, the Co-C1 bond length is significantly longer in the bis-NAP^{Mes} species, $[3b]^+$ (1.933(4) Å), compared to the mono-NAP^{Mes}, $[1a]^+$ (1.859(3) Å), and can be attributed to the *trans*-influence as the increased donor strength provided by the alkyne compared to the Cl in the axial position results in a weaker bond.[13,15,16,26-29] The influence of the electron withdrawing/donating character of the alkynyl ligand on the Co-C1 bond length can be observed across literature with $[Co(cyclam)(C_2CF_3)_2]^+$ (1.917 Å)[30] < $[Co(cyclam)(C_2C_6F_5)_2]^+$ (1.926 Å)[16] < $[3b]^+$ (1.933 Å) < $[Co(cyclam)(C_2C_6H_4\text{-}4\text{-}NMe_2)_2]^+$ (1.942 Å)[15] < $[Co(cyclam)(C_2C_6H_4\text{-}4\text{-}N(Ph\text{-}4\text{-}OMe)_2)_2]^+$ (1.945 Å)[31] < $[Co(cyclam)(C_2Ph)_2]^+$ (2.001 Å)[32]. The electron withdrawing species (CF_3, C_6F_5, and NAP^{Mes}) have notably shortened bond distances (Co-C) compared to the electron donating groups (-NMe_2 and -$N(Ph\text{-}4\text{-}OMe)_2$) due to reduced antibonding contribution from the $\pi(C≡C)$ to the Co $d\pi$.[13,26,33]
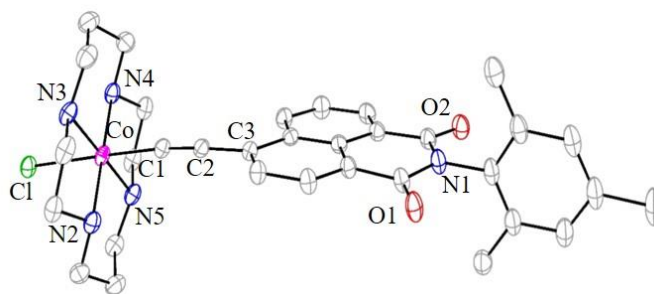
Figure 4.3. ORTEP plot of compound [**1a**]⁺ at 30% probability level; counterion, hydrogen atoms, disorder, and solvent molecules were omitted for clarity.
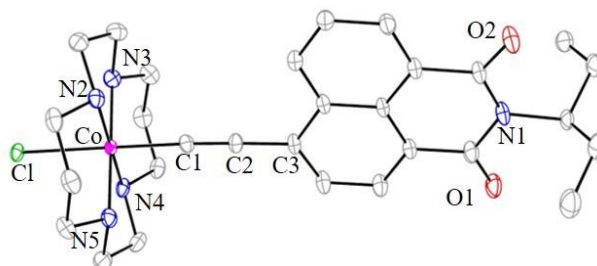
Figure 4.4. ORTEP plot of compound [**1c**]⁺ at 30% probability level; counterion, hydrogen atoms, disorder, and solvent molecules were omitted for clarity.
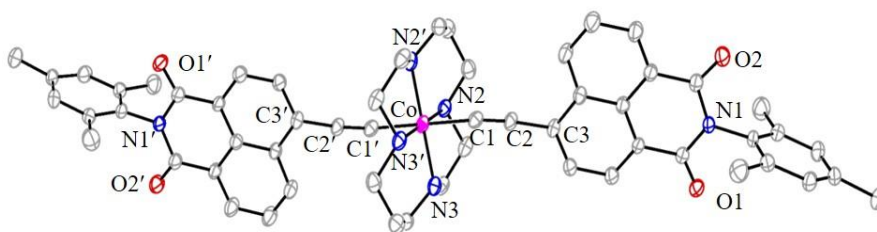
Figure 4.5. ORTEP plot of compound [**3b**]⁺ at 30% probability level; counterion, hydrogen atoms, and solvent molecules were omitted for clarity.

Crystallographic data consistently shows the mesityl group perpendicular to the naphthalimide ligand (Figure 4.1, 4.2, 4.3, and 4.5), suggesting a sterically rigid structure. In contrast, flexible alkyl chains as seen on NAP^{Pen} or NAP^{iPr} can more readily rotate, leaving the imide open to attack. Space filling models of [**1a**]⁺ and [**1c**]⁺ (Figure 4.6) illustrate how the methyl groups on the mesityl "protect" the nitrogen and lock the mesityl group into place. In contrast, the saturated pentyl group does not provide the same protection and could easily rotate depending on the molecular environment.
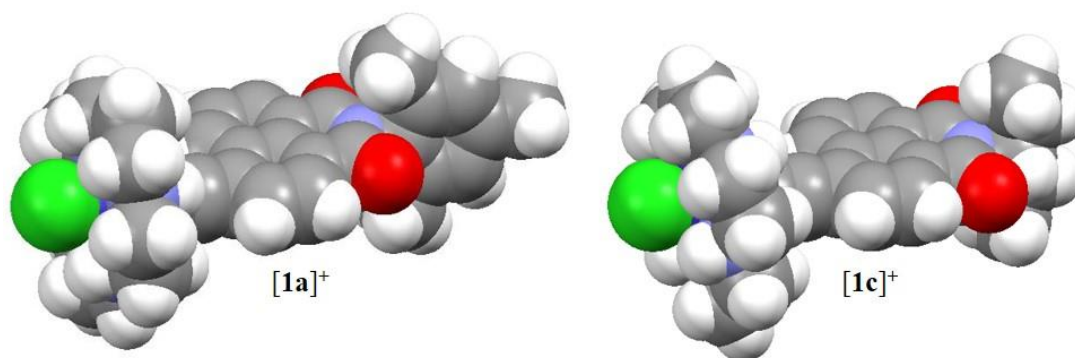
Figure 4.6. Space-filling model of [**1a**]$^+$ (left) and [**1c**]$^+$ (right) demonstrating the steric protection the rigid mesityl group provides compared to the flexible pentyl group.

4.2.3 Electrochemistry
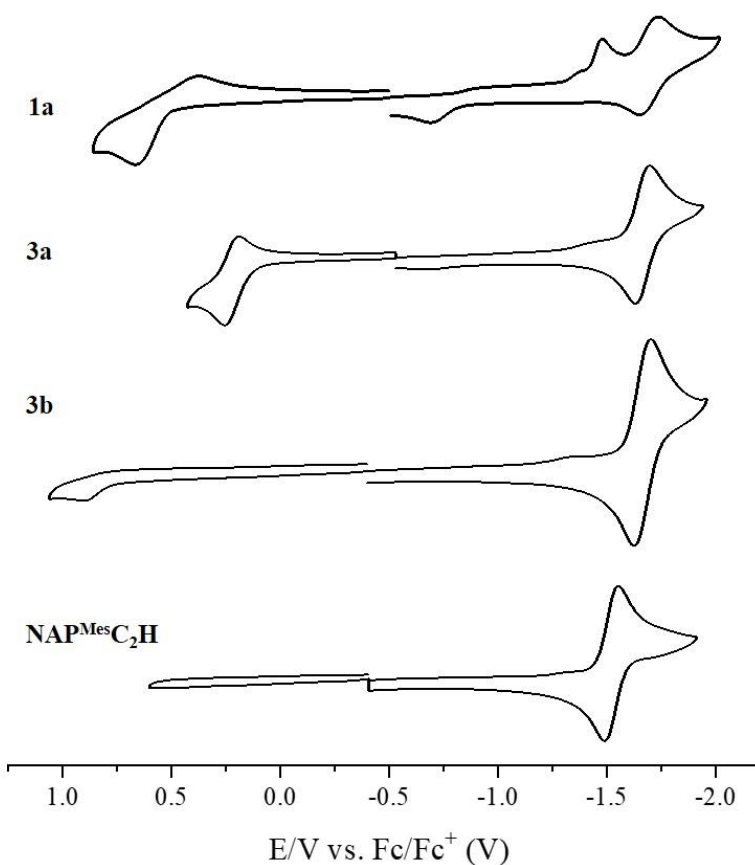
Figure 4.7. Cyclic voltammogram of **1a**, **3a**, **3b** and HC$_2$NAP^{Mes} (vs. Fc/Fc$^+$) in 1.0 mM MeCN solutions with 0.1 M n-Bu$_4$NPF$_6$ as the supporting electrolyte.

Compounds **1a**, **3a**, **3b**, and HC$_2$NAP^{Mes} all have a reversible reduction based on the NAP^{Mes} ligand. Figure 4.7 shows their respective cyclic voltammograms. The Co containing species (**1a** and **3a-3c)** undergo three Co based events, one irreversible 1e$^-$ oxidation (Co^{III}/Co^{IV}) and two irreversible 1e$^-$ reductions (Co^{III}/Co^{II}) and (Co^{II}/Co^I) listed in Table 4.2. Comparison of mono-alkynyl (**1a**) to the bis-alkynyl species (**3a-c**) reveals that the first Co reduction shifts to significantly more negative potentials upon addition of a second alkynyl. This trend is consistent with previous observations and is attributed to the increased donor strength of an alkynyl versus a chloro in the axial position.[14] Comparison of the HC$_2$NAP^{Mes} redox couple (-1.52 V) to **1a** and **3a-c** validates that the assignment of the reversible redox at -1.66 V is attributed to the naphthalimide moiety. Furthermore, it suggests that **3b** undergoes a reversible 2e$^-$ reduction based on NAP^{Mes} as the current at -1.66 V is double those of **1a**, **3a** and HC$_2$NAP^{Mes} (Figure 4.7). The pseudo-reversible redox couple at 0.22 V, observed for the *D-B-A* complex **3a**, was assigned to the donor (-C$_6$H$_4$-4-NMe$_2$) based on similar literature examples that studied the electrochemistry of [Co(cyclam)(C$_2$C$_6$H$_4$-4-NMe$_2$)$_2$]$^+$ and [Co(cyclam)(C$_2$C$_6$H$_4$-4-NMe$_2$)(C$_2$C$_6$F$_5$)]$^+$.[16] Consistent with observations for [Co(cyclam)(C$_2$NAP^{iPr})(C$_2$C$_6$H$_4$-4-NMe$_2$]Cl,[14] this assignment suggests that the HOMO and LUMO for compound **3a** reside on the donor and acceptor, respectively, and provides an estimated electrochemical gap ($E_g = E_{1/2}$(D)-$E_{1/2}$(A)) of 1.88 V.

Table 4.2. Electrode potentials of observed redox couples (V) for **1a**, **3a**, **3b**, **3c**, and HC$_2$NAP^{Mes}

Compound	E$_{1/2}$ (D)	E$_{1/2}$ (A)	E$_{pc}$(Co)	E$_{pc}$(Co)	E$_{pa}$ (Co)
1a	--	-1.69 (0.10)	-1.47	-2.19	0.66
3a	0.22 (0.07)	-1.66 (0.06)	-2.15	-2.26	0.73
3b	--	-1.66 (0.08)	-2.16	-2.32	0.89
3c	--	-1.66 (0.08)	-1.85	-2.30	1.17
HC$_2$NAP^{Mes}	--	-1.52 (0.06)	--	--	--

Potentials vs. Fc/Fc$^+$ in MeCN with 0.1M n-Bu$_4$NPF$_6$ as the supporting electrolyte. Peak separations (ΔE_p) for reversible couples are shown in brackets.

4.2.4   Absorption and Emission Spectroscopy

Absorption and emission spectra were collected at room temperature in CH$_2$Cl$_2$ under ambient condition and the λ_{max} for these techniques are recorded for **1a**, **3a-c**, TMSC$_2$NAP^{Mes}, HC$_2$NAP^{Mes}, [Et$_3$NC$_2$H$_2$NAP^{Mes}]OTf, and NAP^{Mes}C$_4$NAP^{Mes} in Table 4.3. All compounds shown in Figure 4.8 (**1a** and **3a-c**) display a broad absorption band at 400 nm. TD-DFT calculations done on similar compounds, [Co(cyclam)(C$_2$NAP^{iPr})Cl]Cl, [Co(cyclam)(C$_2$NAP^{iPr})(C$_2$C$_6$H$_4$-4-NMe$_2$)]Cl   and   [Co(cyclam)(C$_2$NAP^{iPr})(C$_2$C$_6$H$_4$-4-N(Ph-4-OMe)$_2$)]Cl, indicate that this transition is predominantly the NAP^{Mes} based π-π* transition   with minor MLCT/LMCT character involving Co^{III}(cyclam) and NAP^{Mes}.[14] This assignment is also consistent with Pt^{II}(P^{n}Bu$_3$)$_2$(C$_2$NAP^{Oct})(C$_2$Ar) type complexes reported by Weinstein et al. where the lowest energy transition was observed at 430 nm and was attributed to mixed metal-ligand-to-ligand charge transfer (ML/L'CT).[5] Generally, Co^{III}(cyclam) acetylides generally exhibit a *d-d* transition around 450-500 nm, with higher energy transitions occurring for the *bis*-acetylide complexes and the lower energy for the *mono*-acetylides.[13,15,16,26,27,29,33-36] However, only compound **1a** has an observable *d-d* transition at 480 nm, suggesting the broad MLCT/LMCT transition at 400 nm obscures the *d-d* peaks for **3a-c** (Figure 4.8). Based on previous work published in our group on [Co(cyclam)(C$_2$NAP^{iPr})(C$_2$C$_6$H$_4$-4-NMe$_2$)]Cl,[14] the sharp peak at 287 nm

observed for compound **3a** was assigned to the π-π* transition localized on the donor ligand ($-C_6H_4$-4-NMe_2).
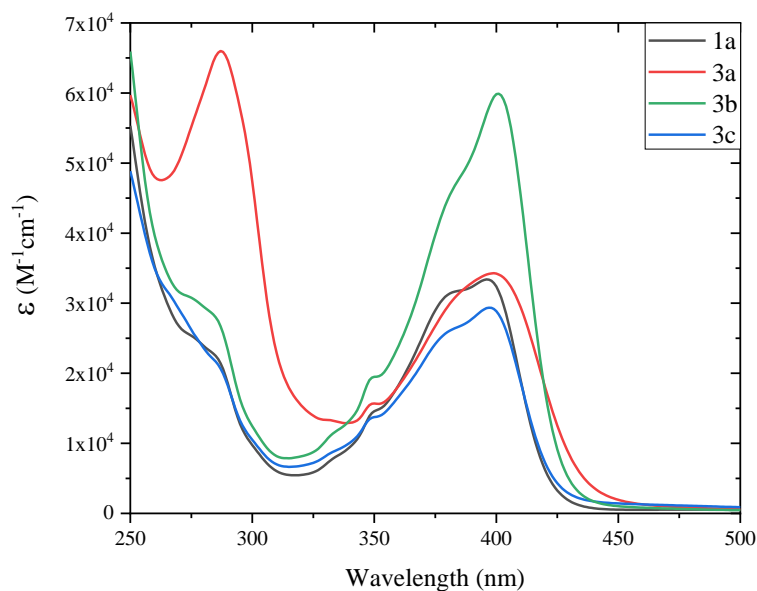
Figure 4.8. Absorption spectra of **1a**, **3a**, **3b**, and **3c** (blue) in CH_2Cl_2 at room temperature.

The electronic absorption spectra of the organic naphthalimide species $TMSC_2NAP^{Mes}$, $NAP^{Mes}C_4NAP^{Mes}$, and $[Et_3NC_2H_2NAP^{Mes}]OTf$ features strong π-π* transitions based on NAP^{Mes} in the visible region (Figure 4.9). $NAP^{Mes}C_4NAP^{Mes}$ has a spectral shape similar to related compounds reported by Liu et al.[37] and has an extinction coefficient double those of TMS/HC_2NAP^{Mes} and $[Et_3NC_2H_2NAP^{Mes}]OTf$ due to increased conjugation. The structured absorption profile observed for $X-C_2NAP^{Mes}$ (X=TMS or H) smooths upon reduction of the alkyne to an alkene ($[Et_3NC_2H_2NAP^{Mes}]OTf$) and is attributed to reduced conjugation.
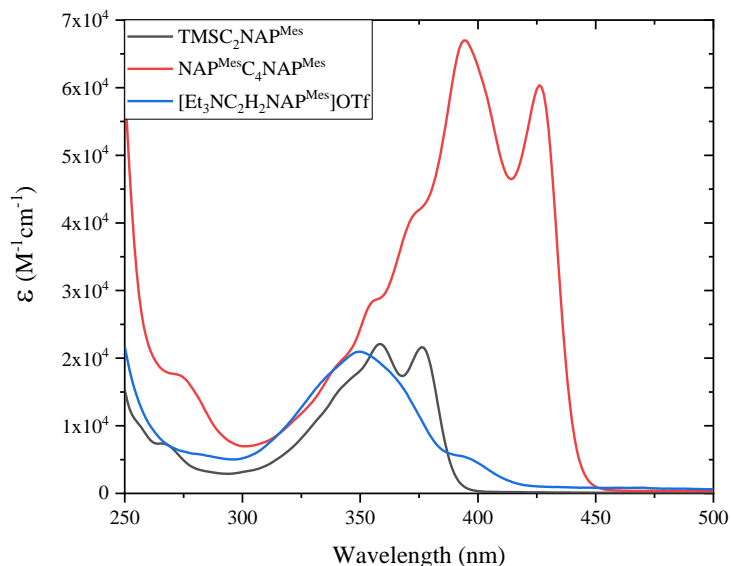
Figure 4.9. Absorption spectra of $TMSC_2NAP^{Mes}$, $[Et_3NC_2H_2NAP^{Mes}]OTf$ versus $NAP^{Mes}C_4NAP^{Mes}$ in CH_2Cl_2 at room temperature.

Use of a simple chromophore as the acceptor allows for analysis of steady-state emission, which can elaborate on the effect the Co^{III}(cyclam) bridge and the donor (-C_6H_4-4-NMe_2) have on the acceptor (NAP^{Mes}) emission. The emission profiles of **1a** and **3a-c** resembled the emission for the X-C_2NAP^{Mes} species, but were significantly red-shifted. The relatively small Stoke shifts between λ_{abs} and λ_{em} suggests that the observed emission originates from the absorption transition around 400 nm. Figure 4.10 shows the normalized emission spectra of $TMSC_2NAP^{Mes}$ versus **1a** and **3a**, demonstrating that the Co^{III}(cyclam) bridge effects the X-C_2NAP^{Mes} electronic states by shifting the emission to lower energy by 42 nm. However, the similarity between the emission of **1a** and **3a** suggests that the donor does not perceivably affect the X-C_2NAP^{Mes} electronic states within the instrument's timescale. Similar findings were reported by us when looking at the NAP^{iPr} analogs of these compounds, which had fluorescent quantum yields (Φ_{fl}) in CH_2Cl_2 on the order of 0.43-0.66% for the Co^{III}(cyclam)(C_2NAP^{iPr}) compounds and 42.3% for HC_2NAP^{iPr}.[14] The dimerized form of -C_2NAP^R (R = ^nBu or Ph) has been recorded in

literature to have Φ_{fl} on the order of 83% and 101%, respectively.[37] While quantum yields were not recorded for this series, compounds **1a** and **3a-c** were observed to have extremely weak emission compared to the organic species listed in Table 4.3. Quenching of fluorophore emission due to the presence of a metal has also been observed by the Weinstein group, who recorded a Φ_{fl} of 5.5% for a $Pt^{II}(P^nBu_3)_2(C_2NAP^{Oct})$ *D-B-A* species,[5] and by McAdam et al., who recorded Φ_{fl} of 0.11% and 0.24% for naphthalimide species linked to ferrocene.[17]
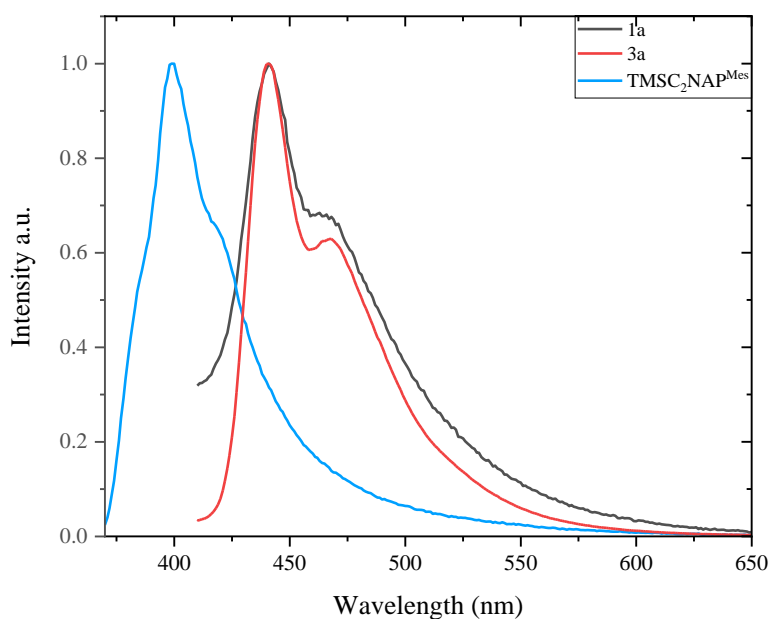
Figure 4.10. Normalized emission spectra of **1a** versus **3a** and $TMSC_2NAP^{Mes}$ in CH_2Cl_2 at room temperature.

Table 4.3. Absorption (λ_{abs}) and emission maxima (λ_{em}) in nm, and excitation (λ_{ex}) wavelength taken in CH_2Cl_2 at room temperature

Compound	λ_{abs} (nm)	λ_{em} (nm)	λ_{ex} (nm)
1a	396	441	390
3a	399	441	390
3b	401	433	390
3c	397	441	390
TMSC$_2$NAP^{Mes}	358 / 376	399	360
HC$_2$NAP^{Mes}	351 / 368	405	340
NAP^{Mes}C$_4$NAP^{Mes}	395 / 425	439	390
[Et$_3$NC$_2$H$_2$NAP^{Mes}]OTf	350	410	330

4.2.5   ATR-FTIR Spectroscopy

ATR-FTIR spectra for compounds **1** and **3** all contain asymmetric $\upsilon(C{\equiv}C)$ stretches around *ca.* 2100 cm^{-1} and C=O stretches *ca.* 1650 cm^{-1} and 1700 cm^{-1}. Figure 4.11 displays the C≡C and C=O stretching modes for compounds **1a**, **3a**, and **3b**. Addition of the second alkyne, to form the asymmetric *D-B-A* (**3a**) or symmetric *A-B-A* (**3b**), increases the absorbance of the C=O and C≡C stretches compared to the *B-A* (**1a**) compound. Compounds **3a-c** all display a single C≡C stretch *ca.* 2090 cm^{-1} and **1a** has a higher $\upsilon(C{\equiv}C)$ at 2103 cm^{-1}. This shift in frequency indicates increased M→C≡CR π-backbonding for the bis-alkynyl species due to the addition of a second alkynyl.[38] The alkyne acting as a π-donor is consistent with reports from the Wagenknecht group looking at [M(cyclam)(C$_2$R)$_2$] type species (M = Rh, Cr, Co; R = -CF$_3$, Fc, or aryl).[29,39]
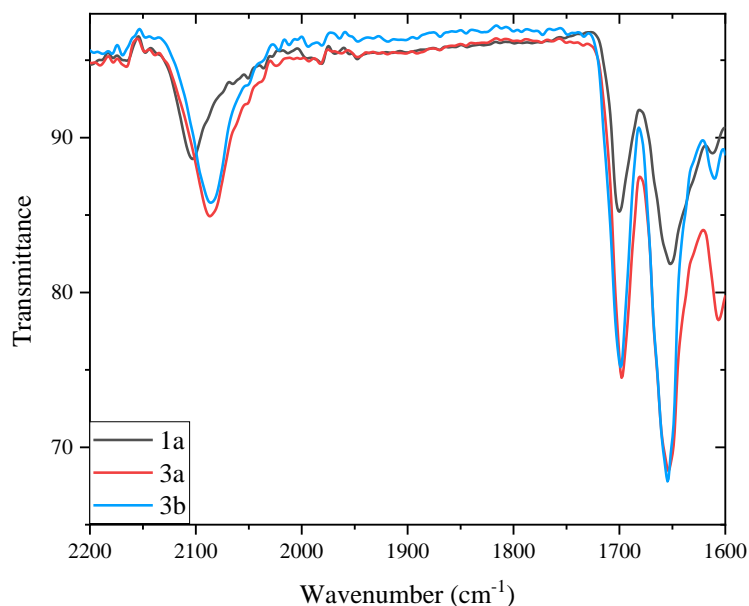
Figure 4.11. ATR-FTIR spectra of **1a** versus **3a** and **3b** showing the C≡C and C=O stretches.

4.3   Conclusions

Discussed in this contribution are several new $Co^{III}(cyclam)(C_2NAP^R)$ type compounds (R = mesityl, methyl, 1-ethylpropyl, 2-ethylhexyl, octyl) that exhibit different crystallinity, stability, and reactivity previously not observed for $Co^{III}(cyclam)(C_2NAP^{iPr})$ [14] species. Careful tuning of the alkyl group on the naphthalimide moiety determined that -C_2NAP^{Mes} type complexes performed the best in the aforementioned categories. The increased stability afforded by the mesityl group allows for selective synthesis of the *D-B-A* compounds under weak base conditions through a triflate intermediate. Furthermore, the perpendicular connection between the mesityl and naphthalimide prevents π-π stacking thereby increasing solubility and crystallinity. These encouraging results suggest other strategies to synthesize the next generation of *D-B-A* complexes could be employed such as through i) Hagihara coupling (CuI / organic amine) as a variation of the

dehydrohalogenation reactions, used to couple arylalkynyls to cobalamin[40] or ii) organo-tin activated arylalkynyls, used by Lewis and co-workers[41,42] to synthesize trans-Ru^{II} acetylides.

4.4 Experimental

4.4.1 Materials and Measurements

[Co(cyclam)Cl$_2$]Cl was prepared according to literature procedures.[43] Also prepared according to literature procedures was 4-ethynyl-*N*-methyl-1,8-naphthalimide,[17] 4-Ethynyl-*N*-2-ethylhexyl-1,8-naphthalimide,[18] and 4-ethynyl-*N*-octyl-1,8-naphthalimide.[5] Diisopropylamine and triethylamine were purchased from ACROS Organics and Fisher chemical, respectively, and then distilled over potassium hydroxide. 4-ethynyl-*N,N*-dimethylaniline was purchased from Sigma Aldrich. Phenylacetylene was purchased from GFS Chemicals. All alkynylation reactions were carried out using Schlenk techniques under dry N$_2$. Crystallographic data for HC$_2$NAP^{Mes}, [Et$_3$NC$_2$H$_2$NAP^{Mes}]OTf, **1a**, **1c** and **3b** is provided in Table 4.4.

4.4.2 Spectroscopic Measurements

UV-Vis-NIR spectra were obtained with a JASCO V-670 UV-Vis-NIR spectrophotometer. Infrared spectra were obtained on a JASCO FT-IR 6300 spectrometer via ATR on a ZnSe crystal. ESI-MS was carried out on an Advion Mass Spectrometer. ^{1}H NMR spectra were recorded on a Varian INOVA300 NMR with chemical shifts (δ) referenced to the solvent signal (CD$_3$OD at 4.88 and 3.31 ppm; CDCl$_3$ at 7.26 ppm). Cyclic voltammograms were recorded in 0.1 M *n*-Bu$_4$NPF$_6$ and 1.0 mM cobalt species solution (CH$_3$CN, Ar degassed) using a CHI620A voltammetric analyzer with a glassy

carbon working electrode (diameter = 2 mm), Pt-wire counter electrode, and an Ag/AgCl reference electrode with ferrocene as an external reference. Emission studies were measured on a Varian Cary Eclipse fluorescence spectrophotometer.

Table 4.4. Experimental Crystal Data for HC_2NAP^{Mes}, $[Et_3NC_2H_2NAP^{Mes}]OTf$, $[\mathbf{1a}]^+$, $[\mathbf{1c}]^+$ and $[\mathbf{3b}]^+$

Compound	HC_2NAP^{Mes}	$[Et_3NC_2H_2NAP^{Mes}]^+$	$[\mathbf{1a}]^+$	$[\mathbf{1c}]^+$	$[\mathbf{3b}]^+$
Chemical Formula	$C_{23}H_{17}NO_2$	$C_{29}H_{33}N_2O_2$ CF_3O_3S	$C_{33}H_{40}ClCoN_5O_2$ $0.518(CH_4O)\cdot Cl$ $2.273(H_2O)$	$C_{29}H_{40}ClCoN_5O_2$ $CH_4O\cdot Cl$	$2(C_{56}H_{56}CoN_6O_4)$ $2(CF_3O_3S)$ $C_4H_{10}O$
Formula Weight	339.38	590.64	762.08	652.53	2244.25
Space group	$P2_1/c$	$P2_1/n$	$C2/c$	$P2_1/c$	$P1$
a, Å	20.3374 (11)	17.6001 (18)	29.8473 (12)	14.7003 (8)	12.3456 (6)
b, Å	7.5418 (4)	10.0526 (9)	10.7485 (4)	10.4012 (6)	14.9708 (6)
c, Å	24.0520 (14)	17.5942 (19)	24.4786 (9)	24.2906 (12)	17.5600 (6)
α, °	--	--	--	--	96.819 (3)
β, °	108.257 (2)	111.929 (3)	90.3918 (14)	107.591 (2)	97.059 (4)
γ, °	--	--	--	--	110.429 (3)
V, Å^3	3503.4 (3)	2887.7 (5)	7852.9 (5)	3540.4 (3)	2972.4 (2)
Z	8	4	8	4	1
$\Delta\rho_{max}$, $\Delta\rho_{min}$ (e Å^{-3})	0.34, −0.26	0.30, -0.30	0.46, −0.93	1.15, −1.22	0.48, −0.42
λ, Å	1.54178	0.71073	0.71073	0.71073	1.54178
T, K	150	150	150	100	150
$(\sin\ \theta/\lambda)_{max}$ (Å^{-1})	0.610	0.668	0.696	0.834	0.610
R	0.059	0.040	0.043	0.081	0.069
R_w (F^2)	0.163	0.108	0.123	0.196	0.190

4.4.3   Preparation of 4-ethynyltrimethylsilyl-*N*-1-R-1,8-naphthalimide

Preparation of 4-ethynyltrimethylsilyl-*N*-1-ethylpropyl-1,8-naphthalimide ($TMSC_2NAP^{Pen}$) and its precursors. To a Schlenk flask charged with 1.3 mL of 3-aminopentane (11.2 mmol) was added 30mL of ethanol and purged with N_2 for 30 min. 4-Bromo-1,8-naphthalic anhydride was added (1.12 g, 4.0 mmol) and the solution was

refluxed for 18 h. Solvent was removed from the resulting dark brown solution. The crude material was dissolved in EtOAc and filtered through a silica plug to remove impurities and then recrystallized from isopropanol to yield 880 mg (2.5 mmol) of 4-bromo-*N*-1-ethylpropyl-1,8-naphthalimide as a light yellow solid (63% based on 4-bromo-1,8-naphthalic anhydride). IR (cm^{-1}): C=O: 1655 (s), 1699 (s).

4-Bromo-*N*-1-ethylpropyl-1,8-naphthalimide (880 mg, 2.5 mmol), Pd(PPh$_3$)$_2$Cl$_2$ (40 mg, 0.057 mmol) and CuI (10 mg, 0.053 mmol) were dried under vacuum for 3 h, upon which 30 mL of diisopropylamine followed by 0.7 mL ethynyltrimethylsilane (4.9 mmol) were added. The solution turned from light yellow to red and was stirred for 20 min at room temperature. The crude solution was filtered through a silica plug with EtOAc and then purified by column chromatography (SiO$_2$, 1:1 CH$_2$Cl$_2$/Hexanes) to yield 0.86 g of 4-ethynyltrimethylsilyl-*N*-1-ethylpropyl-1,8-naphthalimide as a light yellow solid (95% based on 4-bromo-*N*-1ethylpropyl-1,8-naphthalimide). ^{1}H NMR (300 MHz, Chloroform-*d*) δ 8.67 – 8.56 (m, 2H), 8.49 (d, *J* = 7.6 Hz, 1H), 7.89 (d, *J* = 7.6 Hz, 1H), 7.86 – 7.77 (m, 1H), 5.07 – 4.98 (m, 1H), 2.28 – 2.18 (m, 2H), 1.96 – 1.86 (m, 2H), 0.90 (t, *J* = 7.5 Hz, 6H), 0.36 (s, 9H). Visible spectra, λ$_{max}$ (nm): 357, 375; IR (cm^{-1}): C=O: 1657 (s), 1698 (s); C≡C: 2146 (m).

Preparation of 4-ethynyl-*N*-mesityl-1,8-naphthalimide (HC$_2$NAP^{Mes}) and its precursors. 4-Bromo-1,8-naphthalic anhydride (2.2 g, 7.9 mmol) and trimethyl-2,4,6-aniline (6.00 mL, 42.8 mmol) were added to degassed ethanol (70 mL). The solution was refluxed under nitrogen for 84 h to yield a brown solution with a yellow precipitate. The solution was concentrated and filtered to isolate a light yellow precipitate, which was rinsed with methanol (10 mL) to afford 1.9 g of 4-bromo-*N*-mesityl-1,8-naphthalimide

(61% based on 4-bromo-1,8-naphthalic anhydride). ^{1}H NMR (300 MHz, Chloroform-*d*) δ 8.72 (d, *J* = 6.3 Hz, 1H), 8.66 (d, *J* = 8.6 Hz, 1H), 8.48 (d, *J* = 7.9 Hz, 1H), 8.09 (d, *J* = 7.9 Hz, 1H), 7.98 – 7.83 (m, 1H), 7.03 (s, 2H), 2.35 (s, 3H), 2.09 (s, 6H). Visible spectra, λ_{max} (nm): 344, 359.

4-Bromo-*N*-mesityl-1,8-naphthalimide (1.98 g, 5.02 mmol), Pd(PPh$_3$)$_2$Cl$_2$ (68 mg, 0.097 mmol) and CuI (18 mg, 0.095 mmol) were dried under vacuum for 4 h, upon which 30 mL of diisopropylamine followed by 2.0 mL ethynyltrimethylsilane (14.1 mmol) were added. The solution readily turned dark brown and was refluxed for 2 h. The crude solution was extracted from NH$_4$Cl (aq) with CH$_2$Cl$_2$ and dried over MgSO$_4$. Purification by column chromatography (SiO$_2$, 1:2 CH$_2$Cl$_2$/Hexanes) yielded 1.9 g of 4-ethynyltrimethylsilyl-*N*-mesityl-1,8-naphthalimide as a light yellow solid (87% based on 4-bromo-*N*-mesityl-1,8-naphthalimide). ^{1}H NMR (300 MHz, Chloroform-*d*) δ 8.78 – 8.62 (m, 2H), 8.56 (d, *J* = 7.9 Hz, 1H), 7.92 (d, *J* = 7.5 Hz, 1H), 7.86 (t, *J* = 7.4 Hz, 1H), 7.02 (s, 2H), 2.34 (s, 3H), 2.09 (s, 6H), 0.37 (s, 9H). Visible spectra, λ_{max} (nm, ε (M^{-1} cm^{-1})): 358 (22,100), 376 (25,600); IR (cm^{-1}): C=O: 1668 (s), 1708 (s); C≡C: 2148 (m).

Desilylation of 4-ethynyltrimethylsilyl-*N*-mesityl-1,8-naphthalimide (520 mg, 1.27 mmol) was accomplished in a MeOH/THF (v/v 2:1) solution using excess K$_2$CO$_3$ to afford 416 mg of 4-ethynyl-*N*-mesityl-1,8-naphthalimide (97% based on TMSC$_2$NAP^{Mes}). ^{1}H NMR (300 MHz, Chloroform-*d*) δ 8.79 – 8.72 (m, 1H), 8.72 – 8.67 (m, 1H), 8.60 (dd, *J* = 7.5, 1.9 Hz, 1H), 7.99 (dd, *J* = 7.4, 1.6 Hz, 1H), 7.88 (td, *J* = 7.9, 7.3, 2.0 Hz, 1H), 7.04 (s, 2H), 3.77 (s, 1H), 2.36 (s, 3H), 2.09 (s, 6H). Visible spectra, λ_{max} (nm, ε (M^{-1} cm^{-1})): 351 (25,600), 368 (23,000); IR (cm^{-1}): C=O: 1657 (s), 1700 (s); C≡C: 2097 (m); C≡C-H: 3223 (s).

4.4.4 Synthesis of NAP^{Mes} Byproducts

4-(Butadiyne-1,4-diyl)bis-*N*-mesityl-1,8-naphthalimide (NAP^{Mes}C$_4$NAP^{Mes}). This was obtained initially as a byproduct from the synthesis of 4-ethynyl-*N*-mesityl-1,8-naphthalimide. It can be synthesized via oxidative coupling. A round bottom flask was charged with 25 mL of acetone, NAP^{Mes}C$_2$H (30 mg, 0.09 mmol), TMEDA (0.5 mL), and CuI (6 mol%). The solution was stirred under oxygen for 30 min, solvent was removed, and the solution was purified over silica with CH$_2$Cl$_2$. Recrystallization from CH$_2$Cl$_2$ and hexanes afforded 19 mg of bright yellow solid (63% yield based on NAP^{Mes}C$_2$H). ^{1}H NMR (300 MHz, Chloroform-*d*) δ 8.80 (d, *J* = 8.3 Hz, 2H), 8.75 (d, *J* = 7.3 Hz, 2H), 8.65 (d, *J* = 7.6 Hz, 2H), 8.11 (d, *J* = 7.7 Hz, 2H), 7.96 (t, *J* = 7.8 Hz, 2H), 7.05 (s, 4H), 2.36 (s, 6H), 2.11 (s, 12H). Visible spectra, λ$_{max}$ (nm, ε (M^{-1} cm^{-1})): 355 (67,000), 426 (60,400); IR (cm^{-1}): C=O: 1662 (s), 1704 (s); C≡C: 2144 (w), 2207 (w).

(E)-*N,N,N*,-Triethyl-4-ethene-*N*-mesityl-1,8-naphthalimide triflate ([Et$_3$NC$_2$H$_2$NAP^{Mes}]OTf). This was obtained as a byproduct from the synthesis of **3a**, **3b**, and **3c**. It eluted as an orange band prior to the Co species. Recrystallization from MeCN and ether yielded a bright orange solid. ESI-MS: [M]$^+$, 441.3; ^{1}H NMR (300 MHz, Chloroform-*d*) δ 8.72 – 8.61 (m, 1H), 8.45 – 8.34 (m, 1H), 8.08 – 7.92 (m, 2H), 7.76 – 7.65 (m, 1H), 7.03 (s, 1H), 7.01 (s, 1H), 6.50 (s br, 1H), 5.20 (s br, 1H), 3.80 (q, *J* = 7.1 Hz, 2H), 3.16 (qd, *J* = 7.2, 4.8 Hz, 4H), 2.35 (s, 3H), 2.08 (s, 3H), 2.03 (s, 3H), 1.58 – 1.12 (m, 9H). Visible spectra, λ$_{max}$ (nm, ε (M^{-1} cm^{-1})): 350 (21,000), 392 (5,600); IR (cm^{-1}): C-N: 1027 (s), 1148 (s), 1277 (s); C=O: 1661 (s), 1704 (s); N-C=C: 2105 (m); -C=C-H: 3065 (m), 3084 (m).

4.4.5 Synthesis of Compounds **1**, **2** and **3**

Synthesis of [Co(cyclam)(C$_2$NAP^{Mes})Cl]Cl (**1a**). [Co(cyclam)Cl$_2$]Cl (645 mg, 1.77 mmol) was dissolved in 50 mL CH$_3$OH to which a 10 mL solution of THF containing 4-ethynyl-*N*-mesityl-1,8-naphthalimide (677mg, 2.0 mmol) was added and purged with N$_2$. Upon addition of Et$_3$N (4.0 mL, 30 mmol) the solution darkened and was refluxed for 18 h. Silica plug purification with CH$_3$OH/CH$_2$Cl$_2$ (v/v, 1:9) eluted the product as an orange band. Recrystallization from methanol and ether yielded 600 mg of **1** as an orange solid (51% based on [Co(cyclam)Cl$_2$]Cl). ESI-MS: [M]$^+$, 630.2; ^{1}H NMR (300 MHz, Methanol-*d*) δ 9.08 (d, *J* = 9.0 Hz, 1H), 8.65 (d, *J* = 7.4 Hz, 1H), 8.54 (d, *J* = 7.9 Hz, 1H), 8.04 (d, *J* = 7.9 Hz, 1H), 8.00 – 7.90 (m, 1H), 7.06 (s, 2H), 5.38 (s, 4H), 3.10 – 2.90 (m, 4H), 2.89 – 2.64 (m, 14H), 2.57 (d, *J* = 13.3 Hz, 2H), 2.37 (s, 3H), 2.04 (s, 6H). Visible spectra, λ$_{max}$ (nm, ε (M^{-1} cm^{-1})): 396 (33,400), 480 (534); IR (cm^{-1}): C=O: 1652 (s), 1700 (s); C≡C: 2103 (s). Elem. Anal. Found (Calcd) for C$_{34}$H$_{44}$N$_5$O$_3$CoCl$_4$ (**1a**·H$_2$O·CH$_2$Cl$_2$): C, 53.34 (52.93); H, 5.79 (5.75); N, 9.47 (9.08).

Synthesis of [Co(cyclam)(C$_2$NAP^{Me})Cl]Cl (**1b**). [Co(cyclam)Cl$_2$]Cl (138 mg, 0.38 mmol) and TMSC$_2$NAP^{Me} (106 mg, 0.45 mmol) were dissolved in 50 mL CH$_3$OH to which a 1.2 mL (17 mmol) Et$_3$N was added. The solution was refluxed for 16 h and turned from green to bright red. The crude solution was filtered, and ether was added to the filtrate to crash out the desired product. The light orange solid was filtered and dried to yield 103 mg of **1b** (48% based on [Co(cyclam)Cl$_2$]Cl). ESI-MS: [M]$^+$, 528.2; ^{1}H NMR (300 MHz, Methanol-*d*) δ 8.66 – 8.54 (m, 1H), 8.50 (dd, *J* = 12.3, 7.9 Hz, 1H), 8.04 – 7.85 (m, 3H), 5.21 (s, 3H), 4.93 (s br, 4H), 2.88 – 2.59 (m, 14H), 2.10 – 1.93 (m, 4H), 1.75 – 1.63 (m, 2H). Visible spectra, λ$_{max}$ (nm): 395; IR (cm^{-1}): C=O: 1653 (s), 1690 (s); C≡C: 2097 (s).

Synthesis of [Co(cyclam)(C$_2$NAP^{Pen})Cl]Cl (**1c**). [Co(cyclam)Cl$_2$]Cl (99.5 mg, 0.27 mmol) was dissolved in 50 mL CH$_3$OH containing 0.7 mL (5.0 mmol) Et$_3$N. The solution was purged with N$_2$, then 4-ethynyltrimethylsilyl-*N*-1-ethylpropyl-1,8-naphthalimide (115 mg, 0.32 mmol) was added and the solution was refluxed for 16 h. Silica plug purification with CH$_3$OH/CH$_2$Cl$_2$ (v/v, 1:5) eluted the product as an orange band. Recrystallization from methanol and ether yielded 79 mg of **1c** as an orange crystalline solid (47% based on [Co(cyclam)Cl$_2$]Cl). ESI-MS: [M]$^+$, 584.2; ^{1}H NMR (300 MHz, Methanol-*d*) δ 8.97 (d, *J* = 7.2 Hz, 1H), 8.58 (d, *J* = 6.8 Hz, 1H), 8.47 (d, *J* = 7.6 Hz, 1H), 7.97 (d, *J* = 7.7 Hz, 1H), 7.94 – 7.82 (m, 1H), 5.33 (s br, 4H), 5.06 – 5.01 (m, 1H), 2.88 – 2.69 (m, 14H), 2.26 (dd, *J* = 13.8, 7.5 Hz, 2H), 2.12 – 1.95 (m, 4H), 1.89 (dd, *J* = 13.5, 5.9 Hz, 2H), 1.77 – 1.65 (m, 2H), 0.87 (t, *J* = 7.4 Hz, 6H). Visible spectra, λ$_{max}$ (nm, ε (M^{-1} cm^{-1})): 391 (27,900), 483 (245); IR (cm^{-1}): C=O: 1647 (s), 1684 (s); C≡C: 2109 (s). Elem. Anal. Found (Calcd) for C$_{29.5}$H$_{41}$N$_5$O$_2$CoCl$_3$ (**1c**·0.5CH$_2$Cl$_2$): C, 53.51 (53.45); H, 6.61 (6.23); N, 10.72 (10.56).

Synthesis of [Co(cyclam)(C$_2$NAP$^{2-ethhex}$)Cl]Cl (**1d**). [Co(cyclam)Cl$_2$]Cl (150 mg, 0.41 mmol) was dissolved in 80 mL CH$_3$OH to which a 10 mL solution of THF containing 4-ethynyl-*N*-2-ethylhexyl-1,8-naphthalimide (138 mg, 0.41 mmol) was added and purged with N$_2$. Upon addition of Et$_3$N (1.0 mL, 7.5 mmol) the solution darkened and was refluxed for 18 h. Silica plug purification with CH$_3$OH/CH$_2$Cl$_2$ (v/v, 1:6) eluted the product as an orange band. Recrystallization from methanol and ether yielded 122 mg of **1d** as an orange solid (45% based on [Co(cyclam)Cl$_2$]Cl). ESI-MS: [M]$^+$, 626.3; ^{1}H NMR (300 MHz, Methanol-*d*) δ 8.98 (d, *J* = 8.3 Hz, 1H), 8.58 (d, *J* = 6.9 Hz, 1H), 8.47 (d, *J* = 7.4 Hz, 1H), 7.97 (d, *J* = 7.8 Hz, 1H), 7.90 – 7.83 (m, 1H), 5.34 (s, 4H), 4.11 (s,

2H), 2.93 – 2.71 (m, 16H), 2.01 (d, J = 16.7 Hz, 4H), 1.70 (s, 1H), 1.37 (dd, J = 14.8, 7.2 Hz, 8H), 1.04 – 0.83 (m, 6H). Visible spectra, λ_{max} (nm, ε (M^{-1} cm^{-1})): 392 (24,500), 480 (253); IR (cm^{-1}): C=O: 1646 (s), 1691 (s); C≡C: 2101 (s). Elem. Anal. Found (Calcd) for $C_{35}H_{56}N_5O_4CoCl_8$ (**1d**·$2H_2O$·$3CH_2Cl_2$): C, 43.96 (44.09); H, 5.75 (5.92); N, 7.99 (7.35).

Synthesis of [Co(cyclam)(C_2NAP^{Oct})Cl]Cl (**1e**). [Co(cyclam)Cl_2]Cl (500 mg, 1.4 mmol) was dissolved in 90 mL CH_3OH and 4 mL Et_3N (30 mmol) to which 4-ethynyl-*N*-octyl-1,8-naphthalimide (513 mg, 1.5 mmol) was added and purged with N_2. The solution was refluxed for 18 h. Silica plug purification with CH_3OH/CH_2Cl_2 (v/v, 1:5) eluted the product as an orange band. Recrystallization from methanol and ether yielded 345 mg of **1e** as an orange solid (63% based on [Co(cyclam)Cl_2]Cl). ESI-MS: $[M]^+$, 626.3; ^{1}H NMR (300 MHz, Methanol-*d*) δ 8.92 (d, J = 8.2 Hz, 1H), 8.53 (d, J = 7.1 Hz, 1H), 8.42 (d, J = 7.8 Hz, 1H), 7.93 (d, J = 7.7 Hz, 1H), 7.89 – 7.79 (m, 1H), 5.34 (s, 4H), 4.17 – 4.06 (m, 2H), 2.99 – 2.67 (m, 18H), 2.10 – 1.98 (m, 2H), 1.73 (s, 2H), 1.42 – 1.29 (m, 10H), 0.90 (d, J = 7.4 Hz, 3H). Visible spectra, λ_{max} (nm, ε (M^{-1} cm^{-1})): 393 (23,900), 482 (228); IR (cm^{-1}): C=O: 1647 (s), 1684 (s); C≡C: 2110 (s). Elem. Anal. Found (Calcd) for $C_{34}H_{50}N_5O_2CoCl_6$ (**1e**·$2CH_2Cl_2$): C, 48.77 (49.06); H, 6.13 (6.05); N, 8.92 (8.41).

Synthesis of [Co(cyclam)(C_2NAP^{Mes})(MeCN)]OTf_2 (**2a**). [Co(cyclam)(C_2NAP^{Mes})Cl]Cl, compound **1a** (323 mg, 0.49 mmol) was dissolved in 60mL MeCN and purged with N_2. Upon addition of AgOTf (620 mg, 2.41 mmol) the solution was refluxed for 16 h. The solution was filtered through celite with MeCN and concentrated. Recrystallization from MeCN and ether yielded 287 mg of **2a** as a yellow solid (63% based on **1a**). ESI-MS: $[M-OTf]^+$, 744.2.

Synthesis of [Co(cyclam)(C$_2$NAP^{Me})(MeCN)]OTf$_2$ (**2b**). [Co(cyclam)(C$_2$NAP^{Me})Cl]Cl, compound **1b** (203 mg, 0.36 mmol) was dissolved in 70 mL MeCN and AgOTf (460 mg, 1.8 mmol) was added. The solution was refluxed for 72 h, then filtered over celite to remove AgCl. Recrystallization from MeCN and ether yielded 183 mg of **2b** as a yellow solid (57% based on **1b**). ESI-MS: [M-OTf]$^+$, 698.2.

Synthesis of [Co(cyclam)(C$_2$NAP^{Mes})(C$_2$C$_6$H$_4$-4-NMe$_2$)]Cl (**3a**). In a 50 mL round bottom flask, **2a** (95 mg, 0.11 mmol) was dissolved in 20 mL MeCN and purged with N$_2$. After addition of Et$_3$N (0.9 mL, 6.6 mmol) and HC$_2$C$_6$H$_4$-4-NMe$_2$ (62 mg, 0.43 mmol) the solution was refluxed for 24 h. Purification over a silica plug (SiO$_2$, CH$_3$OH/EtOAc v/v, 1:5) eluted the desired product as a light orange band. Recrystallization from methanol and ether yielded 43 mg of **3a** as a light orange solid (39% based on **2a**). ESI-MS: [M]$^+$, 741.3; ^{1}H NMR (300 MHz, Methanol-d) δ 9.22 (d, J = 8.4 Hz, 1H), 8.66 (d, J = 6.9 Hz, 1H), 8.55 (d, J = 8.3 Hz, 1H), 8.06 (d, J = 7.7 Hz, 1H), 7.98 – 7.91 (m, 1H), 7.38 (d, J = 8.8 Hz, 2H), 7.06 (s, 2H), 6.72 (d, J = 8.5 Hz, 2H), 4.86 (s, 4H), 2.94 (s, 6H), 2.76 – 2.68 (m, 12H), 2.65 – 2.52 (m, 8H), 2.37 (s, 3H), 2.06 (s, 6H).Visible spectra, λ$_{max}$ (nm, ε (M^{-1} cm^{-1})): 287 (66,000), 399 (34,300); IR (cm^{-1}): C=O: 1654 (s), 1699 (s); C≡C: 2087 (w). Elem. Anal. Found (Calcd) for C$_{45}$H$_{52}$N$_6$O$_5$CoCl$_2$SF$_3$ (**3a**·CH$_2$Cl$_2$): C, 55.06 (55.39); H, 5.60 (5.37); N, 8.61 (8.99).

Synthesis of [Co(cyclam)(C$_2$NAP^{Me})(C$_2$C$_6$H$_4$-4-NMe$_2$)]Cl (**3ba**). In a 100 mL round bottom flask, **2b** (200 mg, 0.23 mmol) was dissolved in 50 mL MeCN. After addition of Et$_3$N (2.5 mL, 18 mmol) and HC$_2$C$_6$H$_4$-4-NMe$_2$ (203 mg, 1.4 mmol) the solution was refluxed for 16 h. Purification over a silica plug deactivated with Et$_3$N (SiO$_2$, MeCN) eluted the desired product as a light orange band. Recrystallization from MeCN

and ether yielded 42 mg of **3ba** as a light orange solid (29% based on **2b**). ESI-MS: [M]$^+$, 637.3; ^{1}H NMR (300 MHz, Chloroform-*d*) δ 8.38 (d, *J* = 8.1 Hz, 1H), 8.17 − 8.08 (m, 2H), 7.94 (d, *J* = 7.7 Hz, 1H), 7.53 − 7.47 (m, 1H), 7.41 (d, *J* = 9.2 Hz, 2H), 6.70 (d, *J* = 4.9 Hz, 2H), 5.00 (s br, 4H), 3.45 (s, 3H), 3.20 − 3.03 (m, 8H), 2.96 (d, *J* = 12.8 Hz, 6H), 2.91 − 2.67 (m, 12H). Visible spectra, λ_{max} (nm, ε (M^{-1} cm^{-1})): 283 (15,500), 397 (22,300); IR (cm^{-1}): C=O: 1650 (s), 1695 (s); C≡C: 2090 (m).

Synthesis of [Co(cyclam)(C$_2$NAP^{Mes})$_2$]Cl (**3b**). In a 100 mL round bottom flask, **2a** (150 mg, 0.16 mmol) was dissolved in 60 mL MeCN and purged with N$_2$. After addition of Et$_3$N (1.5 mL, 7.9 mmol) and HC$_2$NAP^{Mes} (120 mg, 0.35 mmol) the solution was refluxed for 16 h. Purification over a silica plug (SiO$_2$, CH$_3$OH/CH$_2$Cl$_2$ v/v, 1:7) eluted the desired product as a yellow band. Recrystallization from methanol and ether yielded 20 mg of **3b** as a yellow solid (11% based on **2a**). ESI-MS: [M]$^+$, 935.4; ^{1}H NMR (300 MHz, Methanol-*d*) δ 9.24 (d, *J* = 8.8 Hz, 2H), 8.68 (d, *J* = 7.5 Hz, 2H), 8.58 (d, *J* = 7.9 Hz, 2H), 8.11 (d, *J* = 8.3 Hz, 2H), 8.01 − 7.93 (m, 2H), 7.07 (s, 4H), 5.61 (s, 4H), 3.13 − 3.06 (m, 3H), 2.85 − 2.66 (m, 17H), 2.37 (s, 6H), 2.07 (s, 12H). Visible spectra, λ_{max} (nm, ε (M^{-1} cm^{-1})): 401 (59,900); IR (cm^{-1}): C=O: 1655 (m), 1698 (m); C≡C: 2086 (w). Elem. Anal. Found (Calcd) for C$_{61}$H$_{63}$N$_7$O$_7$CoCl$_4$SF$_3$ (**3b**·2CH$_2$Cl$_2$·MeCN): C, 56.06 (56.53); H, 5.06 (4.90); N, 7.41 (7.57).

Synthesis of [Co(cyclam)(C$_2$NAP^{Mes})(C$_2$Ph)]Cl (**3c**). In a 100 mL round bottom flask, **2a** (150 mg, 0.16 mmol) was dissolved in 30 mL MeCN and purged with N$_2$. After addition of Et$_3$N (1.5 mL, 7.9 mmol) and HC$_2$Ph (0.1 mL, 11 mmol) the solution was refluxed for 16 h. Purification over a silica plug (SiO$_2$, CH$_3$OH/CH$_2$Cl$_2$ v/v, 1:8) eluted the desired product as a yellow band. Recrystallization from methanol and ether yielded

81 mg of **3c** as a yellow solid (60% based on **2a**). ESI-MS: [M]$^+$, 698.3; ^{1}H NMR (300 MHz, Methanol-*d*) δ 9.09 (d, *J* = 7.1 Hz, 1H), 8.66 (d, *J* = 6.3 Hz, 1H), 8.54 (d, *J* = 8.1 Hz, 1H), 8.06 (d, *J* = 6.9 Hz, 1H), 8.03 – 7.92 (m, 2H), 7.52 (d, *J* = 8.8 Hz, 1H), 7.35 – 7.16 (m, 3H), 7.06 (s, 2H), 5.31 (s br, 4H), 3.02 – 2.69 (m, 18H), 2.60 – 2.54 (m, 2H), 2.37 (s, 3H), 2.06 (s, 6H). Visible spectra, λ_{max} (nm, ε (M^{-1} cm^{-1})): 397 (29,400); IR (cm^{-1}): C=O: 1655 (s), 1699 (s); C≡C: 2096 (s). Elem. Anal. Found (Calcd) for $C_{47}H_{55}N_6O_5CoCl_6SF_3$ (**3c**·3CH$_2$Cl$_2$·MeCN): C, 49.09 (49.32); H, 4.23 (4.84); N, 6.98 (7.34).

4.4.6   X-ray Crystallographic Analysis.

Single crystals of **1a** were obtained from the slow diffusion of ether into a CH$_2$Cl$_2$/CH$_3$OH (v/v, 1:1) solution. Single crystals of **1c** were grown from slow diffusion of ether/hexanes (v/v 2:1) into a CH$_3$OH solution. Single crystals of **3b** were grown from slow diffusion of hexanes into a CH$_2$Cl$_2$/CH$_3$OH (v/v, 2:1) solution. Single crystals of HC$_2$NAP^{Mes} were grown from slow evaporation of a CH$_2$Cl$_2$/hexanes (v/v 1:2) solution. Single crystals of [Et$_3$NC$_2$H$_2$NAP^{Mes}]OTf were grown from slow diffusion of ether into a MeCN/MeOH (v/v 1:1) solution. X-ray diffraction data for **1a**, **1c** and [Et$_3$NC$_2$H$_2$NAP^{Mes}]OTf was obtained on a Bruker Quest diffractometer with Mo Kα radiation (λ=0.71073 Å) at 150K. X-ray diffraction data for **3b** and HC$_2$NAP^{Mes} were obtained on a Bruker Quest diffractometer with Cu *K*α radiation (λ= 1.54178 Å) at 150K. Data were collected; reflections were indexed and processed using APEX3.[44] The space groups were assigned and the structures were solved by direct methods using XPREP within the SHELXTL suite of programs[45,46] and refined using Shelxle.[47,48]

4.5   References

(1)   Lu, L. Y.; Zheng, T. Y.; Wu, Q. H.; Schneider, A. M.; Zhao, D. L.; Yu, L. P. Recent Advances in Bulk Heterojunction Polymer Solar Cells. *Chem. Rev.* **2015**, *115*, 12666-12731.

(2)   Albinsson, B.; Mårtensson, J. Long-range electron and excitation energy transfer in donor–bridge–acceptor systems. *J. Photochem. Photobiol. C* **2008**, *9*, 138-155.

(3)   Delor, M.; Scattergood, P. A.; Sazanovich, I. V.; Parker, A. W.; Greetham, G. M.; Meijer, A. J. H. M.; Towrie, M.; Weinstein, J. A. Toward control of electron transfer in donor-acceptor molecules by bond-specific infrared excitation. *Science* **2014**, *346*, 1492-1495.

(4)   Delor, M.; Keane, T.; Scattergood, P. A.; Sazanovich, I. V.; Greetham, G. M.; Towrie, M.; Meijer, A. J. H. M.; Weinstein, J. A. On the mechanism of vibrational control of light-induced charge transfer in donor–bridge–acceptor assemblies. *Nature Chem.* **2015**, *7*, 689-695.

(5)   Scattergood, P. A.; Delor, M.; Sazanovich, I. V.; Bouganov, O. V.; Tikhomirov, S. A.; Stasheuski, A. S.; Parker, A. W.; Greetham, G. M.; Towrie, M.; Davies, E. S.; Meijer, A. J. H. M.; Weinstein, J. A. Electron transfer dynamics and excited state branching in a charge-transfer platinum(II) donor-bridge-acceptor assembly. *Dalton Trans.* **2014**, *43*, 17677-17693.

(6)   Delor, M.; Archer, S. A.; Keane, T.; Meijer, A. J. H. M.; Sazanovich, I. V.; Greetham, G. M.; Towrie, M.; Weinstein, J. A. Directing the path of light-induced electron transfer at a molecular fork using vibrational excitation. *Nature Chemistry* **2017**, *9*, 1099-1104.

(7)   Gauthier, S.; Caro, B.; Robin-Le Guen, F.; Bhuvanesh, N.; Gladysz, J. A.; Wojcik, L.; Le Poul, N.; Planchat, A.; Pellegrin, Y.; Blart, E.; Jacquemin, D.; Odobel, F. Synthesis, photovoltaic performances and TD-DFT modeling of push-pull diacetylide platinum complexes in TiO2 based dye-sensitized solar cells. *Dalton Trans.* **2014**, *43*, 11233-11242.

(8)   De Sousa, S.; Ducasse, L.; Kauffmann, B.; Toupance, T.; Olivier, C. Functionalization of a Ruthenium-Diacetylide Organometallic Complex as a Next-Generation Push-Pull Chromophore. *Chem. Eur. J.* **2014**, *20*, 7017-7024.

(9)   Durand, R. J.; Gauthier, S. b.; Achelle, S.; Groizard, T.; Kahlal, S.; Saillard, J.-Y.; Barsella, A.; Le Poul, N.; Le Guen, F. R. Push-pull D-p-Ru-p-A chromophores: synthesis and electrochemical, photophysical and second-order nonlinear optical properties. *Dalton Trans.* **2018**, *47*, 3965-3975.

(10)   Nisic, F.; Colombo, A.; Dragonetti, C.; Garoni, E.; Marinotto, D.; Righetto, S.; De Angelis, F.; Lobello, M. G.; Salvatori, P.; Biagini, P.; Melchiorre, F. Functionalized Ruthenium Dialkynyl Complexes with High Second-Order Nonlinear Optical Properties and Good Potential as Dye Sensitizers for Solar Cells. *Organometallics* **2015**, *34*, 94-104.

(11)   Banziger, S. D.; Ren, T. Syntheses, structures and bonding of 3d metal alkynyl complexes of cyclam and its derivatives. *J. Organomet. Chem.* **2019**, *885*, 39-48.

(12)   Ren, T. Sustainable metal alkynyl chemistry: 3d metals and polyaza macrocyclic ligands. *Chem. Commun.* **2016**, *52*, 3271-3279.

(13)   Banziger, S. D.; Cook, T. D.; Natoli, S. N.; Fanwick, P. E.; Ren, T. Synthetic and Structural Studies of Mono-acetylide and Unsymmetric Bis-acetylide Complexes based on CoIII-cyclam. *J. Organomet. Chem.* **2015**, *799-800*, 1-6.

(14)   Banziger, S. D.; Li, X.; Zeller, M.; Rubtsov, I.; Ren, T. Unsymmetrical Bis-Alkynyl Complexes Based on Co(III)(cyclam): Synthesis and Ultrafast Charge Separation. *Chem. Sci.* **2019**, manuscript in preparation.

(15)   Natoli, S. N.; Zeller, M.; Ren, T. Stepwise Synthesis of Bis-Alkynyl CoIII(cyclam) Complexes under Ambient Conditions. *Inorg. Chem.* **2016**, *55*, 5756-5758.

(16)   Natoli, S. N.; Zeller, M.; Ren, T. An Aerobic Synthetic Approach toward Bis-Alkynyl Cobalt(III) Compounds. *Inorg. Chem.* **2017**, *56*, 10021-10031.

(17)   McAdam, C. J.; Morgan, J. L.; Robinson, B. H.; Simpson, J.; Rieger, P. H.; Rieger, A. L. Tunable Donor-Acceptor Interactions in 4-Ene/Yne-Ferrocenyl and 4-Enamine Naphthalimides with Ferrocenyl Headgroups. *Organometallics* **2003**, *22*, 5126-5136.

(18)   Saini, A.; Justin Thomas, K. R. Bis-naphthalimides bridged by electron acceptors: optical and self-assembly characteristics. *RSC Adv.* **2016**, *6*, 71638-71651.

(19)   Fischer, G. W. Formylvinylierung tertiarer Amine. *Z. Chem* **1968**, *8*, 269-270.

(20)   Shimada, T.; Nakamura, I.; Yamamoto, Y. Intramolecular C-N Bond Addition of Amides to Alkynes Using Platinum Catalyst. *J. Am. Chem. Soc.* **2004**, *126*, 10546-10547.

(21)   Cacchi, S.; Fabrizi, G.; Pace, P. Palladium-Catalyzed Cyclization of o-Alkynyltrifluoroacetanilides with Allyl Esters. A Regioselective Synthesis of 3-Allylindoles. *J. Org. Chem.* **1998**, *63*, 1001-1011.

(22)   Zeng, X.; Kinjo, R.; Donnadieu, B.; Bertrand, G. Serendipitous Discovery of the Catalytic Hydroammoniumation and Methylamination of Alkynes. *Angew. Chem. Int. Ed.* **2010**, *49*, 942-945.

(23)   McAdam, C. J.; Manning, A. R.; Robinson, B. H.; Simpson, J. Group 8 and 10 metal acetylide naphthalimide dyads. *Inorg. Chim. Acta* **2005**, *358*, 1673-1682.

(24)   McAdam, C. J.; Robinson, B. H.; Simpson, J.; Tagg, T. Ferrocenyl-Naphthalimide Donor-Acceptor Dyads with Aromatic Spacer Groups. *Organometallics* **2010**, *29*, 2474-2483.

(25)   Banziger, S. D.; Judkins, E. C.; Zeller, M.; Ren, T. Diruthenium-DMBA Bis-Alkynyl Compounds with Hetero- and Extended- Aryl Appendant. *Chin. J. Inorg. Chem.* **2017**, *33*, 2103-2109.

(26)   Cook, T. D.; Fanwick, P. E.; Ren, T. Unsymmetric Mononuclear and Bridged Dinuclear Co(III)-cyclam Acetylides. *Organometallics* **2014**, *33*, 4621-4624.

(27)   Judkins, E. C.; Zeller, M.; Ren, T. Synthesis and Characterizations of Macrocyclic Cr(III) and Co(III) 1-Ethynyl Naphthalene and 9-Ethynyl Anthracene Complexes: An Investigation of Structural and Spectroscopic Properties. *Inorg. Chem.* **2018**, *57*, 2249-2259.

(28)   Oxley, B. M.; Mash, B.; Zeller, M.; Banziger, S.; Ren, T. Crystal structures of 5,12-dimethyl-1,4,8,11-tetraazacyclotetradecane cobalt(III) mono-phenylacetylide and bis-phenylacetylide. *Acta Cryst. E* **2018**, *74*, 522-529.

(29)   Thakker, P. U.; Aru, R. G.; Sun, C.; Pennington, W. T.; Siegfried, A. M.; Marder, E. C.; Wagenknecht, P. S. Synthesis of trans Bis-alkynyl Complexes of Co(III) Supported by a Tetradentate Macrocyclic Amine: A Spectroscopic, Structural, and Electrochemical Analysis of p-Interactions and Electronic Communication in the CC-M-CC Structural Unit. *Inorg. Chim. Acta* **2014**, *411*, 158-164.

(30)   Thakker, P. U.; Sun, C.; Khulordava, L.; McMillen, C. D.; Wagenknecht, P. S. Synthetic control of the cis/trans geometry of M(cyclam)(CCR)(2) OTf complexes and photophysics of cis- Cr(cyclam)(CCCF3)(2) OTf and cis-Rh(cyclam)(CCCF3)(2) OTf. *J. Organomet. Chem.* **2014**, *772*, 107-112.

(31)   Banziger, S. D.; Zeller, M.; Ren, T. Macrocyclic Co(III) complexes of TPA acetylide: Synthesis, eta-2 attachment of Cu(I)/Ag(I) and spectroscopic properties. *Eur. J. Inorg. Chem.*, manuscript in preparation.

(32)   Hoffert, W. A.; Kabir, M. K.; Hill, E. A.; Mueller, S. M.; Shores, M. P. Stepwise acetylide ligand substitution for the assembly of ethynylbenzene-linked Co(III) complexes. *Inorg. Chim. Acta* **2012**, *380*, 174-180.

(33)   Cook, T. D.; Natoli, S. N.; Fanwick, P. E.; Ren, T. Dimeric Complexes of CoIII(cyclam) with Polyyndiyl Bridge. *Organometallics* **2015**, *34*, 686-689.

(34)   Cook, T. D.; Natoli, S. N.; Fanwick, P. E.; Ren, T. CoIII(cyclam) Oligoynyls: Monomeric Oligoynyl Complexes and Dimeric Complexes with an Oligoyn-diyl Bridge. *Organometallics* **2016**, *35*, 1329-1338.

(35)   Natoli, S. N.; Cook, T. D.; Abraham, T. R.; Kiernicki, J. J.; Fanwick, P. E.; Ren, T. Cobalt(III) Bridged by gem-DEE: Facile Access to A New Class of Cross-Conjugated Organometallics. *Organometallics* **2015**, *34*, 5207-5209.

(36)   Natoli, S. N.; Azbell, T. J.; Fanwick, P. E.; Zeller, M.; Ren, T. A Synthetic Approach to Cross-Conjugated Organometallic Complexes Based on geminal-Diethynylethene and CoIII(cyclam). *Organometallics* **2016**, *35*, 3594-3603.

(37)   Liu, Y.; Wang, H.-Y.; Chen, G.; Xu, X.-P.; Ji, S.-J. Synthesis and Properties of Novel Ethyne-Linked Compounds Containing Carbazole and 1,8-Naphthalimide Groups. *Aust. J. Chem.* **2009**, *62*, 934-940.

(38)   Manna, J.; John, K. D.; Hopkins, M. D. In *Advances in Organometallic Chemistry*; 38 ed.; Stone, F. G. A., West, R., Eds.; Academic Press, 1995; pp 79-154.

(39)   Sun, C.; Thakker, P. U.; Khulordava, L.; Tobben, D. J.; Greenstein, S. M.; Grisenti, D. L.; Kantor, A. G.; Wagenknecht, P. S. Trifluoropropynyl as a Surrogate for the Cyano Ligand and Intense, Room-Temperature, Metal-Centered Emission from Its Rh(III) Complex. *Inorg. Chem.* **2012**, *51*, 10477-10479.

(40)   Chrominski, M.; Lewalska, A.; Gryko, D. Reduction-free synthesis of stable acetylide cobalamins. *Chem. Commun.* **2013**, *49*, 11406-11408.

(41)   Long, N. J.; Williams, C. K. Metal Alkynyl Complexes: Synthesis and Materials. *Angew. Chem. Int. Ed. Engl.* **2003**, *42*, 2586-2617.

(42)   Younus, M.; Long, N. J.; Raithby, P. R.; Lewis, J.; Page, N. A.; White, A. J. P.; Williams, D. J.; Colbert, M. C. B.; Hodge, A. J.; Khan, M. S.; Parker, D. G. Synthesis and characterisation of mono-acetylide and unsymmetrical bis-acetylide complexes of ruthenium and osmium: X-ray structure determinations on [(dppe)(2)Ru(Cl)(C C-C6H4-p- NO2)], [(dppe)(2)Ru(Cl)(C C-C6H3-o-CH3-p-NO2)] and [(dppm)(2)Os(C C-C6H4-p-CH3)(C C-C6H4-p-NO2)]. *J. Organomet. Chem.* **1999**, *578*, 198-209.

(43)   Bosnich, B.; Tobe, M. L.; Webb, G. A. Complexes of Nickel(2) with a Cyclic Tetradentate Secondary Amine. *Inorg. Chem.* **1965**, *4*, 1109-1112.

(44)   *APEX3 v2016.9-0, Saint V8.34A, Saint V8.37A*Bruker AXS, Inc.: Madison, WI, 2016.

(45)   *SHELXTL suite of programs, version 6.14*Bruker AXS Inc.: Madison, WI, 2000-2003.

(46)   Sheldrick, G. M. A short history of SHELX. *Acta Crystallogr A* **2008**, *64*, 112-122.

(47)   Sheldrick, G. M. Crystal structure refinement with SHELXL. *Acta Crystallogr C* **2015**, *71*, 3-8.

(48) Hübschle, C. B.; Sheldrick, G. M.; Dittrich, B. ShelXle: a Qt graphical user interface for SHELXL. *J. Appl. Cryst.* **2011**, *44*, 1281-1284.

CHAPTER 5.   DIRUTHENIUM-DMBA BIS-ALKYNYL COMPOUNDS WITH HETERO- AND EXTENDED- ARYL APPENDANT

Abstract: Under weak base conditions, diruthenium(III) tetrakis-*N,N′*-dimethylbenzamidinate (DMBA) nitrate (Ru$_2$(DMBA)$_4$(NO$_3$)$_2$) was reacted with arylethyne ligands, where aryl = NAP^{Me} (*N-methyl*-1,8-naphthalimide), NAP^{iPr} (*N-isopropyl*-1,8-naphthalimide), Naphth (naphthalene) and Ant (anthracene), to afford four new compounds: *trans*-Ru$_2$(DMBA)$_4$(C$_2$Ar)$_2$ (Ar = NAP^{Me}, **1**; NAP^{iPr}, **2**; Naphth, **3**; and Ant, **4**). Molecular structures of new compounds were determined using single crystal X-ray diffraction (CCDC 1555598: **1**; 1555599: **2**; 1555609: **3**; 1555611: **4**), and the Ru-Ru bond lengths (2.450 – 2.491 Å) are consistent with the existence of a Ru-Ru single bond. These compounds are diamagnetic and were further characterized with ^{1}H NMR and UV-Vis-NIR spectroscopic techniques. Cyclic voltammograms of compounds **1 - 4** consist of two reversible one-electron processes, an oxidation and a reduction, and their potentials depend on the nature of Ar.

5.1   Introduction

Conjugated metal-alkynyl compounds are of interest to both the inorganic and materials chemistry communities[1-3] and have been studied as prototypical molecular wires,[4-7] light emitting materials[8,9] and photovoltaic materials[10]. Recent interesting examples of linearly conjugated metal alkynyl or metal alkenyl species include those based on mono- and bimetallic Ru compounds supported by phosphine.[11-14] and PtAu$_2$ heterometallics.[15,16]

Diruthenium compounds bearing axial alkynyl ligands are known for their capacity to undergo multiple reversible one-electron oxidations / reductions,[2] strongly couple across oligoyn-diyl bridges,[17-19] mediate couplings between two ferrocenyls,[20] facilitate the formation of supramolecules,[21,22] and function as the active species in molecular devices.[23,24]   Among *N*,*N'*-bidentate ligands used to support the Ru$_2$ core, DMBA (*N*,*N'*-dimethylbenzamidinate) and its derivatives are the most electron donating and support a variety of Ru$_2$(III,III) bis-alkynyls[25-27] and Fe-Ru$_2$ heterometallic complexes.[28] Reported in this contribution are four new *trans*-Ru$_2$(DMBA)$_4$(C$_2$Ar)$_2$ type compounds with Ar as 4-*N*-methyl-1,8-naphthalimide (**1**), 4-*N*-isopropyl-1,8-naphthalimide (**2**) 1-naphthalene (**3**) and 9-anthracene (**4**), as sketched in Scheme 5.1.
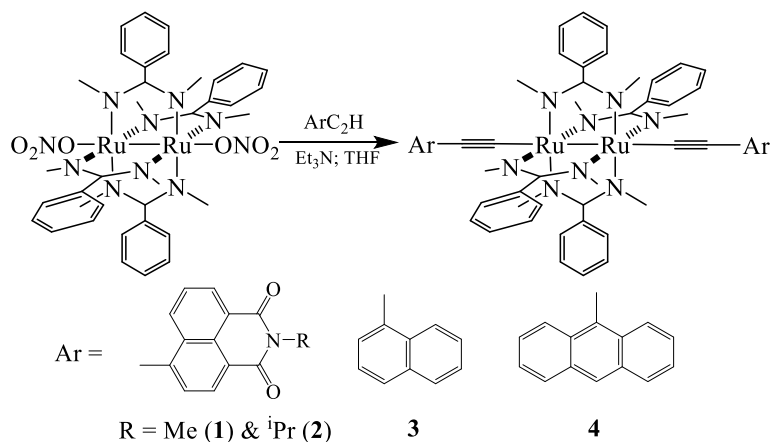
Scheme 5.1. New $Ru_2(DMBA)_4(C_2Ar)_2$ compounds

5.2 Experimental

5.2.1 Materials and measurements

[$Ru_2(DMBA)_4(NO_3)$] was prepared according to literature procedures.[29] Also prepared according literature procedures were 1-ethynylnaphthalene,[30] 9-ethynylanthracene,[31] and 4-ethynyl-*N*-methyl-1,8-naphthalimide.[32] THF was distilled over Na/benzophenone under a N_2 atmosphere. Diisopropylamine was purchased from Acros Organics and distilled over potassium hydroxide. The synthesis of Ru_2 compounds was performed under ambient atmosphere. All other reactions were carried out using Schlenk techniques under N_2. UV-Vis-NIR spectra were obtained with a JASCO V-670 UV-Vis-NIR spectrophotometer. Infrared spectra were obtained on a JASCO FT-IR 6300 spectrometer via ATR on a ZnSe crystal. ^1H NMR spectra were recorded on a Varian MERCURY300 NMR. Cyclic voltammograms were recorded in 0.1 M *n*-Bu_4NPF_6 and 1.0 mM ruthenium species solution (THF, Ar degassed) using a CHI620A voltammetric analyzer with a glassy carbon working electrode (diameter = 2 mm), Pt-wire counter electrode, and a Ag/AgCl reference electrode with ferrocene used as an external reference.

5.2.2   Preparation of 4-Ethynyl-*N*-isopropyl-1,8-naphthalimide.

4-Bromo-1,8-naphthalic anhydride (1.00 g, 3.61 mmol) and isopropylamine (1.00 mL, 11.66 mmol) were added to degassed ethanol (30 mL). The mixture was refluxed under nitrogen for 18 h to yield a dark yellow solution and then placed in an ice bath. A light yellow precipitate formed which was then filtered, and rinsed with methanol (30 mL) to afford 0.89 g of 4-bromo-*N*-isopropyl-1,8-naphthalimide (77% based on 4-bromo-1,8-naphthalic anhydride). ^{1}H NMR (CDCl$_3$, δ): 8.64 (dd, J = 7.3, 1.1 Hz, 1H), 8.55 (dd, J = 8.5, 1.1 Hz, 1H), 8.40 (d, J = 7.9 Hz, 1H), 8.03 (d, J = 7.9 Hz, 1H), 7.84 (dd, J = 8.5, 7.4 Hz, 1H), 5.42 (hept, J = 7.0 Hz, 1H), 1.60 (d, J = 7.0 Hz, 6H). IR (cm^{-1}): C=O: 1656 (s), 1700 (s).

4-Bromo-*N*-isopropyl-1,8-naphthalimide (890 mg, 2.80 mmol), Pd(PPh$_3$)$_2$Cl$_2$ (40 mg, 0.057 mmol) and CuI (11 mg, 0.058 mmol) were dried under vacuum for 3 h, upon which 35 mL of diisopropylamine and ethynyltrimethylsilane (0.8 mL, 5.78 mmol) were added. The dark brown solution was stirred at room temperature for 30 min and then heated to reflux for 30 min until the solvent became black. Upon rotary evaporation, the off-white solid was re-dissolved in EtOAc, rinsed through a short silica plug, and purified by column chromatography (SiO$_2$, 1:1 CH$_2$Cl$_2$/Hexanes) to afford 855 mg of 4-ethynyltrimethylsilyl-*N*-isopropyl-1,8-naphthalimide   (91%   based   on   4-bromo-*N*-isopropyl-1,8-naphthalimide). Desilylation of 4-ethynyltrimethylsilyl-*N*-isopropyl-1,8-naphthalimide (675 mg, 2.01 mmol) was accomplished using K$_2$CO$_3$ in a MeOH/CH$_2$Cl$_2$ (v/v 2:1) solution to afford 524 mg of 4-ethynyl-*N*-isopropyl-1,8-naphthalimide (98%). ^{1}H NMR (CDCl$_3$, δ): 8.63 (dd, J = 8.6 Hz, 2H), 8.51 (d, J = 7.5 Hz, 1H), 7.93 (d, J = 7.7 Hz, 1H), 7.82 (t, J = 7.9 Hz, 1H), 5.43 (hept, 1H), 3.72 (s, 1H), 1.60 (dd, J = 7.0, 0.6 Hz,

6H). Visible spectra, λ_{max} (nm, ε (M^{-1} cm^{-1})): 350 (35,240), 366 (32,580); IR (cm^{-1}): C=O: 1653 (s), 1700 (s); C≡C: 2102 (m); C≡C-H: 3227 (s).

5.2.3 Preparation of compounds 1-4

Preparation of 1. $Ru_2(DMBA)_4(NO_3)_2$ (45.2 mg, 0.049 mmol), 4-ethynyl-*N*-methyl-1,8-naphthalimide (70.1 mg, 0.298 mmol), and Et_3N (0.6 mL) were dissolved in 50mL THF and reacted for 4 h to yield a dark red solution. Upon solvent removal, the residue was purified by column chromatography (SiO_2, hexanes/THF v/v, 9:1). Unreacted ligand eluted first, followed closely by the desired product as a deep red band. Upon solvent removal, the red fraction was recrystallized from hexanes and THF to afford 43.7 mg of **1** (70% based on Ru). ESI-MS: $[M]^+$, 1260.0. ^{1}H NMR ($CDCl_3$, δ): 8.82 (d, J = 8.2 Hz, 2H), 8.54 (d, J = 7.4 Hz, 2H), 8.43 (d, J = 7.8 Hz, 2H), 7.60 (d, J = 7.8 Hz, 2H), 7.53 − 7.46 (m, 12H), 7.41 (d, J = 7.8 Hz, 2H), 7.07 (d, J = 7.1 Hz, 8H), 3.53 (s, 6H), 3.40 (s, 24H). Visible spectra, λ_{max} (nm, ε (M^{-1} cm^{-1})): 322 (16,160), 460 (15,200), 550 (28,200), 877 (1,690); IR (cm^{-1}): C=O: 1654 (s), 1691 (s); C≡C: 2047 (s). Anal. Found (calcd) for $C_{70}H_{68}N_{10}O_5Ru_2$ (**1**·THF): C, 63.28 (63.14); H, 5.04 (5.14); N, 10.52 (10.52).

Preparation of 2. $Ru_2(DMBA)_4(NO_3)_2$ (93 mg, 0.102 mmol), 4-ethynyl-*N*-isopropyl-1,8-naphthalimide (134 mg, 0.508 mmol) and Et_3N (0.3 mL) were reacted in 100 mL of THF for 3 h. The reaction mixture was purified similarly to that of **1** to afford 112 mg of **2** (84% based on Ru). ESI-MS: $[M]^+$, 1316.1. ^{1}H NMR ($CDCl_3$, δ): 8.78 (dd, J = 8.3, 1.3 Hz, 2H), 8.50 (dt, J = 7.3, 1.6 Hz, 2H), 8.40 (dd, J = 7.8, 1.8 Hz, 2H), 7.74 − 7.27 (m, 16H), 7.10 − 7.02 (m, 8H), 5.47 − 5.34 (m, 2H), 3.40 (d, J = 1.8 Hz, 24H), 1.57 (dd, J = 3.1, 1.9 Hz, 12H).Visible spectra, λ_{max} (nm, ε (M^{-1} cm^{-1})): 323 (20,940), 462

(20,050), 549 (37,140), 870 (2,450); IR (cm^{-1}): C=O: 1653 (s), 1690 (s); C≡C: 2049 (s).

Anal. Found (calcd) for C$_{74}$H$_{80}$N$_{10}$O$_7$Ru$_2$ (**2**·THF·2H$_2$O): C, 62.31 (62.43); H, 5.40 (5.66);

N, 9.82 (9.83).

Preparation of 3. Ru$_2$(DMBA)$_4$(NO$_3$)$_2$ (0.095 g, 0.104 mmol) was added to a

solution of 1-ethynylnaphthalene (0.043 g, 0.28 mmol) and 3 mL Et$_3$N in THF (30 mL)

and stirred for 4 h. The crude solution was run over a silica plug, eluting **3** with a 89:10:1

hexanes:EtOAc:THF solvent mixture. The ensuing recrystallization from THF/MeOH

yielded **3** as deep red, crystalline solid (52 mg, 0.048 mmol, 46% based on Ru). ESI-

MS:[M + H]$^+$, 1094 m/z. ^{1}H NMR (CDCl$_3$, δ): 8.59 (dd, J = 7.9, 1.4 Hz, 2H), 7.71 (dd, J

= 6.9, 1.3 Hz, 2H), 7.51 – 7.32 (m, 22H), 7.10 – 7.03 (m, 8H), 3.42 (s, 24H). Visible

spectra, λmax (nm, ε (M^{-1} cm^{-1})): 372sh (32,162), 391 (33,184), 508 (18,195), 681sh

(1,791), 892 (3,214); IR (cm^{-1}): C≡C: 2063 (s). Anal. Found (calcd) for C$_{60}$H$_{60}$N$_8$ORu$_2$

(**3**·H$_2$O): C, 64.85 (64.85); H, 5.64 (5.44); N, 9.97 (10.08).

Preparation of 4. Ru$_2$(DMBA)$_4$(NO$_3$)$_2$ (0.085 g, 0.093 mmol) was added to a

solution of 9-ethynylanthracene (0.055 g, 0.27 mmol) and 1.5 mL Et$_2$NH in THF (20 mL)

and stirred 12 h. The crude solution was purified similarly to that of **3** to afford 50 mg of

4 (0.042 mmol, 45% based on Ru). ESI-MS:[M + H]$^+$,1195 m/z. ^{1}H NMR (CDCl$_3$, δ):

8.88 (d, J = 8.4 Hz, 4H), 7.93 (s, 2H), 7.86 (d, J = 8.5 Hz, 4H), 7.51-7.30 (m, 20H), 7.13

(d, J = 6.8 Hz, 8H), 3.55 (s, 24H). Visible spectra, λmax (nm, ε (M^{-1}cm^{-1})): 283sh

(35,544), 289 (49,953), 502 (41,938), 699sh (1,785), 903 (2,291); IR (cm^{-1}): C≡C: 2045

(s). Anal. Found (calcd) for C$_{72}$H$_{73}$N$_8$O$_{2.5}$Ru$_2$ (**4**·1.5H$_2$O·THF): C, 66.97 (66.91); H, 5.76

(5.69); N, 8.53 (8.67).

5.3 Results and Discussion

5.3.1 Syntheses

As shown in Scheme 5.1, compounds **1** – **4** were prepared from the direct reaction between $Ru_2(DMBA)_4(NO_3)_2$[29] and HC_2Ar in the presence of Et_3N/Et_2NH in satisfactory to very good yields after purification. Consistent with the previous studies of related compounds, compounds **1** – **4** are diamagnetic, which facilitate their characterization using ^{1}H NMR. In addition, the purity of these compounds was also confirmed by combustion analysis.

5.3.2   Crystal structures.

Figure 5.1. ORTEP plots at 30% probability level of compounds **1** (a), **2** (b), **3** (c) and **4** (d); hydrogen atoms were omitted for clarity.

Molecular structures of compounds **1** – **4** have been determined using single crystal X-ray diffraction and structural plots are shown in Figure 5.1. While molecules **2** – **4** do not contain a crystallographic symmetry element, there is a C_2 axis passing through the midpoint of the Ru-Ru bond and relating two adjacent DMBA ligands in **1**. It is clear from Figure 5.1 that all compounds adopt the expected paddlewheel geometry with four equatorial bridging DMBA and two axial arylethynyl ligands. The Ru-Ru bond lengths are within a narrow range of 2.450 – 2.491 Å, which agrees with the values reported for other $Ru_2(DMBA)_4(C_2R)_2$ type compounds[2] and is consistent with the presence of a Ru-Ru single bond. The Ru-C bond lengths in **1 - 4** (1.96 – 2.01 Å) are also in agreement with the previous reports.[2,33]

A notable structural feature of the $Ru_2(DMBA)_4(C_2Ar)_2$ type compounds is the significant distortion of the first coordination sphere of the Ru_2 core from an idealized paddlewheel structure (D_{4h}). The origin of such distortion is rooted in a second order Jahn-Teller effect, as originally proposed to rationalize the structures of the $Ru_2(DArF)_4(C_2Ph)_2$ type compounds (DArF = *N,N'*-diarylformamidinate).[34] The structural distortion is typically reflected by (i) the large variation in Ru-N bond lengths, (ii) both acute and obtuse Ru-Ru-N angles, and (iii) significantly nonlinear Ru-Ru-C angles. These are clearly the case for the structures of **1** – **3**. However, the distortion is completely suppressed in **4**: Ru-N bond lengths are within a narrow range, Ru-Ru-N angles are all acute and Ru-Ru-C angles are fairly linear. We surmise that the steric effect of anthracene may be responsible for a more symmetric structure.

Table 5.1. Selected bond lengths (Å) and angles (°) for compounds **1** – **4**.

1[a]			
Ru1-Ru1'	2.491 (2)	Ru1'-Ru1-C1	162.5 (5)
Ru1-C1	2.01 (2)	Ru1'-Ru1-N2	81.2 (4)
Ru1-N2	2.04 (2)	Ru1'-Ru1-N3	93.4 (4)
Ru1-N3	2.01 (3)	Ru1'-Ru1-N4	79.2 (4)
Ru1-N4	2.18 (1)	Ru1'-Ru1-N5	93.9 (4)
Ru1-N5	2.00 (2)		
C1-C2	1.24 (2)		
2 [a]			
Ru1-Ru2	2.4567 (4)	Ru2-Ru1-N3	91.24 (9)
Ru1-C1	1.971 (4)	Ru2-Ru1-N5	82.59 (8)
Ru2-C18	1.958 (4)	Ru2-Ru1-N7	81.12 (9)
Ru1-N3	2.011 (3)	Ru2-Ru1-N9	90.15 (8)
Ru1-N5	2.083 (3)	Ru1-Ru2-N4	81.62 (9)
Ru1-N7	2.105 (3)	Ru1-Ru2-N6	90.49 (9)
Ru1-N9	1.996 (3)	Ru1-Ru2-N8	92.12 (9)
Ru2-N4	2.099 (3)	Ru1-Ru2-N10	83.24 (9)
Ru2-N6	2.005 (3)	Ru2-Ru1-C1	167.7 (1)
Ru2-N8	1.996 (3)	Ru1-Ru2-C18	167.4 (1)
Ru2-N10	2.065 (3)		
C1-C2	1.206 (6)		
C18-C19	1.214 (6)		
3 [a]			
Ru1-Ru2	2.4498 (6)	Ru2-Ru1-N1	91.6 (2)
Ru1-C1	1.961 (6)	Ru2-Ru1-N3	83.2 (1)
Ru2-C3	1.982 (7)	Ru2-Ru1-N5	81.6 (1)
Ru1-N1	1.990 (5)	Ru2-Ru1-N7	91.0 (2)
Ru1-N3	2.056 (6)	Ru1-Ru2-N2	82.0 (1)
Ru1-N5	2.118 (4)	Ru1-Ru2-N4	90.4 (2)
Ru1-N7	2.006 (6)	Ru1-Ru2-N6	91.8 (2)
Ru2-N2	2.081 (5)	Ru1-Ru2-N8	81.9 (2)
Ru2-N4	2.017 (6)	Ru2-Ru1-C1	167.9 (2)
Ru2-N6	2.008 (5)	Ru1-Ru2-C3	168.4 (2)
Ru2-N8	2.098 (6)		
C1-C2	1.213 (9)		
C3-C4	1.217 (9)		
4			
Ru1-Ru2	2.4506 (3)	Ru2-Ru1-N1	86.87 (6)
Ru1-C1	1.971 (3)	Ru2-Ru1-N3	87.68 (6)
Ru2-C3	1.963 (2)	Ru2-Ru1-N5	85.90 (6)
Ru1-N1	2.039 (2)	Ru2-Ru1-N7	84.87 (6)
Ru1-N3	2.038 (2)	Ru1-Ru2-N2	86.08 (6)
Ru1-N5	2.038 (2)	Ru1-Ru2-N4	84.84 (6)
Ru1-N7	2.063 (2)	Ru1-Ru2-N6	86.70 (6)
Ru2-N2	2.051 (2)	Ru1-Ru2-N8	88.06 (6)
Ru2-N4	2.061 (2)	Ru2-Ru1-C1	177.8 (3)
Ru2-N6	2.045 (2)	Ru1-Ru2-C3	176.7 (2)
Ru2-N8	2.041 (2)		
C1-C2	1.211 (4)		
C3-C4	1.212 (4)		

[a] There are two crystallographically independent molecules; geometric parameters for only one of them are tabulated herein.

5.3.3   Vis-NIR Spectroscopy and Voltammetry

As noted earlier, all four compounds have a deep wine red color with a slight variation in hue. The Vis-NIR absorption spectra of **1** – **4** are shown in Figure 5.2, featuring a distinctive NIR band around *ca.* 880 nm that is responsible for the wine red color. This absorption is likely attributed to the $\pi^*(Ru_2) \rightarrow \delta^*(Ru_2)$ transition according to a prior TD-DFT analysis of related $Ru_2(DMBA)_4(C_2R)_2$ compounds.[20] The Vis region is dominated by a very intense band with a transition energy depending on the nature of Ar. While the λ_{max} for Ar as both NAP^{Me} (**1**) and NAP^{iPr} (**2**) are 550 nm, the λ_{max} for Ar as Naphth (**3**) and Ant (**4**) are blue-shifted to 508 nm and 502 nm, respectively. This absorption may be assigned to the $\delta(Ru_2) + \pi(C{\equiv}C) \rightarrow \sigma^*(Ru\text{-}C)$ transition based on the said TD-DFT study, which provides a ready rationale for the observed energy dependence on Ar. Electron donating Naphth and Ant destabilize $\sigma^*(Ru\text{-}C)$ more significantly than electron withdrawing NAP^{Me} and NAP^{iPr}, which led to significantly wider optical gaps for **3** and **4**. The Vis spectra of both **1** and **2** also feature a shoulder at *ca.* 450 nm that is absent in the spectra of **3** and **4**, pointing to a possible NAP based transition. Also noteworthy is that while all four aryl ligands are strongly fluorescent, compounds **1** – **4** are non-emissive, reflecting the efficient quenching by the $Ru_2(DMBA)_4$ core.
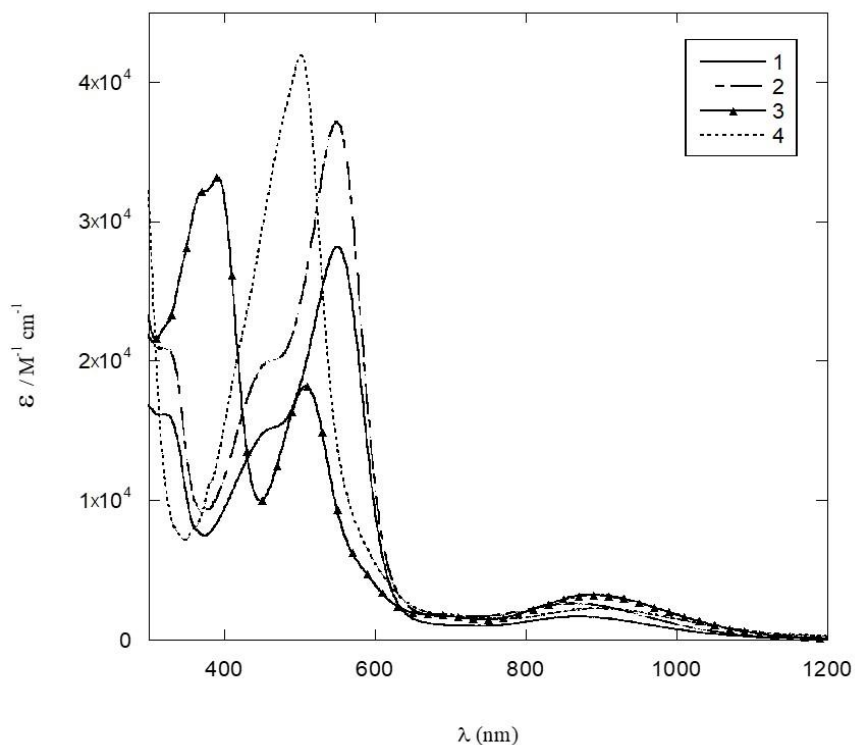
Figure 5.2. Vis-NIR spectra of compounds **1** – **4** recorded in THF solution.

Ru$_2$(DMBA)$_4$(C$_2$R)$_2$ type compounds often display rich electrochemical characteristics[20,26,27,33] and compounds **1** – **4** are no exception. As shown in Figure 5.3, their cyclic voltammograms (CV) all consist of two Ru$_2$-based reversible one-electron couples, an oxidation (**A**) and a reduction (**B**). It is also clear that the electrode potentials of compounds **1** and **2** are far more positive than those of the corresponding couples in **3** and **4**, reflecting the electron-deficient nature of the NAP ligands. Since the oxidation and reduction potentials can be respectively correlated with the HOMO and LUMO energies,[35,36] the electrochemical HOMO-LUMO gap (E_g) can be directly calculated from the difference between $E_{1/2}(\mathbf{A})$ and $E_{1/2}(\mathbf{B})$, and the values for **1** – **4** are listed in Table 5.2. Interestingly, the E_g remains fairly constant across the series despite the large variance in

electrode potentials. Clearly, both the HOMO and LUMO are Ru_2-based, and the inductive ligand effects on their energies are about the same, within experimental error.
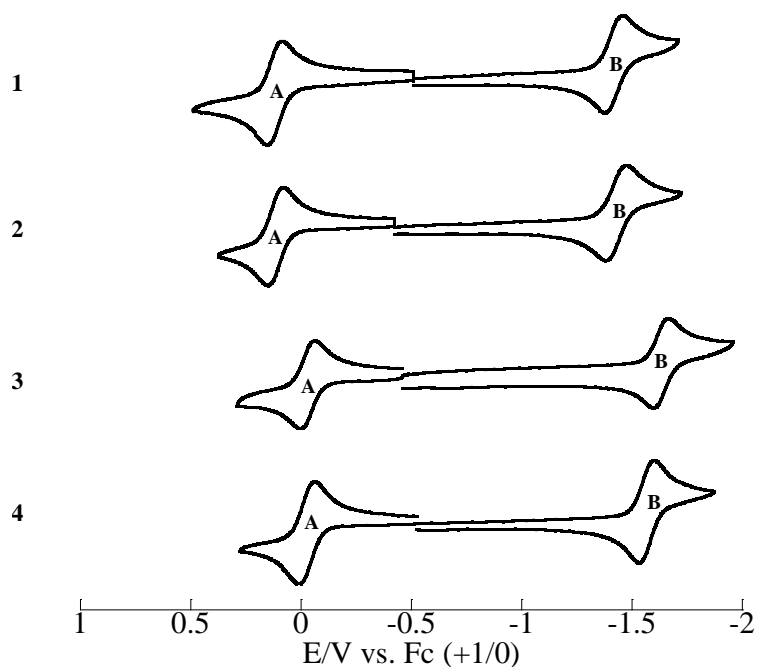
Figure 5.3. Cyclic voltammograms of compounds **1 - 4** recorded in 0.10 M n-Bu$_4$NPF$_6$ THF solution at the scan rate of 100 mV/s.

Table 5.2. Electrode potentials of observed redox couples in $Ru_2(DMBA)_4(C_2Ar)_2$

Ar	$E_{1/2}$ (**A**)/V (ΔE_p/mV, i_{back} / $i_{forward}$)	$E_{1/2}$ (**B**))/V (ΔE_p/mV, i_{back} / $i_{forward}$)	E_g/V = $E_{1/2}$ (**A**) - $E_{1/2}$ (**B**)
NAP^{Me} (**1**)	0.120 (68, 0.90)	-1.42 (73, 0.96)	1.54
NAP^{iPr} (**2**)	0.120 (67, 0.92)	-1.43 (92, 0.92)	1.55
Naphth (**3**)	-0.03 (69, 0.97)	-1.63 (67, 0.97)	1.60
Ant (**4**)	-0.03 (68, 0.92)	-1.57 (76, 0.81)	1.54

5.4   Conclusions

Four new $Ru_2(DMBA)_4(C_2Ar)_2$ compounds have been prepared and structurally characterized. While both the voltammetric responses and electronic absorption spectra are dominated by the Ru_2-centered processes, both the electrode potentials and excitation energies exhibit significant dependence on the arylethynyl ligands.

5.5   References

(1)   Paul, F.; Lapinte, C. Organometallic molecular wires and other nanoscale-sized devices: An approach using the organoiron (dppe)Cp*Fe building block. *Coord. Chem. Rev.* **1998**, *178-180*, 431-509.

(2)   Ren, T. Diruthenium σ-Alkynyl Compounds**:** A New Class of Conjugated Organometallics. *Organometallics* **2005**, *24*, 4854-4870.

(3)   Costuas, K.; Rigaut, S. Polynuclear carbon-rich organometallic complexes: clarification of the role of the bridging ligand in the redox properties. *Dalton Trans.* **2011**, *40*, 5643-5658.

(4)   Blum, A. S.; Ren, T.; Parish, D. A.; Trammell, S. A.; Moore, M. H.; Kushmerick, J. G.; Xu, G. L.; Deschamps, J. R.; Pollack, S. K.; Shashidhar, R. Ru-2(ap)(4)(sigma-oligo(phenyleneethynyl)) molecular wires: Synthesis and electronic characterization. *J. Am. Chem. Soc.* **2005**, *127*, 10010-10011.

(5)   Meng, F. B.; Hervault, Y. M.; Norel, L.; Costuas, K.; Van Dyck, C.; Geskin, V.; Cornil, J.; Hng, H. H.; Rigaut, S.; Chen, X. D. Photo-modulable molecular transport junctions based on organometallic molecular wires. *Chem. Sci.* **2012**, *3*, 3113-3118.

(6)   Zhang, X. Y.; Zheng, Q.; Qian, C. X.; Zuo, J. L. Some New Progress on Molecular Wires. *Chin. J. Inorg. Chem.* **2011**, *27*, 1451-1464.

(7)   Wen, H. M.; Yang, Y.; Zhou, X. S.; Liu, J. Y.; Zhang, D. B.; Chen, Z. B.; Wang, J. Y.; Chen, Z. N.; Tian, Z. Q. Electrical conductance study on 1,3-butadiyne-linked dinuclear ruthenium(II) complexes within single molecule break junctions. *Chem. Sci.* **2013**, *4*, 2471-2477.

(8)   Chen, Z. N.; Zhao, N.; Fan, Y.; Ni, J. Luminescent groups 10 and 11 heteropolynuclear complexes based on thiolate or alkynyl ligands. *Coord. Chem. Rev.* **2009**, *253*, 1-20.

(9)   Yam, V. W.-W. Molecular Design of Transition Metal Alkynyl Complexes as Building Blocks for Luminescent Metal-Based Materials: Structural and Photophysical Aspects. *Acc. Chem. Res.* **2002**, *35*, 555-563.

(10)   Wong, W. Y.; Ho, C. L. Organometallic Photovoltaics: A New and Versatile Approach for Harvesting Solar Energy Using Conjugated Polymetallaynes. *Acc. Chem. Res.* **2010**, *43*, 1246-1256.

(11)   Liu, S. H.; Xia, H. P.; Wen, T. B.; Zhou, Z. Y.; Jia, G. C. Synthesis and characterization of bimetallic ruthenium complexes with (CH)(6) and related bridges. *Organometallics* **2003**, *22*, 737-743.

(12)   Liu, S. H.; Hu, Q. Y.; Xue, P.; Wen, T. B.; Williams, I. D.; Jia, G. C. Synthesis and characterization of C10H10-bridged bimetallic ruthenium complexes. *Organometallics* **2005**, *24*, 769-772.

(13)   Kong, D. D.; Xue, L. S.; Jang, R.; Liu, B.; Meng, X. G.; Jin, S.; Ou, Y. P.; Hao, X.; Liu, S. H. Conformational Tuning of the Intramolecular Electronic Coupling in Molecular-Wire Biruthenium Complexes Bridged by Biphenyl Derivatives. *Chem. Eur. J.* **2015**, *21*, 9895-9904.

(14)   Ou, Y. P.; Zhang, J.; Zhang, F. X.; Kuang, D. Z.; Hartl, F.; Rao, L.; Liu, S. H. Notable differences between oxidized diruthenium complexes bridged by four isomeric diethynyl benzodithiophene ligands. *Dalton Trans.* **2016**, *45*, 6503-6516.

(15)   Xu, L. J.; Zeng, X. C.; Wang, J. Y.; Zhang, L. Y.; Chi, Y.; Chen, Z. N. Phosphorescent PtAu2 Complexes with Differently Positioned Carbazole-Acetylide Ligands for Solution-Processed Organic Light-Emitting Diodes with External Quantum Efficiencies of over 20%. *ACS Appl. Mater. Interfaces* **2016**, *8*, 20251-20257.

(16)   Zhang, L. Y.; Xu, L. J.; Wang, J. Y.; Zeng, X. C.; Chen, Z. N. Photoluminescence and electroluminescence of cationic PtAu2 heterotrinuclear complexes with aromatic acetylides. *Dalton Trans.* **2017**, *46*, 865-874.

(17)   Xu, G.-L.; Zou, G.; Ni, Y.-H.; DeRosa, M. C.; Crutchley, R. J.; Ren, T. Polyyn-diyls Capped by Diruthenium Termini: A New Family of Carbon-Rich Organometallic Compounds and Distance Dependent Electronic Coupling Therein. *J. Am. Chem. Soc.* **2003**, *125*, 10057-10065.

(18)   Cao, Z.; Xi, B.; Jodoin, D. S.; Zhang, L.; Cummings, S. P.; Gao, Y.; Tyler, S. F.; Fanwick, P. E.; Crutchley, R. J.; Ren, T. Diruthenium-Polyyn-diyl-Diruthenium Wires: Electronic Couplings in the Long Distance Regime. *J. Am. Chem. Soc.* **2014**, *136*, 12174-12183.

(19)   Wong, K.-T.; Lehn, J.-M.; Peng, S.-M.; Lee, G.-H. Nanoscale molecular organometallo-wires containing diruthenium cores. *Chem. Commun.* **2000**, 2259-2260.

(20)   Xu, G.-L.; Crutchley, R. J.; DeRosa, M. C.; Pan, Q.-J.; Zhang, H.-X.; Wang, X.; Ren, T. Strong Electronic Couplings between Ferrocenyl Centers Mediated by Bis-Ethynyl/Butadiynyl Diruthenium Bridges. *J. Am. Chem. Soc.* **2005**, *127*, 13354-13363.

(21)   Zuo, J.-L.; Herdtweck, E.; Biani, F. F. d.; Santos, A. M.; Kühn, F. E. Ruthenium(II) alkynyl-hydride and ruthenium(II) bis(-pyridylacetylide) as ligands and linkers for metal–metal-bonded complexes. *New J. Chem.* **2002**, *26*, 889-894.

(22) Zuo, J.-L.; Herdtweck, E.; Kühn, F. E. Diruthenium -alkynyl complexes as potential building blocks for heterometallic molecular rods. *Dalton Trans.* **2002**, 1244-1246.

(23) Mahapatro, A. K.; Ying, J.; Ren, T.; Janes, D. B. Electronic Transport through Ruthenium Based Redox-Active Molecules in Metal-Molecule-Metal Nanogap Junctions. *Nano Lett* **2008**, *8*, 2131-2136.

(24) Zhu, H.; Pookpanratana, S. J.; Bonevich, J. E.; Natoli, S. N.; Hacker, C. A.; Ren, T.; Suehle, J. S.; Richter, C. A.; Li, Q. Redox-Active Molecular Nanowire Flash Memory for High-Endurance and High-Density Non-Volatile Memory Applications. *ACS Appl. Mater. Interfaces* **2015**, *7*, 27306-27313.

(25) Ying, J.-W.; Cordova, A.; Ren, T. Y.; Xu, G.-L.; Ren, T. Bis-alkynyl Diruthenium Compounds with Build-in Electronic Asymmetry: Toward an Organometallic Aviram-Ratner Diode. *Chem. Eur. J.* **2007**, *13*, 6874-6882.

(26) Ying, J.-W.; Liu, I. P.-C.; Xi, B.; Song, Y.; Campana, C.; Zuo, J.-L.; Ren, T. Linear Diruthenium Trimer of Butadiyn-diyl Bridge - A Unique Electronic Wire. *Angew. Chem. Int. Ed.* **2010**, *49*, 954-957.

(27) Cai, X.-M.; Zhang, X.-Y.; Savchenko, J.; Cao, Z.; Ren, T.; Zuo, J.-L. New Linear -Conjugated Diruthenium Compounds Containing Axial Tetrathiafulvalene-acetylide Ligands. *Organometallics* **2012**, *31*, 8591-8597.

(28) Wang, C.-F.; Zuo, J. L.; Ying, J.-W.; Ren, T.; You, X.-Z. Novel Heterometallic Fe-Ru2-Fe Arrays via "Complex of Complexes" Approach. *Inorg. Chem.* **2008**, *47*, 9716-9722.

(29) Xu, G.-L.; Jablonski, C. G.; Ren, T. Ru2(*DMBA*)4(BF4)2 and Ru2(*DMBA*)4(NO3)2: The First Examples of Diruthenium Compounds Containing BF4- and NO3- as Ligands. *Inorg. Chim. Acta* **2003**, *343*, 387-390.

(30) Chang, N.-H.; Mori, H.; Chen, X.-C.; Okuda, Y.; Okamoto, T.; Nishihara, Y. Synthesis of Substituted [6]Phenacenes through Suzuki-Miyaura Coupling of Polyhalobenzene with Alkenylboronates and Sequential Intramolecular Cyclization via C-H Bond Activation. *Chem. Lett.* **2013**, *42*, 1257-1259.

(31) Takahashi, S.; Kuriyama, Y.; Sonogashira, K.; Hagihara, N. A Convenient Synthesis of Ethylarenes and Diethynylarenes. *Synthesis* **1980**, 627-630.

(32) McAdam, C. J.; Morgan, J. L.; Murray, R. E.; Robinson, B. H.; Simpson, J. Synthesis and fluorescence properties of new enaminenaphthalimides. *Aust. J. Chem.* **2004**, *57*, 525-530.

(33)   Xu, G.-L.; Campana, C.; Ren, T. Tetrakis(*N*,*N'*-dimethylbenzamidinato)diruthenium Compounds Bearing Axial Chloro and Alkynyl Ligands: A New Family of Redox Rich Diruthenium Compounds. *Inorg. Chem.* **2002**, *41*, 3521-3527.

(34)   Lin, C.; Ren, T.; Valente, E. J.; Zubkowski, J. D. Synthesis, Spectroscopy, and Electrochemistry of Tetrakis(μ-*N*,*N*-diarylformamidinato)di-(phenylethynyl)diruthenium(III,III). Part 5. Linear Free Energy Relationships in Dinuclear Compounds. *J. Chem. Soc., Dalton Trans.* **1998**, 571-576.

(35)   Ren, T. Linear Free Energy Relationships in Dinuclear Compounds. Electrochemical and Spectroscopic Investigations. *Coord. Chem. Rev.* **1998**, *175*, 43-58.

(36)   Loutfy, R. O.; Loutfy, R. O. Interrelation between Polarographic Half-Wave Potentials and Energies of Electronic Excited-States. *Can. J. Chem.* **1976**, *54*, 1454-1463.

CHAPTER 6. FORMATION OF η^2 CU(I) AND AG(I) ADDUCTS TO CO(CYCLAM)(C$_2$R)

6.1 Introduction

Chemistry of transition metal alkynyls has evolved extensively since the early study of homoleptic complexes $[M(C\equiv CR)_m]^{n-}$ by Nast and co-workers.[1] In addition to continuous interest in new synthesis[2-4] and understanding of structures[5,6] and bonding of metal alkynyls,[7] recent decades have witnessed significant progresses in areas such as molecular electronic wires and devices[8-15] and optoelectronic materials.[16-18] One of the peculiar attributes of metal alkynyl complexes is the propensity to form η^2 adduct of Cu(I) / Ag(I) at the acetylenic unit that bonds to the metal center. Also noteworthy is the demonstration of the influence of η^2-coordination of Cu(I) on the electronic coupling between two Ru(II) centers linked by butadiynyl.[19] Luminescent coordination polymers of Pt-alkynyls provided a template for 2D and 3D MOFs (metal-organic frameworks) designed for small molecule capture.[20] η^2-Coordination of Ag(I) is also a key structural element in the formation of high nuclearity clusters based on Ag$_2$C$_2$ unit.[21]
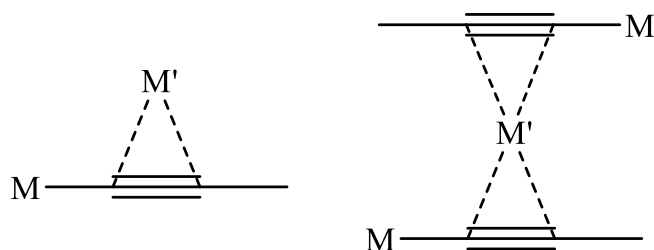
Chart 6.1. Metal alkynyl with η^2 coinage metal adduct

Our laboratory has become interested in alkynyl complexes based on 3d metal supported by both cyclam (1,4,8,11-tetraazacyclotetradecane) and its C-substituted derivatives.[22,23] Though the area is fairly young, Co^{III}(cyclam) based complexes have

been a frequent target due to the possibility of high yield preparation of *trans*-[Co(cyclam)(C$_2$R)Cl]$^+$ under mild conditions, which allows for further synthesis of unsymmetric *trans*-[Co(cyclam)(C$_2$R)(C$_2$R')]$^+$ type complexes in reasonable yield.[24-26] It has been discovered in the course of these studies that *trans*-[Co(cyclam)(C$_2$R)X]$^+$ species readily form η^2-adduct of Cu(I) / Ag(I). Reported herein are the details of synthesis, structures, voltammetric and fluorescent properties of the Co species, and the impact of Cu(I) / Ag(I) addition. To our knowledge, compounds **2a** / **2b** are the first examples of Co-alkynyl with η^2-adduct of Cu(I) / Ag(I).

6.2   Results and discussion

6.2.1   Synthesis
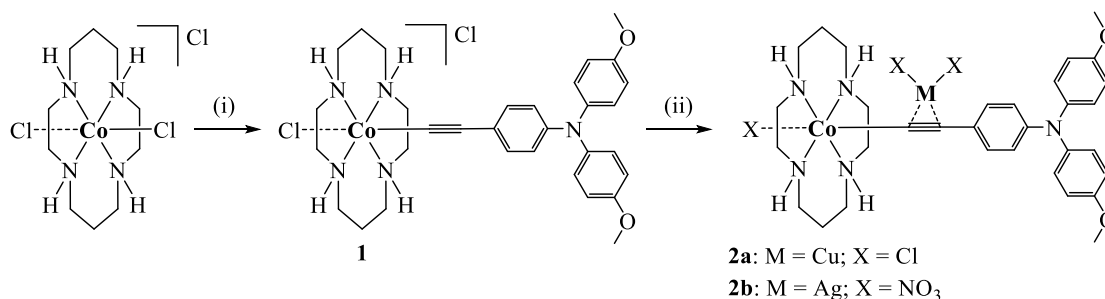
Scheme 6.1. Synthesis of compounds **1**, **2a**, and **2b**. Conditions: (i) HC$_2$TPA; Et$_2$NH, MeOH/THF; 60 °C, 12 h; (ii) **1**, M-X, MeOH/MeCN; 60 °C, 4-12 h.

Synthesis of 4-ethynyl-*N,N*-bis(4-methoxyphenyl)aniline (HC$_2$TPA) was achieved following literature procedures.[27,28] Formation of [Co(cyclam)(C$_2$TPA)Cl]Cl (**1**) was achieved under weak base conditions from the reaction of [Co(cyclam)Cl$_2$]Cl and HC$_2$TPA in a MeOH/THF solution to yield a pink crystalline solid (75% yield). Scheme 6.1 shows the step-wise formation of [Co(cyclam)(C$_2$TPA-η^2-CuCl$_2$)Cl] (**2a)** and [Co(cyclam)(C$_2$TPA-η^2-Ag(NO$_3$)$_2$)NO$_3$] (**2b)**, with **1** as a precursor. Formation of **2a** was

achieved via reflux of **1** and CuCl in MeCN for 12 h. The reaction solution was filtered and **2a** was recrystallized from the filtrate as a light pink solid in 74% yield. **2b** was prepared similarly, starting from $AgNO_3$, resulting in 70% yield of dark red solid. Attempts to synthesize $[Co(cyclam)(C_2TPA-\eta^2-Ag(Cl)_2)Cl]$ proved futile due to the low solubility of AgCl. Furthermore, compound **2b** exhibited extremely low solubility, preventing a thorough investigation of its experimental properties (i.e. absorption and redox properties). Synthesis of $[Co(cyclam)(C_2TPA)_2]Cl$ (**3**) was achieved from the combination of $[Co(cyclam)Cl_2]Cl$ with 3 equiv of LiC_2TPA in THF using standard Schlenck techniques. After silica gel plug purification, compound **3** was isolated as a light brown solid in 84% yield. Attempts to react CuCl or $AgNO_3$ with **3** to form a **3**-η^2-MX_2 type species (M = Cu or Ag; X = Cl or NO_3), resulted in formation of **2a** or **2b**, respectively. All compounds presented herein are low spin Co(III) species, and are readily characterized using ^{1}H NMR, UVvis and FT-IR spectroscopies, ESI mass spectrometry and combustion analysis.

6.2.2   Structure Analysis

Single crystals of **1**, **2a**, **2b** and **3** were grown from slow diffusion of diethyl ether into a concentrated solution of the respective complex. Molecular structures of $[1]^+$ (Fig 6.1), **2a** (Fig 6.2), **2b** (Fig 6.3) and $[3]^+$ (Fig 6.4) were determined using single crystal X-ray diffraction. In all structures, the Co center adopts a pseudo-octahedral geometry with the alkynyl and chloro ligands in the axial positions *trans-* to each other. No additional counterion was observed for **2a** and **2b** suggesting Cu(I) and Ag(I) were coordinated, respectively.   Selected bond lengths and angles can be found in Table 6.1 and experimental details can be found in the experimental section (Table 6.6).
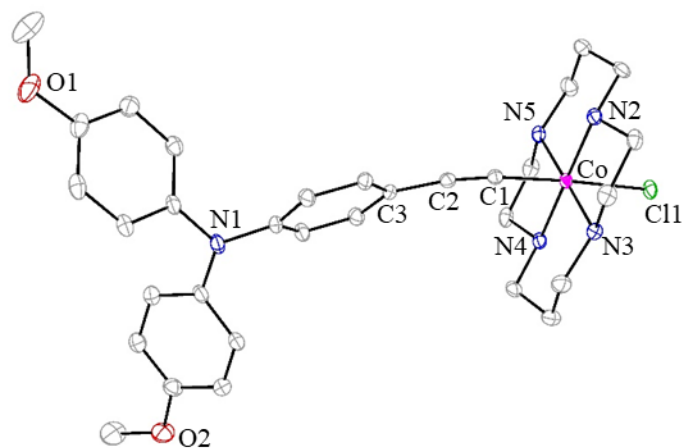
Figure 6.1. ORTEP plot of [**1**]$^+$ at 30% probability level. Hydrogen atoms, solvent molecules and Cl$^-$ were omitted for clarity.
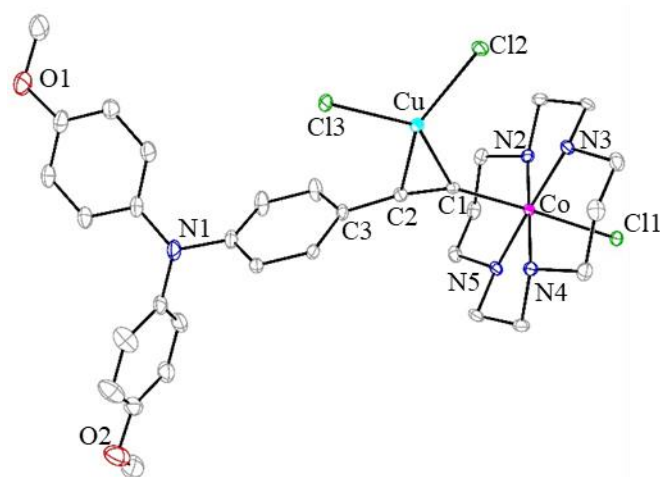
Figure 6.2. ORTEP plot of **2a** at 30% probability level. Hydrogen atoms and solvent molecules were omitted for clarity.
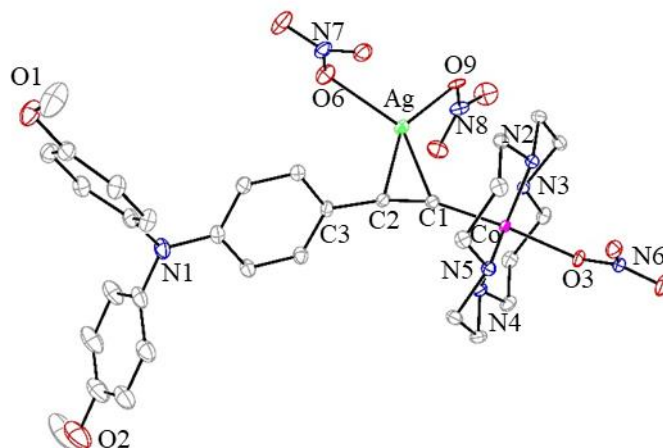
Figure 6.3. ORTEP plot of **2b** at 30% probability level. Hydrogen atoms, solvent and disorder were omitted for clarity.
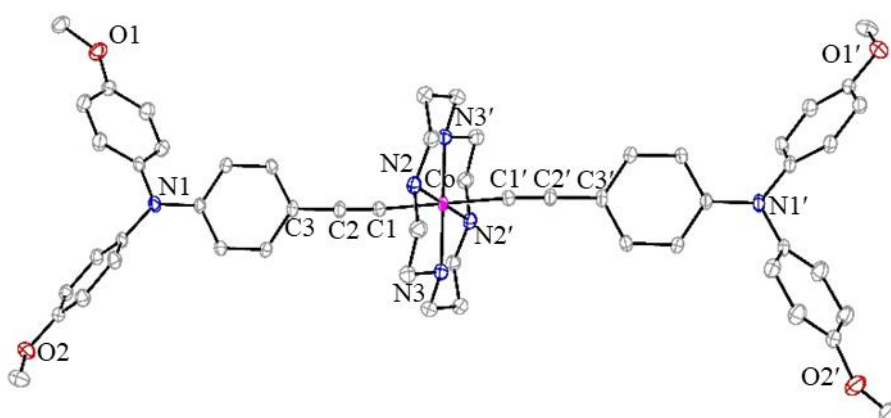
Figure 6.4. ORTEP plot of [**3**]$^+$ at 30% probability level. Hydrogen atoms and the counterion were omitted for clarity.

The C≡C and Co-C1 bond lengths for **1** and **3** follow the canonical trend for mono- vs. symmetric bis-Co^{III}(cyclam) acetylides, in which the C≡C bond length is relatively the same and the Co-C1 bond is shorter for **1** (1.879(3) Å) vs. **3** (1.945(2) Å) due to the trans influence.[29] The Co-C1 bond distances are also consistent with those observed for analogous Co^{III}(cyclam) species coordinated to electron donating ligands,

$[Co(cyclam)(C_2C_6H_4\text{-}4\text{-}NMe_2)(NCMe)]^+$ (1.874(2) Å) and $[Co(cyclam)(C_2C_6H_4\text{-}4\text{-}NMe_2)_2]^+$ (1.942(3) Å).[26,30]

Table 6.1. Selected bond lengths (Å) and bond angles (°) for $[\mathbf{1}]^+$, $\mathbf{2a}$, $\mathbf{2b}$, and $[\mathbf{3}]^+$

	$[\mathbf{1}]^+$	$\mathbf{2a}$	$\mathbf{2b}$	$[\mathbf{3}]^+$
Co-N2	1.969(2)	1.980(2)	1.962(2)	1.992(2)
Co1-N3	1.975(2)	1.984(2)	1.982(2)	1.987(2)
Co1-N4	1.976(2)	1.975(2)	1.983(2)	-
Co1-N5	1.980(2)	1.972(2)	1.968(2)	-
Co1-C1	1.879(3)	1.928(2)	1.891(3)	1.945(2)
Co1-Cl1/O3/C1′	2.3401(7)	2.3228(6)	1.984(2)	1.945(2)
Cu/Ag-C1	-	2.011(2)	2.317(2)	-
Cu/Ag-C2	-	2.042(2)	2.319(3)	-
Cu-Cl2/Ag-O6	-	2.2670(6)	2.33(2)	-
Cu-Cl3/Ag-O7	-	2.2728(6)	2.382(2)	-
C1-C2	1.205(4)	1.232(3)	1.234(4)	1.203(3)
C2-C3	1.434(4)	1.450(3)	1.442(3)	1.446(3)
Cl/O3/C1′-Co1-C1	177.26(8)	177.23(6)	172.99(9)	180.0
Co1-C1-C2	172.6(2)	153.5(2)	158.5(2)	175.8(2)
C1-C2-C3	171.6(3)	165.8(2)	167.3(3)	177.5(3)
C1-Cu/Ag-C2	-	35.37(8)	30.89(9)	-
Co1-C1-C2-C3	-	18.4(12)	-2.0(17)	-

Comparison of $\mathbf{1}$ to $\mathbf{2a}$ and $\mathbf{2b}$ reveals that the $\eta^2(\pi)$-coordination of MX_2 to the acetylide has an appreciable elongation effect on the length of Co-C1, C≡C and C2-C3 bond lengths (Table 6.1). Chen and co-workers also noted elongation of Ru-C and C≡C bonds for Ru-C≡C-C≡C-Ru systems when the alkynes were η^2 coordinated to Cu(I).[19] The length of the Cu-C bond distance (averaged bond length: 2.027[2] Å) was consistent with literature reports for a Cu(I) species,[19] as was the Ag-C bond distance (averaged bond length: 2.318[5] Å) for a Ag(I) species.[21] Significant curvature, compared to compound $\mathbf{1}$ (Fig 6.5), of the Co-C1-C2 and C1-C2-C3 bond angles were noted for compounds $\mathbf{2a}$ and $\mathbf{2b}$ and were attributed to η^2 coordination to Cu(I) and Ag(I), respectively. Similar distortions were noted for Pt-C≡C- polymers coordinated by Cu_2Y_2

(Y = I, Br, or Cl) in which the Cu coordinated species had longer C≡C bonds and curved

C-C≡C motifs.[20]
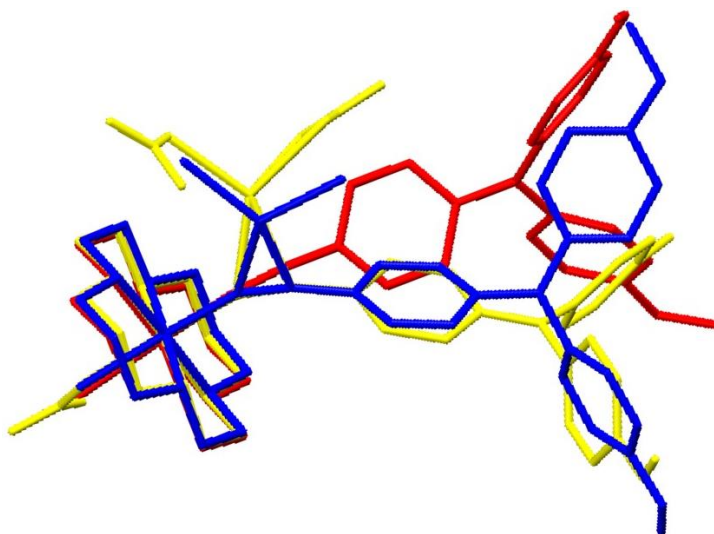
Figure 6.5. Overlay of compounds **1** (red), **2a** (blue) and **2b** (yellow) showing the effect of η^2 coordination on the Co-C1-C2-C3 dihedral angle.

6.2.3   Fourier Transform Infrared Spectra (FTIR)

The FTIR spectra shown in Fig 6.6 highlights the C≡C stretching frequencies for

1, **2a**, **2b** and **3**. Consistent with previous work,[25,26] compound **3** has a lower $v(C≡C)$ than

1 due to the presence of a second alkynyl in place of a chloro in the axial position, which

results in greater antibonding interactions with the filled dπ of the dπ-π(C≡C) and

therefore a lower $\upsilon(C≡C)$.[29] In agreement with the experimentally observed structure data,

compound **2b** (1.234(4) Å; 2030 cm^{-1}) has longer C≡C bond length and a lower $v(C≡C)$

compared to **1** (1.205(4) Å; 2114 cm^{-1}). However, compound **2a** does not follow this

expected trend, with a C≡C bond length of 1.232(3) Å and $\upsilon(C≡C)$ of 2129 cm^{-1}. This

experimental anomaly could be attributed to a number of factors such as i) the relative

atomic weights and identities of the η^2 coordinated metals or ii) the relative π-donor

character of the atom *trans* to the alkyne. The nitro ligand (**2b**) is a better π-acceptor than the chloro (**2a**) and could influence the v(C≡C) more than the η^2 coordinated metal.[31]
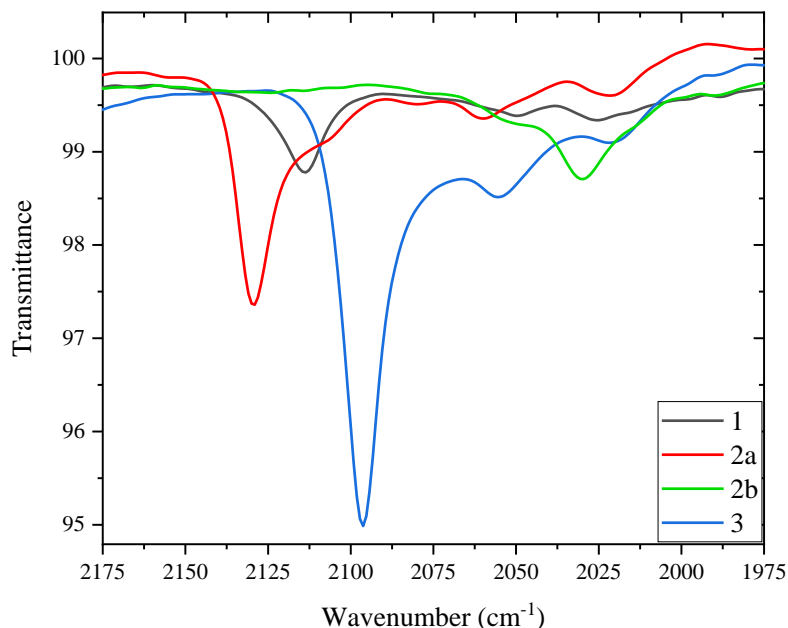
Figure 6.6. ATR-FTIR of **1**, **2a**, **2b** and **3** highlighting the C≡C stretches

6.2.4 UV-vis and Emission Spectroscopic Analysis

Absorption and emission spectra for compounds **1**, **2a**, **2b** and **3** were collected in both CH_2Cl_2 and MeCN under ambient conditions. Table 6.2 lists absorption (λ_{abs}) and emission maxima (λ_{em}) in CH_2Cl_2. Peak locations and extinction coefficients were similar in both solvent systems; however, emission could not be detected in MeCN. Compound **2b** suffered from low solubility and could only be evaluated based on peak location and shape. The normalized absorption spectra in CH_2Cl_2 comparing **1**, **2a**, and **2b** reveals that the three compounds exhibit nearly identical transitions (Fig 6.7), suggesting η^2 coordination of Cu(I) or Ag(I) does not affect the transitions in the ultraviolet and visible regions.
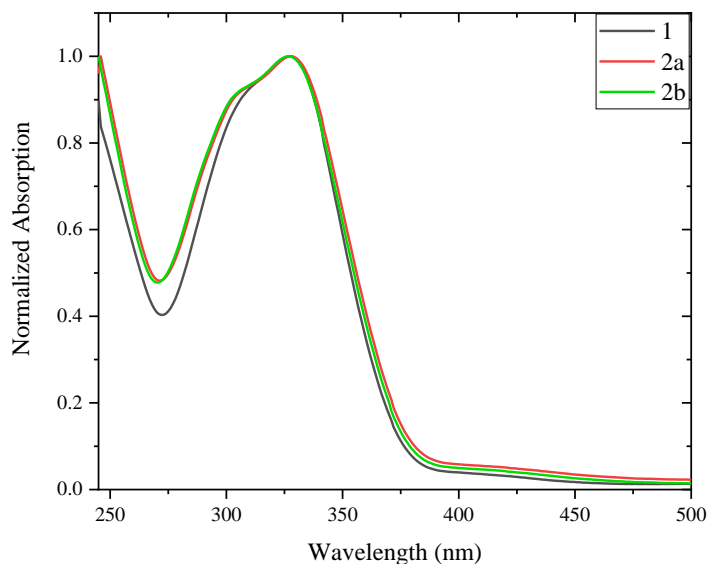
Figure 6.7. Normalized absorption spectra of **1**, **2a** and **2b** in CH$_2$Cl$_2$

All compounds display a strong absorption band ~330 nm (Fig 6.7 and Fig 6.8) with an extinction coefficient on the order of 47,700 M^{-1}cm^{-1} for **3** and ~25,000 M^{-1}cm^{-1} for compounds **1** and **2a**, suggesting this transition is strongly influenced by the TPA ligand. Organometallic and organic compounds bearing triaryl amine ligands, such as Ru^{II}(TPA),[32] Co^{II}(Tara)(ClO$_4$)$_2$ (Tara = o-substituted 2-(pyridine-2-yl)-1,10-phenanthrolines),[33] TPAC$_4$TPA,[28] and TPA-X (X = Cl or Br),[34,35] exhibit similar absorption features under 400 nm, which were attributed to the π→π* transition of TPA. DFT analysis on compounds **1** and **3** (discussed below and Table 6.5) corroborates this assignment and suggests this transition may also have LMCT character (TPA→3d$_{x^2-y^2}$). The broad nature of this peak partially obscures the *d-d* ($^1A_{1g} \rightarrow {}^1T_{1g}$, O_h) transition for compound **3**, however it is clearly defined for compounds **1** and **2a**. Consistent with previous reports, the *d-d* transition is lower in energy for the Co^{III}(cyclam) mono-acetylides and higher in energy for the Co^{III}(cyclam) bis-acetylides (inset Fig 6.8).[24,25,29,30,36] Also noteworthy is the high similarity in peak position and extinction

coefficient for compounds **1** and **2a**, suggesting Cu(I) has little to no effect on the electronic transitions in the ultraviolet and visible regions.
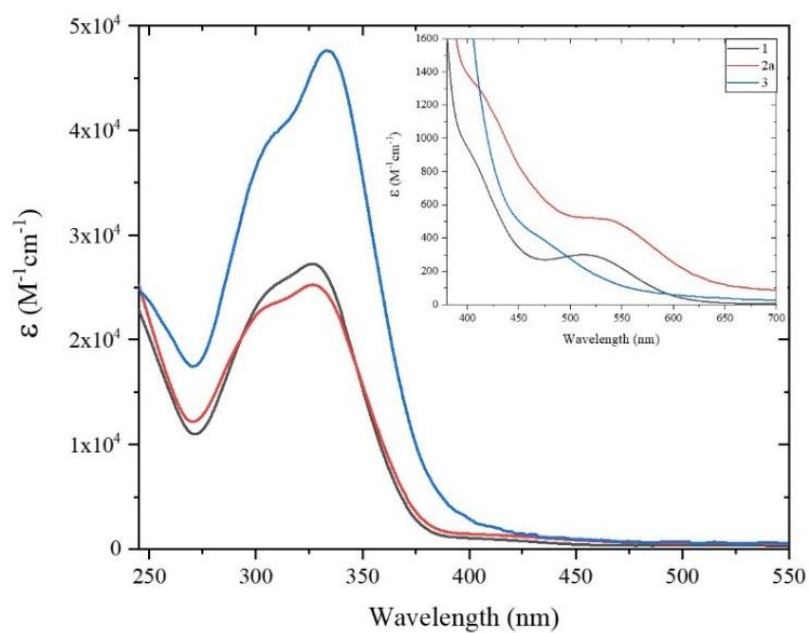
Figure 6.8. Absorption spectra of **1**, **2a** and **3** in CH_2Cl_2
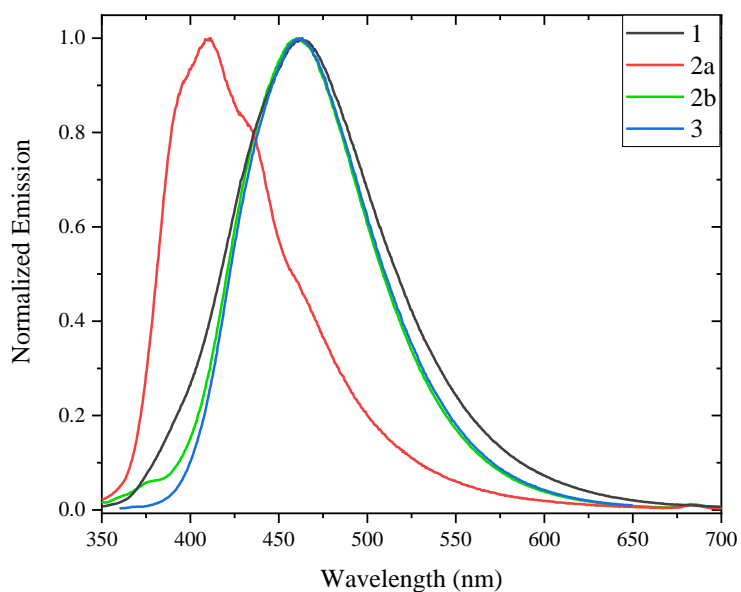
Figure 6.9. Normalized emission spectra of **1**, **2a**, **2b** and **3** in CH_2Cl_2 at room temperature

Steady-state emission of complexes **1**, **2b** and **3** is dominated by $S_0 \rightarrow S_1$ transition of the TPA ligand and originates from the absorption transition ~330 nm (Fig 6.9).[27,28] Direct comparison of the λ_{em}, spectral shape and fluorescence quantum yields (Φ_{fl}) in CH_2Cl_2 of compounds **1** and **3** versus HC_2TPA (Table 6.2) further supports this assignment. Consistent with previous reports of Co^{III}(cyclam) alkynyl species coordinated to simple chromophores, like naphthalene[36] and naphthalimide,[25] Co greatly quenches the fluorophore emission. Compound **3** (6.8%) has a Φ_{fl} ten-fold higher than that of compound **1** (0.64%) due to the presence of two TPA ligands. The emission for **2a** and **2b** was too weak to calculate the Φ_{fl}, likely due to the presence of a second "quenching" metal and is assumed to have a $\Phi_{fl} < 0.64\%$. The λ_{em} for **2a** is blue shifted by 50 nm compared to the rest of the series, indicating η^2 coordination of Cu(I) might cause relaxation through different electronic states or formation of a new fluorescent species upon excitation.[37] The pairing of Co^{III} and Cu in photosensitive materials has been used in a number of systems to generate carbon-centered radicals via irradiation with ultraviolet or visible light.[38-40] Work is ongoing to determine if this type of reactivity explains why the reaction of **3** with CuCl resulted selectively in the formation of **2a**.

Table 6.2. Absorption (λ_{abs}) and emission maxima (λ_{em}) in nm, excitation wavelength (λ_{ex}) in nm, and emission quantum yields (Φ_{fl}) in CH_2Cl_2

	Φ_{fl}	λ_{abs}	λ_{em}	λ_{ex}
TPAC₂H	0.11	301	460	301
1	0.0064	327	463	335
2a	-	328	410	335
2b	-	326	461	335
3	0.068	333	462	360

6.2.5　Electrochemistry
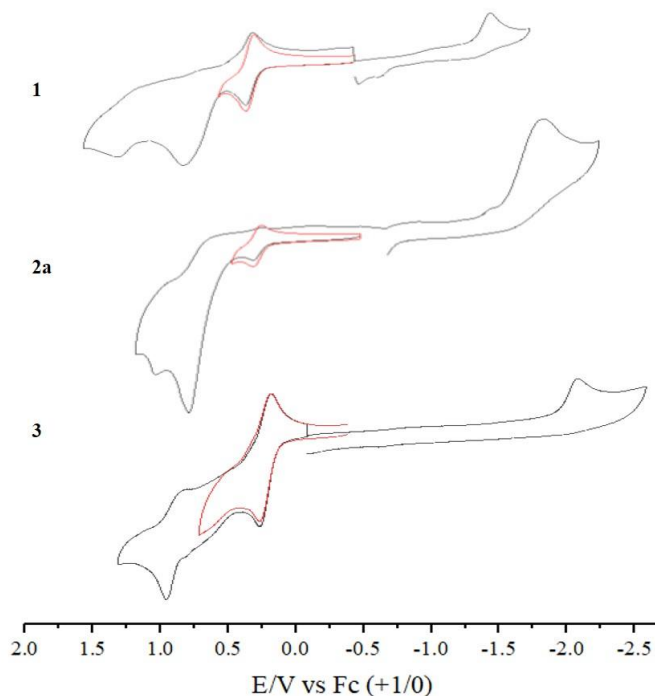
Figure 6.10. Cyclic Voltammogram of a 1.0 mM solution of **1**, **2a**, and **3** in a 0.1 M
solution of n-Bu$_4$NPF$_6$ in MeCN at scan rate = 0.1 V/s

　　　Compounds **1**, **2a** and **3** were studied electrochemically and their cyclic

voltammograms (CVs) are shown in Fig 6.10 and respective redox potentials listed in

Table 6.3. Within the solvent window, Co^{III} undergoes one irreversible 1e$^-$ reductions,

(Co^{III}/Co^{II})　and one irreversible 1e$^-$ oxidation (Co^{III}/Co^{IV}). Although a second Co

irreversible 1e$^-$ reduction (Co$^{II/I}$) was observed　in previous studies of Co^{III}(cyclam)

alkynyl complexes,[22-26] the electron donating nature of the TPA ligand signicantly

increases electron density at the Co center and moves Co$^{II/I}$ couple to more negative

potentials, beyond the solvent window. This is consitent with systems containing a

similar anilino donor studied in MeCN with a Fc external standard, in which the

(Co^{III}/Co^{II}) event occurred at the edge of the solvent window for　　both

[Co(cyclam)(C$_2$C$_6$H$_4$-4-NMe$_2$)$_2$]$^+$ (-2.08 V) and [Co(cyclam)(C$_2$C$_6$H$_4$-4-NMe$_2$)(C$_2$C$_6$F$_5$)]$^+$

(-1.86 V).[30] All complexes (**1**, **2a** and **3**) exhibit two characteristic oxidations attributed to the TPA ligand (Table 6.3), the first is a reversible (**1** and **3**) /pseudo-reversible (**2a**) oxidation occurring at ~0.28 V (TPA/TPA$^{\cdot+}$) and subsequently a pseudo-reversible (**1** and **3**) /irreversible (**2a**) oxidation ~1 V (TPA$^{\cdot+}$/TPA^{+2}). Redox potentials measured experimentally in CH$_2$Cl$_2$ for TPA-Br occur at 0.29 V (1e$^-$) and 0.98 V (1e$^-$). Similar literature examples recorded a reversible 1e$^-$ oxidation at 0.29 V for TPA-Cl,[34] two reversible 1 e$^-$ oxidations at 0.11 V and 0.86 V for TPA-OMe,[34] and a reversible 2e$^-$ oxidation at 0.30 V for TPAC$_4$TPA. [28]

Comparison of the CVs for **1** and **2a** demonstrates that η^2 bonding of Cu(I) to -C≡C-TPA clearly has an impact on the electronic interactions within the system. The Co oxidation is moved 0.05 V more positive for **2a** and the Co reduction for **2a** moves 0.35 V more negative and significantly increases in current compared to **1**. The former is likely due to an overlapping oxidation event based on [CuCl$_2$]$^-$ and the latter due to increased electron density on Co provided by η^2 coordination of [CuCl$_2$]$^-$ to the alkyne, moving the Co reduction to more negative potentials. A similar trend was reported for [MCl$_2$(η^2-N,N-dpksc)] (M = Zn, Cd, Hg and dpksc = di-2-pyridylketone semicarbazone) species, where η^2 coordination of MCl$_2$ pushed the parent compound's (dpksc) reduction to more negative potentials.[41] Additionally, the TPA/TPA$^{\cdot+}$ oxidation for **2a** is pseudo-reversible, preventing spectroelectrochemical study of the complex. Altered redox behavior due to η^2 Cu(I) coordination has been documented in literature for Cp(dppf)Ru-C≡C-C≡C-Ru(dppf)Cp (dppf = 1,1´-bis(diphenylphosphino)ferrocene) type complexes, in which the Cu(I) coordination reduced redox reversibility of the Ru couples.[19] Comparison of the TPA oxidation peak currents of **1** and **2a** to the symmetric bis-alkynyl

species (**3**), suggests that **3** undergoes a reversible 2e⁻ oxidation (TPA/TPA·⁺) and a pseudo-reversible 2e⁻ oxidation (TPA·⁺/TPA⁺²) based on TPA versus the respective 1e⁻ oxidations observed for **1** and **2a**.

Table 6.3. Electrode potentials of all observed redox couples (V) in TPA-Br, **1**, **2a**, and **3**.

	$E_{1/2}$ TPA	$E_{1/2}$ TPA	E_{pa} (Co$^{III/IV}$)	E_{pc} (Co$^{III/II}$)
[a]**TPA-Br**	0.29 (0.08)	0.98 (0.07)	--	--
[b]**1**	0.27 (0.06)	1.20 (0.10)	0.77	-1.55
[b]**2a**	0.28 (0.07)	1.05	0.82	-1.90
[b]**3**	0.28 (0.08)	0.94 (0.10)	0.77	-2.03

Electrode potentials vs. Fc⁺/Fc with peak separation (ΔE_p) for reversible processes shown in brackets. Solutions contain 1.0 mM analyte and 0.1 M n-Bu$_4$NPF$_6$ as the supporting electrolyte. [a]Collected in CH$_2$Cl$_2$. [b]Collected in MeCN solutions.

6.3   Spectroelectrochemistry

UV-vis-NIR spectroelectrochemistry was performed in an OTTLE (optically transparent thin layer electrochemical) cell with a CaF$_2$ window and a path length of 0.02 mm. A CV of compounds **1** and **3** was taken in the OTTLE cell and used to determine the location of the first oxidation event (0.88 V for both species vs Ag ref.). Based on CV data listed above, it was estimated to be a 1e⁻ event for compound [**1**]Cl ([**1**]Cl→{[**1**]Cl}⁺) and a 2e⁻ event for compound [**3**]Cl ([**3**]Cl→{[**3**]Cl}⁺²).
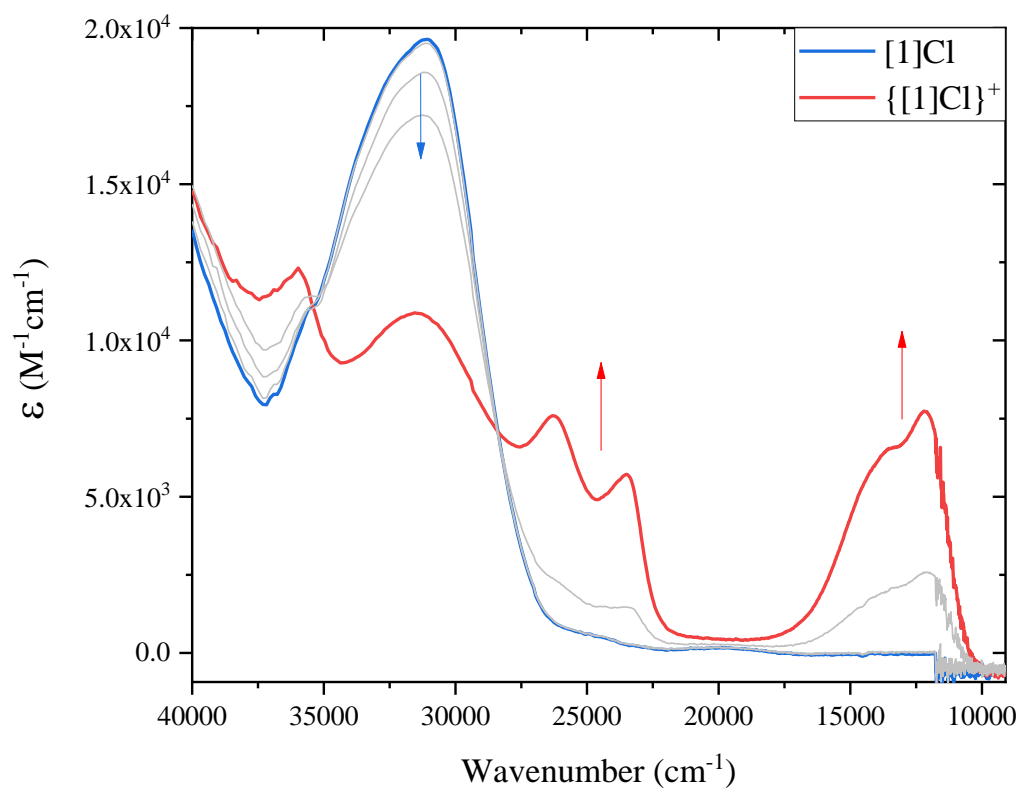
Figure 6.11. Absorption spectra in MeCN of **1** in the ground (blue) and 1e⁻ oxidized (red) states. Red arrows indicate new absorption bands for the oxidized species and blue arrows indicate absorption decay.
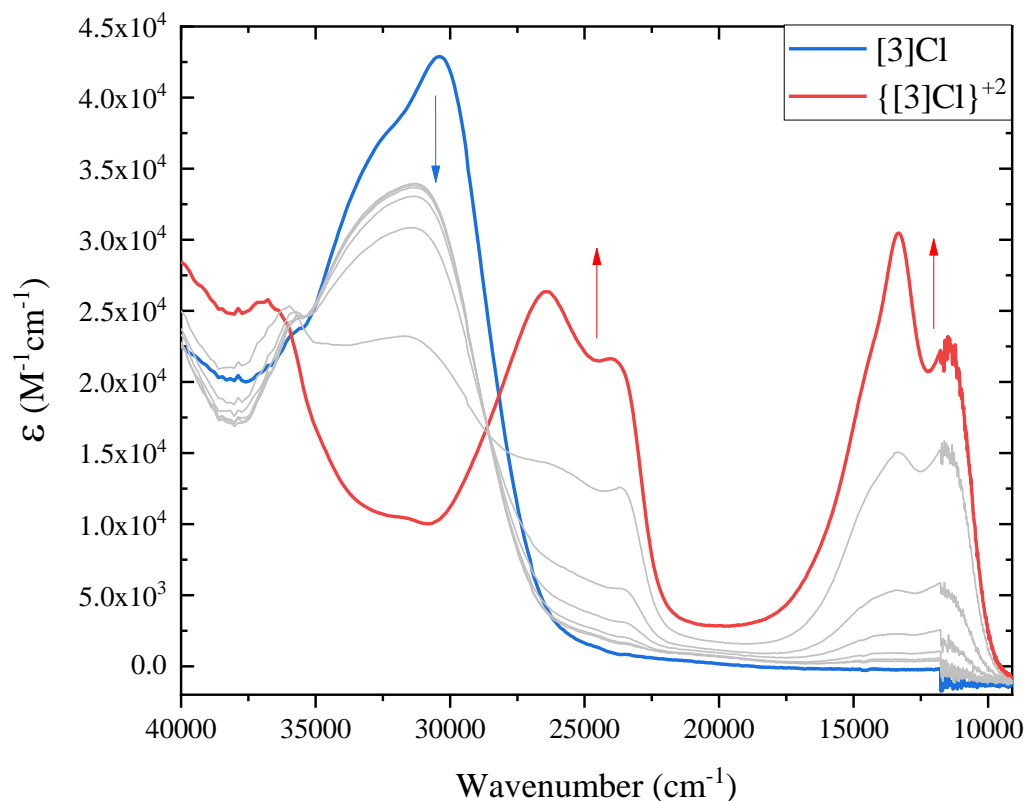
Figure 6.12. Absorption spectra in MeCN of **3** in the ground (blue) and 2e⁻ oxidized (red) states. Red arrows indicate new absorption bands for the oxidized species and blue arrows indicate absorption decay.

Spectroelectrochemical data for **1** (Fig 6.11) shows that upon oxidation the π→π* (TPA) transition (330 nm, 30,000 cm⁻¹) is partially reduced and new transitions grow in around 25,000 cm⁻¹ (400 nm) and 12,500 cm⁻¹ (800 nm). DFT analysis of the oxidized species suggests the former transition (400 nm) is attributed to $(TPA)^+ \rightarrow 3d_{x^2-y^2}$ and the latter (800 nm) attributed to $3d_{xy}/3d_{xz} \rightarrow (TPA)^+$. Compound **3** shows similar spectral features (Fig 6.12), however upon oxidation, the (TPA) π→π* transition is completely bleached and the observed transitions for the oxidized species (~400 nm and ~800 nm) are twice as strong compared to **1**. These differences were attributed to the presence of two TPA ligands trans to each other. DFT modeling of the oxidized form of {[**3**]Cl}⁺²,

suggested the transitions *ca.* 400 nm was also attributed to TPA→$3d_{x^2-y^2}$, however the transitions *ca.* 800 nm likely possesses both TPA→$3d_{x^2-y^2}$ and TPA→TPA character. These transitions are highly reminiscent in shape and λ_{max} of literature examples that claim to undergo MLCT and LMCT between metal center and ligand, like Ru^{II}(TPA) species[32] and Fc-TPA species.[42]

Table 6.4. Gaussian fit peak analysis for transitions between 20,000 cm^{-1} (500 nm) and 8,000 cm^{-1} (1250 nm).

Compound	Peak	[a]E_{OP} (cm^{-1})	[a]ε_{max} (M^{-1}cm^{-1})	[b]$\Delta\nu_{1/2}$ (cm^{-1})	[c]r (Å)
1	A	14003	5928	2928	8.757
1	B	12030	6028	1655	8.757
3	A	15158	19105	2475	8.848
3	B	13277	25244	2119	8.848
3	C	11273	19105	1499	8.848

[a]Measured by spectroelectrochemical oxidation. [b]Determined from deconvoluted spectral analysis ($\Delta\nu_{1/2}$ = fwhm). [c]Determined based on the geometric distance between the Co^{III} metal center and the nitrogen atom of the TPA group in the collected crystal structures.

Overlapping peaks made analysis of the new spectral features difficult, deconvolution of the absorption data between 20,000 cm^{-1} (500 nm) and 8,000 cm^{-1} (1250 nm) was required. The Gaussian fit peak analysis features are listed in Table 6.4 and deconvoluted spectra are shown in Fig 6.13 and Fig 6.14. The black line is a smoothed spectrum of the experimental data, the red line the cumulative spectra of all Gaussian bands needed to fit the spectrum adequately, and the green peaks represent the deconvoluted transitions. Work is ongoing to determine the true nature of these transitions.
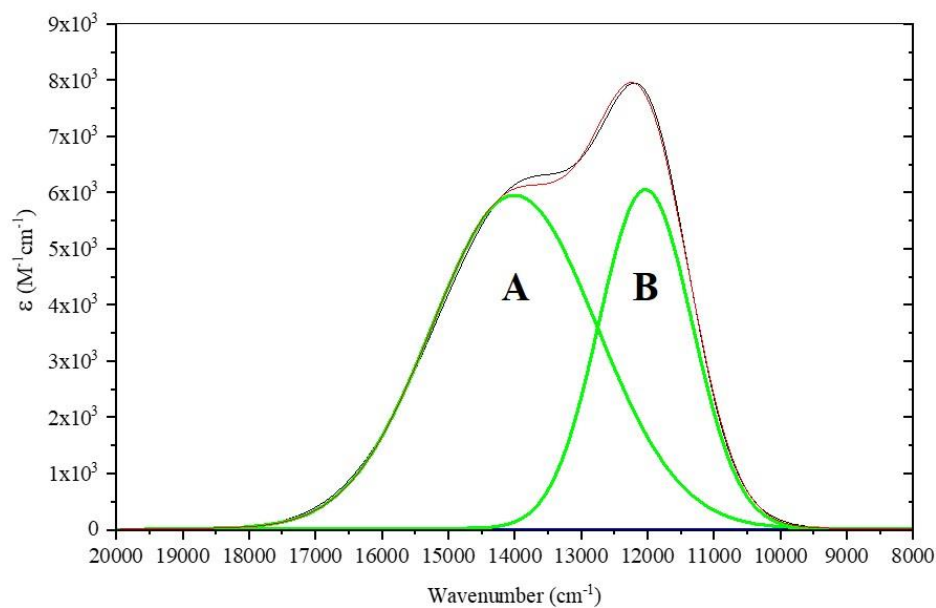
Figure 6.13. Deconvoluted spectra of the first oxidation product formed from holding compound **3** at 0.88 V in a MeCN solution containing 0.1 M *n*-Bu$_4$NPF$_6$.
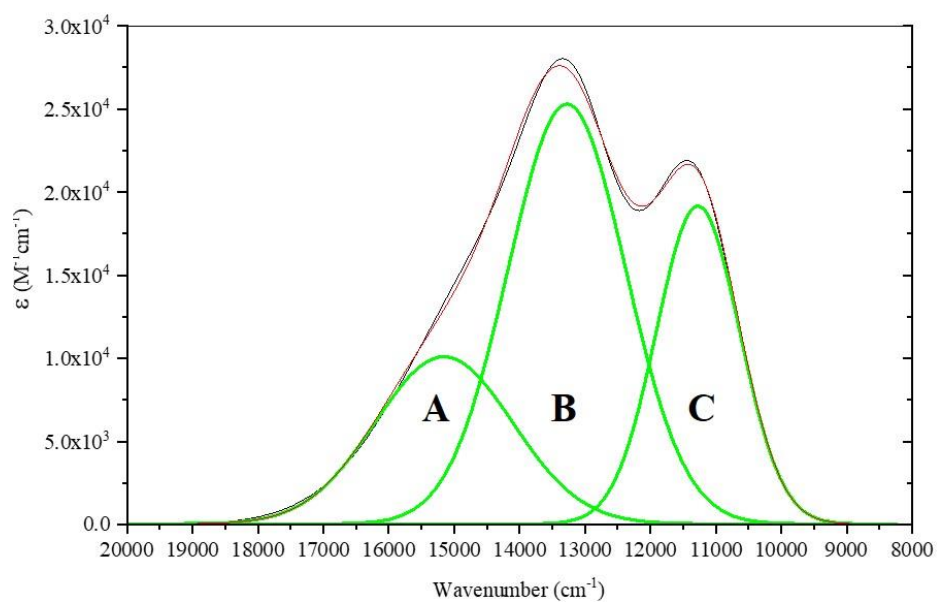
Figure 6.14. Deconvoluted spectra of the first oxidation product formed from holding compound **3** at 0.88 V in a MeCN solution containing 0.1 M *n*-Bu$_4$NPF$_6$.

6.3.1 Density Functional Theory (DFT) calculations
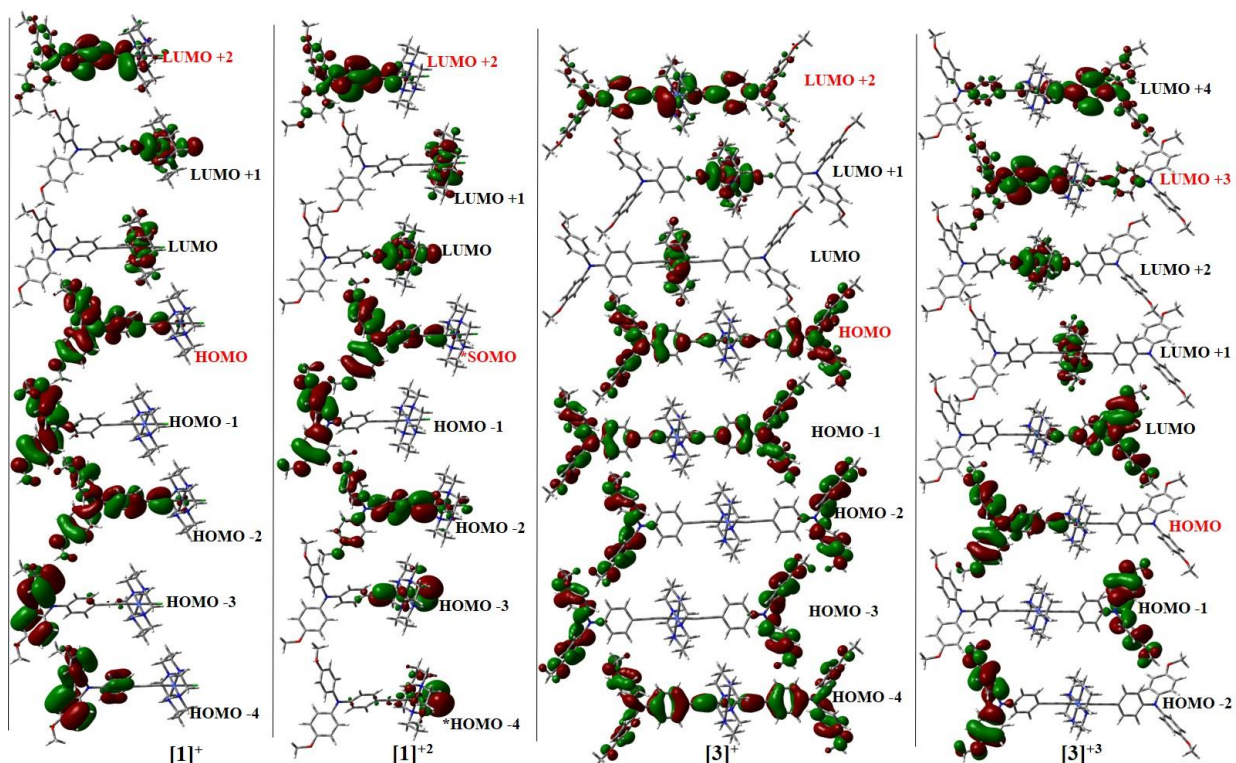
Figure 6.15. Molecular orbital diagrams for [1]+, [1]+2, [3]+and, [3]+3 from DFT calculations; the (TPA)$\pi \rightarrow \pi^*$ transition is noted in red; *SOMO = Singularly occupied MO

To gain a rudimentary understanding of the absorption transitions observed spectroelectrochemically, DFT calculations were performed on geometry optimized structures of [1]+, [1]+2, [3]+ and [3]+3 at B3LYP/LanL2DZ level using Gaussian 16 suite,[43] utilizing the crystal structures of [1]+ and [3]+ as the optimization starting point. The molecular orbital energy level results and assigned transitions are listed in Table 6.5. The calculations and nature of the molecular orbitals (shown in Fig 6.15) suggest that the major absorption band, observed for **1, 2a, 2b** and **3**, at 330 nm is comprised primarily of (TPA)$\pi \rightarrow \pi^*$ character with some contribution from TPA$\rightarrow 3d_{x^2-y^2}$ and TPA$\rightarrow 3d_{z^2}$ (LMCT). The relative energies of the molecular orbitals for the modeled oxidized species

([1]$^{+2}$ and [3]$^{+3}$) are significantly lower in energy than their parent compounds, which is consistent with loss of an electron(s). Analysis of major transitions for [1]$^{+2}$ and [3]$^{+3}$ was based on experimental spectroelectrochemical data and are listed in Table 6.4.

Table 6.5. Relative energies (eV) of Molecular Orbitals and major transitions (eV) calculated at B3LYP/LanL2DZ level

	[1]$^+$	[1]$^{+2*}$	[3]$^+$	[3]$^{+3}$
LUMO +4	-2.37	-5.42	-2.34	-6.72
LUMO +3	-2.48	-5.63	-2.37	-6.86
LUMO +2	-2.78	-6.01	-2.56	-7.16
LUMO +1	-4.60	-6.59	-3.48	-1.70
LUMO	-4.63	-6.64	-4.14	-9.44
HOMO/SOMO*	-6.61	-10.10	-6.34	-10.83
HOMO -1	-7.78	-11.10	-6.37	-11.43
HOMO -2	-7.95	-11.16	-7.62	-11.81
HOMO -3	-8.57	-11.65	-7.62	-11.84
HOMO -4	-8.63	-11.67	-7.67	-12.03
[a](TPA)$\pi \to \pi*$	3.84	4.08	3.78	3.97
	(323 nm)	(304 nm)	(328 nm)	(312 nm)
[b]HOMO/H-1$\to$3d$_{x^2-y^2}$	3.16	3.46	2.23	3.13
	(393 nm)	(359 nm)	(556 nm)	(396 nm)
[c]HOMO/H-1$\to$3d$_{z^2}$	3.18	3.51	2.88	3.67
	(389 nm)	(353 nm)	(430 nm)	(338 nm)
H-3$\to$SOMO	--	1.55	--	--
		(799 nm)		
H-4$\to$SOMO	--	1.58	--	--
		(786 nm)		
HOMO$\to$LUMO	--	--	--	1.39
				(894 nm)
LUMO$\to$L+1	--	--	--	1.74
				(712 nm)

[a][1]$^+$, [1]$^{+2}$ and [3]$^+$ (HOMO$\to$L+2) and [3]$^{+3}$ (HOMO$\to$L+3); [b][1]$^+$ and [3]$^+$ (H-1$\to$3d$_{x^2-y^2}$) and [1]$^{+2}$ and [3]$^{+3}$ (HOMO$\to$3d$_{x^2-y^2}$); [c][1]$^+$ and [3]$^+$ (H-1$\to$3d$_{z^2}$) and [1]$^{+2}$ and [3]$^{+3}$ (HOMO$\to$3d$_{z^2}$).

6.4   Conclusion

Reported herein is new reactivity for *trans*-[Co(cyclam)(C$_2$R)X]$^+$ species to form η^2-adducts of Cu(I) (**2a**) and Ag(I) (**2b**). These compounds exhibit intriguing electronic and fluorescent properties that are being actively investigated. Efforts to understand the

reactivity of **3** with CuCl/AgNO$_3$ are in progress. Electronic coupling between Co^{III}(cyclam) and the TPA ligand was probed for compounds **1** and **3** using spectroelectrochemistry. Further analysis via TD-DFT is also underway to elucidate on the true nature of transitions observed for the respective oxidized species ({[**1**]Cl}$^+$ and {[**3**]Cl}$^{+2}$).

6.5   Experimental

6.5.1   Materials

CuCl was purchased from Alfa Aesar. AgNO$_3$ and *n*-butyl lithium were purchased from Sigma-Aldrich. Dry acetonitrile was purchased from ACROS Chemical. All reagents were used as received. [Co(cyclam)Cl$_2$]Cl was prepared according to literature procedures.[44] Also prepared according to literature procedures was 4-ethynyl-*N,N*-bis(4-methoxyphenyl)aniline (HC$_2$TPA).[27,28] THF was distilled over Na/benzophenone under a N$_2$ atmosphere. Unless otherwise noted, all reactions were carried out using Schlenk techniques under N$_2$.

6.5.2   Physical Measurements and Computational Details

UV-vis spectra were obtained with a JASCO V-670 spectrophotometer. FT-IR spectra were measured as neat samples using a JASCO FT/IR-6300 spectrometer equipped with an ZnSe ATR accessory. ESI-MS were analyzed on an Advion LC/MS. Emission studies were performed on a Varian Cary Eclipse fluorescence spectrophotometer. Fluorescent quantum yields were determined using an anthracene standard. Elemental Analysis was carried out by Atlantic Micro Labs in Norcross, GA. ^{1}H NMR spectra were recorded on a Varian INOVA300 NMR. Electrochemical analysis

was done on a CHI620A voltammetric analyzer with a glassy carbon working electrode (diameter = 2 mm), a Pt-wire auxiliary electrode, and a Ag/AgCl reference electrode; the analyte concentration is 1.0 mM in 4 mL dry acetonitrile at a 0.1 M n-Bu$_4$NPF$_6$ electrolyte concentration. Spectrochemical analysis was performed using an OTTLE[45] (optically transparent thin-layer electrochemical) liquid-sample cell with a 0.2 mm optical path length, 0.3 mL sample volume and a CaF$_2$ window. The cell was equipped with a mesh Pt working electrode; mesh Pt auxiliary electrode, and Ag reference electrode; the analyte concentration was 1.0 mM in 4 mL dry acetonitrile at a 0.1 M n-Bu$_4$NPF$_6$ electrolyte concentration. Spin-restricted DFT calculations were performed with the B3LYP functional and LANL2DZ basis sets, as implemented in the Gaussian 16 program.[43]

6.5.3   Synthesis of Compounds 1, 2a, 2b, and 3

Synthesis of trans-[Co(cyclam)(C$_2$TPA)Cl]Cl (**1**). [Co(cyclam)Cl$_2$]Cl (127 mg, 0.35 mmol) was dissolved in 30 mL of MeOH, a 5 mL solution of THF containing TPAC$_2$H (77 mg, 0.23 mmol) was added and the solution was purged with N$_2$. Upon addition of 0.5 mL of Et$_2$NH (4.9 mmol) the solution turned turquoise. It was then refluxed for 12 h, resulting in a red solution which was then purified over silica, eluting **1** as a dark red band (1:6 MeCN:CH$_2$Cl$_2$). Recrystallization from CH$_2$Cl$_2$, minimal MeOH, and diethyl ether afforded microcrystalline pink solid. Yield: 0.116 g (0.18 mmol; 75% based on HC$_2$TPA). ESI-MS [M$^+$] 622.3 m/z. UV-vis, λ_{max}/nm (ε/M^{-1}cm^{-1}): 327 (27,240), 410 (820), 513 (300). FT-IR, ν(C$\equiv$C)/cm^{-1}: 2114 (w). ^{1}H NMR (300 MHz, CD$_3$OD) δ 7.23 (d, J = 8.8 Hz, 2H), 6.98 (d, J = 9.0 Hz, 4H), 6.86 (d, J = 9.0 Hz, 4H), 6.75 (d, J = 8.7 Hz, 2H), 5.07 (br s, 4H), 3.77 (s, 6H), 2.91 (s, 2H), 2.73 – 2.64 (m, 8H), 2.56-2.45 (m,

6H), 1.95 (t, J = 13.4 Hz, 2H), 1.68 – 1.58 (m, 2H). Elem. Anal. Found (Calcd) for $C_{34}H_{52}N_6O_5CoCl_2$ (**1**·3H$_2$O·MeCN): C, 54.16 (54.11); H, 7.41 (6.95); N, 10.85 (11.13).

Synthesis of trans-[Co(cyclam)(C$_2$TPA-η^2-CuCl$_2$)Cl] (**2a**). Combining **1** (30 mg, 0.045 mmol) with CuCl (10 mg, 0.05 mmol) in 20 mL MeCN yielded **2** after stirring for 12 h under reflux. The precipitate formed was discarded, and the reaction solution was concentrated via rotary evaporation. The desired product was recrystallized from MeCN with diethyl ether to yield a light pink solid. Yield: 0. 029 g (0.034 mmol; 74% based on **1**). ESI-MS [M$^+$] 622.1 m/z. ESI-MS [M$^-$] 132.7 m/z. UV-vis, λ_{max}/nm (ε/M^{-1}cm^{-1}): 328 (25,242), 410 (1310), 515 (523). FT-IR, ν(C≡C)/cm^{-1}: 2129 (w). ^{1}H NMR (300 MHz, CD$_3$OD) δ 7.23 (d, J = 10.1 Hz, 2H), 6.99 (d, J = 9.5 Hz, 4H), 6.86 (d, J = 9.3 Hz, 4H), 6.75 (d, J = 8.7 Hz, 2H), 5.09 (br s, 4H), 3.78 (s, 6H), 2.82 (s, 2H), 2.70 – 2.62 (m, 8H), 2.56 – 2.49 (m, 6H), 1.99-1.90 (m, 2H), 1.86 – 1.55 (m, 2H). Elem. Anal. Found (Calcd) for $C_{32}H_{48}N_5O_5CoCuCl_3$ (**2a**·3H$_2$O): C, 47.68 (47.36); H, 5.99 (5.96); N, 9.13 (8.63).

Synthesis of trans-[Co(cyclam)(C$_2$TPA-η^2-Ag(NO$_3$)$_2$)(NO$_3$)] (**2b**). In a round bottom flask, **1** (17 mg, 0.026 mmol) and AgNO$_3$ (18 mg, 0.11 mmol) was stirred at room temperature in 10 mL of MeOH for 4 h. A grey precipitate formed and was filtered out and rinsed until the filtrate ran clear. The filtrate was concentrated. Recrystallization from CH$_2$Cl$_2$ and ether afforded **3** as dark red crystals. Yield: 0.016 g (0.018 mmol; 70% based on **1**). ESI-MS [M$^+$] 649.2 m/z. ESI-MS [M$^-$] 230.7 m/z. UV-vis, λ_{max}/nm: 326, 410, 519. FT-IR, ν(C≡C)/cm^{-1}: 2030 (w). ^{1}H NMR (300 MHz, CD$_3$OD) δ 7.21 (br s, 2H), 6.98 (br s, 4H), 6.87 (br s, 4H), 6.76 (br s, 2H), 5.17 (br s, 4H), 3.79 (s, 6H), 3.04-2.93 (m, 4H), 2.90 – 2.27 (m, 12H), 2.16 – 1.93 (m, 2H), 2.02 – 1.48 (m, 2H). Elem. Anal. Found (Calcd)

for $C_{33}H_{44}N_8O_{11}CoAgCl_2$ (**2b**·$3CH_2Cl_2$): C, 41.01 (41.01); H, 4.45 (4.59); N, 11.90 (11.59).

Synthesis of trans-[Co(cyclam)(C_2TPA)$_2$]Cl (**3**). A solution of LiC_2TPA (prepared from 1.88 mmol HC_2TPA, 2.5 mmol *n*-BuLi, and 20 mL THF) was added to a flask containing [Co(cyclam)Cl$_2$]Cl (228 mg, 0.63 mmol). Upon addition the reaction turned from red to dark brown. After 3 h the reaction was quenched and purified over silica, **3** eluted as a dark brown band with 1:5 MeOH: CH_2Cl_2. Recrystallization from CH_2Cl_2 with ether yielded a light brown solid. Yield: 0.501 g (0.53 mmol; 84% based on Co). ESI-MS [M$^+$] 915.3 *m/z*. UV-vis, λ_{max}/nm (ε/M^{-1}cm^{-1}): 333 (47,650), 470 (406). FT-IR, ν(C≡C)/cm^{-1}: 2096 (m). ^{1}H NMR (300 MHz, CDCl$_3$) δ 7.38 (d, *J* = 8.7 Hz, 4H), 7.02 (d, *J* = 9.0 Hz, 8H), 6.86 (d, *J* = 6.9 Hz, 4H), 6.81 (d, *J* = 8.9 Hz, 8H), 4.40 (br s, 4H), 3.79 (s, 12H), 2.93 (s, 2H), 2.86 – 2.76 (m, 6H), 2.71 – 2.60 (m, 8H), 1.91-1.86 (m, 2H), 1.65-1.60 (m, 2H). Elem. Anal. Found (Calcd) for $C_{54}H_{63}N_6O_5CoCl_2$ (**3**·$1H_2O$·$0.5CH_2Cl_2$): C, 65.01 (64.69); H, 6.41 (6.27); N, 8.47 (8.30).

6.5.4 X-ray Crystallographic Analysis.

Single crystals of complexes **1**, **2a**, **2b**, and **3** were grown via slow diffusion of diethyl ether into a solution of MeOH for **1**, **2a**, or **2b** and in a solution of EtOAc/MeOH (1:1) for **3**. X-ray diffraction data was obtained on a Bruker Quest diffractometer with Mo Kα radiation (λ=0.71073Å) at 100K. Data were collected; reflections were indexed and processed using APEX3.[46] The space groups were assigned and the structures were solved by direct methods using XPREP within the SHELXTL suite of programs[47,48] and refined using Shelxle.[49,50]

Table 6.6. Crystal data for complexes **1**, **2a**, **2b** and **3**

	1·THF·CH₃OH	**2a·THF**	**2b·CH₃OH**	**3·CH₂Cl₂**
Chemical Formula	$C_{32}H_{42}ClCoN_5O_2 \cdot 0.247(C_4H_{10}O) \cdot 1.507(CH_4O) \cdot 0.05(I) \cdot 0.95(Cl)$	$C_{32}H_{42}Cl_3CoCuN_5O_2 \cdot C_4H_8O$	$C_{32}H_{42}AgCoN_8O_{11} \cdot 1.476(CH_4O) \cdot 0.209(O)$	$C_{54}H_{60}CoN_6O_4 \cdot 0.874(CH_2Cl_2) \cdot 0.415(Br) \cdot 0.585(Cl)$
Formula Weight	729.67	829.63	933.70	1044.11
Space Group	Monoclinic, $P2_1/c$	Triclinic, $P1$	Triclinic, $P1$	Triclinic, $P1$
a, Å	14.2721 (8)	9.3921 (8)	10.5925 (6)	11.8848 (12)
b, Å	24.1352 (13)	13.371 (2)	11.7280 (7)	13.9746 (18)
c, Å	10.4474 (5)	15.203 (2)	16.0527 (9)	15.972 (3)
α, deg	-	86.645 (3)	93.730 (2)	104.155 (6)
β, deg	93.064 (2)	77.678 (4)	98.254 (2)	91.216 (6)
γ, deg	-	85.353 (3)	96.435 (2)	91.053 (4)
V, Å³	3593.6 (3)	1857.4 (4)	1954.4 (2)	2570.8 (6)
Z	4	2	2	2
T, K	150	150	150	150
λ, Å	0.71073	0.71073	0.71073	0.71073
$\Delta\rho_{max}$, $\Delta\rho_{min}$ (e Å⁻³)	0.66, −0.39	0.42, −0.47	1.15, −1.12	0.72, −0.39
R	0.046	0.026	0.041	0.044
$R_w(F^2)$	0.126	0.085	0.103	0.142

6.6 References

(1) Nast, R. Coordination Chemistry of Metal Alkynyl Compounds. *Coord. Chem. Rev.* **1982**, *47*, 89-124.

(2) Bruce, M. I. Transition Metal Complexes Containing Allenylidene, Cumulenylidene, and Related Ligands. *Chem. Rev.* **1998**, *98*, 2797-858.

(3) Bruce, M. I.; Low, P. J. Transition Metal Complexes Containing All-Carbon Ligands. *Adv. Organomet. Chem.* **2004**, *50*, 179-444.

(4) Long, N. J.; Williams, C. K. Metal Alkynyl Complexes: Synthesis and Materials. *Angew. Chem. Int. Ed.* **2003**, *42*, 2586-2617.

(5) Szafert, S.; Gladysz, J. A. Carbon in One Dimension: Structural Analysis of the Higher Conjugated Polyynes. *Chem. Rev.* **2003**, *103*, 4175-4206.

(6) Szafert, S.; Gladysz, J. A. Update 1 of: Carbon in One Dimension: Structural Analysis of the Higher Conjugated Polyynes. *Chem. Rev.* **2006**, *106*, 1-33.

(7) Manna, J.; John, K. D.; Hopkins, M. D. The Bonding of Metal-Alkynyl Complexes. *Adv. Organomet. Chem.* **1995**, *38*, 79-154.

(8)   Paul, F.; Lapinte, C. Organometallic Molecular Wires and Other Nanoscale-sized Devices. An Approach using the Organoiron (dppe)Cp*Fe Building Block. *Coord. Chem. Rev.* **1998**, *178-180*, 431-509.

(9)   Ren, T. Diruthenium s-Alkynyl Compounds**:** A New Class of Conjugated Organometallics. *Organometallics* **2005**, *24*, 4854-4870.

(10)   Costuas, K.; Rigaut, S. Polynuclear carbon-rich organometallic complexes: clarification of the role of the bridging ligand in the redox properties. *Dalton Trans.* **2011**, *40*, 5643-5658.

(11)   Rigaut, S. Metal complexes in molecular junctions. *Dalton Trans.* **2013**, *42*, 15859-15863.

(12)   Blum, A. S.; Ren, T.; Parish, D. A.; Trammell, S. A.; Moore, M. H.; Kushmerick, J. G.; Xu, G.-L.; Deschamps, J. R.; Pollack, S. K.; Shashidhar, R. $Ru_2(ap)_4$(s-oligo(phenyleneethynyl)) Molecular Wires: Synthesis and Electronic Characterization. *J. Am. Chem. Soc.* **2005**, *127*, 10010-10011.

(13)   Wen, H. M.; Yang, Y.; Zhou, X. S.; Liu, J. Y.; Zhang, D. B.; Chen, Z. B.; Wang, J. Y.; Chen, Z. N.; Tian, Z. Q. Electrical conductance study on 1,3-butadiyne-linked dinuclear ruthenium(II) complexes within single molecule break junctions. *Chem. Sci.* **2013**, *4*, 2471-2477.

(14)   Meng, F. B.; Hervault, Y. M.; Shao, Q.; Hu, B. H.; Norel, L.; Rigaut, S.; Chen, X. D. Orthogonally modulated molecular transport junctions for resettable electronic logic gates. *Nature Commun.* **2014**, *5*, Art. 3023.

(15)   Zhu, H.; Pookpanratana, S. J.; Bonevich, J. E.; Natoli, S. N.; Hacker, C. A.; Ren, T.; Suehle, J. S.; Richter, C. A.; Li, Q. Redox-Active Molecular Nanowire Flash Memory for High-Endurance and High-Density Non-Volatile Memory Applications. *ACS Appl. Mater. Interfaces* **2015**, *7*, 27306-27313.

(16)   Wong, W.-Y.; Ho, C.-L. Organometallic Photovoltaics: A New and Versatile Approach for Harvesting Solar Energy Using Conjugated Polymetallaynes. *Acc. Chem. Res.* **2010**, *43*, 1246-1256.

(17)   Ho, C.-L.; Yu, Z.-Q.; Wong, W.-Y. Multifunctional polymetallaynes: properties, functions and applications. *Chem. Soc. Rev.* **2016**, *45*, 5264-5295.

(18)   Ko, C.-C.; Yam, V. W.-W. Coordination Compounds with Photochromic Ligands: Ready Tunability and Visible Light-Sensitized Photochromism. *Acc. Chem. Res.* **2018**, *51*, 149-159.

(19)   Gao, L.-B.; Zhang, L.-Y.; Shi, L.-X.; Chen, Z.-N. Syntheses, Characterization, Redox Properties, and Mixed-Valence Chemistry of Tetra- and Hexanuclear Diyndiyl Complexes. *Organometallics* **2005**, *24*, 1678-1684.

(20) Juvenal, F.; Langlois, A.; Bonnot, A.; Fortin, D.; Harvey, P. D. Luminescent 1D- and 2D-Coordination Polymers Using CuX Salts (X = Cl, Br, I) and a Metal-Containing Dithioether Ligand. *Inorg. Chem.* **2016**, *55*, 11096-11109.

(21) Mak, T. C. W.; Zhao, X. L.; Wang, Q. M.; Guo, G. C. Synthesis and structural characterization of silver(I) double and multiple salts containing the acetylenediide dianion. *Coord. Chem. Rev.* **2007**, *251*, 2311-2333.

(22) Banziger, S. D.; Ren, T. Syntheses, Structures and Bonding of 3d Metal Alkynyl Complexes of Cyclam and Its Derivatives. *J. Organomet. Chem.* **2019**, submitted.

(23) Ren, T. A Sustainable Metal Alkynyl Chemistry: 3d Metals and Polyaza Macrocyclic Ligands. *Chem. Commun.* **2016**, *52*, 3271-3279.

(24) Banziger, S. D.; Cook, T. D.; Natoli, S. N.; Fanwick, P. E.; Ren, T. Synthetic and Structural Studies of Mono-acetylide and Unsymmetric Bis-acetylide Complexes based on CoIII-cyclam. *J. Organomet. Chem.* **2015**, *799-800*, 1-6.

(25) Banziger, S. D.; Li, X.; Zeller, M.; Rubtsov, I.; Ren, T. Unsymmetrical Bis-Alkynyl Complexes Based on Co(III)(cyclam): Synthesis and Ultrafast Charge Separation. *Chem. Sci.* **2019**, manuscript in preparation.

(26) Natoli, S. N.; Zeller, M.; Ren, T. An Aerobic Synthetic Approach toward Bis-Alkynyl Cobalt(III) Compounds. *Inorg. Chem.* **2017**, *56*, 10021-10031.

(27) Heyer, E.; Ziessel, R. Panchromatic Push-Pull Dyes of Elongated Form from Triphenylamine, Diketopyrrolopyrrole, and Tetracyanobutadiene Modules. *Synlett* **2015**, *26*, 2109-2116.

(28) Planells, M.; Abate, A.; Hollman, D. J.; Stranks, S. D.; Bharti, V.; Gaur, J.; Mohanty, D.; Chand, S.; Snaith, H. J.; Robertson, N. Diacetylene bridged triphenylamines as hole transport materials for solid state dye sensitized solar cells. *J. Mater. Chem. A* **2013**, *1*, 6949-6960.

(29) Thakker, P. U.; Aru, R. G.; Sun, C.; Pennington, W. T.; Siegfried, A. M.; Marder, E. C.; Wagenknecht, P. S. Synthesis of trans Bis-alkynyl Complexes of Co(III) Supported by a Tetradentate Macrocyclic Amine: A Spectroscopic, Structural, and Electrochemical Analysis of p-Interactions and Electronic Communication in the CC-M-CC Structural Unit. *Inorg. Chim. Acta* **2014**, *411*, 158-164.

(30) Natoli, S. N.; Zeller, M.; Ren, T. Stepwise Synthesis of Bis-Alkynyl CoIII(cyclam) Complexes under Ambient Conditions. *Inorg. Chem.* **2016**, *55*, 5756-5758.

(31) Tsuchida, R. Absorption Spectra of Co-ordination Compounds. I. *Bull. Chem. Soc. Jpn.* **1938**, *13*, 388-400.

(32) Piechota, E. J.; Troian-Gautier, L.; Sampaio, R. N.; Brennaman, M. K.; Hu, K.; Berlinguette, C. P.; Meyer, G. J. Optical Intramolecular Electron Transfer in Opposite Directions through the Same Bridge That Follows Different Pathways. *J. Am. Chem. Soc.* **2018**, *140*, 7176-7186.

(33) Schnaubelt, L.; Petzold, H.; Dmitrieva, E.; Rosenkranz, M.; Lang, H. A solvent- and temperature-dependent intramolecular equilibrium of diamagnetic and paramagnetic states in Co complexes bearing triaryl amines. *Dalton Trans.* **2018**, *47*, 13180-13189.

(34) Amthor, S.; Noller, B.; Lambert, C. UV/Vis/NIR spectral properties of t riarylamines and their corresponding radical cations. *Chem. Phys.* **2005**, *316*, 141-152.

(35) Dapperheld, S.; Steckhan, E.; Brinkhaus, K.-H. G.; Esch, T. Organic Electron Transfer Systems, II Substituted Triarylamine Cation-Radical Redox Systems - Synthesis, Electrochemical and Spectroscopic Properties, Hammet Behavior, and Suitability as Redox Catalysts. *Chem. Ber.* **1991**, *124*, 2557-2567.

(36) Judkins, E. C.; Zeller, M.; Ren, T. Synthesis and Characterizations of Macrocyclic Cr(III) and Co(III) 1-Ethynyl Naphthalene and 9-Ethynyl Anthracene Complexes: An Investigation of Structural and Spectroscopic Properties. *Inorg. Chem.* **2018**, *57*, 2249-2259.

(37) Ferraudi, G. In *Photosensitive Metal-Organic Systems*; Kutal, C., Serpone, N., Eds.; American Chemical Society: Washington, D.C., 1993; Vol. 238.

(38) Bakac, A.; Espenson, J. H. Preparation, properties, and crystal structure of a novel series of macrocyclic organocobalt complexes. *Inorg. Chem.* **1987**, *26*, 4353-4355.

(39) Roche, T. S.; Endicott, J. F. Saturated macrocyclic (N4) complexes of cobalt(III) containing cobalt-alkyl bonds. Preparation and properties. *Inorg. Chem.* **1974**, *13*, 1575-1580.

(40) Scaiano, J. C.; Leigh, W. J.; Ferraudi, G. Flash photolysis of phenylacetatopentaminecobalt(III) in aqueous solution. Generation of benzyl radicals and their reversible trapping by cupric ions in homogeneous and micellar solutions. *Can. J. Chem.* **1984**, *62*, 2355-2358.

(41) Bakir, M.; McDermot, C.; Johnson, T. Spectroscopic, and electrochemical studies of [MCl2(h·2-N,N-dpksc)] (M=Zn, Cd, Hg and dpksc=di-2-pyridylketone semicarbazone). *J. Mol. Struct.* **2013**, *1040*, 221-225.

(42) Zhang, M.-X.; Zhang, J.; Yin, J.; Hartl, F. e.; Liu, S. H. Anodic electrochemistry of mono- and dinuclear aminophenylferrocene and diphenylaminoferrocene complexes. *Dalton Trans.* **2018**, *47*, 6112-6123.

(43) *Gaussian 16 Rev. B.01*; Frisch, M. J.; Trucks, G. W.; Schlegel, H. B.; Scuseria, G. E.; Robb, M. A.; Cheeseman, J. R.; Scalmani, G.; Barone, V.; Petersson, G. A.; Nakatsuji, H.; Li, X.; Caricato, M.; Marenich, A. V.; Bloino, J.; Janesko, B. G.; Gomperts, R.; Mennucci, B.; Hratchian, H. P.; Ortiz, J. V.; Izmaylov, A. F.; Sonnenberg, J. L.; Williams; Ding, F.; Lipparini, F.; Egidi, F.; Goings, J.; Peng, B.; Petrone, A.; Henderson, T.; Ranasinghe, D.; Zakrzewski, V. G.; Gao, J.; Rega, N.; Zheng, G.; Liang, W.; Hada, M.; Ehara, M.; Toyota, K.; Fukuda, R.; Hasegawa, J.; Ishida, M.; Nakajima, T.; Honda, Y.; Kitao, O.; Nakai, H.; Vreven, T.; Throssell, K.; Montgomery Jr., J. A.; Peralta, J. E.; Ogliaro, F.; Bearpark, M. J.; Heyd, J. J.; Brothers, E. N.; Kudin, K. N.; Staroverov, V. N.; Keith, T. A.; Kobayashi, R.; Normand, J.; Raghavachari, K.; Rendell, A. P.; Burant, J. C.; Iyengar, S. S.; Tomasi, J.; Cossi, M.; Millam, J. M.; Klene, M.; Adamo, C.; Cammi, R.; Ochterski, J. W.; Martin, R. L.; Morokuma, K.; Farkas, O.; Foresman, J. B.; Fox, D. J.: Wallingford, CT, 2016.

(44) Bosnich, B.; Tobe, M. L.; Webb, G. A. Complexes of Nickel(2) with a Cyclic Tetradentate Secondary Amine. *Inorg. Chem.* **1965**, *4*, 1109-1112.

(45) Krejcik, M.; Danek, M.; Hartl, F. Simple construction of an infrared optically transparent thin-layer electrochemical cell: Applications to the redox reactions of ferrocene, Mn2(CO)10 and Mn(CO)3(3,5-di-t-butyl-catecholate)-. *J. Electroanal. Chem.* **1991**, *317*, 179-187.

(46) *APEX3 v2016.9-0, Saint V8.34A, Saint V8.37A*Bruker AXS, Inc.: Madison, WI, 2016.

(47) *SHELXTL suite of programs, version 6.14*Bruker AXS Inc.: Madison, WI, 2000-2003.

(48) Sheldrick, G. M. A short history of SHELX. *Acta Crystallogr A* **2008**, *64*, 112-122.

(49) Sheldrick, G. M. Crystal structure refinement with SHELXL. *Acta Crystallogr C* **2015**, *71*, 3-8.

(50) Hübschle, C. B.; Sheldrick, G. M.; Dittrich, B. ShelXle: a Qt graphical user interface for SHELXL. *J. Appl. Cryst.* **2011**, *44*, 1281-1284.